Mathematical Modeling of the Performance of a Rotating Biological Contactor for Process Optimisation in Wastewater Treatment

Zur Erlangung des akademischen Grades eines

DOKTOR-INGENIEURS

von der Fakultät für

Bauingenieur-, Geo- und Umweltwissenschaften

der Universität Fridericiana zu Karlsruhe (TH)

genehmigte

DISSERTATION

von

Sanjay Dutta, M.Tech.
aus Kalkutta, Indien

Tag der mündlichen
Prüfung: 14. Februar, 2007
Hauptreferent: Prof. Dr. Ing. E.h. Hermann H. Hahn, Ph.D., Karlsruhe
Korreferent: Prof. Dr. rer. nat. habil. Josef Winter, Karlsruhe

Karlsruhe 2007

Dissertation genehmigt von der
Fakultät für Bauingenieur-, Geo- und Umweltwissenschaften

Universität Fridericiana zu Karlsruhe (TH)
2007

Hauptreferent: Prof. Dr. Ing. E.h. Hermann H. Hahn, Ph.D., Karlsruhe
Korreferent: Prof. Dr. rer. nat. habil. Josef Winter, Karlsruhe

Dutta, Sanjay

Mathematical Modeling of the Performance of a Rotating Biological Contactor for Process Optimisation in Wastewater Treatment
Karlsruhe: Universität Karlsruhe – Verlag
Siedlungswasserwirtschaft Karlsruhe, 2007
(Schriftenreihe SWW – Band 126)
Zugl.: Karlsruhe, Univ., Diss., 2007
ISBN 978-3-9809383-9-6

ISBN 978-3-9809383-9-6

Satz: Institut für Wasser und Gewässerentwicklung
Bereich Siedlungswasserwirtschaft
Universität Karlsruhe (TH)
Druck: E&B printware, Digital- und Schnelldruck GmbH, 76131 Karlsruhe
Printed in Germany

Vorwort des Herausgebers

Scheibentauchkörper als biologische Reinigungselemente haben sich bislang einer eher auf spezifische Anschlussgrößen (im mittleren Bereich) und spezifische Abwässer beschränkten Beliebtheit erfreut. In jüngerer Zeit nimmt das Interesse an diesen biologischen Reinigungselementen allerdings zu, insbesondere vor dem Hintergrund der Anwendung für kleinere Anschlussgrößen im Rahmen der sog. "Dezentralisierungsdiskussion" und insbesondere auch im Hinblick auf die Möglichkeiten und Grenzen des Exportes dieser Technologie in Drittweltländer.

Der Autor dieser Schrift, ein indischer Fachkollege, untersucht zum einen die Leistungsfähigkeit dieses Systems und insbesondere auch die Verhaltensweisen der Scheibentauchkörper unter variablen Belastungsbedingungen und veränderten Temperaturen, wie sie möglicherweise in Indien herrschen. - Diese Untersuchung geschieht nicht wie im klassischen Sinne in ausgedehnten experimentellen Reihen, sondern mit Hilfe des Instrumentes der mathematischen Simulation. Die von ihm verwendeten Modelle eicht er an Daten aus halbtechnischen Untersuchungen, die parallel in einer anderen, experimentellen Arbeit gewonnen wurden.

Der Autor schreibt verständlicherweise in seiner Muttersprache Englisch und dies flüssig, flüssig vor allen Dingen auch in einem anwendungsorientierten, wissenschaftlichen Stil. Dadurch fällte es dem Leser nicht schwer, den Ausführungen des Autors zu folgen. Die gesamte Darstellung, etwa des Sauerstoffübergangs oder insbesondere der Prozesse im Biofilm, ist nicht nur detailliert und durch viele Verweise auf relevante Literaturberichte umfassend gestaltet sondern auch mit zahlreichen Gleichungen und Formeln versehen.

Die Arbeit ist insofern auch als ein gelungener Zwischenbericht zum Stand der Technik und Wissenschaft für den Bereich der Scheibentauchkörper oder auch Biofilmverfahren zu sehen und für nachfolgende Bearbeitungen von Interesse. – In dieser Art von Kombination eigener Vorstellungen, eigener Erkenntnisse und Berichte Dritter ist die Arbeit Duttas sicherlich als eine sehr aufwändige und wissenschaftsorientierte zu betrachten und geht über den Rahmen typischer Ingenieurarbeiten hinaus.

Karlsruhe im März 2007 H.H.Hahn

Kurzfassung

Das Scheibentauchkörperverfahren bietet die prozessspezifischen Vorteile des Biofilmverfahrens zur Entfernung von gelösten organischen Inhaltsstoffen und Nährstoffverbindungen aus Abwässern. Diese Adaptation des Biofilmverfahrens ermöglicht einen einfachen und effektiven Sauerstoffeintrag in den Biofilm. Kreisrunde, glatte oder geriffelte Scheiben werden dabei auf einer horizontalen Welle angeordnet, teilweise in Wasser eingetaucht und in einem kontinuierlich von Abwasser durchströmten Reaktor gedreht. Die kompakte Bauweise und der sparsame Betrieb lassen das Verfahren gerade für dezentrale Abwasserbehandlungsanlagen praktikabel erscheinen. Um eine effiziente Anwendung der Technologie zu ermöglichen, besteht weiterer Forschungsbedarf bezüglich der Prozessoptimierung und des Anpassungsvermögens bei unterschiedlichen Umwelt- und Zuflussbedingungen. Mathematische Modellierungen helfen das Systemverhalten unter verschiedenen Rahmenbedingungen vorauszusagen. Aufgrund der dynamischen Beschaffenheit des Systems fehlen jedoch nach wie vor befriedigende mathematische Darstellungen.

Mit dieser Arbeit wird versucht in einfacher und realistischer Weise mathematische Modelle für diesen Prozess zu formulieren. Das Modell beruht auf dem Prinzip des eindimensionalen Massen- und Stoffaustausches. Sauerstoff ist als wichtiger und oft limitierender Faktor im aeroben Behandlungsprozess anerkannt. Die Modellierung des physikalischen Sauerstoffeintrages in den Wasserfilm einer rotierenden Scheibe zeigte, dass der Sauerstoffübergangskoeffizient mit der Umdrehungsgeschwindigkeit und dem betrachteten Ort auf der Scheibe variiert. Ein Anstieg der Umgebungstemperatur hatte eine abfallende Sauerstoff eintragsrate zur Folge. Basierend auf einer kontinuierlich beaufschlagten halbtechnischen Versuchsanlage wurde das Modell für eine dreikaskadige Scheibentauchkörperanlage realisiert. Die Prozesskinetik wurde dem *Activated Sludge Model No. 3* entnommen, was der Abbildung einer bakteriellen Mischkultur entspricht. Die Simulierung des Modells wurde in *Matlab* durchgeführt, mit der Finite-Differenzen-Methode zur numerischen Lösung der Differenzialgleichungen. Die schwierige Beschaffenheit des Lösungsalgorithmuses machte die Verwendung von veränderlichen Zeitschritten notwenig, um schnelle und stabile Resultate zu erreichen. Das Modell wurde mit den Untersuchungsergebnissen bei 25°C Umgebungstemperatur kalibriert. Bei ansteigender Substrat- oder hydraulischer Belastung zeigte der Scheibentauchkörper

ansteigende Eliminationsraten im optimalen Bereich. Die Konzentration an gelöstem Sauerstoff im Wasserkörper war ausreichend hoch, um aerobe Verhältnisse aufrecht zu erhalten. Bei hoher Nährstoffbelastung der ersten Kaskade lag die Sauerstoffeindringtiefe bei 250 bis 300 µm. In tieferen Schichten lagen anoxische Verhältnisse mit entsprechender Denitrifikation vor. Bei 25°C, hoher Substratbelastung und reduzierter Scheibenfläche in der zweiten und dritten Kaskade konnte ein nahezu vollständiger Abbau der gelösten organischen Substanzen und des Ammoniums erreicht werden. Dies deutet auf einen potenziellen Kosteneinsparungsfaktor bei gleichzeitiger Prozessoptimierung hin. Die Simulation zeigte einen allgemeinen Anstieg der Eliminationsleistung mit steigender Temperatur im Bereich von 10 bis 32.5°C. Die Nitrifikation war weitaus empfindlicher gegenüber der Temperatur und erwies sich als limitierender Faktor bei der Auslegung des Systems. Eine Sensitivitätsanalyse des Modells wurde durchgeführt, um die Bedeutung der Variation der Systemparameter, die normalerweise bei der Modellierung als konstant angenommen werden, zu untersuchen. Die Rezirkulation von Abwasser erhöht zwar die Nitrifikationsleistung der ersten Kaskade, die gesamte Eliminationsleistung wird jedoch nicht entscheidend beeinträchtigt. Dies bedeutet, dass Scheibentauchkörper die Vorteile einer Propfenströmung berücksichtigen, um Stoßbelastungen abzufangen und eine hohe Abbauleistung ohne Rückführung gewährleisten. Das Modell zeigte weiterhin, dass angemessene Prozessanpassungen mit verschiedenen Eintauchverhältnissen in unterschiedlichen Kaskaden und Wasserrückführung in den Scheibentauchkörpern möglich sind.

Zusammenfassend lässt sich festhalten, dass das Modell eine adäquate Möglichkeit darstellt, um die Flexibilität des Scheibentauchkörperverfahrens darstellen zu können und dementsprechend eine Optimierung der Technologie zu erreichen.

Abstract

The rotating biological contactor process offers the specific advantages of a biofilm system in treatment of wastewater for removal of soluble organic substances and nitrogen compounds. It is a unique adaptation of the moving-medium biofilm system which facilitates easy and effective oxygen transfer. Media in the form of several large flat or corrugated discs with biofilm attached to the surface is mounted on a common shaft partially submerged in the wastewater and rotated through contoured tanks in which wastewater flows on a continuous basis. The compactness of the system and its economical operation makes it a viable option specially suited for decentralized wastewater treatment technologies. The process optimisation and adaptability under different environmental conditions and influent characteristics remain challenging tasks for the efficient use of this technology.

Mathematical modelling helps to predict the system performance under various external conditions. However, satisfactory mathematical representation is still lacking due to the dynamic nature of the system. In this work, it has been attempted to frame mathematical models for the process in simple and realistic ways. The models are based on the principles of one-dimensional mass transfer and transport of substances. Oxygen is accepted to be one of the most important and often limiting substrates in an aerobic treatment process. Modelling of the physical oxygen transfer through the water film developed on a rotating disc revealed that the oxygen transfer coefficient varies with the rotational speed and the location on the exposed disc surface. Increase of ambient temperature resulted in decrease of the oxygen mass transfer rate. The biofilm model was implemented for a three stage rotating biological contactor based on a laboratory-scale experimental set-up. The process kinetics was adopted from the Activated Sludge Model No. 3 which represents a mixed-culture biomass environment. The model simulations were conducted in *Matlab* based on numerical solution of the differential equations by finite-difference methodology. The stiff nature of the solution algorithm necessitated the use of variable time step solver to achieve fast and steady results. The model was calibrated with the experimental data available at 25°C. With the increase of the substrate or hydraulic loading rate, the RBC shows increasing removal rates within an optimal range. The dissolved oxygen concentration in the bulk liquid was high enough to maintain an aerobic environment. Under high nutrient loading rate in stage-1, the penetration depth of oxygen ranged between 250 to 300µm. Anoxic conditions set in and resulted in some denitrification after this depth. At 25°C and

high substrate loading rate, the compact design with reduced interfacial area in stage-2 and stage-3 showed nearly complete removal of soluble organic substrate and ammonia. This indicates a potential cost saving measure with process optimization. The simulations showed that overall removal efficiency improves with temperature in the range from 10 to 32.5°C. Nitrification was more sensitive to temperature and proved to be the limiting factor in design of the system. Sensitivity analysis of the model was performed to study the significance of variation of system parameters which are usually taken as constant in RBC modeling. Flow recirculation improves nitrification in stage-1 although the overall removal efficiency does not get affected substantially. This establishes that RBCs incorporate the advantages of a plug-flow system to sustain load surges and provide high efficiency without requirement of flow recirculation. The model also indicates that suitable process adaptations with variation of submergence ratio in different stages as well as flow recirculation are possible in a RBC system for enhanced denitrification or other specific requirements. In essence, the model helps to explore the flexibilities within a RBC system and optimise the process design accordingly.

Acknowledgements

This dissertation would not have been possible without the encouragement and active support of a number of people to whom I would like to offer my sincere thanks.

I would like to convey my sincere thanks to Professor Hermann H. Hahn for supervising my studies for the past three years. He had been my professor during the time of my Master's thesis under DAAD program as well. I would like to express my sincere gratitude and profound regards to him for having me as a Ph.D. student in his institute. Without his help, broad-mindedness and incessant support I could not have laid the foundation of my Ph.D. work. Being under the umbrella of his knowledge and guidance, I have been sheltered from many problems which might have affected my work otherwise.

I would like to acknowledge Dr. Ulrike Schaub, Director of the IPSWaT programme under BMBF, for honouring me with a scholarship. The financial support gave me an opportunity to come to Germany and broaden the horizons of my knowledge. It changed my future aspirations and helped me to pursue my dreams in the field of research.

Right from the nascent stages of my student career in this institute, it was my supervisor and guide, Prof. Erhard Hoffmann who kept me motivated and steered me out of all the stumbling blocks on the way. He gave me a free hand in my work and at the same time guided me at all times. I would like to thank him most sincerely for his help, advice and competent guidance.

I would like to offer my sincere thanks to Professor Josef Winter for agreeing to be my co-referee and willing to review my work. Attending his lectures during the course of my PhD. programme helped me to develop better insight into the biological treatment processes which were essential to develop the model. Without his help I could not have accomplished this task.

My special thanks go to Prof. Willi Gujer, EAWAG, Dübendorf, Switzerland for reviewing my dissertation work. It has been a great help to improve the quality of my work with his comments. The roots of my current work on mathematical modelling and simulation are embedded in the pioneering contributions made by him to this field. My visit to his institute in August 2005 and the meeting with him, Dr. Oscar Wanner and Prof. H. Siegrist helped me develop a better insight of the model. I am thankful to all of them for the valuable time they had spent on me. I would also like to acknowledge the help and guidance extended to me from time to time by Prof. Eberhard Morgenroth, University of Illinois at Urbana Champaign, USA.

Standing at the threshold of my dissertation work, I feel truly indebted to my friend and guide, Dr. Imre Takacs, Envirosim Inc., Canada for his relentless support, encouragement and motivation. His knowledge and constant guidance has been a stepping stone which helped me from the basics of understanding a biofilm model to the making of the mathematical model. Although we were continents apart, our co-ordinated efforts, discussions and regular exchange of mail helped me ride a smooth journey. I thank him wholeheartedly for all the co-operation extended to me especially during the critical stages of my work.

My friends and colleagues in this institute have helped and encouraged me in many different ways and I thank them all for the wonderful times I spent here. Mr. Andreas Blank has been the key person to provide me with the experimental data and help me with the model structure. Without his help and back-up, it would have been very difficult to make constant progress in my work. Dr. Martin Schwarz has helped me to frame the dissertation write-up and guided me with his valuable suggestions from time to time. I would like to sincerely thank Ms. Katja Friedrich, Mr. Robertino Turkovic, Mr. Tobias Morck and all others of my institute for their help and encouragement during my stay here. My special thanks go to Mrs. Christiana Nollert and her husband Mr. Kurt Nollert who has always been a friend in need. They have helped me and my family in innumerable ways. I would like to highlight and acknowledge the pivotal help received from Mrs. Kay Dittner of Resources Engineering at key times. Her congenial and helpful attitude made my stay in Germany pleasant and memorable. Mrs. Ruth Petters-Raskob, librarian from IWG has helped me and my family in many different ways and I would like to thank her earnestly.

I am thankful to my friend Dr. Laltu Chandra who had helped me with the basics of programming in Matlab and had given me a platform to start with. From a personal standpoint, I would like to thank my neighbour Mrs. Heidi Graf who has been a part of our day to day family life. She provided great strength and stood by us with compassion and kindness at all times during our stay over here.

In the end, I would like to thank my parents and family for being the source of constant support and inspiration. Last but not the least, I thank my wife Mrs. Pubali Dutta who has stood by me and walked hand in hand during the entire journey and supported me in every way. She has been the greatest critic of my work and at the same time provided me with moral support and strength at every step. I thank her especially for taking care of our daughter during the entire period of my research work here. Without her support, it would have been impossible to complete this dissertation work.

List of contents

List of tables

List of figures

List of symbols

Physical oxygen transfer model

K_L	Physical oxygen mass transfer coefficient from air to film [LT^{-1}]
δ	Thickness of the liquid film boundary layer over exposed disc surface[L]
t	Time [T]
x	Space coordinate from liquid film surface (x = 0) [L]
D	Diffusivity coefficient of oxygen in liquid film i.e. water [L^2T^{-1}]
C	Concentration of dissolved oxygen in the liquid film [ML^{-3}]
C_0	Initial concentration of oxygen in liquid film [ML^{-3}]
C_S	Saturation concentration of oxygen in air [ML^{-3}]
C_t	Concentration of oxygen in liquid film after time t [ML^{-3}]
N_t	Oxygen flux through the boundary layer [$ML^{-2}T^{-1}$]
t_R	Time of exposure of the liquid film in air [T]
$\overline{t_R}$	Average time of exposure of the liquid film in air [T]
$\overline{N_t}$	Time averaged flux of oxygen into liquid film over time interval t_R [$ML^{-2}T^{-1}$]
R	Radius of disc [L]
H	Distance between water surface and centre of the shaft [L]
I	Immersion factor, $\frac{R-H}{R}$
d	Diameter of the disc, i.e. 2R [L]
υ	Kinematic viscosity of liquid [L^2T^{-1}]
ω	Rotational speed in revolutions per minute [rpm]
n	Rotational speed [T^{-1}]
η	Dynamic viscosity of water [$ML^{-1}T^{-1}$]
v	Velocity of withdrawal of a flat plate from liquid [LT^{-1}]
ρ	Density of water [ML^{-3}]
g	Acceleration due to gravity [LT^{-2}]
v_C	Vertical component of the peripheral velocity v at the point of emergence of disc from the liquid surface in the trough [LT^{-1}]
δ_b	Average submerged boundary layer thickness [L]

K_L'	Oxygen transfer coefficient in the submerged boundary layer [LT^{-1}]
S_C	Schmidt number, v/D
Re	Reynolds number, vx/ν_C
r	Radial distance of any point on the disc from the shaft centre [L]
ϕ	Angle subtended for a distinct depth of immersion as shown in Figure 18 [rad]
$K_L a$	Volumetric oxygen transfer coefficient [T^{-1}]
a	Specific surface area of exchange, A/V [L^{-1}]
A	Interfacial surface area of exchange [L^2]
V	Control volume of the physical medium [L^3]
ϕ_{H_2O}	Association factor for the solvent (water)
T	Temperature [°C/°K]

Biofilm model

μ	Growth rate of a bacterial cell [T^{-1}]
μ_{max}	Maximum growth rate of bacterial cell [T^{-1}]
k_d	Decay rate of bacterial cell [T^{-1}]
P	1-D property such as substrate concentration or biomass density [ML^{-3}]
N	1-D property flux or the amount of property transported per unit time [$ML^{-2}T^{-1}$]
R	Net property production rate [$ML^{-3}T^{-1}$]
x	Spatial coordinate representing the depth of the biofilm from the sub-stratum [L]
X_j	Density of the biomass species j [ML^{-3}]
S_i	Concentration of substrate i affecting the growth of biomass species j [ML^{-3}]
i	Substrates: organic carbon (S_S), ammonia-nitrogen (S_{NH}), nitrate-nitrogen (S_{NO}), alkalinity (S_{ALK}), oxygen (S_O)
j	Particulate species: heterotrophs (X_H), autotrophs (X_A), inerts (X_I), suspended solids (X_S)
μ_{obs}	Observed growth rate of a species [T^{-1}]
$Y_{j,max}$	Maximum yield of biomass species j [-]
$R_{X_S,V}$	Rate of hydrolysis of the suspended solids X_S [$ML^{-3}T^{-1}$]
k_h	Specific hydrolysis rate constant [T^{-1}]

$R_{X_j end,V}$	Rate of endogenous resp. of bacteria species X_j under aerobic conditions [$ML^{-3}T^{-1}$]
$R'_{X_j end,V}$	Rate of endogenous resp. of bacterial species X_j under anoxic conditions [$ML^{-3}T^{-1}$]
$k_{X_j end}$	Specific endogenous resp. rate constants of X_j under aerobic conditions [T^{-1}]
$k'_{X_j end}$	Specific endogenous resp. rate constants of X_j under aerobic conditions [T^{-1}]
R_{S_i}	Rate of transformation of soluble substrate i per unit volume of biofilm [$ML^{-3}T^{-1}$]
A	Total interfacial area of the disc [L^2]
A_{sub}	Submerged area of the disc into the bulk liquid [L^2]
$A_{\exp}$	Exposed area of the disc in air [L^2]
δ_{Bf}	Total thickness of the biofilm [L]
N_{S_i}	Flux of soluble component i due to molecular diffusion within biofilm [$ML^{-2}T^{-1}$]
S_i^{Bf}	Concentration of the soluble component i within the biofilm [ML^{-3}]
D_{S_i}	Effective diffusivity coefficient of the soluble component i within biofilm [L^2T^{-1}]
D_O	Effective diffusivity coefficient of the oxygen within biofilm [L^2T^{-1}]
K_{S_i}	Mass transfer coeff. of substrate S_i at the liquid film - biofilm interface [LT^{-1}]
V_{Lf}	Average volume of the liquid film, i.e. $\delta_{Lf}.A$ [L^3]
δ_{Lf}	Average thickness of the liquid film over the whole disc area [L]
S_i^T	Concentration of substrate i in tank (bulk) [ML^{-3}]
S_i^{Lf}	Concentration of substrate i in liquid film [ML^{-3}]
$S_i^{Bf}\Big\vert_{x=\delta_{Bf}}$	Concentration of substrate i at the biofilm surface [ML^{-3}]
$S_{O_2}^{Lf}$	Dissolved oxygen concentration in the liquid film [ML^{-3}]
$S_{O_2}^{T}$	Dissolved oxygen concentration in tank [ML^{-3}]
$S_{O_2}^{Bf}\Big\vert_{x=\delta_{Bf}}$	Dissolved oxygen concentration at the biofilm surface [ML^{-3}]
$S_{O_2}^{*}$	Equilibrium concentration of oxygen in the bulk at a given temperature [ML^{-3}]
K_L	Average oxygen transfer coefficient in the liquid film [LT^{-1}]
K_{S_i}	Average mass transfer coefficient of substrate S_i in the liquid film [LT^{-1}]
K_1a	Oxygen transfer coefficient of the air drive unit [T^{-1}]
V_T	Tank volume [L^3]
Q	Volumetric flow rate through the tank [L^3T^{-1}]
Q_r	Recycle flow rate to the tank [L^3T^{-1}]
$S_i^{T\,ini}$	Initial concentration of soluble substrate i in the tank [ML^{-3}]
$S_{O_2}^{T\,ini}$	Initial concentration of oxygen in the tank [ML^{-3}]
$R_{S_i}^T$	Reaction rate of soluble substrate i in tank [$ML^{-3}T^{-1}$]

X_j^{Bf}	Concentration of particulate species j within the biofilm in terms of COD [ML^{-3}]
R_{X_j}	Rate of production of particulate species j within the biofilm [$ML^{-3}T^{-1}$]
N_{X_j}	Flux of particulate species j within the biofilm [$ML^{-2}T^{-1}$]
u	Advective velocity of displacement of the particulate species j [LT^{-1}]
D_{X_j}	Effective diffusive coefficient of particulate species j [L^2T^{-1}]
ρ	Density of the biofilm in units of COD, i.e. sum of concentrations of all particulate species within the biofilm [ML^{-3}]
$N_{att,j}$	Attachment flux of the particulate species j [$ML^{-2}T^{-1}$]
$k_{att,j}$	Attachment rate coefficient of the particulate species j [LT^{-1}]
u_{att}	Attachment velocity at the biofilm surface [LT^{-1}]
X_j^T	Concentration of particulate species j in the bulk liquid [ML^{-3}]
$N_{\det,j}$	Detachment flux of particulate species j [$ML^{-2}T^{-1}$]
$k_{\det,j}$	Detachment rate coeff. of X_j in case of linear biomass loss [T^{-1}]
$k'_{\det,j}$	Detachment rate coeff. of the X_j in case of exponential biomass loss [$L^{-1}T^{-1}$]
$k''_{\det}$	Detachment coefficient which can be any decimal fraction [-]
$u_{\det}$	Detachment velocity at the biofilm surface [LT^{-1}]
$R_{X_j}^T$	Reaction rate of particulate species j in the tank [$ML^{-3}T^{-1}$]
V_{Bf}	Average volume of the biofilm on disc surface [L^3]
$T1$	First stage tank
Tr	Tank stage from where the recycle flow is initiated
N	Number of layers considered for spatial discretization of biofilm in simulation
ε_l	Liquid phase volume fraction [-]
ε_{S_j}	Solid phase volume fraction of particulate species j [-]

List of abbreviations

1D	One-dimensional
3D	Three-dimensional
AOM	Ammonia oxidizing micro-organisms
ASM	Activated Sludge Model
ASP	Activated Sludge Process
Aut	Autotrophs
BOD_5	Biochemical oxygen demand (5 day)
CLSM	Confocal laser scanning microscope
COD	Chemical oxygen demand
DO	Dissolved oxygen
eps	Extra cellular polymeric substances
HCO_3^-	Bicarbonate alkalinity
Het	Heterotrophs
MCB	Mixed culture biofilm
NH_4-N	Ammonium nitrogen
NO_2-N	Nitrite-nitrogen
NO_3-N	Nitrate-nitrogen
NOM	Nitrite oxidizing micro-organisms
ode	Ordinary differential equation
pde	Partial differential equation
RBC	Rotating biological contactor
rpm	rotations per minute
TSS	Total suspended solids
VSS	Volatile suspended solids

1 Introduction

The implementation of suitable methods for the disposal of wastewater dates back to the times of Roman civilisation. However, it was only in the later part of the 19th century that a spurt of activity in the realm of wastewater treatment took place. The growth of the human population, urbanisation and industrialisation necessitated the treatment of wastewater. It became evident that the untreated wastewater which was discharged directly into water bodies caused pollution and posed health hazards. In case of streams and rivers, the pollution load was high in the immediate neighbourhood downstream of the disposal point. Growing industrialisation added to the pollution burden on nature and sometimes exceeded the self purification capacity of the flowing water bodies. The link between disease and untreated wastewater appears to be first made in Europe in the middle of the 19th Century. The first instance happened in 1854 in London when a community well contaminated by sewage from a nearby residence cess pit was identified as a source of a major cholera outbreak which led to numerous deaths. But it was not until 1892 that the German scientist Robert Koch identified the bacteria which cause cholera and the link between contaminated water and this deadly disease was confirmed. All these developments initiated the search for suitable means of wastewater treatment. A lot of research followed in the late 19th century and led to the development of the biological treatment process using aerated suspended biomass, known as activated sludge process (ASP). This was adapted for large-scale treatment applications and involved separate aeration and recirculation mechanisms. In 1923, Los Angeles became one of the first big cities to use an activated sludge process in its wastewater treatment plant.

However, the advent of fixed biofilm systems as a secondary wastewater treatment process seems to precede the use of ASP process. The instance came with first full-scale operation of trickling filters in early 1880s in Wales (Lazarova & Manem 2000). But the application of biofilm systems was limited till the middle of 20th century. It increased after new biofilm media material and reactor configurations were developed (Rodgers et al. 2003). The attached growth biofilm systems rendered several advantages over the suspended growth biomass systems. The specific advantages vary with the type of biofilm system and reactor configuration. In general, a biofilm system offers the following advantages (Tchobanoglous 1995):

- High biomass packing density and reactor compactness due to a large specific surface area

- Short contact periods and co-habitation of aerobic and anoxic micro-organisms within the same ecosystem
- Reduced sludge bulking and better sludge thickening qualities
- Lower sensitivity and better recovery from shock loadings
- Low energy requirements and more economy in operation and maintenance
- Low sludge production and superior process control
- Simple in operation and maintenance

Over the years, the treatment of wastewater using biofilm technologies has been established to be an efficient and proven technology with relatively stable end-products. They offer an ideal alternative, mainly as a secondary or tertiary biological treatment unit for the simultaneous removal of organic substances, nitrogen and other nutrients in municipal wastewater (Müller et al. 1980, Masuda et al. 1990, Boller et al. 1990). The first two authors studied secondary biological treatment systems while Boller et al. (1990) studied specifically biofilm affected nitrification in tertiary treatment systems. The most specific advantage of a biofilm system is the coexistence of aerobic, anoxic and sometimes anaerobic environment in a single composite system, facilitating different removal regimes, such as carbon oxidation, nitrification and denitrification. They offer a greater flexibility and can be suitably modified by changing the boundary environment in order to achieve a specific nutrient removal processes, such as the P-elimination in a Sequencing Batch Biofilm Reactor (Dutta 2002).

Biofilm systems may be broadly divided into two categories: fixed-medium systems and moving-medium systems. In the former system, the biofilm media is static in the reactor and the biochemical reactions occur in the biofilm developed on the static surface. Trickling filters and biological aerated filters are examples of such systems. In moving-medium systems, the biofilm media is continuously moving by means of mechanical, hydraulic or pneumatic forces. Examples of such systems include rotating biological contactors, moving-bed biofilm reactors and fluidised bed biofilm reactors. The major advantages of the moving-medium systems are:

- Prevention or better control of biological clogging, which is rather common in biofilters
- Hydraulic film diffusion facilitates an easy transport of substrate from the bulk liquid into the biofilm through the boundary layer

The latter is also true in fixed-medium biofilm systems. Biological clogging is controlled in moving-medium systems due to the higher detachment rate as a consequence of the

generation of hydraulic shear forces. Trulear et al. (1982) observed that the biofilm detachment rate increased with the rotational speed in a rotating annular reactor. Therefore, it is apparent that moving-medium systems provide an edge over other systems although the scale of operation and the economy are big factors affecting the selection of a suitable treatment process. In fact, these systems offer one of the most efficient wastewater treatment processes with potential for a widespread application (Rodgers et al. 2003).

The rotating biological contactor (RBC) is a unique adaptation of the moving-medium attached growth biofilm system which offers an alternative technology to the conventional ASP treatment process. Media in the form of several large flat or corrugated discs with biofilm attached to the surface are mounted on a common shaft partially submerged in the wastewater and rotated through contoured tanks in which the wastewater flows on a continuous basis. RBC systems offer a typical specific surface area of the order of 150-250 m^2/m^3 of liquid. The principal advantage of the RBC system stems from its high oxygen transfer efficiency which provides greater economy in the long run compared to other processes employing surface aerators or diffusers. It is operationally very economical and efficient at low power consumption values. Though RBC systems are inclined to be sensitive to temperature, and involve capital costs initially, they have proved to be very efficient systems with excellent sludge quality and low sludge volume index values in the secondary clarifier (Antonio et al. 1974). Properly designed RBCs provide other specific advantages such as high capacity to withstand fluctuations arising in the wastewater characteristics and substrate concentrations and to dampen shock loadings (Tchobanoglous 1995). Estimations reveal that RBCs require about 40-50% of the energy requirements of an activated sludge system (Droste 1997) and 70-80% of a Trickling filter system (Rodgers et al. 2003).

The first instance of the use of RBC as a biofilm remediation technology is documented in 1928 (Winkler 1981). The availability of polystyrene marked the beginning of commercial application of RBCs with the first full-scale RBC being installed in Germany in 1958. There are several different designs available today world-wide depending upon specific requirement criteria. More than 16% of all wastewater treatment plants in Switzerland and nearly 31% of the small treatment units with a capacity of the equivalent of a population of 5000 are RBCs (Boller et al. 1990). Today, the increasing complexity and inadequate efficiency in operation and maintenance of large and sometimes mammoth sized wastewater treatment plants based on ASP process has paved the way towards the concept of small wastewater treatment plants (decentralized wastewater technologies). The increasing

demand for such small and medium sized plants for urban or sub-urban habitations created the need for alternative processes which are required to be equally effective and more economical. The RBC concept fits in ideally in such cases. Trickling filters have also proven to be an effective biofilm treatment system but the disadvantage is their complexity in operation and requirement of proper recirculation (Fruhen 1997). Apart from the easy and effective oxygen transfer in RBCs, the compact design with separate compartments provides the advantages of a plug-flow system to sustain load surges and provide high efficiency without the requirement of flow recirculation.

1.1 Basis of mathematical modelling

Process optimisation and adaptability under different environmental conditions and influent characteristics remain challenging tasks in the design of any wastewater system like RBCs. Apart from the experimental methods to study and observe the system behaviour under different physical and biological conditions, mathematical modelling can help to predict the system performance under various external conditions. Models save money and time and once calibrated properly can help to provide sensitivity analysis with ease. Models can be broadly classified into two categories depending upon their structure. The first category represents the family of empirical models based on empirical formulations of the processes which cannot be fully understood. They rely on the fitting of statistical data and symbolise a top to bottom approach. The other category is the mechanistic models based on the numerical solution of partial differential equations defining the physical phenomena occurring in the real system. The latter category defines a bottom to top approach and is based on the first principle, i.e. implementation of the fundamental laws of natural sciences. These include the use of physical, chemical and biological processes and principles to define a system. Mechanistic models are superior in nature due to their firm base and robust and realistic outlook. However, they are often limited by the poor understanding of the phenomena occurring in reality and are based on simplified assumptions. The modern biofilm models rely on a combination of both of the approaches although the purpose of the model often defines the complexity level.

Models can be used either as an interesting research tool or as a practical engineering tool. The aim of the latter kind is to describe the dynamics of a real plant in the best possible way. Its response to influent variations or process changes is of main importance. Models also help in designing reactors. In this application, they are used to predict full-scale operation after evaluating pilot plant data. It may be noted that besides the general belief

that models are merely interesting research tools, modelling should be considered as an inherent part of engineering design and operation of a wastewater treatment system. In the most fundamental approach, the engineer reduces the complex physical system into a conceptual image of how it functions. In order to overcome the limitation of inadequate knowledge of many processes occurring in nature, biofilm modellers have over the years tried to incorporate complex empirical expressions into the mechanistic model. This tendency of including almost all processes envisaged to be occurring in reality has its advantages and disadvantages. Although complex models are ideal as a research tool, they often require a lot of computational effort and time in solving processes which are not fully understood. This factor often leads to simulation times which are too long to permit practical application of the model as a design and engineering tool and for process optimisation.

Therefore, the level of complexity in models intended for engineering usage is desired to be kept medium to low depending upon the level of accuracy to be maintained for practical purposes. It is true that a very simple model will not be able to describe all the dynamics of the system precisely because of its simplifications. But at the same time, it does not call to justify and include all those processes which are very complex in nature and cannot be measured experimentally on a laboratory-scale or a pilot-scale biofilm treatment plant (Vanhooren 2002).

The aim of the current dissertation work has been to build and test simple and realistic mathematical models for studying the dynamic processes occurring in an RBC system. The physical oxygen transfer model (chapter 5) helps to identify the characteristics of oxygen transfer in a rotating disc system. The biofilm model (chapter 6) is concerned with the biological treatment of wastewater in a RBC system under variations of feed concentrations and the ambient conditions. It is calibrated on experiments at a laboratory-scale as described in chapter 4. The results obtained from the simulation runs using the biofilm model are summarised in chapter 7. Chapter 8 discusses and reviews the results obtained from the physical oxygen transfer model and the biofilm model. Chapter 9 summarizes the work with conclusions and future recommendations. The models are intended to be robust and provide fast simulations while being moderately accurate at the same time.

2 Aim of dissertation

The inherent advantages of having a RBC biofilm system in municipal wastewater treatment have been discussed in chapter 1. The economic advantage and compactness of the system compared to conventional treatment processes such as activated sludge plants make it a favourable choice especially suited to the concept of decentralized wastewater treatment systems (Patwardhan 2003). Their only big disadvantage is the limitation in size (maximum capacity ~ 50,000 population equivalents, maximum disc diameter ~ 3.50 m) but this is compromised by the savings in cost of operation and maintenance as well as the removal efficiency under varied loading conditions. Although a lot of research has been done on biofilm systems and their modelling, not much research has been aimed towards the behaviour of RBC systems under different physical conditions such as temperature variations, usage of flat plastic discs as media support and effect on removal efficiency with reduction of the number of RBC stages from the conventional four to three stages. Although experimental observations are important for verification, a mathematical model based on the experimental structure is equally important to analyse and optimise the process under the different conditions. The physical factors affecting the aerobic treatment process such as oxygen transfer rate and temperature can be easily studied with the help of numerical modelling.

Rodgers et al. (2003) mentioned that it is very difficult to model the RBC process because of the complication of the system regarding aeration, nutrient and oxygen mass transfer, biofilm growth and detachment and the participation of suspended biomass in the treatment process. Of course a whole range of commercial biofilm models is available today, ranging from relatively simple one-dimensional models to comprehensive three dimensional descriptions of the biofilm structure in time and space. The first models focussed on the one-dimensional solution to mass transport in the biofilm (Müller et al. 1980, Trulear et al. 1982, Kissel et al. 1984, Wanner et al. 1986). More complex models included equations describing the microbial species growth and distribution in a biofilm in all the three spatial dimensions with time (Picioreanu, 1999).

Each model has its value and specific application. The complexity of the model should normally be relevant to the intended purpose and possible application. It has not been the aim of this work to compare or promote one or the other model or its complexity. The principal goal is to apply the fundamental concepts underlying the system and develop an efficient modelling tool which can predict the system performance steadily and effectively. It is essential to formulate the interdependency between substrate transport and solids displacement inside the biofilm matrix as well as surface processes such as attachment and detachment of biomass. At the same time, the model needs to be suitably customised to take into account the dynamic boundary conditions of the

RBC system. In addition to the requirement of being a robust prediction tool, the required computational time is also an important factor in choosing the level of complexity. Many of the complex 3D models are often slow unless suitable compromises have been made in obtaining solutions to the partial differential equations for the slow and fast dynamics simultaneously. These models are commercially available as packages and sometimes require dedicated hardware because they are computationally intensive in nature. In most cases, where the principal aim is to study biofilm growth and population dynamics at the individual cell level (e.g. 3D models), the compromise is made by using an analytical solution to the substrate profiles in the biofilm. In many cases, the biological transformation processes are too simplified in order to study slow processes such as biofilm growth, attachment and detachment. Although the high-end models clearly have the advantage of including a lot of the available knowledge about biofilm processes, the high complexity of the model also increases the number of unknown parameters and the possible dependencies between them (Noguera et al. 2004). These factors make the accurate estimation of parameter values very difficult. Moreover, even for very sophisticated models, many biofilm processes like attachment and detachment of solids, particulate diffusive transport, the influence of higher organisms etc. are still poorly understood and estimated using empirical formulae which seem to be crude approximations of reality.

The dissertation work was carried out in 3 phases:

a) Physical model of oxygen transfer for identification and determination of the factors affecting the oxygen transfer in rotating disc systems
b) Development of the 1D mixed-culture biofilm (MCB) model for a single stage RBC
c) Extension of the MCB model from single to three stages based on the experimental set-up

Previously, a mathematical model for RBC had been described by Gujer et al. (1990). The use of the model as a design tool was restricted due to inadequacy in predicting the dynamic behaviour of the RBC operation (section 3.4 and 6.3.3) and limited computing capacity of personal computers considering the short-time response required in the simulation. The diffusive transport of the solids inside the biofilm matrix was not included in this model.

The current mixed-culture biofilm model has been developed based on one-dimensional solution to the governing processes. The functional aspects such as the layered structure of the biofilm, transport processes etc. stem from the RBC model of Gujer et al. (1990). Additionally, a new correlation which considers the effect of the dynamic boundary conditions in operation of a RBC has been included. The dynamic boundary condition relates to the transient oxygen transfer through the liquid boundary layer in RBC system due to the rotation of the disc. Further changes include the process kinetics and stoichiometry for the microbiological transformation reactions,

which have been adapted from the up-to-date Activated Sludge Model No. 3 (Gujer et al. 1999). The reaction rates have not only been incorporated for the biofilm layers but also for the bulk liquid in the reactor. Some other concepts such as particulate transport by diffusion have been based upon the universally accepted mixed-culture biofilm model of Wanner and Reichert (1995), although suitable complexity compromises had to be attempted in processes where not much is known or experimentally determinable. In effect, the model is easy to run, takes relatively less time and helps to estimate the parameters values easily. And despite its simplifications it can be used to describe processes occurring in different depths of the biofilm.

Results from laboratory-scale experiments have been used for the calibration of the model and validation of the model results where available. Many parameter values have been obtained from literature sources where experimental determination has not been possible. The parameter values at higher temperatures have been calculated using temperature functions and the results compared with laboratory-scale experiments where available. In essence, the model helps to give an insight into the dynamics of the RBC treatment process under different design conditions and ambient environment. It may be used as an efficient prediction tool to investigate the system performance under varying temperature conditions provided it is fine calibrated with kinetics parameters at each step. It can help in sensitivity studies and process optimisation.

The physical and the MCB model can be used to answer some of the typical questions that a wastewater engineer might like to ask:

- How does the oxygen transfer coefficient vary with temperature and liquid film thickness?
- Is it possible to achieve high performance efficiency by using three stages instead of the conventional four stage design at high loading rates?
- Where does substantial nitrification take place and how effective is the denitrification in RBC?
- How far is the oxygen diffusion limited inside the biofilm?
- What is the effect of temperature on removal efficiency?
- What is the optimum range of nutrient and hydraulic load that the RBC system can sustain?
- Does flow recirculation help to improve the system performance?
- How does a variation of the submergence ratio affect the system behaviour?
- How does the biofilm thickness vary with time?

Although some of the sensitivity investigations done with the MCB model could not be supported with experimental evidence, it has been attempted to compare the trend with data from literature wherever available. For higher numerical accuracy of model predictions, a model needs to be fine calibrated at each scale-up. The current model may also run with dynamic data sets as input.

3 Literature review

3.1 Background of biofilm research

Biofilms represent a complex assembly of surface-associated microbial cells that are in biocenosis in an extracellular polymeric substance matrix. Van Leeuwenhoek, using his simple microscopes, first observed microorganisms on tooth surfaces and can be credited with the discovery of microbial biofilms. Heukelekian and Heller (1940) noticed the "bottle effect" for marine microorganisms, i.e., bacterial growth and activity were substantially enhanced by the incorporation of a surface to which these organisms could attach. However, a detailed examination of biofilms would await the electron microscope, which allowed high-resolution microscopy at much higher magnifications than did the light microscope. Using scanning and transmission electron microscopy, Jones et al. (1969) studied biofilms on trickling filters in a wastewater treatment plant and showed them to be composed of a variety of organisms (based on cell morphology). Early in 1973, Characklis examined microbial slimes in industrial water systems and showed that they were not only very tenacious but also highly resistant to disinfectants such as chlorine. Since that time, the studies of biofilms in industrial settings and in systems concerned with public health such as municipal wastewater treatment have basically run parallel to each other. Much of the work in the last two decades has relied on tools such as scanning electron microscopy or standard microbiological culture techniques for biofilm characterization. Additionally, two major innovations in the last few years have dramatically impacted the understanding of biofilms, namely the utilization of the confocal laser scanning microscope (CLSM) to characterize biofilm microstructure, and an investigation of the genes involved in cell adhesion and biofilm formation.

Biofilms play an important role in natural as well as artificial systems. We often come across situations where conventional methods of killing bacteria using antibiotics and disinfectants are ineffective with biofilm bacteria. The huge doses of antimicrobials required to rid systems of biofilm bacteria are sometimes environmentally undesirable and medically impractical since what is required to kill the biofilm bacteria would also kill the patient. Conversely, on the brighter side, attached biofilm processes offer opportunities for positive industrial and environmental effects, such as municipal wastewater treatment, bioremediation of hazardous wastes, biofiltering of industrial water, and forming biobarriers to protect soil and groundwater from contamination. The technology using biofilms is

currently gaining renewed attention, especially in places were space is limited and loading rates are highly irregular. Fixed biofilm mechanisms have inherent advantages as a consequence of the high biomass packing density and compactness of the system. Increased urbanisation and stricter environmental regulations have necessitated augmentation as well as modernisation of existing wastewater treatment plants in densely populated area. However, due to physical and economic constraints, the extension is often a problem. Optimisation using biofilm systems come as a viable alternative approach which can be suitably amalgamated with the existing system or can be used as a separate system. Apart from the economic advantage, biofilm systems are moderately easy to control and maintain. They can survive shock loads and short toxic waste dosing because of the relatively short hydraulic retention time in the reactor. The shock usually affects the microbes at the biofilm surface and deeper layers normally remain unaffected (Grady and Lim 1980). The operation of biofilm plants is further simplified by the limited need for sludge sedimentation and sludge recirculation (Henze et. al 1995). In most systems, effluent recirculation can be omitted.

Biofilms find their use not only in sewage treatment, but also a range of other promising applications including detoxification of water containing hazardous organic chemicals and treatment of industrial wastewaters. The short hydraulic retention times and excellent biomass retention in biofilm reactors make them highly attractive when the compound to be treated are inhibitory or slowly degradable in nature (Jeppsson, 1996).

3.2 Composition and structure of the biofilm

Biofilms exhibit very dynamic behaviour in nature. In wastewater treatment, they comprise of a multitude of bacterial species, protozoa and metazoa, inorganic and organic inerts, extracellular polymeric substances (eps), pore water and interstitial water. The eps are composed of polysaccharides, proteins, uronic acids, lipids and DNA. Polysaccharides usually predominate with 65% of the eps, while proteins constitute 10-15% (Lazarova and Manem 1995). Activated sludge flocs are often considered as suspended biofilm particles without substratum, although there are a number of properties which differentiate biofilms from activated sludge flocs, the most significant of them being the density and transport mechanisms. Unlike activated sludge flocs, which are not so much affected by transport limitations, biofilm performance is largely affected by transport mechanisms. Interfacial transfer and transport by molecular diffusion remain the governing mechanism and often lead to stratification of biomass activity and bacterial species distribution (Lazarova et

al.1995). The outer layers comprise the active zone with densely populated aerobic species while the inner regions may be populated by different species, such as anoxic or anaerobic bacteria. Moreover, the same species may exhibit different behaviour under different local conditions. The transformation and displacement of the particulate species in the biofilm matrix occur as a consequence of a combination of biochemical processes and physical mechanisms. The substrate supply contributes to the transformation processes such as growth, decay and cellular maintenance mechanisms of the microbial species. The net effective growth or decay of the biomass generates density differences within different regions of the biofilm. This contributes to advective transport of the solids as a consequence

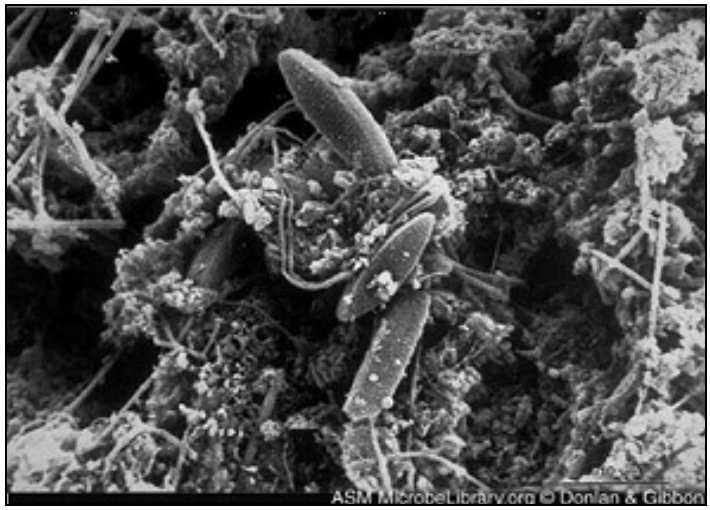

Figure 1 Scanning electron micrograph of a native biofilm developed on a mild steel surface in an eight week period in an industrial water system.
(Donlan, 2002)

of development of mass gradient. Surface reactions such as attachment of flocs and detachment of biomass at the biofilm surface may generate an additional diffusive transport flux which may further augment to the transport of solids within the biofilm matrix (Drury et al 1993). Figure 1 reveals a typical biofilm structure with solids and interspatial voids as revealed under scanning electron microscope.

3.2.1 Growth pattern of bacterial species in pure culture

Although there is a multitude of micro-organisms present in the biofilm, bacteria appear to be the primary species in biological removal. These uni-cellular micro-organisms reproduce by binary fission and can range in size from 0.5 µm to 5.0µm. The time required for each fission may vary from days to around 20min. Environmental conditions such as temperature and pH have important influence on survival and growth of these species. However, the general growth pattern of bacteria in pure culture under favourable conditions may be

represented as shown in Figure 2. The pattern shows four distinct time phases relative to the time scale:

- Lag phase: After the introduction of an inoculum to a culture medium, the lag phase represents the time required for the organisms to acclimatise into the new environment and start fission.
- Exponential growth phase: It represents rapid cellular division based on generation time. There is abundance of nutrient and a sustainable environment surrounding the bacterias and growth is a function of ability of the micro-organisms to process the substrate.
- Stationary phase: The organisms maintain steady-state, i.e. they remain stationary. The cells seem to have exhausted the substrate requirement for growth and new cells are offset by the death of old degenerating cells.
- Endogenous respiration and decay: During this phase, the cells undergo slow degeneration. They are forced to metabolise their own protoplasm without replacement because the available nutrient concentration is very less. With lysis, the nutrients remaining in dead cells may diffuse out while new cells constantly take their place for food.

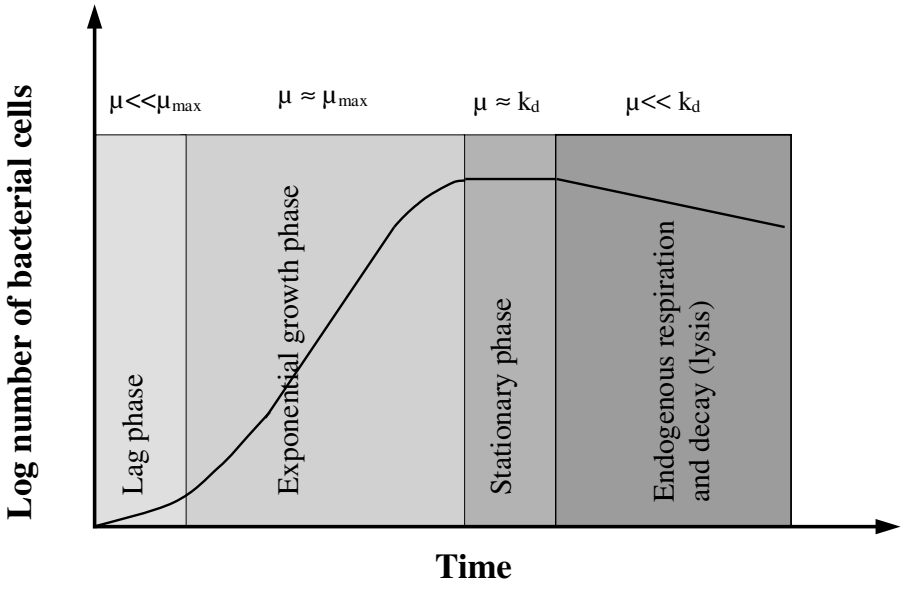

Figure 2 Typical bacterial growth and degeneration profile
(Tchobanoglous, 1995)

where

μ Growth rate of a bacterial cell [T^{-1}]

μ_{max} Maximum growth rate of bacterial cell [T^{-1}]

k_d Decay rate of bacterial cell [T^{-1}]

It is found that the endogenous respiration and decay rate of bacteria in a mixed-culture biofilm is comparatively lower than in activated sludge process and depend upon the supply of substrate and oxygen (parameter values in MCB model of Horn and Hempel 1997). Under starvation conditions, the micro-organisms degenerate faster in the ASP system compared to the biofilm system.

3.2.2 Growth in mixed culture biofilms

The behaviour and development of the microbial species in biocenosis inside a biofilm may be very different based on complex interaction among different species in competition for food and space. Each particular species in the system has its own growth curve. The position and shape of a particular growth curve on a time scale in the system depend upon the availability of specific nutrients and on local environmental conditions such as temperature, pH and whether the system is aerobic or anaerobic at that location. While bacteria are the main source of stabilisation of organic substances, there remain a vast multitude of other species such as fungi, protozoa, algae which help in wastewater treatment as well and often maintain symbiotic relationship with bacterias. The biofilm surface remains very dynamic due to the intrinsic as well as extrinsic activities taking place all the time. The suspended particulate flocs from the bulk may attach or reattach to the surface and get transported inside the matrix, while biofilm may shed bio-solids from the surface at a random rate due to regular wear and tear as well as combination of physical and biochemical forces such as surface turbulence, flow rate, influent quality, media roughness, biofilm age, ambient temperature and denitrification gases formed in the inner layers. Figure 3 gives a pictorial representation of the various processes taking place at the biofilm surface due to the attachment (1), growth (2) and detachment (3) of the solids at the surface. The early attachment of the active microbial flocs at the media surface occur due to a variety of reasons, e.g. surface roughness causing colonization and growth, production of eps.

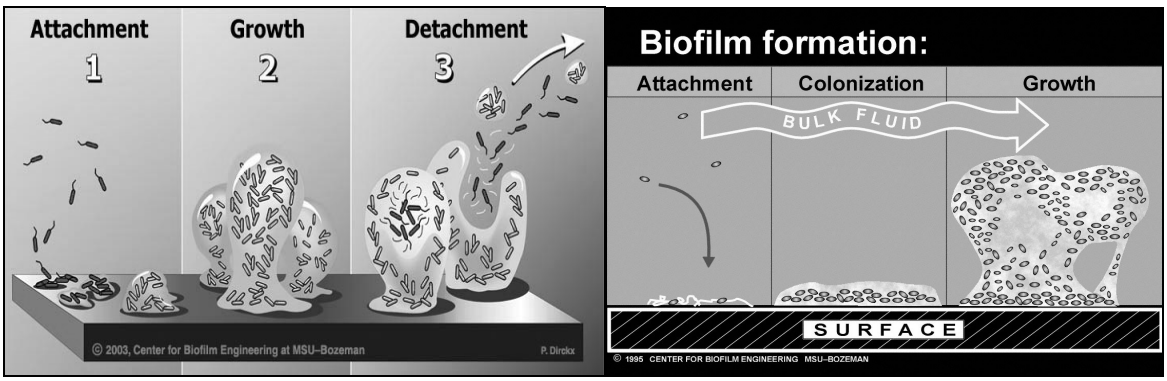

Figure 3 Development of biofilm over sub-stratum due to surface activities
(Source: Peg Dirckx, Center for Biofilm Engineering, Montana State University, USA)

3.3 Biofilm reactors in wastewater treatment

Different reactors have been developed to take advantage of the biofilm processes in wastewater treatment. The oldest is the traditional biofilter, introduced before the 20th century. It was initially used as screening device but later on it became clear that the mechanism of purification was not purely physical screening, but biological as well (Jeppsson, 1996). This led to the trickling filters where the biofilm grows over stone or plastic carrier material which acts as a media bed and the wastewater trickles down through this media bed. Few years later, at the turn of the century, RBCs were introduced using wood as solid media for the attachment of the biofilm (Arvin and Harremoës, 1990). The original patent of RBC was filed by A.T. Maltby in 1928 (Winkler 1981), The essential difference between the two aerobic systems is that in trickling filters, the media remain fixed in the reactor bed and the water flows over the biofilm exposed in air, while in RBCs, the media rotates through a nearly stagnant bulk water and air. Further development in biofilm technology led to usage of novelty processes like fluidised bed reactors, membrane reactors and moving bed biofilm carriers. However, many of these state-of-the-art biofilm treatment processes come with extra costs which need to be compensated with treatment efficiency. The criterion for selection of a suitable system is often a question of economy, quality of raw influent, desired treatment efficiency and availability of space. In some processes such as membrane filters, the capital costs may be very high, but the operational costs are minimal and it is often economical in the longer run. Each process has its own specific advantage and disadvantage and it remains for the designer and the users to choose a suitable treatment process based on specific requirements and economic factors. The main reactor types are briefly compared in Table 1 below.

Table 1 Typical properties of some biofilm reactors

Reactor	Specific surface area	Biofilm thickness	Hydraulic loading	Organic loading*	Conversion capacity
	m^3/m^2	mm	$m^3/(m^2 \cdot h)$		$kgO_2/m^3.d$
Trickling Filter	150	5.0-10.0	0.50-2.0	200-800 gBOD/(m^3.d)	1.50
RBC	200	1.0-4.0	0.7-3.8 +	5-20 gBOD/(m^2.d)	2.0
Submerged Filter	700	0.5-1.0	10.0-15.0	-	7.0
Fluidised Bed	2000	0.2	30.0	-	5.0

(Tijhuis et al. 1994, *Henze et al. 2002, +Table 2)

The comparative thickness of biofilm in different biofilm processes are illustrated in Figure 4. The thicknesses are only representative in nature for the purpose of comparison and exact thickness may vary depending upon system configuration and nutrient loading conditions. A thick biofilm doesnot necessarily result in a high nitrification rate. Adsorbed suspended matter and heterotrophs are mainly responsible for higher thickness in the first stage of RBC.

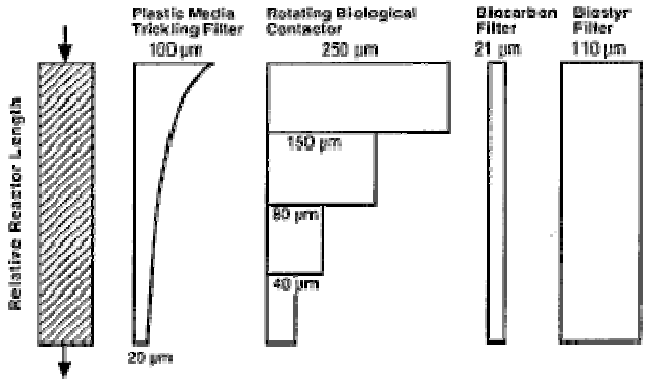

Figure 4 Distribution of biofilm thickness in different biofilm reactors
(Boller et al. 1994)

3.4 Features of a RBC system

As discussed in section 3.3 above, the selection of a suitable system is often influenced by performance efficiency at minimal cost. RBCs offer a low cost solution with high efficiency and inherent advantages. The most stand-alone feature is facilitating easy transfer of oxygen from air while enabling biofilm affected treatment simultaneously. Due to remarkably low energy consumption, efficient aeration of water due to rotation while simultaneously making efficient contact between biofilm and water, they offer an ideal choice as small wastewater treatment units under situations where space is limited (Henze et al. 2002). Oxygen remains as one of the most limiting substrates in biofilm treatment, and the deeper and faster the oxygen diffusion is inside the biofilm, the better the aerobic treatment. The advantages of this system are extremely low cost for mixing and high oxygen provision (Rodgers et al. 2003). The system is also less susceptible to fluctuating hydraulic loadings as compared to the trickling filters (Henk 2002). The typical sketch of an RBC disc in operation is shown in Figure 5. In its simplest form, an RBC unit consists of a series of closely placed discs that are mounted on a horizontal shaft and are partially submerged in wastewater. In other words, a part of the discs is immersed in the bulk liquid while the other part remains exposed in air. In some cases, the disc is completely submerged in bulk liquid to initiate anoxic conditions of treatment. The shaft is driven mechanically using an electric motor or pneumatically with compressed air drive so that the discs rotate perpendicular to

the flow of wastewater. The rotation helps to maintain oxygen diffusion through the air-liquid interface and enables aerobic biofilm growth and resultant nutrient removal. In practice, RBCs are preceded by a primary clarifier and succeeded by a secondary clarifier.

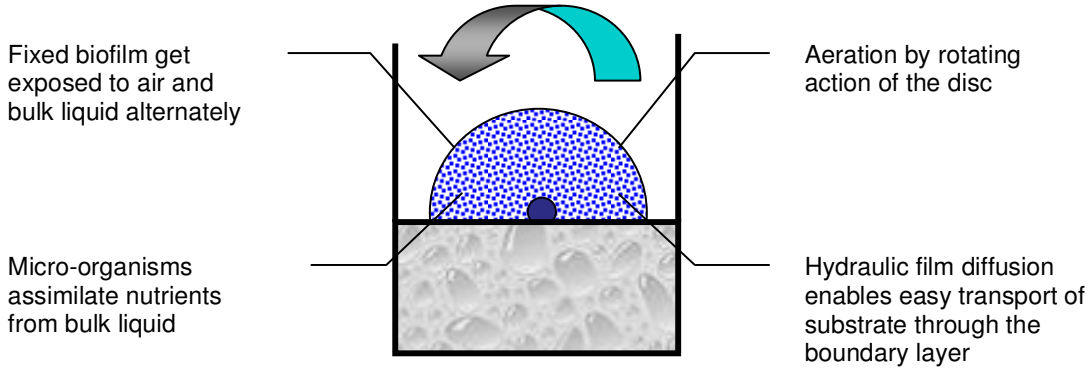

Figure 5 Sketch of RBC disc in operation

As stated, the wastewater previously undergoes primary treatment in settling tanks before entering into the RBC unit. The effluent from the RBC also requires a secondary clarifier to separate out the sludge from the treated wastewater. Figure 6 shows the schematic arrangement of a typical RBC treatment system. The repeated rotation of the disc media by the shaft not only supplies oxygen to the micro-organisms in the biofilm but also to the suspended biomass in the bulk liquid. The discs are usually made of plastic (polythylene, polyvinyl chloride or polystyrene) and are contained in a trough so that about 40% of their area is typically immersed in wastewater. They are arranged in groups or packs with baffles in between them to reduce surging or short-circuiting. Normally RBCs are designed and operated in a series of stages, ranging from three to four stages, separated by baffles. The purpose of staging is to make the RBC behave like a plug-flow system and eliminate short circuiting. Typically, the first stage always receives the highest organic loading and provides maximum organic removal efficiency. The latter stages are used for nitrification as well as residual organic carbon removal. After the fourth stage, improvement of organic removal is insignificant (Rodgers and Zhan 2003). When there is recycling of wastewater from the last tank to the first one, denitrification may be achieved in the first tank, where there is high organic loading (due to the influent) and low dissolved oxygen content. In specific set-ups like Figure 6(a), the rotational speed may be varied in each stage depending upon the oxygen requirement at that stage so as to optimise removal efficiency under given loading conditions and to enable variation of hydraulic shear forces to initiate detachment of biomass. This can help to control biofilm thickness.

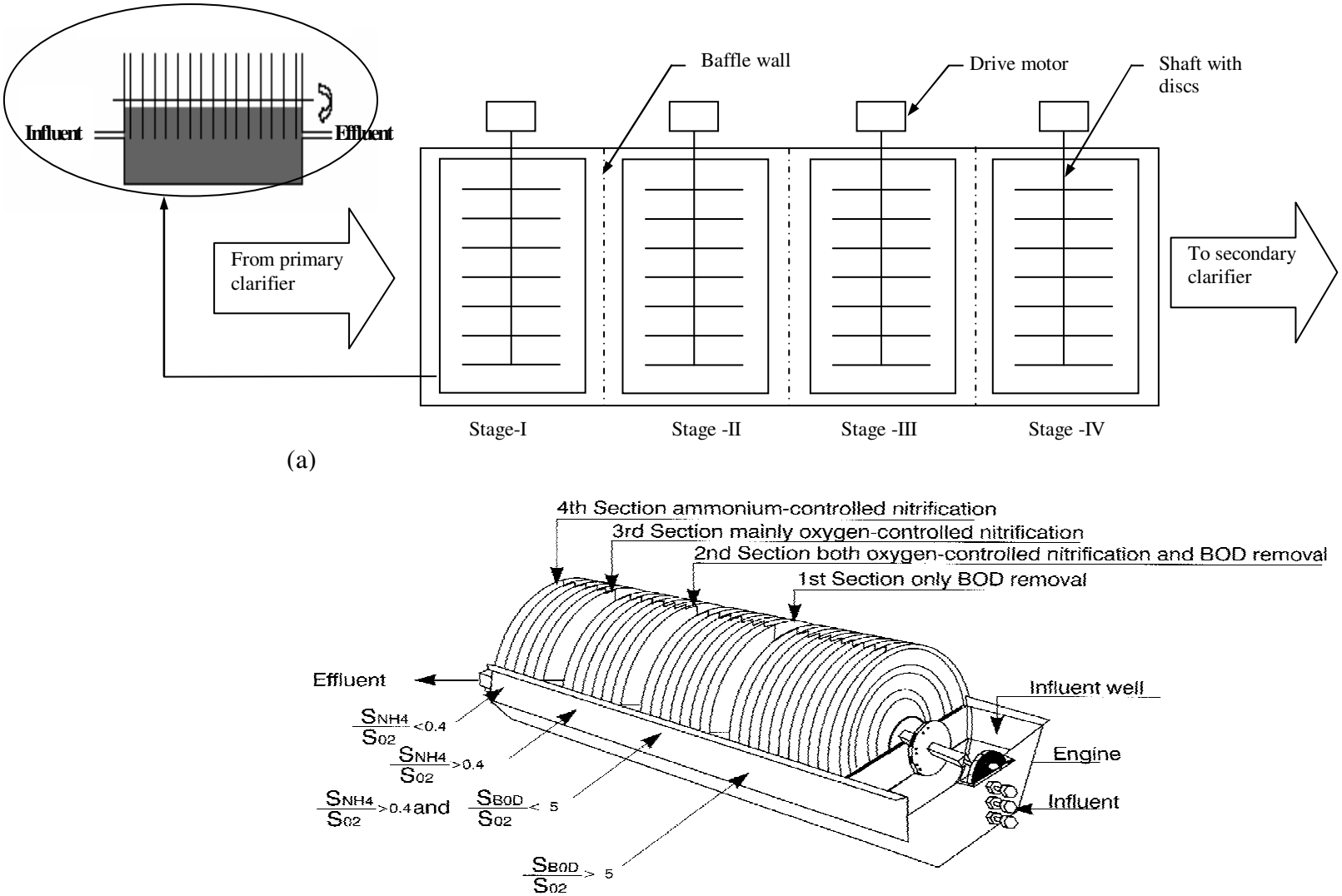

Figure 6 Typical arrangement of 4-stage RBC systems: (a) Flow perpendicular to shaft, view in plan, (b) Flow parallel to shaft
(Henze et al. 2002)

Normally the rotational speed cannot be made very high and there is disc size restriction. This checks high peripheral velocities, which may cause shearing off of the liquid film and consequently substrate limitations in the biofilm. To protect the biofilm from exposure to temperature extremities and heat loss and to prevent the growth of algae, RBC units are almost always covered. It is also important to protect the plastic discs from direct exposure to UV rays and weather. Discs may also be immersed up to 80-90% submergence, which provides less loading on the shafts due to buoyancy and larger media contact volume. This design is used especially suited for denitrification effects (Teixeira & Oliveira 2001). But for aerobic treatment of wastewater, deeper submergence of discs does not allow adequate aeration and dissolved oxygen levels in the liquid lower down. Consequently, additional aeration units need to be used to provide sufficient aeration and suspension of biomass in the trough. Fully submerged RBCs can be used for anaerobic mode of treatment (Lu et al. 1997). Overall performance of RBC systems for nutrient removal from wastewater depends upon several factors:

- Influent wastewater characteristics
  - hydraulic loading rate
  - organic loading rate
  - ammonium loading rate
  - pH
- System configuration
  - rotational speed
  - specific surface area of discs
  - disc submergence
  - number of stages
  - recirculation rate
  - drive mechanisms
  - shaft arrangement (common shaft with single rpm or separate shaft for each stage)
- oxygen transfer rate
- ambient and wastewater temperature
- media density

The most important physical factors affecting the overall removal efficiency of the system are oxygen mass transfer rate and temperature. Oxygen transfer rate is again dependent on operating temperature and physical set-up of the system. The thickness of the biofilm is controlled by the availability of nutrients and surface turbulence due to rotational speed.

However, during scale-up, it is the peripheral speed on the discs which is the governing factor in the growth of the biofilm and the resultant thickness. Usually the peripheral velocity at the rim of the disc needs to be below 20cms^{-1}.

Table 2 Design criteria for RBC units

Parameter	Treatment level			Units
	BOD removal	Combined nitrification	Post nitrification	
Hydraulic loading	0.08-0.16	0.03-0.08	0.04-0.10	$m^3/m^2.d$
Organic loading (avg)	5-10	2.5-8	0.5-1.0	g $SBOD_5/m^2.d$[a]
	8-20	4-16	1-2	g $TBOD_5/m^2.d$[b]
Maximum organic loading on 1st stage	12	12		g $SBOD_5/m^2.d$[a]
	24-30	24-30		g $TBOD_5/m^2.d$[b]
NH_4-N loading (avg)		0.75-1.5		g $N/m^2.d$
Hydraulic retention time	0.7-1.5	1.5-4	1.2-3.0	h

(Tchobanoglous et al. 2003) a $SBOD_5$ = Soluble BOD_5, b $TBOD_5$ = Total BOD_5

3.4.1 Process design and nutrient removal performance

3.4.1.1 Organic substrate removal

The critical hydraulic retention time for removal of carbonaceous substrate in RBCs is about 3-4 hours and studies have revealed that further increase in retention has little effect on improvement in performances. For a given system, as the applied loading rate increases, the removal efficiency decreases. Under normal operating conditions, carbonaceous substrate is mainly removed in initial stages of the RBC.

3.4.1.2 Nitrification

The oxidation of ammonia is an important feature in assessing the performance of a biological reactor. Heterotrophic bacterias offer strong competition to nitrifiers in the initial stages with high BOD concentrations. So the maximum nitrification rate occurs when the soluble BOD load reduces sufficiently. Studies suggest that full nitrification can only be achieved when the organic loading rate is less than 5gBOD/(m^2.day) (WEF and ASCE 1998). The recommended initial BOD_5 loading rate as per ATV-DVWK standard (2001) is 8-10g/(m^2.d). Therefore, nitrification always occurs prominently in the later stages of RBC set-up. The highest nitrification rate depends upon oxygen concentration in the boundary layer and dissolved oxygen concentration in the bulk liquid, which should not be oxygen

limited. Also concentration of ammoniacal Nitrogen should not go below 3-5 mg/l in the bulk liquid for best results.

3.4.1.3 Denitrification

The usage of RBC systems for denitrification is not very widespread. Laboratory scale studies indicate that for an influent NO_3-N concentration of 50mg/l, the maximum denitrification rate is 15.2gNO_3-N/m^2.day at a rotational speed of 2rpm (Teixeira & Oliveira 2001).

Typical design criteria for RBCs when the wastewater temperature exceeds 13°C are listed in Table 2. In case of liquid temperature going below 13°C, temperature correction factors need to be taken into account. These can be obtained from pilot studies and literature. In general, when the temperature drops from 13 to 5°C, nearly 2.5 times more media surface area is required for achieving the same performance (Rodgers and Zhan 2003).

3.4.2 RBC biofilm

A layer of biological growth, slimy in nature and about 1-3 mm in thickness is established on the surface of the disc. This biological slime that becomes attached to the disc surface assimilates the dissolved and suspended organic materials from the wastewater. Excess biomass is sheared off into the tank, while the rotating action of the discs maintains the solids in suspension. Eventually, the effluent carries these solids out of the system and into a secondary clarifier, where they are separated.

Structurally the composition of the biofilm is highly heterogeneous. It is made up of a matrix of microbial cell clusters and intermediate voids with spatial distribution of autotrophs, heterotrophs, other bacterial cells and protozoa. Microscopic studies reveal that the outer biofilm layer is more heterogeneous and complex. It is composed of filamentous bacteria, protozoa, eukaryotic algae and small metazoans. The inner layers are relatively more uniform and compact (Martin-Creceda et al. 2001). During the initial stages of RBC set-up for BOD removal, heterotrophs compete with autotrophs (nitrifying bacteria) in the outermost biofilm layers for oxygen and space. The bacterial population gets diminished in the inner biofilm layers, because it contains a major fraction of non viable bacteria compared to the outer layers (Rodgers and Zhan 2003). The active metabolic cell fraction reduced from 35 ± 13% in the outermost biofilm layer to 15 ± 4% in the innermost biofilm layer (Okabe et al. 1996). Filamentous mirco-organisms present in the biofilm such as Beggiatoa ssp. and Sphaerotilus natans often cause flotation problems and the sheared sludge refuses to settle (Galvan et al. 2000). Excess growth of Beggiatoa serves as a caution signal to the

performance of RBC units because the blooming of these sulphur oxidising bacterias prevents the sloughing of thick biofilm from the discs, which may result in overloading on the media supports (Surampalli and Baumann 1997).

Studies show that there are several means to control the biofilm thickness. These are increasing rotational speed, reversing the rotation-direction periodically to develop shear stresses in opposite direction, supplementary aeration for pre-oxidation of reduced-sulphur so that Beggiatoa growth is sulphur-limited, step feeding the influent and chemically stripping with alkali, chlorine and other chemicals. The most influential parameters controlling biofilm growth and decay are wastewater temperature, oxygen supply, organic and hydraulic loading rates.

3.4.3 Operational problems

Mechanical failures often occur in RBC units. The most common are shaft failures, bearing failures and media support structure failures. This may arise due to overloading conditions from high hydraulic loading rate, excess biofilm growth, microbially influenced corrosion, low frequency corrosion fatigue, improper greasing and inadequate locking of nuts and bolts (Mba et al.1999). If the RBC unit is not housed properly, the discs may get exposed to UV radiations and bad weather conditions in tropical climates, which can damage the disc material. Another problem associated with this is excess growth of algae which may clog the shaft and disc movement. So the RBC units need to be adequately covered.

3.5 Modelling of biofilm systems

Defining biofilm systems by way of mathematical modelling helps to understand how biofilms grow, what mechanisms play their role in the transport and transformation processes and how the system behaves under a given set of conditions. It helps to predict the degradation capacity and hence the treatment efficiency of the system and in optimisation of the system operation. The relative complex nature of biofilm modelling arises from the fact that there is not only the microbial conversion of substrates needed to be considered, but also the transport of nutrients and particulate species inside the biofilm. There has been considerable development in the field of mathematical models over the last 30 years. Early modelling approaches neglected the aspect of biomass growth and particulate transport and assumed a predefined biomass distribution with a fixed biofilm thickness (Williamson and McCarty 1976; Harremöes 1978; Müller et al. 1978, 1980). It was only in the mid-eighties that the particulates mass transfer aspect was taken into consideration. The pioneering works of Kissel et al. (1984) and Wanner and Gujer (1986) introduced a more generalised

description of the multi-cultural biofilms in space and time. It made possible to predict the microbial species development over the depth of biofilm as a function of the substrate flux and the attachment and detachment fluxes at the biofilm surface. Further developments in mathematical modelling were guided by experimental results. The displacement of particulate species in the matrix was assumed to be not only as a result of advective forces, but also diffusive forces (Wanner and Reichert 1996). The diffusive flux of particulates species depends upon surface reactions and external hydraulic forces causing bioturbulation. Recent advances in biofilm research reveal the heterogeneous matrix of the biofilm which challenged the continuum approach to biofilm modelling. The quantitative approach to describe this development has been attempted in the revised biofilm model of Wanner and Reichert 1996. However, such a detailed and complex mathematical description of the processes often increases the computational effort for solving the set of partial and ordinary differential equations (Rauch et al. 1999).

3.5.1 Basis of the mechanistic-deterministic biofilm model

In any mechanistic-deterministic mathematical model, the basic approach is to apply the conservation laws to properties such as mass, volume, energy and momentum for a system based on the system configuration and behaviour with time. The time based solution to the differential form of these conserved properties predicts the system behaviour. The system needs to be defined properly based on its physical as well as chemical-biological characteristics. In biofilm systems, the conservation of mass and volume remain the most governing aspects for the definition of system behaviour, at a given temperature. The difference in temperature and resultant energy transfer during the treatment process is neglected since the influence is much smaller as compared to the mass transfer. However, the system parameters such as process kinetics and transport characteristics are greatly influenced by temperature. Traditionally, the development of biofilm is seen as the formation of a layered structure growing from the substratum outwards. This led to the traditional one-dimensional models (Rittmann and Manem 1992; Wanner and Gujer 1986) where all the property gradients are one-dimensional and vary in the direction perpendicular to the substratum. The properties include substrate concentrations, biomass density, porosity and attachment and detachment of solids at the biofilm surface. The differential one-dimensional form of equation describing the biofilm system can be summarized by the equation 3.1 below (Wanner and Reichert 1996).

$$\frac{\partial P}{\partial t} + \frac{\partial N}{\partial x} = R \qquad (3.1)$$

where

P represents the 1-D property such as substrate concentration or biomass density [ML^{-3}]

N is the 1-D property flux or the amount of property transported per unit time [$ML^{-2}T^{-1}$]

R represents the net property production rate (amount of property produced per unit time, per unit length) [$ML^{-3}T^{-1}$]

t time [T]

x space coordinate (perpendicular to the sub-stratum) [L]

Till the middle of 80s, the modellers described in detail the mass transport of substrate through the biofilm assuming a constant biofilm density profile. Initially, only one species of micro-organisms i.e. heterotrophs was considered and carbonaceous substrate removal was modelled (Williamson and McCarty 1976, Müller et al. 1978; Rittmann et al. 1978). Later on, organic substrate removal was extended with simultaneous nitrification in a mixed species biofilm with a defined biomass distribution (Müller et al. 1980, Jansen et al. 1985, Gujer et al. 1986). Watnabe et al. (1978) observed denitrification in a RBC biofilm. Parallel studies in understanding the dynamics of biomass transport inside the biofilm matrix and attachment-detachment mechanism of solids at the surface were attempted (Trulear and Characklis 1982). However, till the beginning of 80s, the aspect of spatial and temporal development of biofilms could not be correlated to the substrate transport and transformation in a single model. The difference in time scales between the development of the different processes were too high to be put together into one computational model.

Figure 7 shows the characteristic times of the biofilm processes relative to each other. It was first discussed by Kissel et al. (1984) when they modelled the biofilm system as a whole.

The left hand side of the partial differential equation 3.1 depicts the behaviour of the transport phenomena of the substrate as well as displacement of biomass inside the biofilm matrix. This is discussed in detail in chapter-6 wherein the underlying concepts of the current RBC model is explained. The boundary layer and the reactor model equations are also explained therein. The right hand side of equation 3.1 reflects the transformation processes by the biomass in the biofilm and the reactor. The kinetics and stoichiometry of these conversion processes are discussed in the subsequent sections of this chapter.

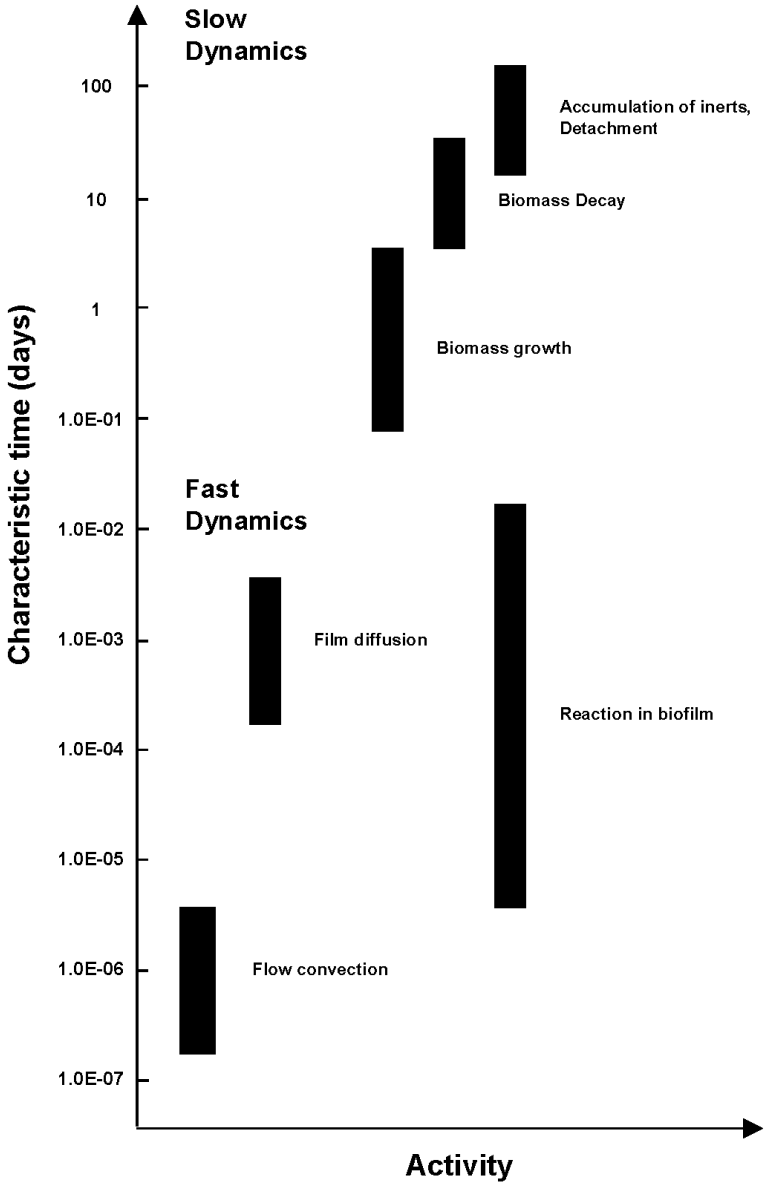

Figure 7 Characteristic times of different processes in a biofilm
(Based on Kissel et al.1984)

3.5.2 Kinetics of microbiological conversions in biofilm

Each hypothetical layer in a biofilm acts as a biological unit for biochemical transformation reactions based upon physical conditions and nutrient supply. For the degradation of nutrients in a biofilm unit, it is necessary to provide an electron donor (substrate) and an electron acceptor (oxygen or nitrate). It is possible that aerobic conditions are present only in the upper layer of the film. In the lower parts of the biofilm, oxygen transport can be insufficient and anoxic or anaerobic conditions can be present. Measurements using micro-electrodes showed that these conditions are possible at only 100 µm deep in the biofilm (Bishop et al. 1995). The value is only an indication since large variations are possible,

dependent on the oxygen and substrate concentrations in the bulk liquid, the mass transfer to the biofilm and the conversion speed. At different depths in the biofilm, micro-organisms will thus develop that use different electron donors and acceptors. Reduced organic substances can serve as donors along with ammonium (for nitrification). A wide variety of acceptors are possible: oxygen (aerobic metabolism), nitrate (denitrification), sulphate (sulphate reduction), hydrogen (methanogenesis) and other organic molecules (fermentation). In most domestic wastewaters, nutrients will be available abound, although this might not be true in case of some industrial wastewaters.

In the world of modelling, the complex biological processes are simplified into three important steps (Henze et al. 2002):

- Biological growth based on nutrient supply
- Hydrolysis and storage
- Endogenous respiration and decay

The basic models for biological treatment in activated sludge treatment plants which had been built by IAWQ teams [ASM No.1, Henze et al. (1987); ASM No.2d, Henze et al. 1999; ASM No.3, Gujer et al. (1999)] are based on the above hypothesis. ASM No.1 however did not consider storage of biomass as an intermediate step. It was included in the ASM No.3. The models were basically built and implemented for the activated sludge plants, and its extension to a biofilm unit is just an analogy as the bacteriological processes are nearly the same, although their rates can vary depending upon density and porosity.

3.5.2.1 Biological growth

The bacterias are assumed to be the primary organisms in conversion reactions and they are able to utilize the small and simple molecules for growth. It may be substances such as acetic acid, ethanol, methanol, propionic acid, glucose, ammonium, nitrite etc. The major difficulty in most biological conversions is that only a certain part of the substrate to be removed or treated in the process is immediately available for microbial removal. The process can be described using the following relation:

$$R_{X_j,V} = \mu_{max}.f(S).X_j \qquad (3.2)$$

where

$R_{Xj,V}$ is the volumetric biological growth rate [$ML^{-3}T^{-1}$]

μ_{max} is the maximum specific growth rate [T^{-1}]

f(S) is the reaction kinetics (e.g. zero, first order or Monod kinetics)

X_j is the density of the biomass species j [ML^{-3}]

The growth kinetics f(S) is commonly assumed to be a Michaelis-Monod expression (Henze et al. 2002):

$$f(S) = \frac{S}{K_S + S} \tag{3.3}$$

where

S is the principal substrate concentration affecting the growth of biomass species j [ML^{-3}];

K_S is the half-saturation rate constant for substrate S [ML^{-3}]

Equation 3.3 can easily switch between first and zero order kinetics with respect to substrate. In case of high substrate concentrations, e.g. industrial wastewater, the kinetics may be described by zero order expression, i.e. if $S>>K_S$, then K_S can be neglected. The observed growth rate of a species μ_{obs} then approaches a finite maximum value μ_{max}. In case of biofilm, this transition can be gradual from zero-order (substrate saturation) at biofilm surface (Maier et al., 1967) to first-order (substrate limitation) in the deeper layers. On the other hand, the growth rate can approach zero when the concentration of the limiting substrate approaches zero. A special case of first-order kinetics occurs if $S<<K_S$. Then the growth rate μ_{obs} is expressed as follows:

$$\mu_{obs} = k_1 . S \tag{3.4}$$

with

$$k_1 = \frac{\mu_{max}}{K_S} \tag{3.5}$$

The volumetric growth of biomass results in change of substrate concentration which is based upon the yield of biomass species j. The rate of substrate uptake may be given by the equation 3.4 below.

$$R_{S_i,V} = \frac{\mu_{max}}{Y_{j,max}} . f(S) . X_j \tag{3.6}$$

where

$R_{S_i,V}$ is the rate of substrate utilization [$ML^{-3}T^{-1}$]

$Y_{j,max}$ is the maximum yield of biomass species j [-]

The rate of substrate utilization shown in equation 3.6 may also be represented in terms of μ_{obs} as shown in equation 3.7 below.

$$R_{S_i,V} = \frac{\mu_{obs}}{Y_{j,max}} . X_j \tag{3.7}$$

Both μ_{max} and $Y_{j,max}$ are very sensitive kinetic parameters and depend upon a number environmental factors such as temperature, oxygen, pH, alkalinity and presence or absence of other nutrients and toxic substances. The observed growth rate may then be represented mathematically by equation 3.8.

$$\mu_{obs} = \mu_{max}.f(S).f(S_O).f(pH).f(T) \tag{3.8}$$

where

S_O is the oxygen concentration [ML^{-3}]

T is the temperature [°C]

In case of multiple substrate limitations, the growth kinetics is usually described by a multiple Monod expression. For dependency on DO, the growth kinetics is modelled as shown below.

$$\mu_{obs} = \mu_{max}.\frac{S}{K_S + S}.\frac{S_O}{K_O + S_O} \tag{3.9}$$

where

K_O is the half-saturation rate constant for oxygen [ML^{-3}]

The effect of other nutrients such as ammonium and alkalinity on the observed growth rate μ_{obs} can similarly be modelled by extending the double Monod expression in equation 3.9 with similar expressions for the above nutrients so that the microbial growth is inhibited when those nutrient concentrations are low (Bae and Rittmann, 1996).

A temperature correction factor θ_T needs to be applied to μ_{max} in equation 3.9 for variations in temperature in the range 0-32°C as against standard growth rate at 20°C. The temperature dependency for the biological process can be described by the van't Hoff exponential expression as shown below.

$$\mu_{max,T^\circ C} = \mu_{max,20^\circ C} e^{\theta_T (T-20)} \tag{3.10}$$

Figure 8 shows the relative growth rate of nitrifying bacteria as a function of temperature, while Figure 9 depicts the sensitivity of maximum growth rate of nitrifiers with temperature. When the temperature rise is fast, the increase in the growth rate is lower than expected, whereas a sudden drop of temperature gives a much higher decline in the activity than expected from Figure 8. Normally, nitrifying processes does not take place at thermophilic temeperatures (50-60°C) (Henze et al. 2002). Similarly, temperature corrections need to be applied for the half-saturation rate coefficient K_i for each nutrient i as expressed by equation 3.11.

$$K_{i,T^\circ C} = K_{i,20^\circ C}.e^{\theta_T^{'}(T-20)} \tag{3.11}$$

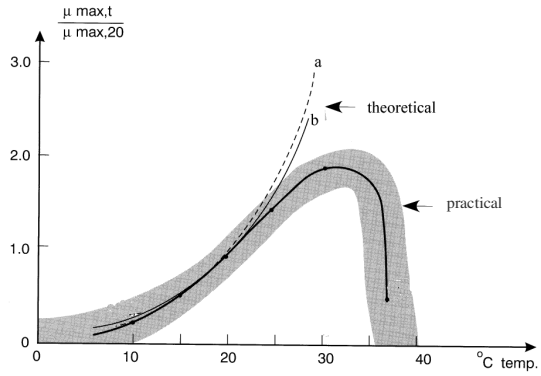

Figure 8 Variation of theoretical and actual growth rate of nitrifiers with temperature.
(Henze et al. 2002), a (Knowles 1965), b (Gujer 1977), c (Buswell 1954)

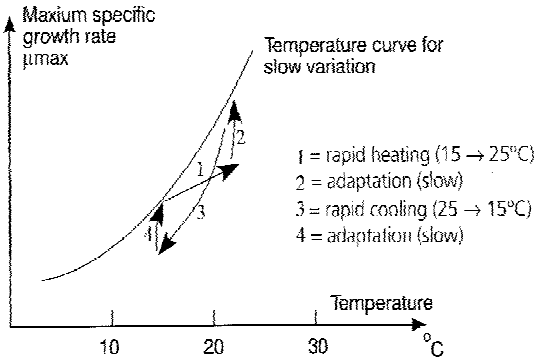

Figure 9 Effect of rapid and slow temperature changes on the growth rate of nitrifiers.
(Henze et al. 1978)

In activated sludge treatment processes under aerobic environment, experience shows that the removal rate increases with temperature in the range 0-32°C, remains nearly constant in the temperature range from 32-40°C, after which it usually starts declining at around 45°C.

3.5.2.2 Hydrolysis and storage

The hydrolysis process converts macro molecules into small, readily degradable molecules. It can be a degradation of both particulate as well as dissolved components. This process is very slow compared to biological growth process and is basically of major importance in ASP systems. Due to lack of adequate knowledge about the process, it is usually represented by simple first-order kinetics in the activated sludge models.

$$R_{X_S,V} = k_h . X_S \tag{3.12}$$

where

$R_{X_S,V}$ is the rate of hydrolysis of the suspended solids X_S [$ML^{-3}T^{-1}$]

k_h is the specific hydrolysis rate constant [T^{-1}]

X_S is the concentration of the suspended solids [ML^{-3}]

However, hydrolysis is neglected in most biofilm models. This process is slow and is rarely the principal rate limiting step when compared with fast diffusing substrates, oxygen etc. described using Monod's expressions previously. Similarly, storage of readily biodegradable substrate in the form of cell internal storage product for subsequent degradation by the biomass is a hypothesis which is principally employed in ASP models and is not considered in biofilm models as little is known about the kinetics of the storage process.

3.5.2.3 Endogenous respiration and decay

This process describes collectively all forms of biomass degeneration and energy requirements not associated with growth in aerobic as well as anoxic conditions. The anoxic

endogenous respiration process is relatively slower than the aerobic respiration. Degeneration results from all the processes that reduce bacterial mass and number. It includes mechanisms such as decay (lysis), endogenous respiration, cell maintenance, predation, motility and death (Henze et al. 2002). When there is no more food, the bacteria start to metabolise substances inside their own cells. This metabolism can play an important role in the survival of a biofilm under substrate limiting conditions. This is an essential element in the biological conversion of nutrients. Although a very slow process in the biofilms, it generates particulate inerts in the nutrient limited or starved layers which eventually get displaced to the biofilm surface and are removed by detachment processes into the reactor. The endogenous respiration was earlier modelled as a first order decay process in ASM No.1. The updated ASM No.3 assumes the mechanism to be based on Michaelis-Monod equation and the surrounding environment. Under aerobic environment, the endogenous metabolism is modelled as shown in equation 3.13, while under anoxic conditions, it is represented as shown in equation 3.14.

$$R_{X_j end,V} = k_{X_j end} \cdot \frac{S_O}{K_O + S_O} X_j \tag{3.13}$$

$$R'_{X_j end,V} = k'_{X_j end} \cdot \frac{K_O}{K_O + S_O} X_j \tag{3.14}$$

where

$R_{X_j end,V}$ and $R'_{X_j end,V}$ are the rate of endogenous respiration of bacterial species X_j under aerobic and anoxic conditions respectively [$ML^{-3}T^{-1}$],

$k_{X_j end}$ and $k'_{X_j end}$ represent the specific endogenous respiration rate constants for X_j under aerobic and anoxic conditions respectively [T^{-1}].

3.5.3 Stoichiometry of biological conversions in biofilm

The stoichiometry of the biochemical reactions is essentially based upon the redox reactions by the electron donors and acceptors, depending upon aerobic or anoxic conditions in each biofilm layer. The reaction stoichiometry is essentially sub-divided into three major categories based upon the conversion processes in treatment of municipal wastewater: aerobic degradation of organic matter; nitrification and denitrification. These processes are of principal importance in treatment of municipal sewage.

3.5.3.1 Aerobic degradation of organic substrate

The degradation of organic matter by micro-organisms may result in the following transformations:

- oxidation to CO_2 and different inorganic compounds
- assimilation in biomass for growth and cell maintenance
- conversion into other organic matter

In case of non-biodegradable inert substances, there is no transformation. Organic matter in wastewater has an approximate chemical composition as $C_{18}H_{19}O_9N$. The chemical oxidation of organic matter chiefly by the heterotrophic bacterias may be represented by the following expression (Henze et al. 2002):

Without nitrification :

$$\underset{(393g)}{C_{18}H_{19}O_9N} + 17.5\,O_2 + H^+ \xrightarrow{bacteria} 18CO_2 + 8H_2O + \underset{(560g)}{NH_4^+} + energy \qquad (3.15)$$

With nitrification :

$$\underset{(393g)}{C_{18}H_{19}O_9N} + 19.5\,O_2 \xrightarrow{bacteria} 18CO_2 + 9H_2O + H^+ + \underset{(624g)}{NO_3^-} + energy \qquad (3.16)$$

The microbial oxygen consumption without and with nitrification is calculated to be 1.42 and 1.59gO_2/g organic matter respectively. The COD measured with $K_2Cr_2O_7$ will be 1.42g O_2/g organic matter in both cases as ammonium is not oxidised in connection with COD analysis. The energy resulting from the exothermic oxidation reaction of the organic matter is about 110kJ/e-equivalent. The organic substrate is primarily composed of carbohydrates, fats and proteins in municipal sewage. In terms of weight, these substances are present in almost equal amounts. However, the oxygen requirement may vary considerably depending upon individual components chemical structure and equations 3.14 and 3.15 reflect only average values.

The yield in a microbial heterotrophic conversion is the mass of biomass growth per unit mass of substrate utilized. Heterotrophs have a typical energy efficiency β of about 55-60% and typical yield in aerobic degradation is around 0.5gCOD VSS/gCOD organic substrate (Loosdrecht et. al. 1997). The rest of the energy efficiency and biomass yield is contributed to the storage phenomenon. Organic matter metabolised aerobically (or anoxically) maybe used for different purposes:

- biomass growth
- energy production by oxidation with oxygen (or nitrate) to CO_2
- storage as cell internal products (intracellular polymers)
- extracellular polymers (eps)

The maximum yield constant Y_{max} for the aerobic growth process is wastewater is around 0.60-0.65 gCOD VSS/gCOD organic substrate and this value is used in mathematical models

(ASM 2d, Henze et al.1999). The observed yield Y_{obs} is often much lower (0.3-0.4gCOD VSS/gCOD org. matter) due to maintenance/endogenous respiration. Again, in case of less organic loading, yield is less due to substrate limitation resulting in the micro-organisms entering into endogenous respiration phase. Chemically, if x moles of organic substrate (composition $C_{18}H_{19}O_9N$) is utilized to produce y moles of biomass (assumed composition $C_5H_7NO_2$), the observed yield may be represented as shown in 3.18.

$$\underset{(x.393)\ g}{x\ C_{18}H_{19}O_9N} + \ldots\ldots\ldots \longrightarrow \underset{(y.113)\ g}{y\ C_5H_7NO_2} + \ldots\ldots\ldots\ldots \tag{3.17}$$

$$Y_{obs} = \frac{(y.113)}{(x.393)} \tag{3.18}$$

If Y_{obs} is 0.5, then one mole of organic substrate gives 1.74 moles of biomass, i.e. for x =1, y = 1.74. Therefore, the mass balance equation of chemical conversion may be represented as shown in 3.19 below.

$$\underset{(org.\ substrate)}{C_{18}H_{19}O_9N} + 0.74\ NH_3 + 8.8\ O_2 \longrightarrow \underset{(bacterial\ cell)}{1.74\ C_5H_7NO_2} + 9.3\ CO_2 + 4.52\ H_2O \tag{3.19}$$

It is observed that some nitrogen needs to be present in the form of ammonium as there is not sufficient nitrogen in the organic matter for complete assimilation and utilization in the biomass. If the organic matter is fed to more than one organism type (high food chain factor), more organic matter will be utilized for energy through oxidation, resulting in a lower overall yield. In a multi-species biofilm model, the observed yield is very often much less and different in different layers due to competition between micro-organisms for the nutrients. In case of low organic loadings, cells enter into endogenous respiration phase in which they start consuming their own cell protoplasm with some requirement of oxygen and thereby generate energy.

$$C_5H_7NO_2 + 5\ O_2 \xrightarrow{bacteria} 5\ CO_2 + 2\ H_2O + NH_3 + energy \tag{3.20}$$

3.5.3.2 Nitrification

In municipal wastewater, nitrogen compounds originate from the biological decomposition of proteins and urea. Organic nitrogen may be biologically converted to free ammonia (NH_3^0) or ammonium ion (NH_4^+). The two chemical species are together termed as ammonia nitrogen and exist in equilibrium depending upon pH as per the following reversible reaction.

$$NH_4^+ \Leftrightarrow NH_3^0 + H^+ \tag{3.21}$$

At pH above 11, ammonia nitrogen can be stripped as gaseous ammonia based on equation 3.21. However, normal pH of wastewater is much below that and so biological oxidation of

ammonia nitrogen with molecular oxygen by the autotrophic organisms is one of the conventional methods to achieve nitrification. This oxidation is usually modelled as a two step process wherein ammonium is first oxidised into nitrite by one set of nitrifying species and then nitrite is eventually converted to nitrate by another set of nitrifying organisms. The first step is believed to involve a complex series of reactions. The chemical conversion process by ammonium oxidizing micro-organisms (AOM) and nitrite oxidizing micro-organisms (NOM) could be expressed in a simple way by equation 3.22 and 3.23 respectively.

$$\underset{(14g)}{NH_4^+} + \underset{(48g)}{\frac{3}{2}O_2} \xrightarrow{aom} NO_2^- + H_2O + 2H^+ + energy \qquad (3.22)$$

$$\underset{(14g)}{NO_2^-} + \underset{(16g)}{\frac{1}{2}O_2} \xrightarrow{nom} NO_3^- + energy \qquad (3.23)$$

The above nitrification reactions result in the utilization of 4.57g of oxygen for each gram of ammonia-nitrogen oxidised to nitrate-nitrogen. The first step requires about 3.43g of oxygen to oxidise 1g of ammonia-nitrogen to nitrite-nitrogen by the ammonia oxidising micro-organisms. In the second step, 1.14g of oxygen is used to convert 1g of nitrite-nitrogen to nitrate-nitrogen by the nitrite oxidising bacteria.

The energy released during the oxidation reaction of ammonium is about 270kJ/mol NH_4^+-N and 80kJ/mol NO_2^--N. The nitrifiers have a characteristic lower growth rate than heterotrophs due to low energy yield compared to the latter. They have to compete with heterotrophs for food and oxygen and hence nitrification is often a more sensitive process in biological treatment. Nitrifying bacterias are chemoautotrophs and require inorganic carbon source such as CO_2 along with nitrogen compounds for their sustenance. The reduction of carbon dioxide to inorganic carbon for access into cell mass occurs through the oxidation of the nitrogen source of the concerned nitrifying bacteria.

Oxidation of ammonium - nitrogen :

$$13\,NH_4^+ + 15\,CO_2 \longrightarrow 3\,C_5H_7NO_2 + 10\,NO_2^- + 23\,H^+ + 4\,H_2O + energy \qquad (3.24)$$

Oxidation of nitrite - nitrogen :

$$10\,NO_2^- + NH_4^+ + 5\,CO_2 + 2\,H_2O \longrightarrow C_5H_7NO_2 + 10\,NO_3^- + H^+ + energy \qquad (3.25)$$

When the observed yield constants of nitrifiers are known, i.e. $Y_{obs,NH4}$ for AOM and $Y_{obs,NO2}$ for NOM, the equations of reaction can be specified. Combining the equations (3.22) and (3.24) and by using the carbonate equilibrium system and considering $Y_{obs,NH4}$ as 0.10gVSS/gNH_4^+-N (i.e. 0.142gCOD VSS/ gNH_4^+-N), the growth of AOM can be written as follows (Henze et al. 2002):

$$80.7\,NH_4^+ + 114.55O_2 + 160.4HCO_3^- \longrightarrow C_5H_7NO_2 + 79.7\,NO_2^- + 82.7\,H_2O + 155.4\,H_2CO_3 \quad (3.26)$$

(1129.8 gN) *(113 g)*

In case of NOM, combining equations 3.23 and 3.25 and considering $Y_{obs,NO2}$ as 0.06gVSS/gNO_2^--N (i.e. 0.085gCOD VSS/gNO_2^--N) yields the following expression (Henze et al. 2002):

$$134.5\,NO_2^- + 62.25\,O_2 + NH_4^+ + HCO_3^- + 4H_2CO_3 \longrightarrow C_5H_7NO_2 + 134.5\,NO_3^- + 3\,H_2O \quad (3.27)$$

(1883 gN) *(113 g)*

However, the above chemical balance may change with $Y_{obs,NH4}$ value for AOM and $Y_{obs,NO2}$ for NOM. It has been noted that the oxidation of ammonium to nitrite takes place in several steps while that of nitrite to nitrate is a single step process. The intermediate states are avoided in modelling the reaction stoichiometry and only the end-products are considered for simplification (ASM No.3). Moreover, the intermediate nitrite-nitrogen production is unstable and denitrification occurring from it cannot be easily determined. In one step nitrification, the nitrite-nitrate concentrations are combined together and in effect, denitrification occurring from it is thereby taken into account (Gujer et al. 1999).

From the chemical equations, it is clear that nitrification process reduces the alkalinity in waste water. For every mole of NH_4^+-N which is oxidized to NO_2^--N, approximately 2 moles of HCO_3^- are consumed which corresponds to 2 equivalents of alkalinity. In case of soft water, presence of alkalinity is an essential requirement for nitrification where pH of water can be so low that the process is limited. Nitrifying bacterias are especially sensitive to sudden variations in temperature as shown in Figure 8 previously. They are extremely susceptible to a wide variety of inhibitors as well. For example, high concentrations of nitrous acid can be inhibitory. Dissolved Oxygen concentrations above 1 mg/l is necessary to maintain nitrification and if the DO level diffusing into the biofilm drops below that value, oxygen becomes the limiting nutrient and nitrification slows down or ceases (Tchobanoglous 1995).

3.5.3.3 Denitrification

The reduction of nitrite and nitrate into molecular nitrogen is carried out mainly by facultative bacteria in the deeper layers of the biofilm where oxygen diffusion is limited. Denitrification usually occurs under anoxic conditions, when nitrate is present and molecular oxygen is absent. Nitrate acts as the electron acceptor or oxidising agent. In the past, the conversion process was identified as anaerobic denitrification. But the principal biochemical pathways are not anaerobic but rather a modification of the aerobic pathways. Hence, the use of the term anoxic instead of

anaerobic is considered more suited here. Most heterotrophic bacterias have the ability to change their metabolism from using oxygen as the final electron acceptor to using nitrate instead. The so called choice made by the bacterial cell to determine the terminal electron acceptor depends upon the redox potential between the last cytochrome in the electron transport system and oxygen or nitrate. Cytochrome is a class of cell protein whose principle biological function is to carry electrons or protons by virtue of the reversible charging/discharging of an iron atom in the centre of the protein, thereby undergoing alternate reduction and oxidation. Usually the cells favour oxygen, so that under circumstances where both oxygen and nitrate are present, the bacteria will respire with oxygen instead of denitrifying nitrate. This is because molecular oxygen generates a higher redox potential with the cell cytochrome compared to nitrate and make the electron acceptance easier.

The denitrification process occurs stepwise with several intermediate products which are all toxic and undesirable. The symbolic representation of denitrification steps is as follows:

$$NO_3^- \rightarrow NO_2^- \rightarrow NO \rightarrow N_2O \rightarrow N_2 \tag{3.28}$$

The last three compounds are gaseous i.e. nitric oxide, dinitrogen oxide and nitrogen and can be released into the atmosphere. In mathematical models, denitrification is assumed to be a single step process and intermediate stoichiometry is neglected for simplicity. Further, the amount of intermediate product will normally be miniscule. Alkalinity is produced during denitrification resulting in an increase of pH. The stoichiometric energy yielding expression for denitrifying bacteria which uses organic matter in wastewater as carbon and energy source may be given as below:

$$\frac{1}{70}C_{18}H_{19}O_9N + \frac{1}{5}NO_3^- + \frac{1}{5}H^+ \rightarrow \frac{1}{10}N_2 + \frac{17}{70}CO_2 + \frac{1}{70}HCO_3^- + \frac{1}{70}NH_4^+ + \frac{1}{5}H_2O \tag{3.29}$$

The above conversion results in about 103kJ/e-equivalent of energy, a part of which maybe used in biological growth and remaining ends up as heat energy. When the energy is used for growth, the maximum yield constant of the process is 15-20% lower than that of aerobic heterotrophic conversion. Assuming an approximate maximum yield of 0.40gVSS/g organic matter (i.e. 0.56gCOD VSS/gCOD organic substrate), the chemical balance when the bacteria uptakes ammonium is as follows:

$$0.52\,C_{18}H_{19}O_9N + 3.28\,NO_3^- + 0.48\,NH_4^+ + 2.80\,H^+ \longrightarrow C_5H_7NO_2 + 1.64\,N_2 + 4.36\,CO_2 + 3.80\,H_2O \tag{3.30}$$

In case of assimilation of nitrate by the microbes, the reaction equation is based on a maximum yield constant of 0.36gVSS/g organic matter (3.31). When ammonium is present, bacterias will

always use it as a nitrogen source as shown by equation (3.30). This is true for most municipal wastewaters.

$$0.57\,C_{18}H_{19}O_9N + 3.73\,NO_3^- + 3.73\,H^+ \longrightarrow C_5H_7NO_2 + 1.65\,N_2 + 5.26\,CO_2 + 3.80\,H_2O \quad (3.31)$$

The denitrification process is temperature dependent because of the heterotrophic bacteria. Moreover, presence of oxygen inhibits the denitrification process. The inhibitory effect of a component I is introduced in modelling (ASM 2d, Henze et al.1999) by multiplying the reaction rates with the approximated expression in 3.32.

$$\frac{K_I}{K_I + I} \quad (3.32)$$

where K_I is the concentration of the inhibitor I giving 50% inhibition of the growth rate of the species. Thus, when oxygen is the inhibitor, the growth rate of heterotrophs during denitrification process may be expressed by a modified form of equation 3.9 as shown below:

$$\mu_{obs} = \mu_{max} \cdot \frac{S}{K_S + S} \cdot \frac{K_O}{K_O + S_O} \quad (3.33)$$

K_O represents the saturation constant for oxygen in inhibition. The optimum pH range for denitrification process is 7 to 9 as in case of other biological processes.

4 Experimental set-up

4.1 Description

The mathematical model of the RBC is based on the laboratory-scale experimental set-up. The experiments are part of the project funded by the German Ministry for Education and Research (BMBF) to my colleague (Mr. Andreas Blank) in this institute in a joint venture programme with Indian Institute of Technology, New Delhi, India and a private partnership with a RBC manufacturing company in Germany (Dr. Scholz and Partner GmbH, Kirchberg). A part of the results obtained from the experiments have been used for model verification and calibration. The experiments were divided into two phases: (a) Measurement of physical oxygen transfer phenomenon into the liquid film with pure water and (b) Biological nutrient removal in laboratory-scale experimental set-up using synthetic wastewater from molasses and ammonium chloride.

4.2 Physical oxygen transfer on discs without biofilm

Initial studies were aimed at determining the physical oxygen transfer coefficient (K_L) across the air-liquid interface formed on a flat plastic disc mounted on a horizontal shaft and rotating in a still basin of water kept inside a trough. Non-steady state re-aeration experiments were conducted at different rotational velocities with the 25cm diameter disc. The submerged area of the disc was about 42% of the total surface area. The ambient temperature was about 19°C. Figure 10 displays the experimental set-up initially used for the measurements. A schematic representation of the disc in the laboratory scale experimental set-up with the list of common physical specifications is displayed in Figure 11.

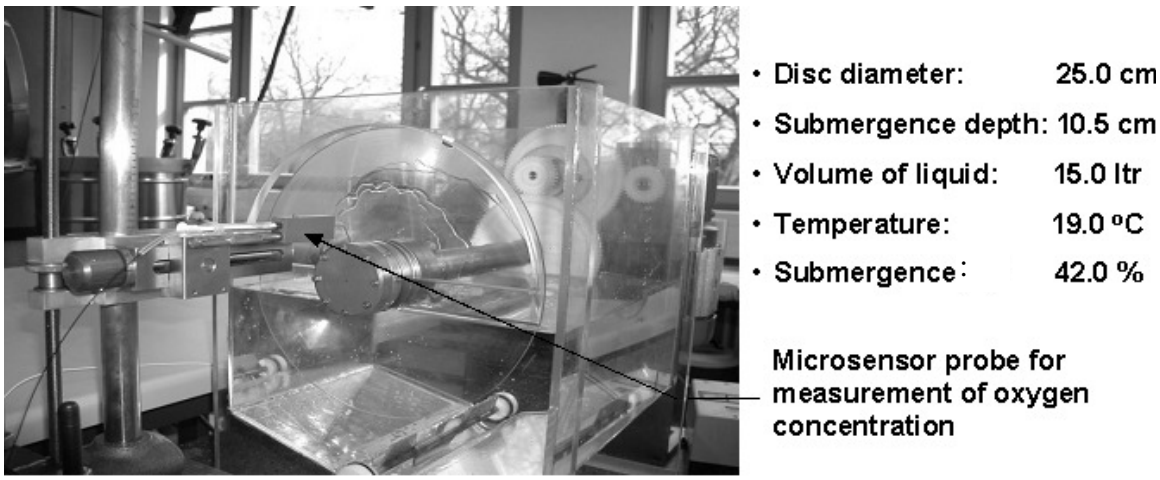

Figure 10 Experimental arrangement for measuring oxygen concentration in liquid film
(Courtesy: A. Blank, IWG, University of Karlsruhe (TH))

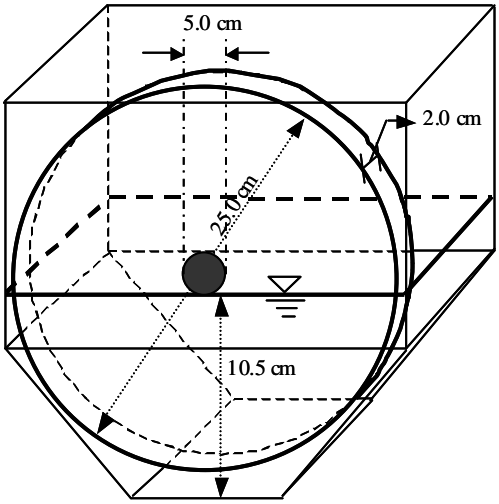

Parameter	Dimension	Unit
Disc diameter	25	cm
Disc thickness	2	cm
Depth of immersion	10.5	cm
Submergence ratio	42	%
Diameter of shaft	5	cm

Figure 11 Schematic sketch and specifications of RBC disc used in the laboratory experimental set-up

In order to deoxygenate the water, a stoichiometric excess of sodium sulphite was used with cobalt chloride as catalyst in a still basin of water in a trough. The oxygen concentration in the liquid film over the exposed disc surface was measured directly using an optical oxygen-sensor probe mounted on a micromanipulator and controlled by a microprocessor (MICOS GmbH). The oxygen-sensor, manufactured by the company PreSens Precising Sensing GmbH (MICROX TX3), functions on the principle of nullification of the effect of luminescence active molecules by molecular oxygen (A. Blank, 2006). The sensor arrangement can be more clearly observed in Figure 12. The diameter of the sensor point was less than 5mm. Due to the small dimension of the sensor and the accuracy of the micromanipulators, it was possible to determine the oxygen concentration on the disc with high precision.

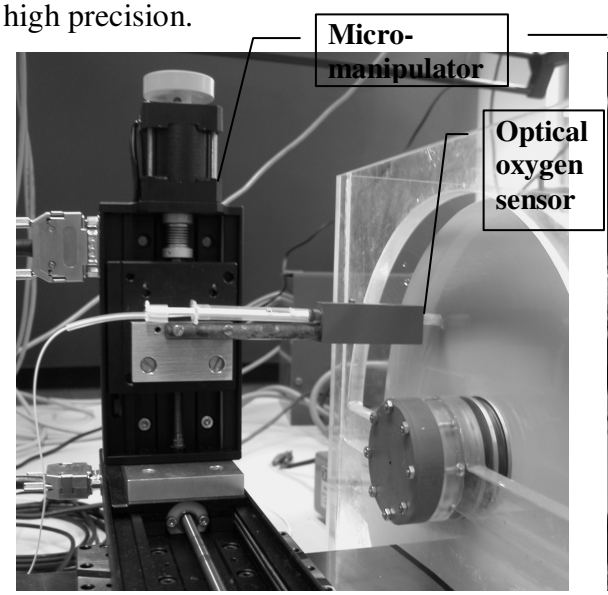

Figure 12 Oxygen sensor for measurement of oxygen concentration at any disc location

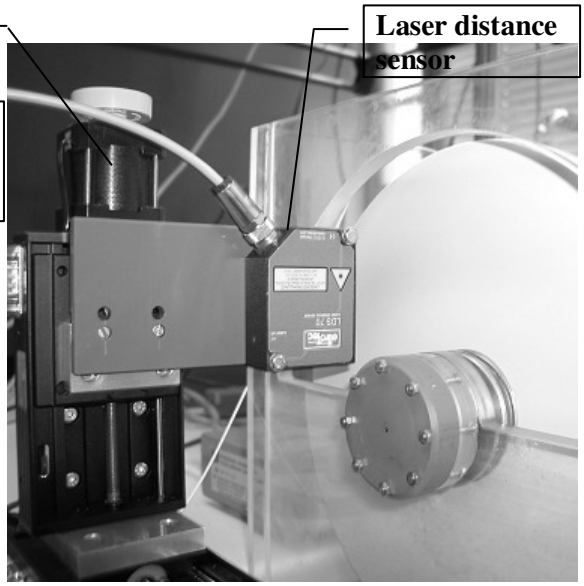

Figure 13 Laser Distance Sensor for determination of film thickness (Courtesy: A. Blank, 2006)

For accurate measurement of liquid film thickness, a laser distance sensor manufactured by the company LEUZE GmbH was used. This sensor was also mounted on the travelling micromanipulator for controlling the measurement location as shown in Figure 13. The laser sensor is based on the triangulation principle. The film thickness is determined indirectly by the difference of the distance between sensor and the dry disc surface and the distance between sensor and moistened disc surface. The position of the water surface on the disc could be specified by means of the addition of titanium dioxide into water which reflected the laser beam. The speed of rotation was adjusted using a belt drive powered by electric motor. All the experiments were conducted by colleague Mr. A. Blank (IWG) of this university.

4.3 Nutrient removal with synthetic wastewater in RBC biofilm

The laboratory-scale experiments were conducted at two different scales. The purpose of two different scales was to observe the variation in performance efficiency with scale-up operation. Each RBC reactor configuration has three stages (cascades) separated by baffles to prevent mixing and initiate desired removal processes. A field-scale model for 150 population equivalent is underway for installation in New Delhi, India for operational observation and process optimisation in tropical climate. Table 3 lists the salient physical specifications for each of two experimental set-ups.

Table 3 Physical specifications of the RBC experimental set-up

Parameter	Stage	Set up-I	Set-up-II	Unit
Disc diameter	I	25	50	cm
	II	25	50	
	III	25	50	
Number of discs	I	12	12	-
	II	10	10	
	III	10	10	
Spatial distance between discs	I	18	18	mm
	II	15	15	
	III	15	15	
Disc thickness		2	2	mm
Depth of immersion		10.5	21	cm
Immersion ratio		42	42	%
Diameter of shaft		5	5	cm

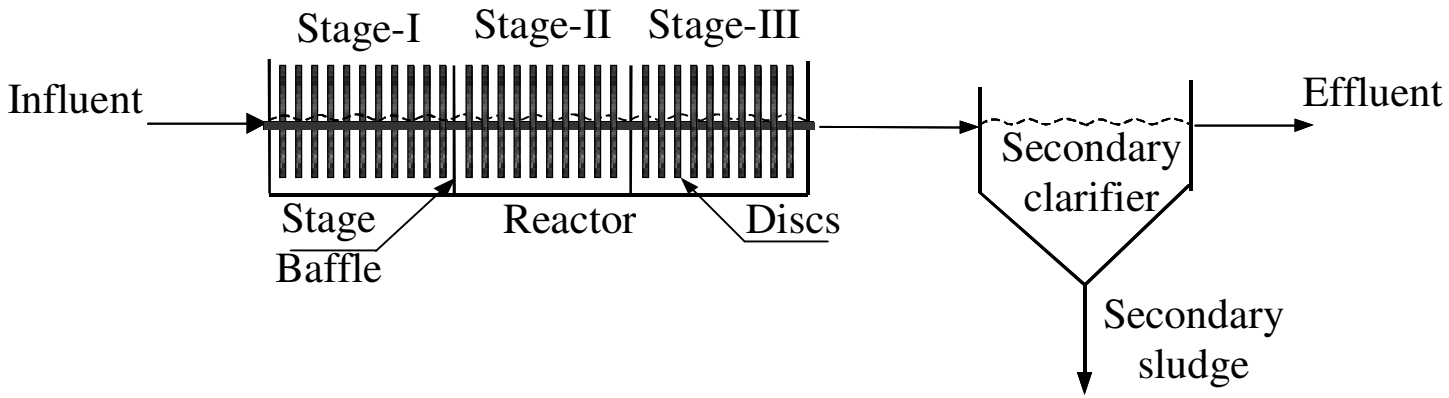

Figure 14 Schematic view of the laboratory-scale RBC set-up used in the experiments

Table 4 Technical data of the 3-stage experimental set-up at two different scales

Set up-I (Small scale laboratory)				Set up-II (Medium scale laboratory)			
Reactor Volume		**Interfacial biofilm area**		**Reactor Volume**		**Interfacial biofilm area**	
Stage-I	5.80 l	Stage-I	1.18 m^2	Stage-I	23.50 l	Stage-I	4.40 m^2
Stage-II	4.20 l	Stage-II	0.98 m^2	Stage-II	17.60 l	Stage-II	3.70 m^2
Stage-III	4.20 l	Stage-III	0.98 m^2	Stage-III	17.60 l	Stage-III	3.70 m^2
Total Volume (V)	14.20 l	Total Area (A)	3.14 m^2	Total Volume (V)	58.70 l	Total Area (A)	11.80 m^2
Flow rate		**Nutrient loading rates**		**Flow rate**		**Nutrient loading rates**	
Q	68.0 l/d	Org. load (molasses) ~ 4.7 gCOD/(m^2d)		Q	280.0 l/d	Org. load (molasses) ~ 5.1 gCOD/(m^2d)	
Q_R	0	Total-N load (NH_4Cl) ~ 1.0 gN/(m^2d)		Q_R	0	Total-N load (NH_4Cl) ~ 1.0 gN/(m^2d)	
HRT		**Rotational speed**		**HRT**		**Rotational speed**	
θ	~ 5.0 h	ω	~ 2-3 rpm	θ	~ 5.0 h	ω	~ 2-3 rpm
Disc submergence		**Ambient Temperature T**		**Disc submergence**		**Ambient Temperature T**	
(R-H)/2R	42 %	Phase-I ~ 25°C	Phase-II ~ 30°C	(R-H)/2R	42 %	Phase-I ~ 25°C	Phase-II ~ 30°C

A schematic view of the experimental set-up is displayed in Figure 14. The two laboratory-scale set-ups have the same schematic layout. Table 4 enumerates the physical dimensions and the loading rates for the two set-ups. The overall hydraulic loading rate was approximately $0.02 m^3/(m^2.d)$ and hydraulic retention time per reactor is 5.0 hrs. The COD loading rate was approximately $14 g/(m^2.d)$ in first stage and $4 g/(m^2.d)$ in the second stage. As per DIN 4261 (II) standards, the organic loading rate should not exceed $4 gCOD/(m^2.d)$ to achieve nitrification in small wastewater plants. The ATV-DVWK standard (2001) specifies a maximum BOD loading rate of $8 g/(m^2.d)$ and a maximum ammonia loading rate of $1.6 g/(m^2.d)$ for a 3-stage RBC treating wastewater with nitrification. The dissolved oxygen concentration in stage-1 was found to vary between 3 to 4mg/l. The discs were rotated at about 2-3 rpm. Excess oxygenation at higher rotational speed may displace the dissolved carbon dioxide (buffer) which is in equilibrium by hydrolysis of carbonic acid in the tanks.

$$H_2CO_3 \Leftrightarrow H_2O + CO_2$$

This may shift the pH equilibrium in the tank resulting in excessive alkaline conditions (pH >8.0) which might deteriorate overall performance. Therefore, the rotational speed was kept low. It also prevents unwanted biomass shearing. High organic loading in the first stage of the reactor was aimed to achieve some denitrification. There was often excess sludge production due to sloughed biomass and it needed to be removed from the bottom of the first stage compartment after a period of time. Table 5 lists the average influent concentrations of nutrient fed to the RBC system. This average concentration data was used for model calibration and steady-state simulations.

Table 5 Average influent concentrations of nutrients into the RBC set-up I
(Ref. A. Blank, 2006)

Component	Average influent concentration	Range	Unit	Temp. (°C)
COD, filtered:	215.0	170.0-260.0	$gCOD/m^3$	25/30
NH_4-N :	45.0	36.0-54.0	gN/m^3	
NO_3-N :	0.7	0.5-1.5	gN/m^3	
DO in bulk (Stage-I):	1.1	0.7-1.3	gO_2/m^3	
HCO_3:	6.0	4.5-6.0	mol/m^3	

The inoculum needed to seed the RBC discs for biofilm growth was obtained from municipal sewage sludge. The synthetic wastewater was mainly composed of molasses and was nearly 90-95% biodegradable. The effluent from the RBC was clarified using a secondary clarifier at the end of the treatment process. Figure 15 displays the laboratory-scale set-up in operation (Set-up-I) with thick biofilm in the initial stage, while it was thinner in the second and third stages of the RBC.

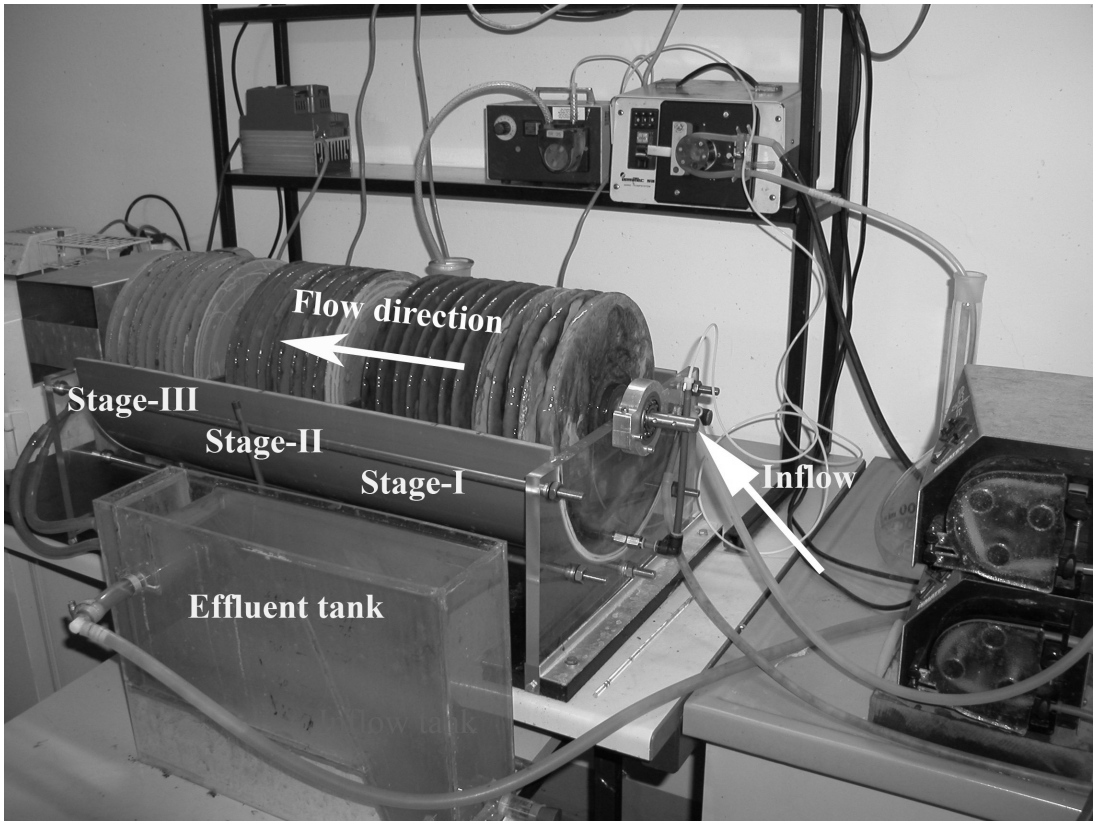

Figure 15 Picture of the 3-stage laboratory-scale experiment of RBC (set-up I)
(Courtesy: A. Blank, IWG, University of Karlsruhe (TH))

The experiments were conducted in climate chamber with controlled ambient temperature. The selected temperature ranges were all in the mesophilic zone. At the beginning of the experiments in the first phase, the inoculum was administered at around 20°C. Once the biofilm was formed on the disc surface, temperature was adjusted to 25°C in the climate chamber. The measurements were taken from September 2005 to December 2005. In the second phase beginning January 2006, the temperature was increased to 30°C. The relative humidity in the experiments was maintained at 70% in both the phases.

Table 6 shows the measured influent and effluent concentrations in the laboratory set-up-I over a period of 9 months during the above two phases. This data was used in the simulations. Although the nutrient concentrations varied over time, the flow rate was nearly constant in the experiments. It is third phase, it is planned to increase the temperature up to 35°C and observe the performance of the system. RBC operation at higher mesophilic temperatures has not been studied in much detail for nitrification and denitrification processes so far. Although the experiments are still continuing, the mathematical model based on the above experimental configuration helps to analyse and predict the results under varied physical boundary conditions.

Table 6 Measured influent and effluent concentrations in the RBC set-up I in first and second phases

Date	S_{O_2} in	S_{O_2} out	S_COD in	S_COD out	S_{NH_4} in	S_{NH_4} out	S_{NO_3} in	S_{NO_3} out	S_ALK in	S_ALK out
	[mg/l]	mg/l	[mg/l]	[mg/l]	[mg/l]	[mg/l]	[mg/l]	[mg/l]	[mmol/l]	[mg/l]
T = 25°C	Phase -I									
01.09.2005	1,10	6,20	215,00	17,93	45,00	7,64	0,70	32,63	6,00	1,60
28.09.2005	1,10		184,00	12,40	44,80	1,19	0,13	32,10	6,10	1,58
30.09.2005		6,20	215,00	19,10	43,30	2,86	0,27	36,00		
04.10.2005	1,30	6,18	200,00	6,78	43,50	4,78	0,24	35,80	6,00	1,61
24.10.2005	1,10	6,25	200,00	5,20	45,70	3,38	1,69	35,50	6,10	1,60
31.10.2005	1,10		211,00	22,50	41,90	6,27	0,18	35,00		
07.11.2005	0,90	6,20	120,00	5,20	36,50	1,08	0,17	26,30	6,12	1,60
14.11.2005	1,10	6,10	185,00	16,80	43,50	4,78	0,60	38,20	6,00	1,62
24.11.2005			151,00	15,70	51,30	9,38	0,19	35,63		
28.11.2005	1,10	6,23	220,00	45,70	59,00	12,80	1,69	35,80	6,00	1,60
02.12.2005			182,00	23,50	53,40	12,40	0,32	28,40	5,98	1,59
05.12.2005			146,00	11,40	53,30	9,50	0,22	26,70		1,60
12.12.2005	1,10	6,20	187,00	19,10	51,20	8,70	0,20	25,40	6,00	
19.12.2005			184,00	25,20	51,96	17,29	0,21	26,80	6,15	1,70
27.12.2005	1,10	6,10	186,00	22,50	56,20	12,50	0,26	39,20	6,00	1,60
T = 30°C	Phase -II									
01.01.2006	1,61	1,80	231,74	19,12	43,11	8,15	0,68	26,89	5,85	1,40
09.02.2006	0,98	2,83	201,00	20,10	32,61	6,83	0,19	31,50		1,40
13.02.2006	2,01		176,00	14,70	28,60	11,73	0,22	15,80	5,85	1,40
15.02.2006	1,92	4,20	210,00	13,70	28,60	1,57	1,31	3,68	5,85	1,45
17.02.2006	1,93	2,32	245,00	14,30	28,50	9,89	1,48	27,50	5,85	1,40
20.02.2006	2,23	2,23	165,00	18,80	45,20	13,95	0,20	33,50		
22.02.2006	2,33	0,56	190,00	17,80	44,13	5,82	0,23	33,80	5,85	1,45
24.02.2006	2,42	0,29	185,00	20,60	51,00	13,31	0,12	31,60	5,80	1,40
06.03.2006	2,43	1,23	447,00	19,40	41,10	12,20	0,26	33,90		1,40
17.03.2006	0,95	2,93	249,00	26,80	53,20	15,20	0,21	24,10	5,85	1,40
21.03.2006	1,23		263,00	27,40	42,00	13,00	0,69	31,80	5,85	
24.03.2006	0,98	2,22	249,00	18,30	48,50	5,65	0,15	22,30		1,40
27.03.2006	2,08	0,92	206,00	20,10	59,70	5,27	2,86	25,54	5,85	1,40
30.03.2006	2,23	1,98	258,00	19,20	46,80	5,87	1,26	25,30	5,85	1,40
04.04.2006	0,98	0,63	213,00	22,70	46,60	5,26	0,62	31,00	5,85	1,35
10.04.2006	1,35		258,00	19,50	48,70	1,92	1,88	26,40	5,90	1,40
17.04.2006	1,14		210,00	14,40	43,11		0,68		5,85	1,25
21.04.2006	0,98		235,00	23,20	43,60	1,19	0,14	28,50	5,85	1,40
27.04.2006	0,90	1,83	187,00	12,00	48,70	8,90	0,24	29,60		1,40
02.05.2006	1,46	1,46	256,00	20,20	38,50	9,20	0,20	28,20	5,85	1,40

(Ref. A. Blank, 2006)

Flat discs have been used for reasons of economy. It is also observed that such discs allow thin biofilm thereby reducing the weight on the load bearing shaft. Another alternative would have been corrugated surface discs. The removal efficiency has been observed to remain steady with about 95% removal of soluble organic substrate and above 90% removal of ammonia-nitrogen under the given influent loading conditions (Table 5). Although the first stage has a typically higher biofilm thickness of the order of 0.6 to 1.5 mm on average due to high nutrient loading rates, it gradually decreases in the later stages (Figure 15).

5 Physical oxygen transfer model

5.1 Principle

5.1.1 Physical oxygen transfer across the boundary layer

In fixed film processes like RBC, the mass transfer phenomenon plays an important role in system performance in addition to biological reaction kinetics. These transfer aspects associated with both the liquid phase as well as biofilm result in concentration gradients from bulk liquid to reaction sites and normally control the system performance. Aeration is one of the important aspects in design of a RBC system. Oxygen mass transfer from air to the RBC unit occurs in nature in two ways: oxygen transfer to the liquid film that adheres to the biofilm surface when the disc is exposed to air; direct oxygen transfer into the bulk liquid at the air-water interface due to the turbulence generated by the rotating movement of the disc (Rittmann et al 1983, Lim et al. 1980). In addition, oxygen transfer can be initiated by air drive modes such as surface aerators or diffused air aerators.

The index for measurement of the oxygen transfer capacity in any system is the physical oxygen mass transfer coefficient K_L (Bintanja et al. 1975). It represents the velocity at which oxygen is transferred into the system across the gas-liquid boundary. For biofilms, K_L value is guided by the oxygen diffusivity coefficient D, thickness of laminar boundary layer and uptake rate by the micro-organisms in the biofilm. However, in purely physical oxygen transfer study, uptake rate is zero as no biofilm is present and diffusion phenomenon becomes the driving criteria. In case of RBCs, K_L depends upon a number of other physical factors such as rotational speed (exposure time), liquid film thickness, temperature and concentration gradient as highlighted in Figure 16 below.

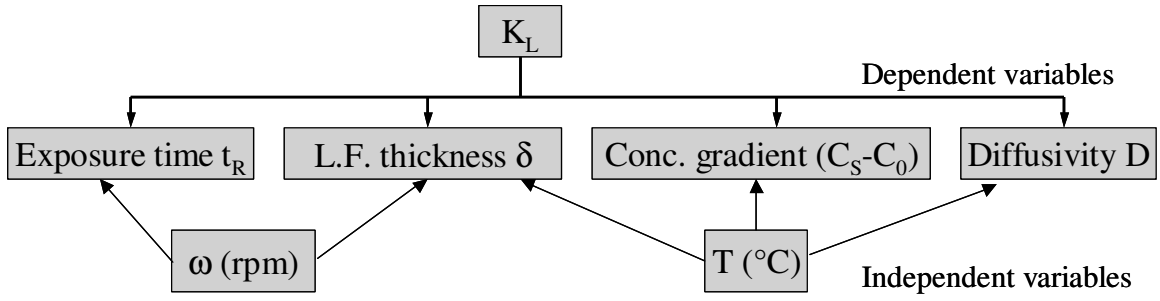

Figure 16 Physical factors affecting oxygen transfer coefficient K_L in RBCs

A number of studies have been undertaken concerning gas-liquid diffusion processes since 1950s. Yamane and Yoshida (1972) were one of the earliest to investigate the characteristics of physical mass transfer across the boundary layer in RBCs. The elementary mathematical

equation for mass transfer of oxygen by diffusion into the thin liquid film developed over a flat rotating plate is dependent on time and space co-ordinates. Diffusion equation for concentration distribution of oxygen in a liquid film (Crank, 1955) is as follows.

$$\frac{\partial C}{\partial t} = D\frac{\partial^2 C}{\partial x^2} \tag{5.1}$$

With initial condition: at t = 0, $0 < x < \delta$, $C = C_0$;

and boundary conditions:

at t > 0 and x = 0 (air-liquid boundary surface), $C = C_S$;

at t > 0 and $x = \delta$ (media support), oxygen flux $(\partial C / \partial x) = 0$

where

δ Thickness of the liquid film boundary layer [L]

D Diffusivity coefficient of oxygen in liquid film i.e. water [L^2T^{-1}]

C Concentration of dissolved oxygen in the liquid film [ML^{-3}]

C_0 Initial concentration of oxygen in liquid film [ML^{-3}]

C_S Saturation concentration of oxygen in air [ML^{-3}]

x Space coordinate from surface (x = 0) [L]

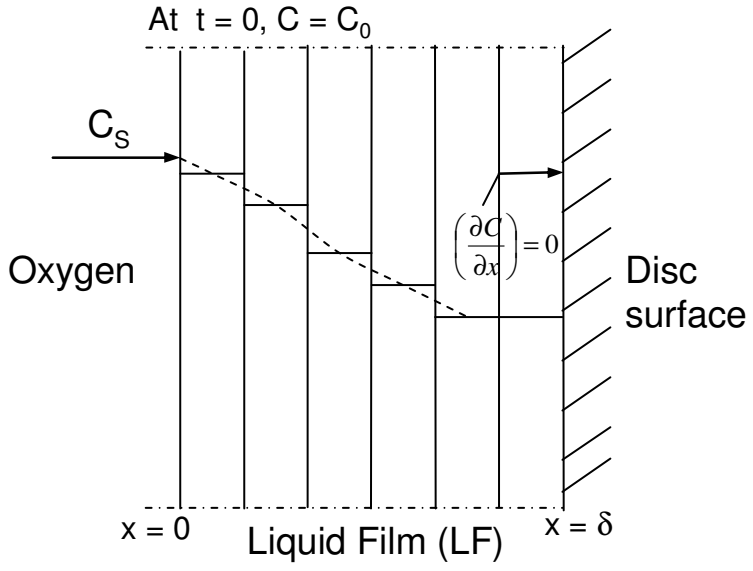

Figure 17 Schematic diagram of oxygen diffusion into the liquid film (boundary layer)

Figure 17 shows the schematic representation of oxygen diffusion across the air-liquid boundary. The time-dependent flux of the solute (oxygen) at the boundary layer surface (i.e. x = 0) is given by equation 5.2 below (Yamane and Yoshida, 1972).

$$N_t = -D\left(\frac{\partial C}{\partial x}\right)_{x=0} \tag{5.2}$$

The oxygen transfer coefficient may be calculated using equation 5.3.

$$K_L = \frac{\left|\overline{N_t}\right|}{(C_S - C_0)} \tag{5.3}$$

where

$$\overline{N_t} = \frac{\int_0^{t_R} N_t\, dt}{\int_0^{t_R} dt} \tag{5.4}$$

N_t Oxygen flux through the boundary layer [$ML^{-2}T^{-1}$]

K_L Oxygen transfer coefficient from air to liquid film [LT^{-1}]

t_R Time of exposure of the liquid film in air [T]

$\overline{N_t}$ Time averaged flux of oxygen into liquid film over time interval t_R [$ML^{-2}T^{-1}$]

Yamane and Yoshida (1972) obtained the approximate solution of the above equations based on some assumptions. The basic assumptions were that the velocity of rotation of the liquid film remained same as that of the rotating disc and there was complete mixing of the liquid film into the bulk liquid once the disc re-enters the trough. Another important assumption was that the thickness of the liquid film entrained over the disc surface is uniform throughout the air-liquid mass transfer phase. These assumptions were valid for relatively high velocities of rotation with depths of immersion equal to that of the radius of the disc. Based on these assumptions, the oxygen transfer coefficient K_L was obtained from the solution of equation (5.3) and (5.4) as follows:

$$K_L = 2\sqrt{\frac{D}{\pi . t_R}}\left[1 + 2\sqrt{\pi}\sum_{n=1}^{\infty}(-1)^n \, ierfc\left(\frac{n.\delta}{\sqrt{D.t_R}}\right)\right] \tag{5.5}$$

Yamane and Yoshida (1972) found by graphical representation that the above equation is reduced to Higbie's equation (Higbie, 1935) as shown in expression (5.6).

$$K_L = 2\sqrt{\frac{D}{\pi . t_R}} \quad \text{when} \quad \frac{\delta}{\sqrt{D.t_R}} \geq 1.7 \tag{5.6}$$

The parameter $K_L / 2\sqrt{D/\pi.t_R}$ can be stated as a dimensionless mass transfer coefficient K_h, whereas $\delta / \sqrt{D.t_R}$ is a measure of the film thickness against the depth of penetration of oxygen by diffusion. It becomes evident from Yamane and Yoshida's theoretical model that

for high velocities of rotation (i.e. when t_R is small or $\delta / \sqrt{D.t_R} \geq 1.7$), the penetration model of Higbie remains valid since $K_L / 2\sqrt{D/\pi.t_R} \cong 1$ from the graphical plots. In other words, for high values of rotational speed ω, the depth of penetration of oxygen from air into the film during a revolution of the disc is small compared with the film thickness δ. This model held good resonance with experimental values of K_L for mean contact times (t_R) between 0.2 to 1.5 sec. The experiments were conducted using 80mm diameter PVC plates and 12mm diameter shaft at 40% disc submergence and a temperature of 30°C (Yamane et al. 1972). The oxygen concentration was measured from the liquid in the trough using oxygen electrode. For lower velocities of rotation, however, the Higbie's equation was no longer valid since the water film on the disc is saturated with oxygen from air due to longer contact time. Consequently, the assumption that the thickness of the liquid film was infinite compared to the depth of penetration of oxygen into the film was no longer valid. Moreover, the liquid film thickness δ and the diffusion coefficient of oxygen in water D were approximated in their model.

Bintanja et al. (1975) improved this model by deriving the K_L value for lower rotational velocities from graphical plots based on their experimental results. They used 10 numbers of 60cm diameter discs with a submergence ratio of 24% and a temperature of 17°C. Oxygen concentrations were measured from the trough liquid using Beckmann-Process Analyser. The result is expressed in equation (5.7) below.

$$K_L = \frac{\delta}{t_R} \text{ when } \frac{\delta}{\sqrt{D.t_R}} \leq 0.8 \tag{5.7}$$

Zeevalkink et al (1979) made further investigations on gas-liquid mass transfer with varying depths of immersion of the discs in water at different rotational velocities of the disc. They made further contribution to the determination of K_L values for intermediate ranges of rotational speed ω as expressed below.

$$K_L = 2\sqrt{\frac{D}{\pi.t_R}}\left[1 - 4.21\exp(-3.2\frac{\delta}{\sqrt{D.t_R}})\right] \text{ when } 0.8 \leq \frac{\delta}{\sqrt{D.t_R}} \leq 1.7 \tag{5.8}$$

Their experimental set-up consisted of 10 numbers of 60cm diameter dics with varying submergence ratio at a temperature of 20°C. The experiments confirmed the findings of Bintanja et al. for lower velocities of rotation. However, the explanations provided by Bintanja regarding the governing principle behind the lower values of K_L measured when compared to the theoretical ones were questioned. It was reasoned that when the film layer became saturated with each revolution for lower values of rotational speed (i.e.

when $\delta \leq 0.8\sqrt{D.t_R}$), too low values of K_L could not be possibly caused due to the somewhat lower velocity of rotation of the film compared to the rotating disc. Moreover, at lower values of rotational speed, the film thickness δ would not be expected to vary substantially across the disc surface. The probable explanation for this deviation from experimental results was cited to be incomplete mixing of the liquid film into the bulk liquid after the disc enters the trough during each revolution. This is due to the development of a submerged boundary layer adjacent to the disc surface when the disc is rotating under water. The effect of incomplete mixing is greater with decreasing immersion depth (R-H) because of the decreasing time of contact between the water film and the bulk liquid in the trough. This incomplete mixing explains why at very low as well as at high rotational velocities, the measured K_L values tend to approach the values predicted from theoretical model. At substantial low values of ω (say $\delta / \sqrt{D.t_R} \leq 0.5$), there is increased contact time between the water in the film and the water in the trough, consequently resulting in the anticipated K_L values. At high values of ω where Higbie's equation is valid (equation 5.6), oxygen penetrates only up to the surface layers of the liquid film, so that incomplete mixing has not any significant effect on the K_L value. The major discrepancy between theory and experimental value remains in the intermediate rotational velocities (when $\delta / \sqrt{D.t_R}$ is between 0.8 to 1.7 approximately) where the consequence of incomplete mixing is dominant. For this range, Zeevalkink introduced an empirical solution for determination of K_L value based on $\delta / \sqrt{D.t_R}$ and immersion factor I, through least squares regression analysis on his experimental data as expressed below.

$$K_L = 0.4\sqrt{\frac{D}{\pi.t_R}}\left(\frac{R-H}{R}\right)^{0.4}\left[2+\left(\frac{\delta}{\sqrt{D.t_R}}\right)^2\right] \text{ when } \frac{K_L}{2\sqrt{D/\pi t_r}} < 0.90 \qquad (5.9)$$

where

R Radius of disc [L]

H Distance between water surface and centre of the shaft [L]

$\frac{R-H}{R}$ Immersion factor, I

The formulation for the boundary layer in the submerged disc was theoretically introduced by Suga and Boongorsrang (1984). This boundary layer formation resulted in incomplete mixing of the liquid film into the bulk liquid in the trough during the submerged phase. Suga et al. proposed different values of K_L for the states when the disc was exposed and during submerged condition based on thickness of the respective boundary layer.

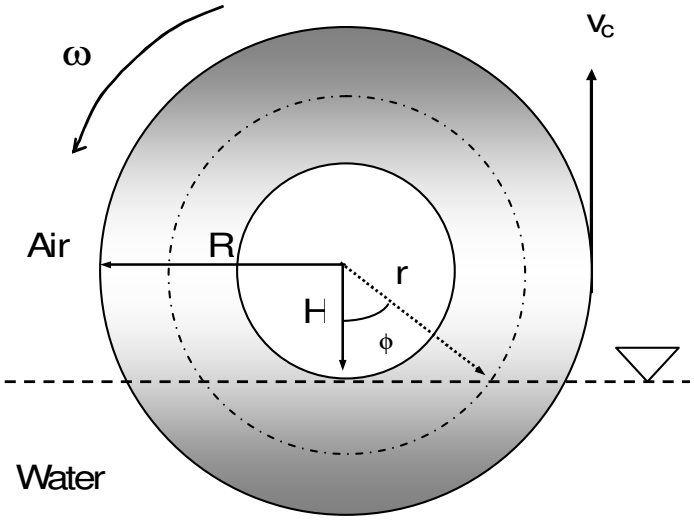

Figure 18 Schematic diagram of RBC disc in water

The mass-balance equation for oxygen transfer was modified to accommodate additional oxygen transfer across the free surface of liquid in the trough from atmosphere. A term for continuous inflow of water into the trough and also for boundary layer oxygen transfer at steady state during the submerged condition of the disc had been introduced. It was assumed that the difference in the volume of liquid entrained on the disc surface when exposed to air and that when submerged was mixed completely at every revolution of the disc. Although this model was an improvement over the previous models, the basic assumption of uniform film thickness δ over the disc surface during exposed state still remained. Not much work has followed since then for improvement of the mathematical model for mass transfer of oxygen over the air-liquid interface. Some empirical models have been developed for determination of K_L through dimensional analysis methods and experimental data regression analysis.

The empirical model derived by Boumansour and Vasel (1997) based on Sant'Anna's model (1980) came closest to the experimental values of most authors. It established a relation between Sherwood's number Sh, Reynolds's number R_e, Froude's number Fr and the Immersion factor I.

$$Sh = 2.673\ (R_e)^{0.769}\ (Fr)^{0.135}\ (I)^{0.865} \qquad (R^2 = 0.97) \tag{5.10}$$

In terms of K_L, equation (5.10) may be expressed as follows.

$$\frac{K_L.d}{D} = 2.673\left[\frac{n.d^2}{\upsilon}\right]^{0.769}\left[\frac{n^2.d}{g}\right]^{0.135}\left[\frac{R-H}{R}\right]^{0.865} \tag{5.11}$$

where

d Diameter of the disc, i.e. 2R [L]

υ Kinematic viscosity of liquid [L^2T^{-1}]

ω Rotational speed in revolutions per minute [rpm]

n Rotational speed [T^{-1}]; n = ω/60

This dimensional model for evaluation of oxygen transfer in the RBC system depends on physical properties like coefficient of molecular gas diffusion in the liquid, physical properties of the liquid and dynamic factors characterising the turbulence effects in the system. The turbulence effects near the interface are created as a result of the rotational movement of the discs, distance from the axis of the disc and the immersion factor. However, no dependence of K_L on the film thickness δ has emerged here. Therefore, the above dimensional model remains true when $\delta / \sqrt{D.t_R} \geq 1.7$, i.e. for higher velocities of rotation. For intermediate range of rotational velocities, the film thickness δ influences the oxygen transfer coefficient value to a substantial extent as reflected in equation (5.9).

Nevertheless, it is best to avoid using the above empirical formulations including error functions since they are based on many assumptions and generalisations. With the use of numerical modelling, the theoretical partial derivative equation for diffusion, i.e. expression (5.1) can be solved through spatial discretization of the boundary layer. In the current physical oxygen transfer model, the solution to the diffusion equation is obtained numerically by dividing the liquid film into a number of layers and applying the boundary conditions. However, to obtain a solution, it becomes necessary to estimate the thickness of the liquid film as well as time of exposure (t_R) of the liquid film in air when exact experimental data is not available. The K_L value can be easily obtained using equation (5.3) provided C_S is known at a given temperature and $\overline{N_t}$ is obtained from equations (5.2) and (5.4) for a given value of t_R and δ.

5.1.2 Estimation of boundary layer thickness and exposure time

Liquid film thickness

The flat plate withdrawal theory (Groenveld, 1970) states that withdrawal of a smooth infinitely long flat plate from a liquid with a velocity v results in an adhering film of thickness δ which can be calculated as a function of the effects of gravity, withdrawal velocity and physical properties of the fluid. This may be expressed as follows:

$$\delta = k\left(\frac{\eta.v}{\rho.g}\right)^{1/2} \tag{5.12}$$

where

η Dynamic viscosity of water [$ML^{-1}T^{-1}$]

v Velocity of withdrawal of a flat plate from liquid [LT^{-1}]

ρ Density of water [ML^{-3}]

g Acceleration due to gravity [LT^{-2}]

Bintanja et al. (1975) gave a value for constant k as 0.93 and expressed the withdrawal velocity in terms of rotational velocity (i.e.v = rω). However, the theoretical values predicted by equation (5.7) were not in good agreement with the experiments conducted by Bintanja for lower values of ω. This was argued to be the consequence of lower average velocity of rotation of the film compared to the rotating disc. K_L values in this case is directly dependent on the actual film thickness δ. Zeevalkink et al. (1978) made an independent study and obtained a theoretical derivation for the film thickness δ on rotating discs based on the flat plate withdrawal theory of Groenveld (1970). He related δ to be a function of the rotational velocity as well as depth of immersion in addition to the forces of gravity and viscosity at a given temperature. This is expressed in equation (5.13) and (5.14).

$$\delta = \frac{4\sqrt{2}}{15}\left(\frac{\eta.v_C}{\rho.g}\right)^{1/2} \tag{5.13}$$

where

$$v_C = \omega\sqrt{\left(R^2 - H^2\right)} \tag{5.14}$$

v_C Vertical component of the peripheral velocity v at the point of emergence of disc from the liquid surface in the trough [LT^{-1}]

The above formula showed good correlation with their experimental results under different rotational velocities and depth of immersion. It also fitted the experimental data reported by Bintanja et al. with a correlation coefficient of 0.99. Therefore, equation (5.13) has been used for the theoretical calculation of average δ values over the exposed disc surface in the model.

Submerged boundary layer thickness

Boundary layer transfer from the submerged disc to the water in the trough is a function of temperature, viscosity of liquid, rotational velocity and the boundary layer thickness. For laminar interfaces, the oxygen transfer coefficient in the boundary layer is given by the relation [Bird 1960].

$$K_L' = \frac{D}{\delta_b} \tag{5.15}$$

where

δ_b Average submerged boundary layer thickness [L]

K_L' Oxygen transfer coefficient in the submerged boundary layer [LT^{-1}]

Schlichting (1960) and Bird (1960) [both authors cited by Zeevalkink et al. 1978] developed a correlation for determination of submerged boundary layer concentration thickness δ_b for a plate travelling a distance x under water with a tip velocity v_c as given below.

$$\delta_b = 5(Re)^{1/2} S_c^{-1/3} \tag{5.16}$$

where

S_c Schmidt number, v/D

Re Reynolds number, $\frac{vx}{\nu_c}$

In case of rotating discs, equation (5.16) is modified as shown by Suga and Boongorsrang (1984) as shown below.

$$\delta_b = 5\left(\frac{v.r(2\phi)}{\omega.r}\right)^{1/2} S_c^{-1/3} \tag{5.17}$$

where

r Distance of any point on the disc from the centre as shown in Figure 18 [L]

ϕ Angle subtended for a distinct depth of immersion as shown in Figure 18 [radian]

Integrating equation (5.17) over the submerged disc area and dividing it by this area would yield the average δ_b at a given rotational velocity. It is shown in equation (5.18).

$$\overline{\delta_b} = \frac{5\sqrt{2}}{\pi R^2\left(\frac{\phi}{\pi}\right)} S_c^{-1/3} \int_{r=H}^{R} \int_{\phi=0}^{\cos^{-1}\left(\frac{H}{R}\right)} \left(\frac{V}{2\pi\varpi}\right)^{1/2} (r.dr)(\theta^{1/2}.d\theta) \tag{5.18}$$

where

θ Any angle between $\phi = 0$ to $\phi = \cos^{-1}(H/R)$ [rad]

The submerged boundary layer thickness is basically governed by physical properties of the liquid in motion such as Reynolds number and Schmidt number. It has been observed in experiments that δ_b is generally greater than the film thickness δ on the exposed disc surface (Zeevalkink et al. 1978). Therefore, a portion of the boundary layer mixes with the bulk liquid as the disc emerges out from the trough. Similarly, the liquid film entrained on the exposed disc surface is only partially mixed with the bulk liquid in the trough through the boundary layer that re-forms over the submerged disc surface. This partial mixing is again dependent upon the temperature, viscosity of the liquid and rotational speed. Since direct

transfer into the bulk is comparatively less, so it can be inferred that the oxygen transfer coefficient will be less when measured in the trough than that on the exposed liquid film surface. Most experimental studies on determination of K_L values in rotating discs have so far been carried out with physical oxygen concentration measurements in the trough. However, from the point of view of actual oxygen transfer to the system, the coefficient values on the liquid film boundary layer seem to be of primary importance. The current study is reinforced by actual measurement of δ formed on the disc surface (Blank, 2006).

Exposure time

The exposure time at any point on the ring element of the exposed liquid film (Figure 18) at a distance r from the shaft centre may be calculated using equation (5.19), based upon the dimensions of the disc.

$$t_R = \frac{1}{\omega}\left(1 - \frac{1}{\pi}\cos^{-1}\left(\frac{H}{r}\right)\right) \tag{5.19}$$

Bintanja et al. (1975) estimated the average contact time for the whole surface area of the disc by an approximate expression based upon the values of H, R and the rotational velocity ω. For high rotational velocities, the expression is as shown in equation 5.20 below:

$$\overline{t_R} = \frac{1}{\omega}\frac{\left(P_0 - \frac{1}{\pi}P_1\right)^2}{\left(P_0 - \frac{P_1}{2\pi} - \frac{P_2}{8\pi^2} - .....\right)^2} \tag{5.20}$$

where

$\overline{t_R}$ Average time of exposure of the liquid film in air [T]

$$P_0 = \int_H^R r dr = \frac{1}{2}\left(R^2 - H^2\right)$$

$$P_1 = \int_H^R r\cos^{-1}\left(\frac{H}{r}\right)dr = \frac{1}{2}R^2\cos^{-1}\left(\frac{H}{R}\right) - \frac{1}{2}RH\sqrt{1-\left(\frac{H}{R}\right)^2}$$

$$P_2 = \int_H^R r\cos^{-2}\left(\frac{H}{r}\right)dr = \frac{1}{2}R^2\cos^{-2}\left(\frac{H}{R}\right) - RH\sqrt{1-\left(\frac{H}{R}\right)^2}.\cos^{-1}\left(\frac{H}{R}\right) - H^2 ln\left(\frac{H}{R}\right)$$

In case of low rotational velocities, i.e. for large contact times, the above equation is simplified by Bintanja to be as follows:

$$\overline{t_R} = \frac{1}{\omega}\left(\frac{P_0 - \frac{1}{\pi}P_1}{P_0}\right) \tag{5.21}$$

Both the equations 5.20 and 5.21 represent a common form as shown below:

$$\overline{t_R} = \frac{1}{\omega} P \tag{5.22}$$

For the current experimental set-up, using the values of H and R as given in section 4.2, the value of P calculated using the above relations yield 0.583 for large values of ω and 0.591 for small values of ω respectively. Thus, the average contact time may be taken as follows:

$$\overline{t_R} = \frac{0.587}{\omega} \tag{5.23}$$

In the model, the contact time has been calculated using equation (5.19) for different points on the disc surface at different exposure levels. For an average value over the whole surface area of the disc, expression (5.23) has been used.

5.2 Results of oxygen transfer at constant temperature

5.2.1 Theoretical estimation of K_L and comparison with experiment

In order to study and compare the theoretical predictions made by previous researchers so far, the empirical formulations for determination of liquid film thickness and K_L value of oxygen on the exposed disc surface is applied to the experimental set-up described in section 4.2. The expressions in equation (5.13) and (5.14) given by Zeevalkink et al. (1978) have been used for calculation of average liquid thickness at different radial distances on the exposed disc surface. The calculations have been made at rotational speeds of 20, 30 and 40 rpm. For determination of average oxygen transfer coefficient values at different radial distances, the $\delta / \sqrt{D.t_R}$ value is used as the criteria for selection among the equations (5.6), (5.7) and (5.8). Figure 19 illustrates the theoretical values of liquid film thickness and the calculated K_L values at different radial distances of the 12.5cm radius disc mounted on a cylindrical shaft of 2.5cm radius. It may be noted that equations (5.13) and (5.14) give only the average δ values at different radial distances r from the disc centre based on the vertical component of the peripheral velocity at the point of emergence. It can be inferred from Figure 19(a) that the average water film thickness increases with increase of angular velocity. Simultaneously, the average thickness tends to increase over the radius of the disc from centre towards the rim due to the increase of the peripheral velocity. However, the theoretical predictions for average δ should be considered only for a certain range of rotational velocity and disc diameter. Figure 19(b) predicts that with the increase of angular velocity, the K_L value should rise. This is an effect of the increasing liquid film thickness. There is a gradual increase of K_L along the surface of the disc from centre towards the periphery.

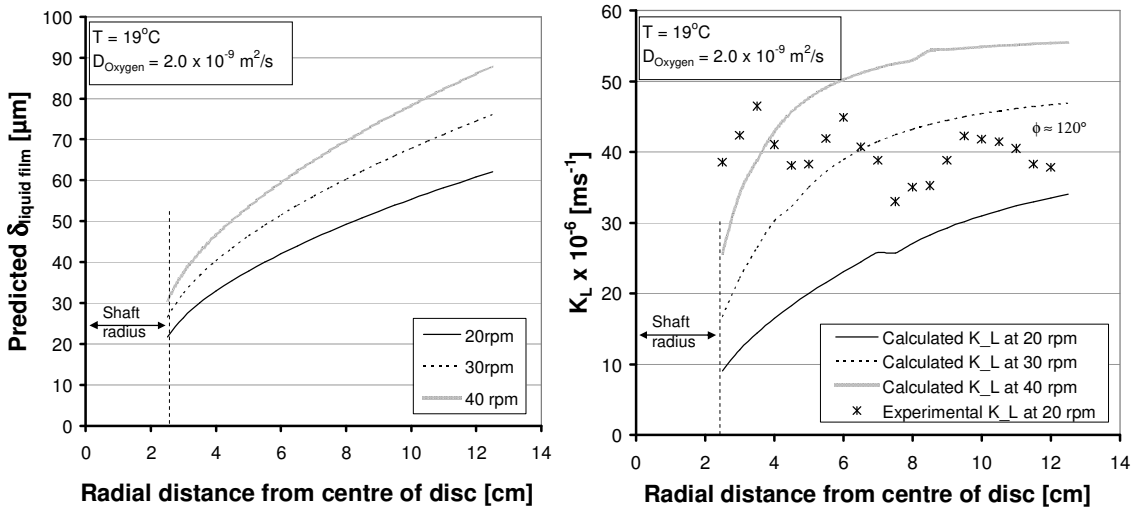

Figure 19 Theoretical determination of liquid film thickness and K_L value

The cause can be attributed to the increase in the peripheral velocity with increasing radius from the centre. The K_L plots reflect a similar trend with δ and the initial slopes of the curves look alike. However, at higher angular velocities or radial distances, the dependence of K_L on film thickness decreases and it tends to approach a constant value based on Higbie's equation (5.6). The graphs reveal a similar trend with the works of Zeevalkink et al. (1978) and Suga and Boongorsrang (1984). The experimental determination of K_L value at a given temperature is given by equation (5.24).

$$K_L = \frac{1}{t_R} \ln\left(\frac{C_S - C_0}{C_S - C_t}\right)\left(\frac{V}{A}\right) \qquad (5.24)$$

where

C_t Concentration of oxygen in liquid film after time t [ML^{-3}]

For a given temperature, when the C_t value at a given point on the liquid film surface is known from experimental measurements, K_L value may be easily determined from the δ at that point. In the current case, comparison with the experimentally determined K_L values obtained at an angular velocity of 20 rpm and an angular disposition of $\phi \approx 120^\circ$ shows that the K_L values get lower towards the periphery of the disc. This effect is more pronounced as the disc rises further from the water surface. It is observed that for higher values of angular disposition (ϕ), the water film thickness is less affected by the centrifugal and viscous forces. The effect of gravity tends to dominate in such situations and there is shearing off of the film from the disc surface near the top. This cascading effect of the film causes less thickness near the top. However, at very low rotational velocity (ω<5rpm), the viscous forces are more predominant and may effect less variation in film thickness over the disc surface. Again, larger disc diameters during scale-up operation would show less shearing

effect due to high peripheral velocities (centrifugal force) at the rim. Thus, the determination of average δ by equation (5.13) holds true only within a range of rotational velocity and disc diameter. Zeevalkink used this formula for his experiments with rotational velocity between 5-30 rpm and disc diameter of 60cm. Bintanja had earlier used a similar expression (5.12) for average δ for rotational velocities between 7.5-35rpm using same disc diameter. Therefore, it is best to determine the exact film thickness at a given position of the disc experimentally. This value could be used in the numerical model to determine the K_L value at that point on the disc. The t_R value may be calculated at a given position using equation (5.19).

5.2.2 Determination of K_L by numerical modelling

5.2.2.1 Characterisation of K_L variation over liquid film with disc position

Simulations have been conducted for the determination of K_L values at some specified locations of the disc surface based on experimentally determined values of δ at these spots. The purpose of these runs is to reflect the non-uniformity of the K_L values on the disc surface. For any point at a distance r_p' from the shaft centre on the emerged disc surface, the contact time is calculated based upon the ϕ and the α values. Using the experimental axes measurements r_p (x-axis) and H´ (y-axis) as shown by the schematic representation in Figure 20 below, r_p' and α can be calculated. Depending upon which section the point is located and knowing the rotational speed ω, the exposure time t_R at the point is thereby calculated using equation (5.19).

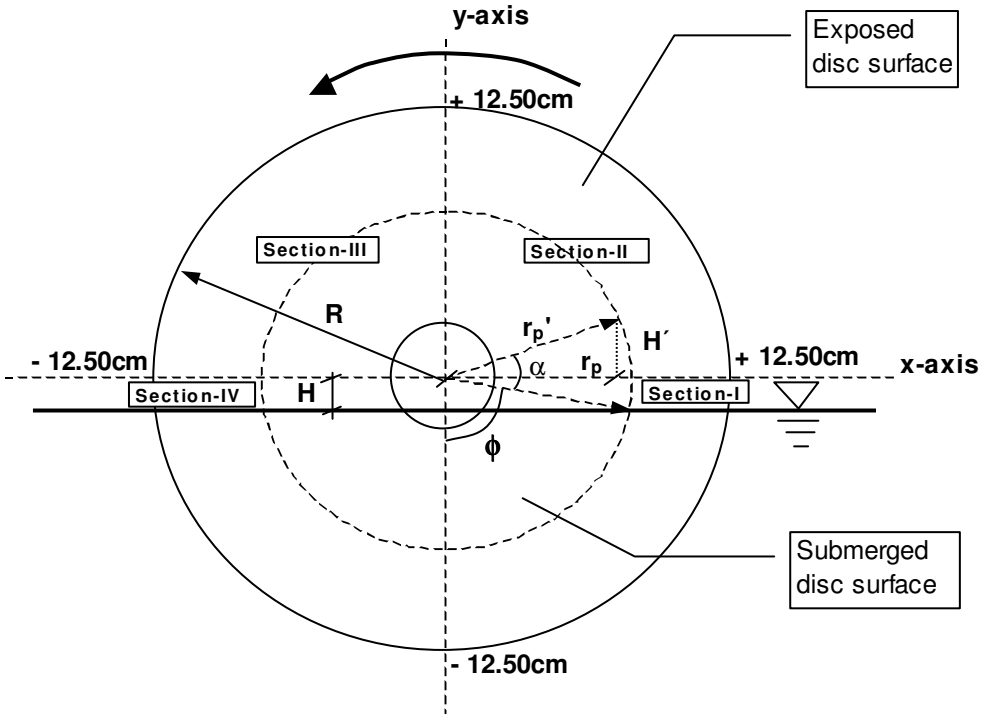

Figure 20 Schematic representation of disc surface for calculation of exposure time at any location

The simulation results have been obtained by numerically solving the diffusion equation (5.1) under the given boundary conditions (δ, t_R, C_S, C_0 and D values). Figure 21 shows the typical characteristic of the oxygen transfer coefficient simulated at different radial positions of the disc based on the experimentally measured values of film thickness for a rotational velocity of 20 rpm. Although the disc radius is 12.5cm, only a part of the disc surface in x and y-axis has been displayed. The negative part of y-axis is not shown as it represents the submerged sector of the disc.

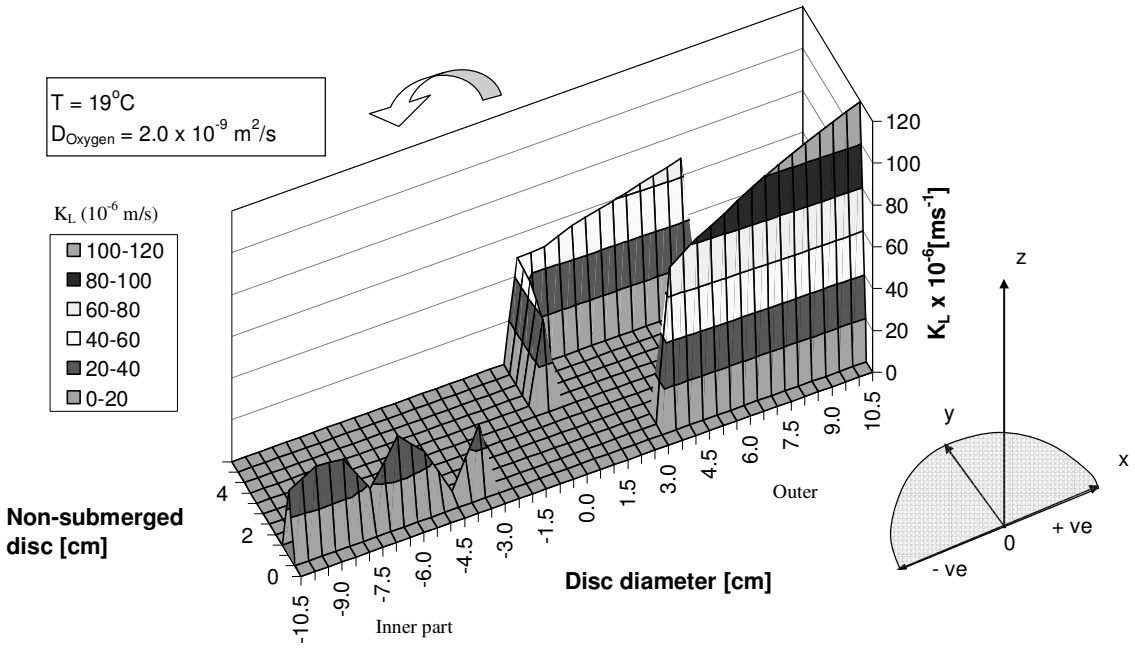

Figure 21 Sample display of variation of K_L on disc surface with position at 20 rpm

As the disc rotates from the positive side (outer part) to the negative side (inner part), K_L goes on decreasing with decrease in oxygen flux between the ambient air and the liquid film surface. This indicates that the oxygen concentration in the liquid film is approaching the saturation level. It is also being observed that the rate coefficient tends to increase towards the outer periphery from the center when emerging out from the liquid surface. This is because of increasing film thickness δ towards the outer periphery, which is again a function of the centrifugal forces acting at that point. It has been assumed that velocity of rotation of the liquid film is same as that of the disc. From the above plot, it transpires that the rate of oxygen transfer in the liquid film is discrete over the disc surface exposed to air as it revolves during each cycle. It is a function of the film thickness at a radial position and the time taken to reach that position from the water surface in the trough. The saturation concentration of oxygen in ambient air and the diffusion coefficient at a given temperature are important physical parameters controlling the rate of oxygen transfer into a given liquid.

As discussed in the theory section previously, the film thickness at a point on the disc depends upon the physical properties of the liquid, such as viscosity, specific gravity and surface tension, apart from the centrifugal force acting at that point. It is non-uniform over the disc surface and thereby affects the K_L value.

5.2.2.2 Characterisation of K_L value with δ, ω and H

Although the K_L value is non-uniform over the disc surface and varies with film thickness and radial position from the point of emergence, it is advantageous to calculate an average value for a given exposure time of the disc. This helps to correlate variation of K_L with other variable parameters. Therefore, for a given rotational velocity, the average time of exposure (t_R) has been calculated using the expression (5.23) of Bintanja et al. (1975) for the purpose of trend analysis. This t_R value has been subsequently used to determine K_L values at different film thickness by way of simulation. In Figure 22 (a), the variation of the K_L with liquid film thickness has been displayed at different rotational velocities. At a given rotational velocity, the oxygen transfer coefficient increases with increasing film thickness, but only up to a certain domain of film thickness. After that, it stabilizes and remains almost constant. For lower rotational speeds up to 10rpm, the significant film thickness value is about 100-120µm, while in case of higher rpm, this domain reduces to about 50-70µm. Overall, it can be inferred that at a given rotational velocity ω and average exposure time t_R, the oxygen transfer coefficient K_L does not enhance beyond a certain significant film thickness. This significant film depth value decreases as the rotational velocity increases. At high rotational velocities, the oxygen is not able to penetrate into the innermost layers of the film as the film depth is increased. Whereas at low rotational velocities, there is more exposure time to enable deeper penetration.

Moreover, increasing the rotational speed should increase the transfer coefficient since the exposure time of the disc to air gets reduced. This means that a higher flux is generated at a given point for the same film thickness because the time taken by the disc to reach that point is less (equation 5.24). Figure 22 (b) depicts this phenomenon more clearly. The above simulation plots are comparable with the trend of results shown by Yamane and Yoshida (1972) and Bintanja et al (1975). However, these authors measured the K_L values in the trough and not in the liquid film surface. In their case, the results were not very accurate for lower rotational speeds. When the liquid film thickness is small or the contact time is high, K_L value is significantly smaller than the value predicted by Higbie's model (equation 5.6). Higbie's equation relates the dependence of K_L value only on contact time and not film

thickness. This is true only at higher rotational speeds when the assumption that film thickness is virtually infinite compared with the depth of penetration of oxygen is justified.

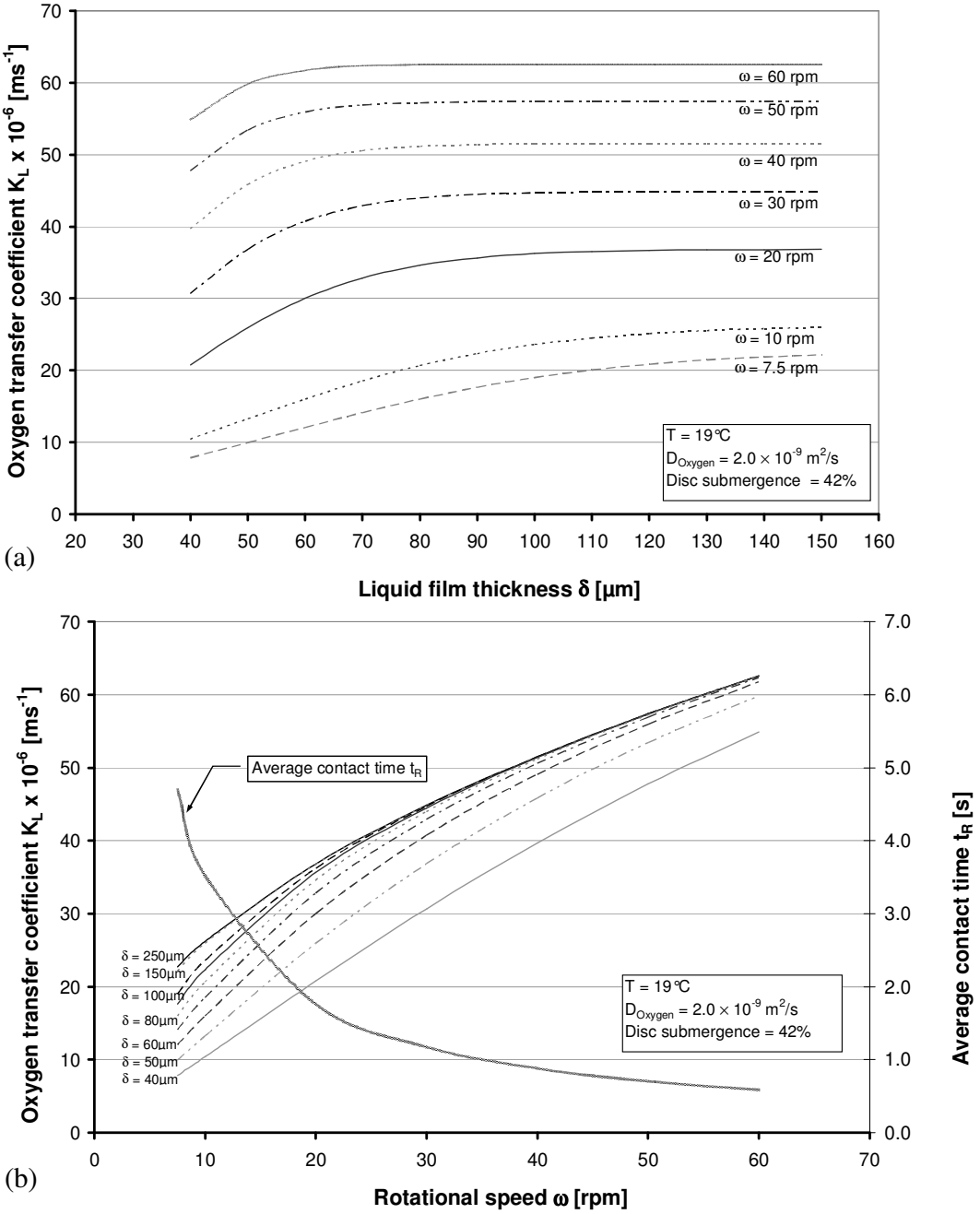

Figure 22 Variation of average K_L on disc surface with liquid film thickness and rotational speed

Figure 23 shows the oxygen transfer coefficient as a function of both velocity of rotation and submergence depth. For each submergence depth, the average liquid film thickness at a given rotation velocity is calculated using expression 5.13 while the average exposure time is determined using expression 5.22. The simulation results reveal that with the increase in the submergence depth, the average K_L value on the disc increases. The plots compare well with the theoretical and experimental results of Zeevalkink et al. (1979). However, at low submergence depth, i.e. increased contact time, the latter found less degree of agreement

between experiment and theory. They suggested incomplete mixing of the liquid film into water in the trough when the disc re-submerges as the possible explanation for lower K_L values in the trough compared to the theoretical results.

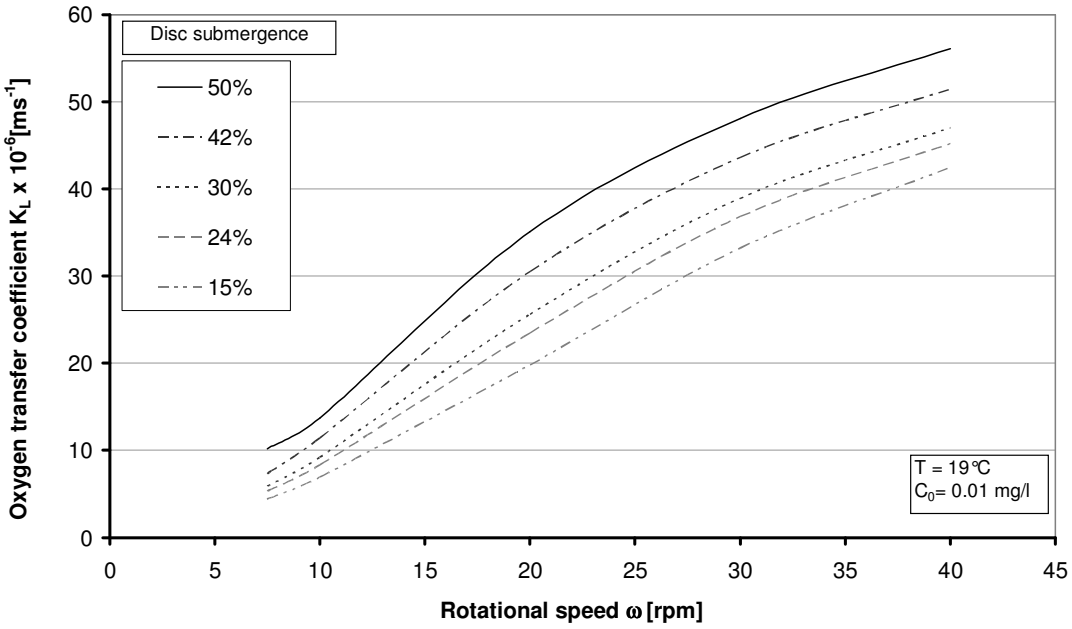

Figure 23 Variation of average K_L on disc surface with disc submergence and rotational speed

Considering the dimensionless parameters K_h and t_d, Figure 24 analyses the empirical relation between K_h and t_d calculated from the above simulation results based on average contact time t_R over the considered range of rotational velocities.

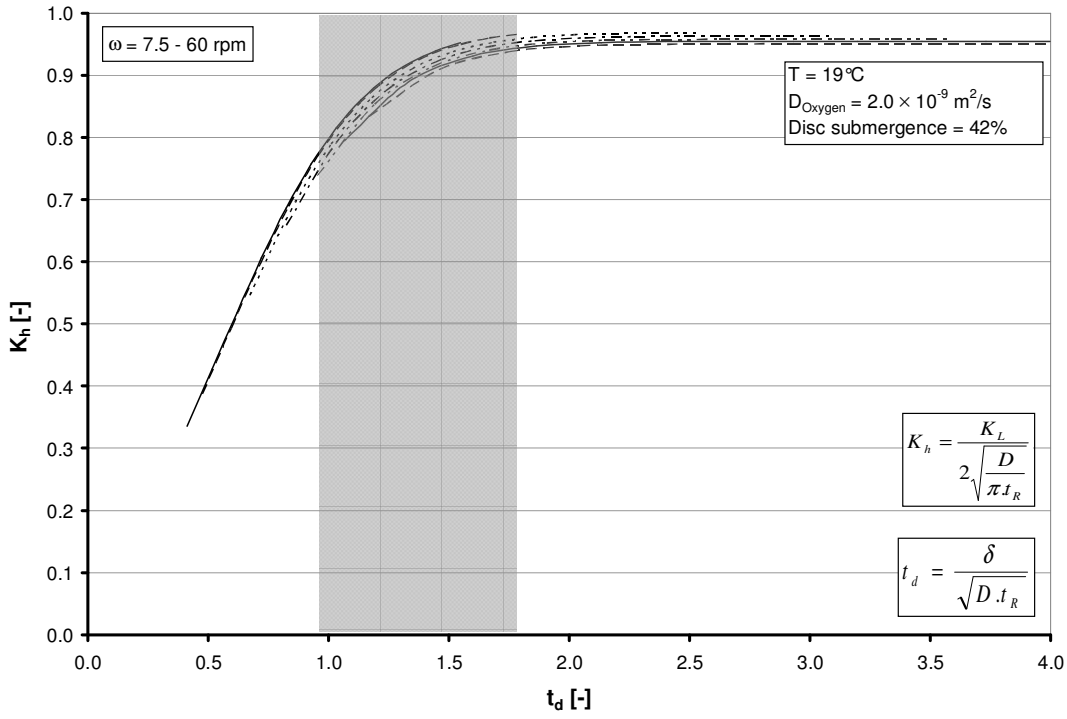

Figure 24 Relationship between dimensionless mass transfer coefficient K_h and liquid film thickness t_d

As noticed by previous authors, the K_h value stabilises where the Higbie's relation holds true. It follows that when $\delta / \sqrt{D.t_R} \geq 1.70$, K_L value tends to be independent on liquid film thickness δ. But in the region where $\delta / \sqrt{D.t_R} \leq 0.8$, K_L value varies directly with δ. This point towards the fact that when rotational velocity is less or film thickness is small, accurate determination of film thickness δ remains an important tool for correctly estimating the value of oxygen transfer coefficient. The simulated results verify and uphold the empirical relations developed by the former researchers.

From the point of view of benefit, higher rotational velocity provides higher oxygen transfer coefficient but up to a limit. At the same time, it increases the energy costs. In real systems with biofilm, it is necessary to restrict the rotational velocity. Otherwise, biomass may get sheared off from the disc surface. From economic criteria, lower rotational speed involves lower costs.

5.3 Temperature effects on physical oxygen transfer

The diffusion phenomenon is highly sensitive to temperature. Oxygen mass transfer is not only dependent on physical parameters like diffusion coefficient, concentration gradient, rotational speed and liquid film thickness, but also the temperature effects onto these parameters. The ambient temperature can vary from 0°C to above 40°C in physical systems. So it is important and worthwhile to study the effects of temperature change on physical oxygen transfer across the air-liquid boundary layer in a rotating disc system. The general equation for oxygen transfer from air into a physical medium such as water film may be written as follows.

$$\frac{dM}{dt} = K_L a(C_S - C_0)V \tag{5.25}$$

where

$$K_L a = K_L\left(\frac{A}{V}\right) \tag{5.26}$$

$K_L a$ Volumetric oxygen transfer coefficient [T^{-1}]

a Specific surface area of exchange, A / V [L^{-1}]

$\frac{dM}{dt}$ oxygen mass transfer rate [MT^{-1}]

A Interfacial surface area of exchange [L^2]

V Control volume of the physical medium [L^3]

K_La represents the oxygen transfer rate coefficient which is only time specific whereas K_L represents the oxygen transfer coefficient in terms of both time and space. Therefore K_L has been used as the basis for comparison. From equation 5.25, it can be observed that the mass transfer mechanism is controlled by two governing parameters which are again functions of temperature. These are the concentration gradient (C_S-C_0) and the transfer coefficient K_La.

5.3.1 Temperature effects on concentration gradient

For a given initial DO concentration (C_0), the concentration gradient (C_S-C_0) across the boundary surface which acts as the mass transfer driving force always decreases with increasing temperature. This is because solubility of oxygen in water decreases with increasing temperature and hence C_S gets reduced with temperature. Table 7 displays the saturation concentration of oxygen in clean water at different temperatures using Henry's coefficients. A comparison is shown with the standard tables for reference.

Table 7 Saturation concentration of oxygen in water as a function of temperature

Partial pr. of O_2 in air, p_g	Temperature	Henry's Coeff., H	Saturation conc. C_S	$C_{S,ref}^*$
% fraction	°C	(atm/mol fraction)× 10^{-4}	mg/l	mg/l
0.21	0	2.55	14.61	14.60
0.21	5	2.91	12.80	12.76
0.21	10	3.27	11.39	11.28
0.21	20	4.01	9.29	9.08
0.21	30	4.75	7.84	7.54
0.21	40	5.35	6.96	6.41

* Tchobanoglous et al. (1995), C_S value at 0 salinity and 1 atm pr. in clean water

To take into account the changes in the diffusive flux (C_S-C_0) with temperature, a correction factor θ' can be introduced with respect to the standard concentration flux at 20°C (i.e. $C_{S,20}$) as shown in expression 5.27 and 5.28 below (Rittman et al. 1983).

$$(C_S - C_0) = (C_{S,20} - C_0)\theta'^{(T-20)} \tag{5.27}$$

$$\Rightarrow \ln(C_S - C_0) = \ln(C_{S,20} - C_0) + (T-20)\ln\theta' \tag{5.28}$$

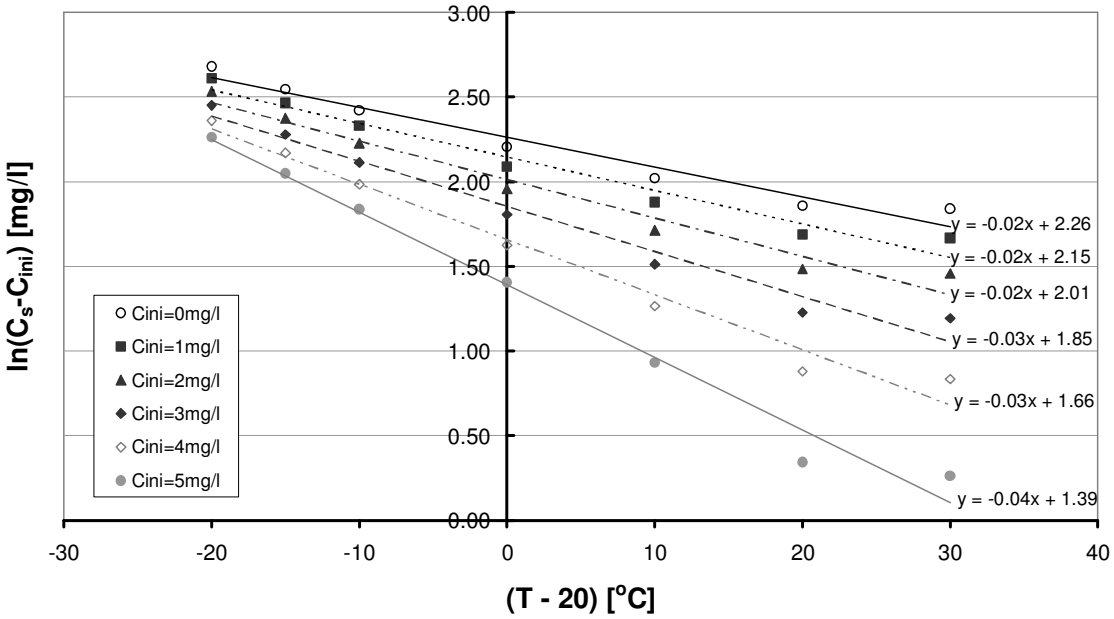

Figure 25 Determination of temperature correction factor for oxygen conc. flux (C_S-C_{ini}) at 20°C

When $\ln(C_S - C_0)$ is plotted against (T-20) at different values of C_0 (denoted as C_{ini}), the slope of the curve gives $\ln\theta'$ and the intercept is $\ln(C_{S,20} - C_0)$. Figure 25 displays the aforesaid plot. The values of θ' at different initial concentration values of oxygen (C_{ini}) are listed in Table 8. The result indicates that θ' decreases as the C_{ini} value increases in a temperature range from 0-50°C, which is in agreement with the correction factors determined by Rittman (1983).

Table 8 Temperature correction factors for the changes in concentration gradient with T

Temperature, T	C_S	C_{ini}[mg/l]					
		0.0	1.0	2.0	3.0	4.0	5.0
[°C]	[mg/l]	Overall concentration flux (C_S - C_{ini}) [mg/l]					
0	14.60	14.60	13.60	12.60	11.60	10.60	9.60
5	12.76	12.76	11.76	10.76	9.76	8.76	7.76
10	11.28	11.28	10.28	9.28	8.28	7.28	6.28
20	9.08	9.08	8.08	7.08	6.08	5.08	4.08
30	7.54	7.54	6.54	5.54	4.54	3.54	2.54
40	6.41	6.41	5.41	4.41	3.41	2.41	1.41
50	6.30	6.30	5.30	4.30	3.30	2.30	1.30
Correction factor θ′		0.983	0.980	0.978	0.974	0.968	0.958

5.3.2 Temperature effects on oxygen transfer coefficient K_La

Apart from the concentration gradient which acts as the driving force, the other factor controlling the oxygen mass transfer is the oxygen transfer coefficient K_La. This value depends upon the diffusivity coefficient D and the film thickness δ, both of which vary with

temperature. The temperature correction factor θ to correct $K_L a$ for temperature variations may be expressed by equation 5.29 as shown below (Metcalf & Eddy: Tchobanoglous et al. 1995).

$$K_L a = K_L a_{20} \theta^{(T-20)} \tag{5.29}$$

$$\Rightarrow ln\, K_L a = ln\, K_L a_{20} + (T-20) ln\, \theta \tag{5.30}$$

If the natural logarithm of the experimentally determined $K_L a$ values (i.e. $ln\, K_L a$) at specific temperatures are plotted against (T-20), the slope of the curve gives $\ln \theta$ and the intercept is $ln\, K_L a_{20}$. A common value for θ used in aeration devices is 1.024 (Rittman et al. 1983).

Therefore, for the overall correction of the mass transfer rate at any temperature, equation (5.25) may be revised as shown in equation (5.31).

$$\frac{dM}{dt} = V \frac{dC}{dt} = V K_L a_{20} (C_{S,20} - C_0)(\theta\theta')^{(T-20)} \tag{5.31}$$

where

$K_L a_{20}$ Oxygen transfer coefficient from air to liquid at 20°C [T^{-1}]

The combined correction factor $\theta\theta'$ can be obtained by multiplying the θ value described above with the θ' values in Table 8 corresponding to the initial concentration value C_0. A product value above unity indicates that dM/dt increases with increasing temperature, while a value under unity symbolises that that the overall mass transfer decreases with temperature. To have an overall effect of increasing mass transfer rate $\frac{dM}{dt}$ with increasing temperature, $K_L a$ needs to increase more than the decrease in the driving force $(C_S - C_0)$. The results from Rittman (1983) revealed that θ value is not constant at 1.024 but very dynamic in RBC.

This was so far the variation of experimentally determined $K_L a$ value with temperature. In mathematical modelling, the temperature variation of K_L value is obtained indirectly from the temperature corrected values of diffusion coefficient D, film thickness δ and the concentration gradient (C_S-C_0) as shown in Figure 16. The variation of film thickness with temperature can be easily calculated using equation (5.13) and (5.14), depending upon the variation of the physical properties of water with temperature.

5.3.2.1 Determination of oxygen diffusivity coefficient at different temperature

Theoretical determination of molecular diffusivity of gas in water D° is based on the physical properties of the gas and water. Bird et al (1960) cited the empirical correlation

developed by Wilke and Chang (1955) on the basis of Stokes-Einstein equation as represented by equation 5.32 below.

$$D^{0}{}_{O_2-H_2O} = 7.4\times10^{-8}\,\frac{\left(\phi_{H_2O}.m_{H_2O}\right)^{0.5}T}{\eta_{H_2O}.\nu_{O_2}{}^{0.6}} \qquad (5.32)$$

where

T absolute temperature (°K)

ϕ_{H_2O} association factor for the solvent (water)

m_{H_2O} molecular weight of solvent (18g/mole)

$\eta_{\cdot H_2O}$ dynamic viscosity of solvent at T (centipoises)

ν_{O_2} molar volume of oxygen at its normal boiling temperature(-183°C) 25.6 cm^3/g.mole

Wilke and Chang recommended that ϕ_{H_2O} be taken as 2.6 when the solvent is water. Bird (1960) mentioned that Wilke and Chang equation, which is used in developing the gas mixture equations, is accurate within a range of ±10% for dilute solutions of non-dissociating solutes. However, Perry et al. (1984) stated that the said equation is most accurate when ϕ_{H_2O} is 2.26 for a solute diffusing into water. They cited Laudie (1974) who studied diffusion coefficients for different solutes in water and reported that the average error is about 0.4% when ϕ_{H_2O} is 2.26. The molar volume of oxygen at its boiling point is estimated using the empirical correlation given by Tyn and Calus (cited in Perry et al. 1984).

$$\nu_{O_2} = 0.285\times\left(\nu_c\right)^{1.048} \qquad (5.33)$$

where

ν_c Critical volume of oxygen

Handbook of Chemistry and Physics (Weast 1964) gives a value of 73.37 cm^3/mole for ν_c. Therefore, ν_{O_2} is calculated to be 25.60cm^3/g.mole. Assuming that the solvent is pure water without dissolved substrates, the values of D for oxygen in an aqueous solution at different temperatures have been calculated and listed in Table 9 below. The value of D has been calculated taking both the literature values of ϕ_{H_2O} as 2.60 and 2.26 respectively. However, the value of D at ϕ_{H_2O} as 2.26 has been used in the physical model for determination of K_L at different temperatures. Figure 26 shows the variation of diffusion coefficient of oxygen in water and dynamic viscosity of water with temperature.

Table 9 Values of diffusivity coefficient of oxygen in water at different temperatures

Temperature	Dynamic viscosity of water*	D_{Oxygen} (ϕ_{H_2O} = 2.60)	D_{Oxygen} (ϕ_{H_2O} = 2.26)
[°C]	[Nsm^{-2}] $\times 10^{-3}$	[m^2s^{-1}] $\times 10^{-9}$	[m^2s^{-1}] $\times 10^{-9}$
5	1.518	1.322	1.235
10	1.307	1.563	1.460
15	1.139	1.825	1.705
20	1.002	2.111	1.972
25	0.890	2.417	2.258
30	0.798	2.741	2.561
35	0.725	3.064	2.863
40	0.653	3.460	3.233

* Tchobanoglous et al. (1995)

Essentially, the value of $\frac{D_{Oxygen} \cdot \eta_{H_2O}}{T}$ remains constant at a given temperature T(°K) as deduced from equation (5.32).

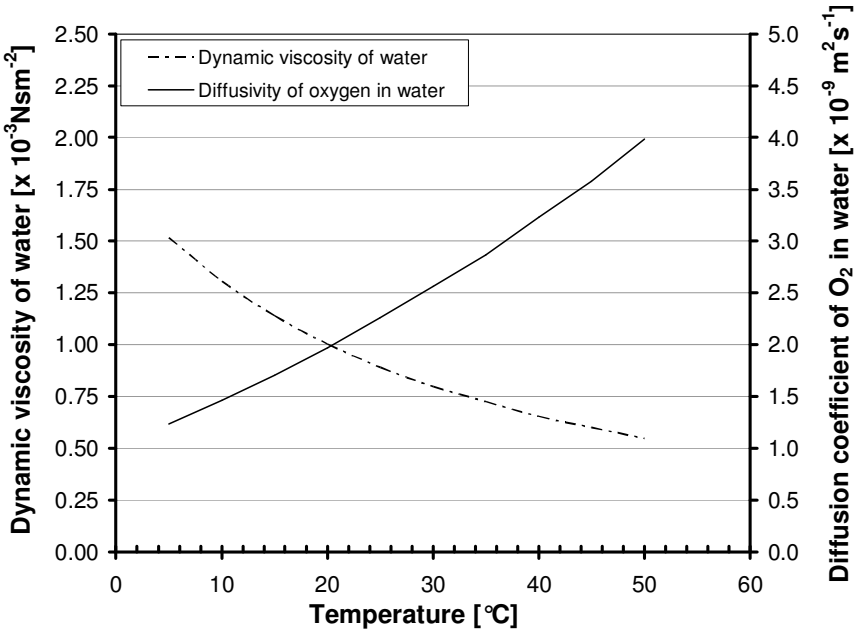

Figure 26 Correlation between diffusion coefficient of oxygen in water and viscosity of water at different temperature

5.4 Simulation results on oxygen transfer at varying temperature

Any temperature change will affect the viscosity of the fluid which will in turn affect the δ and D values. The geometry of the experimental set-up described in section 4.2 has been used for the physical data such as disc diameter. Figure 27 displays the variation of average K_L on the disc surface with ω and temperature. At a given temperature and rotational speed,

δ has been calculated using equations (5.13) and (5.14) at five different radial distances over the exposed disc surface and then averaged to obtain a mean value. The runs have been conducted for a temperature range from 5-40°C. The rotational speed has been varied from 7.5 rpm to 40 rpm, and initial oxygen concentration in the bulk liquid is assumed to be 0.01 mg/l. It follows from the plots that at lower rotational speeds, oxygen transfer coefficient decreases with increase of temperature. This may be substantiated by the fact that at high temperatures, the film entrained on the disc has a lesser thickness due to reduced viscosity. Additionally, the diffusion is faster due to higher diffusivity coefficient value. Therefore, the film is quickly saturated and this lowers the average oxygen transfer speed (K_L). However, as the rotational speed increases, film thickness also increases (expression 5.13). Although film thickness should decrease with increasing temperature, the rise of rotational speed compensates this effect and eventually the reduced exposure time causes partial saturation of the film. The liquid film is no longer fully saturated in the reduced exposure time. Hence the average K_L value shows a rise with temperature reversing its earlier trend.

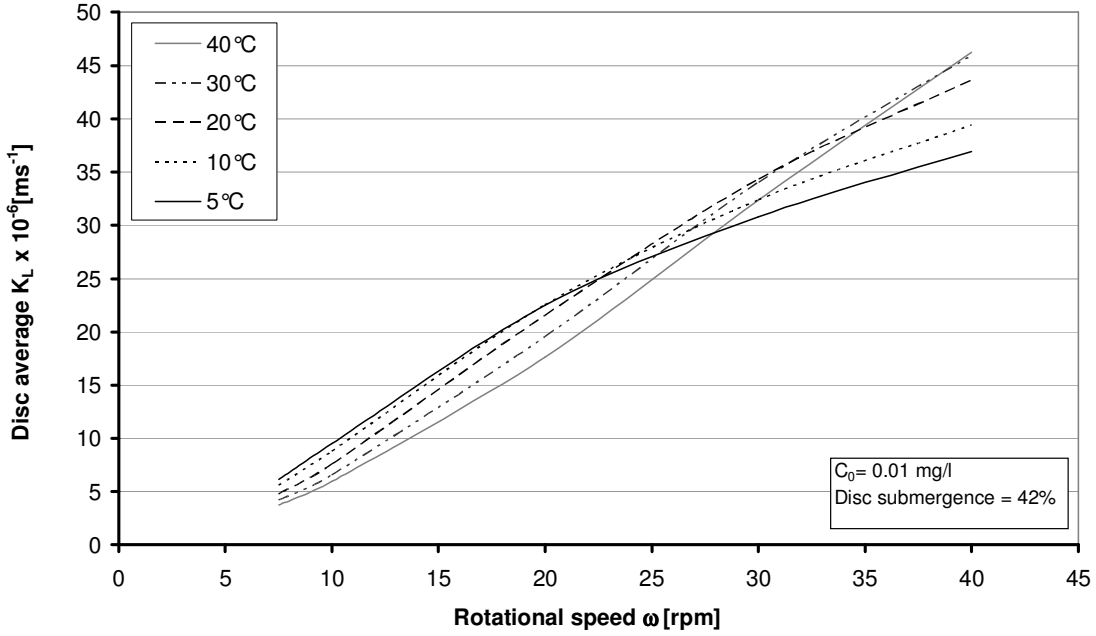

Figure 27 Variation of average K_L on disc surface with rotational speed at different temperatures

The behaviour of the oxygen transfer coefficient with rotational speed at 20°C and 30°C as studied through experimental measurements by Rittman et al. (1983) show a similar trend although the measurements were done in the trough and not spontaneously over the disc surface. This is illustrated clearly in Figure 28. It can be inferred that the measured oxygen transfer coefficient in the trough is less than the simulated average value on the disc surface. Incomplete mixing of the liquid film into the liquid in the trough and hence partial oxygen transfer through the submerged boundary layer is believed to be the cause.

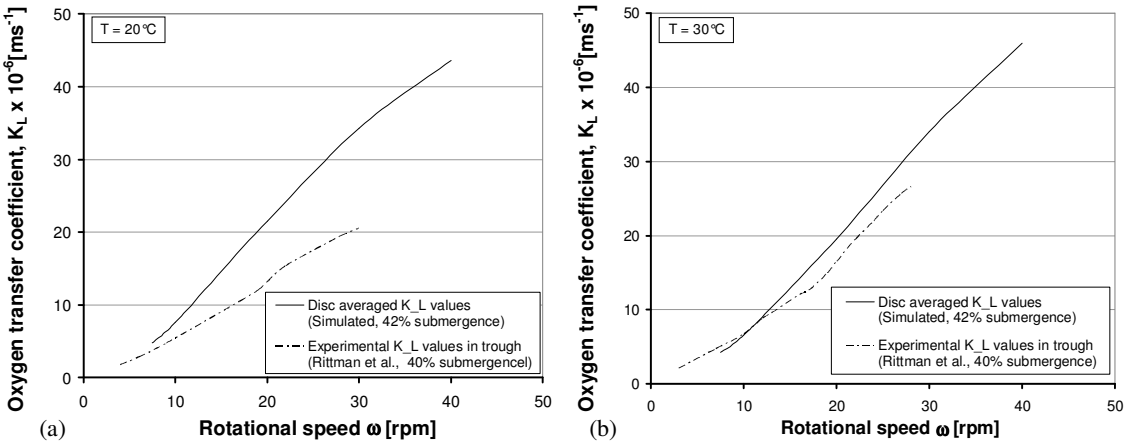

Figure 28 Comparison between simulated K_L value on the disc surface and experimentally determined K_L value in trough at different rotational speeds

With the increase in temperature, however, there is greater mixing and hence the gap between the experimentally determined K_L value in the water basin (Rittman et al.) and the modelled average K_L values on the disc surface closes down as shown in Figure 28(b). This is in agreement with the conclusion made by Rittman that for a given rotational speed, effectiveness factor η for mixing increases with increasing temperature.

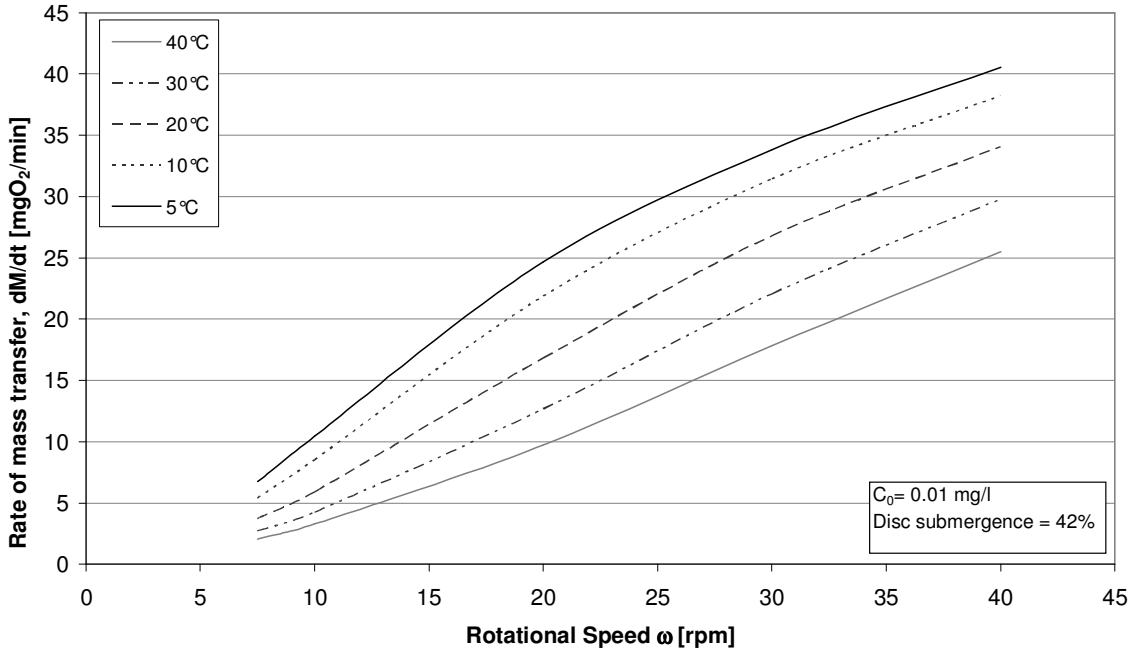

Figure 29 Variation of oxygen mass transfer rate with rotational speed at different temperatures

In Figure 29, the variation of overall oxygen mass transfer rates have been depicted with rotational speed at different temperatures. In general, the mass transfer rate dM/dt (equation 5.25) decreases with increasing temperature at a given rotational speed. This is because the driving force, i.e. the concentration gradient (C_S-C_0) decreases with increasing temperature. The temperature correction factor θ' is usually less than 1 (Table 8). The overall mass

transfer rate reduces with increasing temperature because θ' appears to have a more dominating effect (equation 5.31). The plots may be compared with the trend and the range of values obtained by Rittmann (1983) experimentally. It may also be observed that with increase in rotational speed, the domain of variation of transfer rate increases. In other words, at lower rotational speeds, the mass transfer rates are less affected by temperature than at higher speeds. Therefore, it can be conclusively stated that temperature creates a more pronounced effect over oxygen transfer rate at higher rotational speeds only.

6 Biofilm model for RBC

6.1 Fixed biofilm in wastewater treatment

The processes involved in fixed-film wastewater treatment are complex and dependent on a multitude of factors which are physical, chemical and biological in nature. The vast majority of biofilm models available today try to simplify these processes into suitable mathematical forms which obey the laws of physics and chemistry. In reality, what happens and what might happen under a set of external conditions is still fairly unpredictable and in some cases inconceivable. There are many different species and cultures of bacteria, protozoa, fungi and other filamentous as well as non-filamentous organisms that are present in the biofilm. Their type and number is specific to the type of biofilm, its nutrient source and other physical and biochemical conditions. In general, the organisms in biofilms treating municipal or commercial wastewater have been classified into the following groups: heterotrophic species, ammonium oxidising micro-organisms (AOM, Nitrosomonas clusters), nitrite oxidising micro-organisms (NOM, Nitrobacter clusters), phosphate accumulating organisms, and anaerobic ammonium oxidising organisms (anammox). Each of these species have a specific growth rate and decay kinetics depending on nutrition, temperature, pH, alkalinity and availability or non-availability of oxygen.

6.2 Governing principles behind the mathematical modelling of biofilms

The models for biofilms are more complicated than conventional Activated Sludge Process (ASP) models due to the fact that diffusion (transport) limitation of substrates in the different reaction processes need to be considered. This necessitates accounting by zonation of the biofilm. Each zone or layer presents its individual processes which vary from adjoining layers because of difference in redox-conditions. The kinetics of the chemical transformation reactions considered to be occurring in a biological treatment process had been previously discussed in section 3.5.2. The layered structural representation of the biofilm, wherein the mass balance is incorporated in each layer based upon the known reaction processes (ASM1, 2 or 3) as well as the physical boundary conditions specific for a given system, makes the biofilm model slow and cumbersome. The processes usually considered to be occurring inside biofilms in general are as follows:

- Molecular diffusion of the substrates into and of the end-products out of the biofilm

- Metabolic reactions within the biofilm
- The growth and endogenous respiration of biomass which govern the population dynamics inside the biofilm
- Displacement of the solids by advection and diffusion and finally,
- Attachment and detachment (loss) of biomass at the biofilm surface

Many of the parameters are often relatively uncertain in the model due to less consistent a priori knowledge of model structure and its parameters.

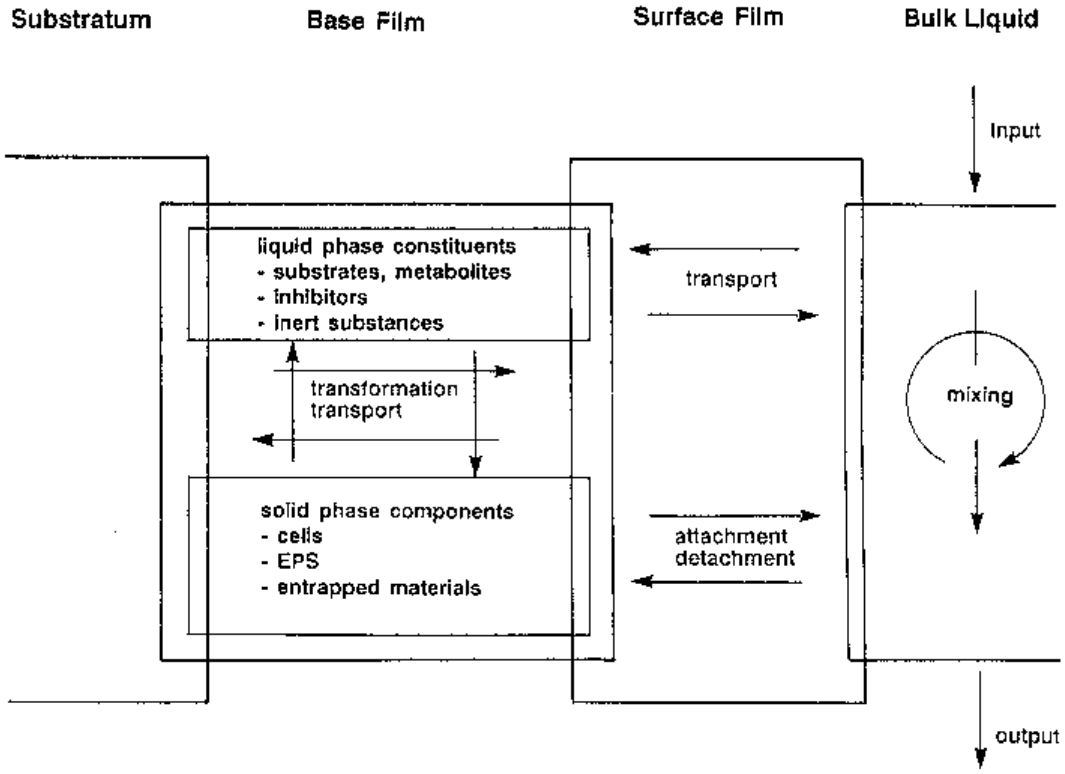

Figure 30 Characterisation of the various processes occurring in a biofilm system

The commonly considered physical boundary conditions in a biofilm reactor include:

- Flow rate or volumetric loading rate,
- Recycling rate
- Organic loading rate,
- System parameters (tank volume, specific surface, detention time and sludge age)

The specific boundary conditions may vary from one biofilm plant to another. For RBCs, the important physical constraints affecting the process dynamics are as follows:

- Diffusivity coefficient of substrates and gases through the dynamic liquid film
- Rotational speed and hence the thickness of laminar boundary layer (liquid film)
- The immersion ratio of the disc in tank
- Number of stages (cascades)

A major advancement in biofilm modelling took place with the one-dimensional multi-species models of Kissel et al.(1984) and Wanner and Gujer (1985, 1986). The concepts behind these models are similar, but the work of the latter group has been continued and subsequently developed into the commercially available scientific software AQUASIM (Reichert 1994). In essence, mechanistic mathematical models, such as biofilm systems in wastewater treatment, are formulated on the basis of non-steady state mass balances of all substrates (nutrient source), particulates (biomass species, extracellular polymeric substances and inerts) and physical states (biofilm thickness, density, advective velocity). The energy balance has been avoided as the mass transfer processes are supposed to occur at a given temperature. For any change in temperature, a corresponding set of parameter values are considered, thereby reducing further complexity of the model as a result of additional energy balance equations. The mass balance of a biofilm system helps to predict the time history of the state of a system as a function of the physical transport and the biochemical reaction processes. The dominant transport processes are as follows:

- physical diffusion of substrates through liquid-liquid (bulk-boundary layer) interface
- physical diffusion of substrates through air-liquid (air-liquid film) interface
- molecular diffusion of substrates into biofilm
- advective and diffusive displacement of solids (biomass) in the biofilm matrix
- attachment-detachment of solids at the biofilm surface.

The processes are extremely specific for the location within the reactor. On the other hand, the reaction processes depend only on the immediate surroundings like temperature, concentrations and are described within a common model subroutine for the entire system.

6.3 Elements of RBC biofilm model

6.3.1 Basic assumptions

Defining a mathematical model for a multi-species biofilm system necessitates several assumptions to be made in order to make it a suitable predictive tool for fast performance with less complexity. However, it is important to note that these assumptions do not overlook any important phenomenon of the system, thereby reducing its accuracy.

The following assumptions have been considered in the biofilm model:

1 The biofilm consists of a liquid phase and several solid phases in each layer.

2 Each solid phase represents one particulate component. The fluid present inside the solid phase is assumed to remain unaffected.

3 The liquid phase represents the interstitial fluid filling the pores between the solid

phases. It contains the dissolved components.

4 The variables in a biofilm such as concentration of substrates and solids are described by averaging the quantities over a given volume.

5 The flux of the components is significantly higher in the direction perpendicular to the substratum as compared to the other directions. Therefore, the mass transfer is modelled in one space dimension only.

6 The constituent particulate components are bound to each other and form a continuous solid matrix with the liquid phase.

7 The transport of the dissolved components in the liquid phase is governed by molecular diffusion which is modelled based on Fick's law of diffusion.

8 The dry densities of the solid components, as well as the volume fraction of the liquid phase, are constant in time

9 The stoichiometry and kinetics of biological transformation processes are constant in the biofilm.

One of the most important assumptions made in the multi-cultural biofilm model is that the biomass in biocenosis is treated as a continuum. This implies that the concentrations and all other properties are averaged over each differential element of the biofilm and this element is treated as homogenous, disregarding the individual characteristics such as the shape or size of each micro-organism in that layer.

6.3.2 Kinetic model

The kinetic model for the bio-chemical reactions and transformation processes occurring in the RBC biofilm is based on the Activated Sludge Model No. 3 developed by the IAWQ Task Group on Mathematical Modelling for Design and Operation of Biological Wastewater Treatment Processes. Conceptually, it predicts the oxygen consumption, sludge production, nitrification and denitrification of activated sludge systems and is typically defined by a set of bio-chemical kinetic equations with its stoichiometry. This model is a modification of the original Activated Sludge Model No.1 (Henze et al. 1987) with an additional process for the storage of organic substrates by the heterotrophs. It also revises the decay process in the original model into aerobic and anoxic endogenous respiration process. This represents the state-of-art development in activated sludge system modelling and corrects some of the deficiencies of ASM No.1. Moreover, it has been subsequently calibrated and validated for several Swiss municipal wastewater treatment plants (Koch et al. 2000).

Therefore, ASM No.3 model forms the basis for the selection of the reaction kinetics for the present RBC biofilm model. The stoichiometry and process kinetics for the reaction rates

and bio-chemical conversion processes in the RBC model has been adopted from this basic model with suitable simplifications. The heterotrophic storage of biodegradable organic substrate as cell internal storage product (intermediate step) for its subsequent breakdown by process of hydrolysis has not been considered in the model kinetics, since this process is of less dominating importance for the rates of oxygen consumption and denitrification (Henze et al.2002). It does not affect the degradation products substantially. Simultaneously, this simplification speeds up the numerical calculations for a biofilm with multiple layer constitution vis-à-vis activated sludge process.

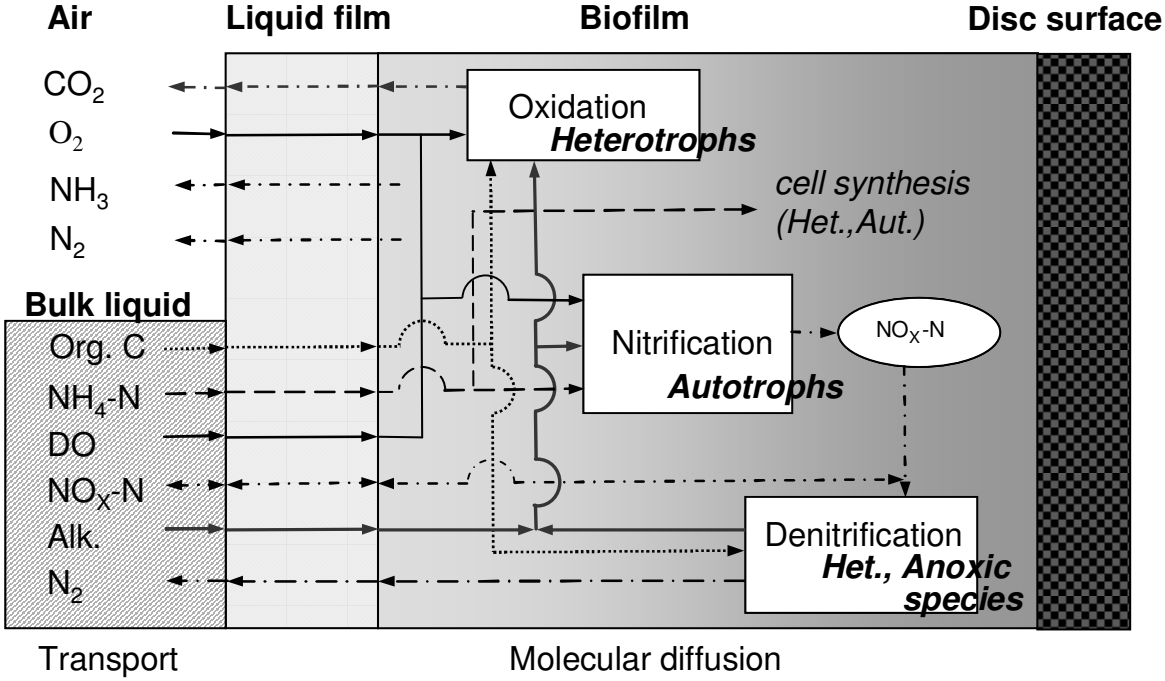

Figure 31 The schematic illustration of redox reactions in a RBC biofilm system

The conceptual illustration of the removal of organic substances and nitrogen compounds in a RBC biofilm is shown in Figure 31. The conversion processes and the chemical kinetics vary with the depth of the biofilm depending upon availability or limitation of substrate and oxygen and the type of bacterial species active at that depth. Table 10 and Table 11 present the stoichiometric model and the kinetic rate expressions in matrix form for the simultaneous removal of organic substances and nitrogen compounds in a mixed-culture biofilm as developed for the RBC system. It considers the aerobic and anoxic degradation of organic components, denitrification and nitrification. The kinetics of the ammonium oxidising micro-organisms and nitrite oxidising micro-organisms have been clubbed together as autotrophic organisms as per ASM No.3 with single-step nitrification from NH_4-N to NO_3-N. This overcomes the difficulty in predicting the fate of nitrite during denitrification.

Table 10 Stoichiometric matrix for aerobic and anoxic degradation of organic components and nitrification-denitrification in biofilm (*Source: ASM No. 3*)

Model matrix ν_{mn}		Dissolved Components						Particulates			
Component →	m	1	2	3	5	6	7	8	9	10	11
n	Processes ↓	S_O	S_S	S_{NH}	S_{NO}	S_{N2}	S_{ALK}	X_I	X_S	X_H	X_A
Heterotrophic organisms, X_H											
1	Aerobic growth of X_H	$1-\frac{1}{Y_{H,O_2}}$	$-\frac{1}{Y_{H,O_2}}$	$-i_{NBM}$			$\frac{-i_{NBM}}{14}$			1	
2	Anoxic growth of X_H (denitrification)		$-\frac{1}{Y_{H,NO}}$	$-i_{NBM}$	$\frac{Y_{H,NO}-1}{2.86.Y_{H,NO}}$	$-\frac{Y_{H,NO}-1}{2.86.Y_{H,NO}}$	$-\frac{Y_{H,NO}-1}{40.Y_{H,NO}}-\frac{i_{NBM}}{14}$			1	
3	Aerobic endogenous respiration of X_H	$-(1-f_I)$		$i_{NBM}-f_I.i_{NXI}$			$\frac{i_{NBM}-f_I.i_{NXI}}{14}$	f_I		-1	
4	Anoxic endogenous respiration of X_H			$i_{NBM}-f_I.i_{NXI}$	$-\frac{(1-f_I)}{2.86}$	$\frac{(1-f_I)}{2.86}$	$\frac{i_{NBM}-f_I.i_{NXI}}{14}+\frac{1-f_I}{40}$	f_I		-1	
Autotrophic organisms, X_A											
5	Aerobic growth of X_A	$1-\frac{4.57}{Y_A}$		$-i_{NBM}-\frac{1}{Y_A}$	$\frac{1}{Y_A}$		$\frac{-i_{NBM}}{14}-\frac{1}{7Y_A}$				1
6	Aerobic endogenous respiration of X_A	$-(1-f_I)$		$i_{NBM}-f_I.i_{NXI}$			$\frac{i_{NBM}-f_I.i_{NXI}}{14}$	f_I			-1
7	Anoxic endogenous respiration of X_A			$i_{NBM}-f_I.i_{NXI}$	$-\frac{(1-f_I)}{2.86}$	$\frac{(1-f_I)}{2.86}$	$\frac{i_{NBM}-f_I.i_{NXI}}{14}+\frac{1-f_I}{40}$	f_I			-1
Hydrolysis											
8	Hydrolysis of X_S		1						-1		

Table 11 Kinetic rate expressions for the aerobic and anoxic degradation of organic components and nitrification-denitrification in RBC biofilm *(Based on ASM No.3)*

n	Process	Process rate ρ_n [$ML^{-3}T^{-1}$]
Heterotrophic organisms, X_H		
1	Aerobic growth of heterotrophs	$\mu_H\left(\frac{S_S}{K_{Ss}+S_S}\right)\left(\frac{S_O}{K_{O_2,H}+S_O}\right)\left(\frac{S_{NH}}{K_{NH,H}+S_{NH}}\right)\left(\frac{S_{ALK}}{K_{ALK,H}+S_{ALK}}\right)X_H$
2	Anoxic growth of heterotrophs (denitrification)	$\rho_1\left(\frac{K_{O2,H}}{S_O}\right)\left(\frac{S_{NO}}{K_{NO,H}+S_{NO}}\right)\eta_{den}$
3	Aerobic endogenous respiration of heterotrophs	$b_H\left(\frac{S_O}{K_{O2,H}+S_O}\right).X_H$
4	Anoxic endogenous respiration of heterotrophs	$\eta_H b_H\left(\frac{K_{O_2,H}}{K_{O_2,H}+S_{O_2}}\right)\left(\frac{S_{NO}}{K_{NO,H}+S_{NO}}\right).X_H$
Autotrophic organisms, X_A		
5	Aerobic growth of autotrophs	$\mu_A\left(\frac{S_{NH}}{K_{NH,A}+S_{NH}}\right)\left(\frac{S_O}{K_{O_2,A}+S_O}\right)\left(\frac{S_{ALK}}{K_{ALK,A}+S_{ALK}}\right)X_A$
6	Aerobic endogenous respiration of autotrophs	$b_A\left(\frac{S_O}{K_{O2,A}+S_O}\right).X_A$
7	Anoxic endogenous respiration of autotrophs	$\eta_A b_A\left(\frac{K_{O_2,A}}{K_{O_2,A}+S_O}\right)\left(\frac{S_{NO}}{K_{NO,A}+S_{NO}}\right)X_A$
Hydrolysis		
8	Hydrolysis of slowly biodegradable substrates	$K_{Hyd}\left(\frac{X_S/X_H}{K_{XS}+(X_S/X_H)}\right)X_H$
Observed reaction rate [$ML^{-3}T^{-1}$]		$r_j=\sum_n \rho_n.\nu_{n,m}$

The kinetic expressions are based on switching functions (Monod terms) for all soluble components considered (section 3.5.2). This eases the mathematical calculations and helps to stop the biological activity when the concentrations approach zero. The model code checks the value of the variables at each time step to ensure that they remain non-negative during the time step integrations by using the *max* function. From Table 11, the expression for aerobic growth rate of heterotrophs and autotrophs as a function of temperature may be expressed as shown below:

$$R_{X_H}=\mu_{H,20^\circ}e^{\theta_T(T-20)}\left(\frac{S_S}{K_{Ss}+S_S}\right)\left(\frac{S_O}{K_{O_2,H}+S_O}\right)\left(\frac{S_{NH}}{K_{NH,H}+S_{NH}}\right)\left(\frac{S_{ALK}}{K_{ALK,H}+S_{ALK}}\right)X_H \quad (6.1)$$

$$R_{X_A}=\mu_{A,20^\circ}e^{\theta_T'(T-20)}\left(\frac{S_{NH}}{K_{NH,A}+S_{NH}}\right)\left(\frac{S_O}{K_{O_2,A}+S_O}\right)\left(\frac{S_{ALK}}{K_{ALK,A}+S_{ALK}}\right)X_A \quad (6.2)$$

For each dissolved or particulate component, m in Table 10, the net rate expression is calculated by multiplying the matrix elements of a component ν_{mn} with the corresponding processes n in Table 11 and making a summation for all the elements at the end. This form of matrix

representation (Peterson matrix) of the process kinetics was originally used in ASM No.1 model and has been subsequently considered in IAWQ as standard form for such expressions. Thus, expressions 6.1 and 6.2 would add up more processes such as aerobic and anoxic endogenous respiration to obtain the net growth rate of heterotrophs and autotrophs.

The transformation processes considered in the RBC biofilm based on the process kinetics as depicted in the above tables are described in detail below:

1. *Aerobic growth of heterotrophs*: A fraction of the readily biodegradable substrate (S_S) is used for the growth of heterotrophic biomass and the rest is oxidized for energy giving rise to an associated oxygen demand. Ammonia is used as a nitrogen source for cell synthesis and incorporated into the cell mass. The growth is modelled using Monod-Michaelis kinetics. Both the concentration of S_S and S_O may be limiting the rate of the growth process. This process is usually the main contributor to the production of new biomass and degradation of the biodegradable organic substrate.
2. *Anoxic growth of heterotrophs (denitrification)*: In the absence of oxygen, the heterotrophic organisms are capable of using nitrite and nitrate as a terminal electron acceptor with S_S as the substrate. This leads to the production of new biomass and nitrogen gas. The nitrogen gas is a result of the reduction of nitrite and nitrate with an associated alkalinity change. The same Monod-Michaelis kinetics as used for the aerobic growth is applied here except that the kinetic rate expression is reduced by multiplication with a factor η_{den} (<1). This reduced rate is assumed to be either due to a lower maximum growth rate under anoxic conditions or because only a fraction of heterotrophic biomass is able to function with NO_x-N as an electron acceptor. Ammonia serves as the nitrogen source for cell synthesis.
3. *Aerobic endogenous respiration of heterotrophs*: This process considers all forms of biomass loss and energy requirements not associated with growth by considering related respiration under aerobic conditions, for example decay (maintenance), endogenous respiration, lysis, predation, death etc.
4. *Anoxic endogenous respiration of heterotrophs*: This process is similar to the aerobic one except that it is slower. Presumably, protozoa (predation) are considerably less active here.
5. *Aerobic growth of Autotrophic organisms (AOM, NOM)*: In biofilm, ammonia is oxidised to nitrate via a multiple-step process resulting in the production of autotrophic biomass and giving rise to an associated oxygen demand. Ammonia is first oxidised into nitrite by one set of nitrifying species (AOM) involving a complex series of reactions.

Nitrite is eventually converted into nitrate by another set of nitrifying organisms (NOM) as described in section 3.5.3. However, this conversion is modelled in a single step (ASM No.3) so that denitrification from both nitrite and nitrate could be accounted together. Moreover, nitrite as an intermediate unstable product is difficult to tune in modelling and can accumulate when nitrification gets inhibited. Apart from oxidation, ammonia is also used as the nitrogen source for synthesis and incorporated into autotrophic cell biomass. The process has a marked effect on the alkalinity and the total oxygen demand. The effect on the amount of biomass production is small as the yield of autotrophic nitrifiers is comparatively low.

6. *Aerobic endogenous respiration of autotrophs*: This process is modelled in a similar way as described for the heterotrophs.
7. *Anoxic endogenous respiration of autotrophs*: Similar to heterotrophs, this process is slower than the aerobic process.
8. *Hydrolysis*: This process breaks down the slowly biodegradable substrate (X_S) contained in the influent into readily degradable substrate (S_s) through extra cellular enzymatic reactions which is then available for the growth of micro-organisms. It is assumed to be active independent of the electron acceptors (S_O, S_{NO}).

Table 12 lists the key parameters used in the model and cites the literature reference. Although many parameter values have been adopted from the ASM No.3 model, some values were based upon previous authors who worked with biofilm modelling (Gujer and Boller 1990, Wanner and Reichert 1995, Fruhen-Hornig thesis, 1997). The exact value of certain parameters like growth rate of heterotrophs and autotrophs were adjusted during the calibration of the model by the author based upon the experimental data (Courtesy: Andreas Blank, 2006, IWG). The table of kinetic parameters calculated at different temperatures based upon Table 12 values at 20°C can be found in the next chapter (Table 15). A comprehensive list of parameter values used from different literature sources that has been used by various modelers and referred to in the current model has been listed in Table 13.

6.3.3 Mass balance aspects of the RBC Model

The mass transfer characteristic of a RBC biofilm is essentially similar to biofilm systems, except for the physical boundary conditions. For each stage, three types of mass balance equations are required both for substrates as well as for the particulate components.

Table 12 Kinetic and stoichiometric parameters at 10°C and 20°C used in the RBC model
(Source: ASM No. 3, Gujer and Boller, 1990 (at 10°C), Wanner and Reichert, 1995, Fruhen 1997)

Parameter	Description	Temperature		Units	Reference (at 20°C)
		10°C	20°C		
Kinetic parameters					
Hydrolysis					
K_{Hyd}	Hydrolysis rate constant	1.50	1.50	$gX_S/(gX_H.d)$	Fruhen-Hornig thesis (1997)
K_{XS}	Saturation constant for Hydrolysis	0.02	0.02	gX_S/gX_H	Fruhen-Hornig thesis (1997)
Heterotrophic organisms, X_H					
μ_H	Maximum growth rate of X_H	2.00	4.50	1/d	Wanner & Reichert (1996), Wanner & Gujer (1986)
K_{Ss}	Saturation constant for substrate S_S	5.00	5.00	$gCOD/m^3$	Wanner & Reichert (1996), Wanner & Gujer (1986)
$K_{O_2,H}$	Saturation constant for oxygen S_O	0.20	0.20	gO_2/m^3	ASM No.3 (1999), Fruhen-Hornig thesis (1997)
$K_{NH,H}$	Saturation constant for ammonium S_{NH}	0.10	0.10	gN/m^3	Fruhen-Hornig thesis (1997)
$K_{NO,H}$	Saturation constant for nitrite-nitrate S_{NO}	0.50	0.50	gN/m^3	Fruhen-Hornig thesis (1997)
$K_{ALK,H}$	Saturation constant for bicarbonate S_{ALK}	0.10	0.10	mol HCO_3^-/m^3	ASM No.3 (1999)
b_H	Aerobic endogenous respiration rate of X_H	0.10	0.20	1/d	Wanner & Reichert (1996), Wanner & Gujer (1986)
η_H	Anoxic reduction factor for endogenous respiration	0.50	0.50	-	ASM No.3 (1999)
η_{den}	Anoxic reduction factor for denitrification	0.30	0.30	-	Model calibration
Autotrophic organisms (X_A)					
μ_A	Maximum growth rate of X_A	0.35	1.00	1/d	Koch et al. (2000), ASM No.3 (1999)
$K_{O_2,A}$	Saturation constant for oxygen S_O	0.30	0.30	gO_2/m^3	Fruhen et al. (1991)
$K_{NH,A}$	Saturation constant for ammonium S_{NH}	1.00	1.00	gN/m^3	Wanner & Reichert (1996), Fruhen-Hornig thesis (1997)
$K_{NO,A}$	Saturation constant for nitrite-nitrate S_{NO}	0.50	0.50		ASM No.3 (1999)
$K_{ALK,A}$	Saturation constant for bicarbonate S_{ALK}	0.50	0.50	mol HCO_3^-/m^3	ASM No.3 (1999)
b_A	Aerobic endogenous respiration rate of X_A	0.05	0.15	1/d	ASM No.3 (1999), Fruhen-Hornig thesis (1997)
η_A	Anoxic reduction factor for endogenous respiration	0.001	0.001	-	Personal correspondence with Prof. Siegrist
Stoichiometric parameters					
Y_{H,O_2}	Aerobic yield of heterotrophic biomass	0.63	0.63	gX_H/gS_S	ASM No.3 (1999), Fruhen-Hornig thesis (1997)
$Y_{H,NO}$	Anoxic yield of heterotrophic biomass	0.54	0.54	gX_H/gS_S	ASM No.3 (1999)
Y_A	Aerobic yield of X_A	0.24	0.24	$gX_{NH}/gN\ S_{NH}$	ASM No.3 (1999), Fruhen et al. (1991)
i_{NBM}	Nitrogen content of biomass, X_H, X_A	0.07	0.07	$gN/g\ X_{H/A}$	ASM No.3 (1999), Fruhen-Hornig thesis (1997)
i_{NXI}	Nitrogen content of inerts, X_I	0.02	0.02	gN/gX_I	ASM No.3 (1999)
f_I	Production of X_I in end. respiration	0.20	0.20	$gX_I/gX_{H/A}$	ASM No.3 (1999)

Table 13 Kinetic and stoichiometric parameters at 10°C and 20°C (literature reference)

Parameter	Description	Units	10° ASM3	10° Gujer-Boller	20° ASM 3	20° Koch-Siegrist	20° Fruhen-Gujer	20° Wanner-Reichert	20° Horn-Hempel	20° Fruhen PhD Thesis	20° Literature ranges_Muller	20° Literature ranges_Fruhen
			1999	1990	1999	2000	1990	1996	1997	1997	1980	1997
Kinetic parameters												
Heterotrophic organisms, X_H												
μ_H	Max. growth rate of X_H	1/d	1.00	2.00	2.00	-	4.00	4.80	5.50	2.00	1.90 - 6.30	0.5 - 10
K_{Ss}	Saturation constant for substrate S_S	gCOD/m^3	2.00	10.00	2.00	-	10.00	5.00	10.00	10.00		5.0 - 20.0
$K_{O_2,H}$	Saturation constant for oxygen S_O	gO$_2$/m^3	0.20	0.10	0.20	-	0.10	0.10	0.50	0.25		0.1 - 1.0
$K_{NH,H}$	Saturation constant for ammonium S_{NH}	gN/m^3	0.01	0.10	0.01	-			0.50	0.10		0.01 - 1.0
$K_{NO,H}$	Saturation constant for nitrate S_{NO}	gNO$_3^-$-N/m^3	0.50	0.50	0.50	-				0.50		0.1 - 1.0
$K_{ALK,H}$	Saturation constant for bicarbonate S_{ALK}	mol HCO$_3^-$/m^3	0.10	0.10	0.10	-				-		-
b_H	Aerobic end. resp. rate of X_H	1/d	0.10	0.35	0.20	-	0.15	0.20		0.50	0.04 - 0.20	0.1 - 1.0
η_H	Anoxic reduction factor for end.respiration	-	0.50	-	0.50	-		0.50				
η_{den}	Anoxic reduction factor for denitrification	-	0.60	0.70	0.60	-				0.80		0.6 - 1.0
Autotrophic organisms												
μ_{NH}	Max. growth rate of X_{NH}	1/d	0.35	0.35	1.00	1.00	0.83	0.95	0.14	0.61	0.08 - 0.56	0.3 - 1.5
$K_{O_2,AOM}$	Saturation constant for oxygen S_O	gO$_2$/m^3	0.50	0.20	0.50	1.00	0.30	0.10		0.50		0.1 - 1.0
$K_{NH,AOM}$	Saturation constant for ammonium S_{NH}	gN/m^3	1.00	0.70	1.00	35.00	2.80	1.00		1.00		0.1 - 5.0
$K_{ALK,AOM}$	Saturation constant for bicarbonate S_{ALK}	mol HCO$_3^-$/m^3	0.50	0.20	0.50	-				-		-
b_{NH}	Aerobic end. resp. rate of X_{NH}	1/d	0.05	0.05	0.15	0.20	0.05	0.05		0.13	0.01 - 0.05	0.01 - 0.5
η_{NH}	Anoxic reduction factor for end.respiration	-	0.33	-	0.33	0.50		-				
Autotrophic organisms (Only Nitrite oxidising micro-organisms. X_{NO})												
μ_{NO}	Max. growth rate of X_{NO}	1/d		0.60		1.30						-
$K_{O_2,NOM}$	Saturation constant for oxygen S_O	gO$_2$/m^3		0.10		0.20						-

			10° ASM3	10° Gujer-Boller	20° ASM 3	20° Koch-Siegrist	20° Fruhen-Gujer	20° Wanner-Reichert	20° Horn-Hempel	20° Fruhen PhD Thesis	20° Literature ranges_Muller	20° Literature ranges_Fruhen
$K_{NH,NOM}$	Saturation constant for ammonium S_{NH}	gN/m^3		0.05		-						-
$K_{NI,NOM}$	Saturation constant for nitrite S_{NI}	gNO_2^-N/m^3		0.50		5.00						-
b_{NO}	Aerobic end. resp. rate of X_{NH}	1/d		0.09		0.26						-
η_{NO}	Anoxic reduction factor for end.respiration	-		-		0.50						-
Stoichiometric parameters												
Y_{H,O_2}	Aerobic yield of heterotrophic biomass	$g\ X_H/gS_S$	0.63	0.57	0.63		0.57	0.40	0.920	0.65		0.5 - 0.8
$Y_{H,NO}$	Anoxic yield of heterotrophic biomass	$g\ X_H/gS_S$	0.54	-	0.54					-		-
Y_{NH}	Aerobic yield of X_{NH}	$g\ X_{NH}/gN\ S_{NH}$	0.24 (only X_A)	0.18	0.24 (only X_A)	0.21	0.24 (only X_A)	0.22	0.062 (only X_A)	0.24	0.38 or 0.17 (obs)	0.2 - 0.3
Y_{NO}	Aerobic yield of X_{NO}	$g\ X_{NO}/gN\ S_{NI}$		0.06	-	0.03	-	-	-	-	-	-
i_{NBM}	Nitrogen content of biomass. X_H, X_{NH}, X_{NO}	$gN/g\ X_{H\,/\,NH\,/\,NO}$	0.07	0.06	0.07					0.08		0.06 - 0.1
i_{NXI}	Nitrogen content of inerts, X_I	$gN/g\ X_I$	0.02	0.05	0.02							
f_I	Production of X_I in end. respiration	$g\ X_I/g\ X_{H\,/\,NH\,/\,NO}$	0.20	0.08	0.20	0.20				0.10		0.05 - 0.2
Biofilm parameters												
ρ	Biofilm density (dry)	$KgVSS/m^3$								50.00		20 - 100
ε_l	Water fraction in biofilm	-								0.85		0.5 - 1.5

The mass balance equations are categorically explained in three sub-units:

- Mass balance equations for biofilm layers
- Mass balance equations for liquid film
- Mass balance equations for the bulk reactor

However, when the system is simulated as a whole, there is substantial difference in the rates of the transport processes between the dissolved components and particulates. While the characteristic accounting time of the mass transfer for dissolved components is typically in the order of a few minutes, it runs into days for the particulate solids. In other words, it only takes a few minutes for the substrate concentrations to reach nearly steady-state profiles together with changes in bulk liquid concentrations, while it takes days for changes in the bacterial concentrations to settle down. Therefore, the former is categorized under fast dynamics while the latter falls under slow dynamics. Although both of the processes have to be computed together to reach a true steady-state, the time-scale difference often makes the numerical algorithms slow and time-consuming especially in sensitivity analysis. The runs are guided by the fast dynamic processes which require very small time steps.

6.3.3.1 Model structure for mass balance

The laminar boundary layer (liquid film) surrounding the RBC biofilm is continuously exposed to air and bulk liquid alternatively due to the rotational motion of the discs. The dominating factors affecting the thickness of the liquid film are rotational speed, temperature and surface roughness (section 5.2). Although the liquid film varies in thickness depending

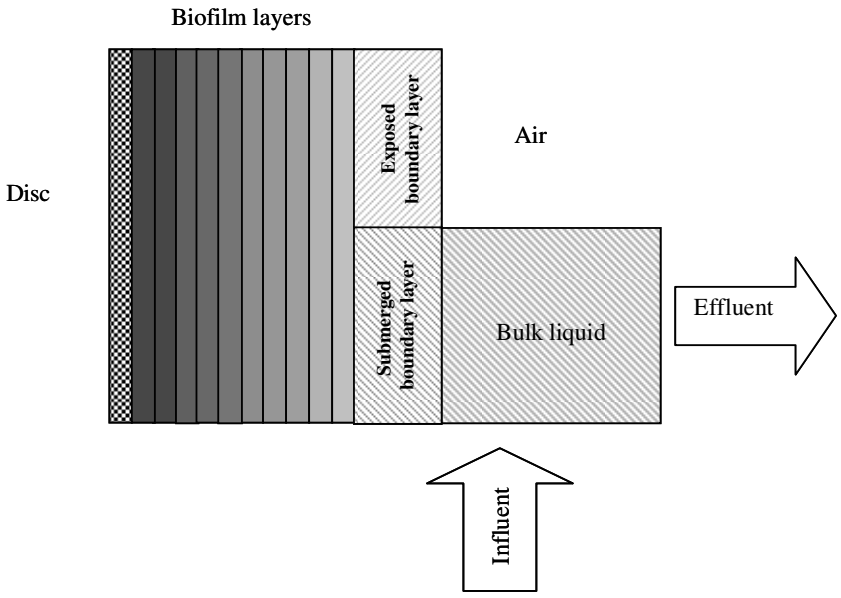

Figure 32 Schematic diagram of the modeled RBC biofilm system

upon the radial position and whether it is exposed to air or inside the bulk liquid, this non uniformity does not have a significant influence in the deeper regions of the biofilm in the

long run. What seems to be of major importance is the concentration of the limiting substrate in diffusion. Therefore, the liquid film is assumed to be stationary and of constant average volume in the model framework. Further, it is assumed to be completely mixed and the concentrations are averaged over the whole rotation. A part of the liquid film is in contact with air while the other part is in contact with bulk liquid at all times. Figure 32 displays the schematic layout of the modelled liquid film entrained over the biofilm surface. In reality, thesubmerged liquid film (boundary layer) may not have the same thickness as the liquid film exposed to air. In the model however, this difference gets averaged during the mass balance of the entire boundary layer. The biofilm is assumed to be composed of several layers of equal thickness and specific surface. The sketch of a typical RBC disc rotating in the bulk liquid reactor is shown in Figure 33. Although many models assume the liquid film to get completely mixed once inside the reactor, in reality there exists a boundary layer inside the reactor as well. Therefore, the average thickness of the exposed liquid film is multiplied by the total exposed surface area (A_{exp}) to obtain the volume of the liquid film in contact with air, while the submerged disc area (A_{sub}) multiplied by the submerged liquid film thickness gives the volume of the film in contact with the bulk liquid.

The RBC model built here is a mixed culture biofilm (MCB) model defined by a set of one-dimensional mass balance equations which govern the spatial distribution and propagation of the dissolved components and particulate components with time, based upon the transport and transformation processes. The dissolved components include nutrients, electron donors (S_S, S_{NH}) and electron acceptors (S_O, S_{NO}) which principally govern the redox reactions while particulate components include biomass cells (X_H, X_A, eps), slowly biodegradable substrates (X_S) and inert organic material (X_I).

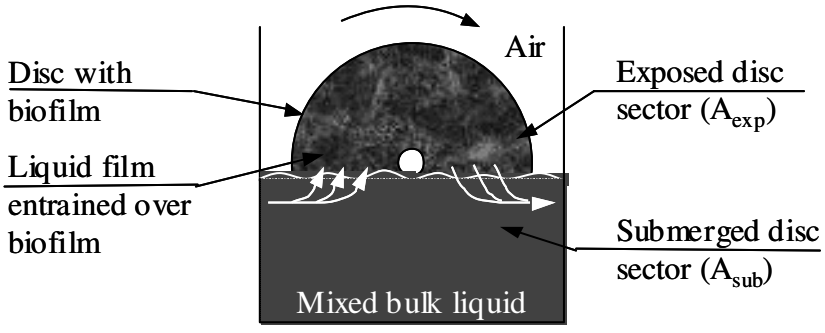

Figure 33 Sketch of the RBC disc with the liquid film and biofilm in operation

6.3.3.2 Mass balance equations for dissolved components: Fast dynamics

Biofilm model equations

Although the other conservation properties of energy and momentum are necessary for the complete balance of any system, the biofilm system is assumed to operate at a constant

temperature and low rotational speed where the changes in the other properties are negligible compared to the mass transfer. The mass transfer through the biofilm is assumed to follow the Fick's law of diffusion. Similar to the liquid film, each biofilm layer is assumed to be a perfectly mixed system and concentration is averaged over the layer thickness. Fick's law essentially states that the mass flux (or driving force) is equal to the diffusivity coefficient multiplied by the concentration gradient. Mathematically, the flux equation may be represented as follows:

$$N_{s_i} = -D_{S_i} \frac{\partial S_i^{Bf}}{\partial x} \tag{6.3}$$

where

N_{S_i} Flux of soluble component i due to molecular diffusion within the biofilm [$ML^{-2}T^{-1}$]

S_i^{Bf} Concentration of the soluble component i within the biofilm [ML^{-3}]

D_{S_i} Effective diffusivity coefficient of the soluble component i within the biofilm [L^2T^{-1}]

x Spatial coordinate representing the depth of the biofilm from the sub-stratum [L]

Figure 34 shows the diffusive transport flux of the soluble component S_i through an infinitesimal slice *dx* of biofilm. A material balance around the differential thickness *dx* of the biofilm would result in the following equation for the state of substrate concentration:

$$\frac{\partial S_i^{Bf}}{\partial t} = -\frac{\partial N_{S_i}}{\partial x} + R_{S_i} \tag{6.4}$$

Where

R_{S_i} Rate of transformation of soluble substrate i per unit volume of biofilm [$ML^{-3}T^{-1}$]

A Total interfacial area of the disc [L^2]

δ_{Bf} Total thickness of the biofilm [L]

The first term on the right of equation 6.4 represents the concentration gradient associated with the diffusive flux through the biomass in a direction normal to the media. Diffusion in the direction of the rotation of the media has been neglected. At any given time step, the advective transport through the biofilm layers is assumed to be negligibly small when compared to the diffusion process (Famularo et al. 1978, Wanner et al. 1995). This can be envisaged from the first-order transport phenomena in case of advection which is extremely slow compared to the second order diffusion process. Therefore diffusion, which is exponentially faster, is considered to be the dominant process in case of biofilms which usually have a thickness of the order of 1-3mm. This speeds up numerical iterations simultaneously. The overall mass transfer occurring by way of the transport process is guided by the concentrations of the substrates at the boundary and neglecting the slow advection process does not make any significant difference to it.

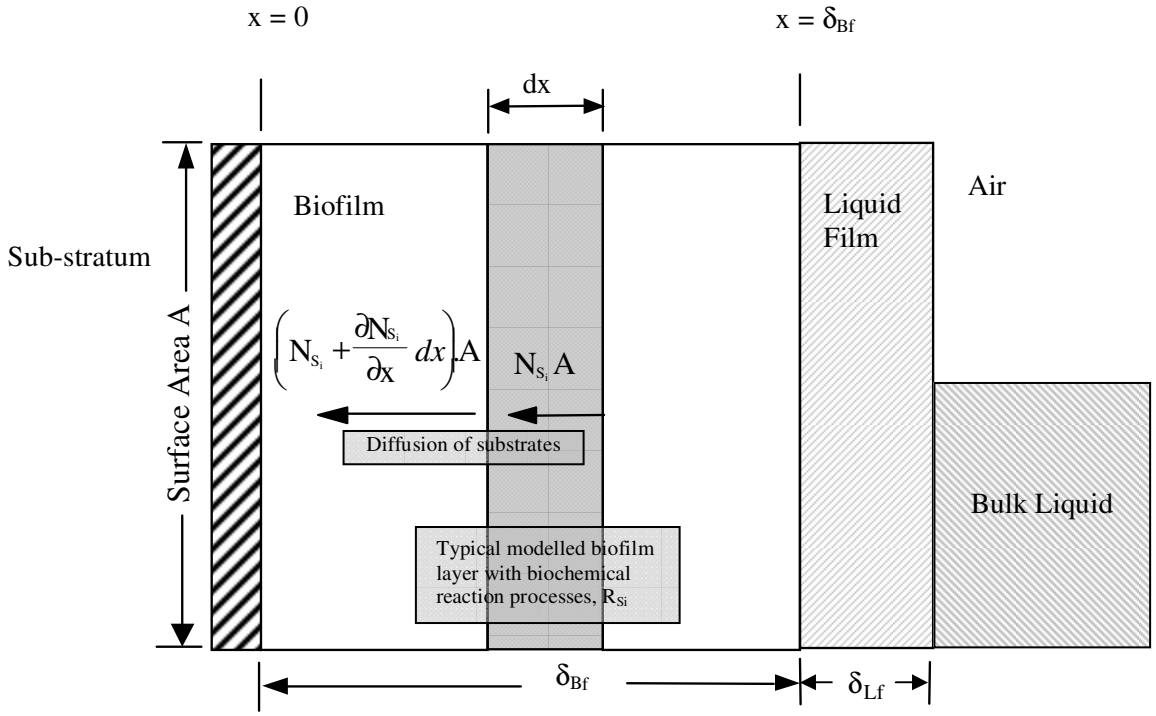

Figure 34 Substrate mass flux through a differential element of biofilm

The last term denotes the reactive transformation of the component based on biochemical kinetics (section 6.3.2). Thus, equation 6.4 may be rewritten as follows:

$$\frac{\partial S_i^{Bf}}{\partial t} = D_{S_i} \cdot \frac{\partial^2 S_i^{Bf}}{\partial x^2} + R_{S_i} \qquad (6.5)$$

(Diffusion) (Reaction)

Boundary condition at biofilm surface

The boundary conditions applying to equation (6.5) at the are as follows:

Flux corresponding to transport at the biofilm-liquid film interface ($x = \delta_{Bf}$):

$$-D_{S_i} \left.\frac{\partial S_i}{\partial x}\right|_{x=\delta_{Bf}} = K_{S_i}\left(S_i^{Lf} - S_i^{Bf}\right) \qquad (6.6)$$

where

K_{S_i} Mass transfer coefficient of substrate S_i at the liquid film - biofilm interface [LT^{-1}]

Flux corresponding to transport at the support media - biofilm interface ($x = 0$) :

$$-D_{S_i} \left.\frac{\partial S_i}{\partial x}\right|_{x=0} = 0 \qquad (6.7)$$

The first boundary condition integrates the biofilm concentrations with the liquid film while the second condition effectively blocks all transport at the media. It is assumed that the support media is non-reactive and allows no transport across it. So flux is zero here. Apart from the boundary conditions, dividing the biofilm into a large number of layers, i.e. high spatial discretization is important in solving the equation 6.5 by means of numerical modelling.

Boundary layer model equations

The liquid film is assumed to be stagnant and concentrations are averaged over the total volume of the liquid film (section 6.3.3.1). A material balance over the liquid film volume V_{Lf} is necessary to maintain mass transport across the system as shown below.

For Oxygen:

$$\frac{dS_{O_2}^{Lf}}{dt} = K_L^{air}.\frac{A_{exp}}{V_{Lf}}\left(S_{O_2}^{*} - S_{O_2}^{Lf}\right) + K_L.\frac{A_{sub}}{V_{Lf}}\left(S_{O_2}^{T} - S_{O_2}^{Lf}\right) - K_L.\frac{A}{V_{Lf}}\left(S_{O_2}^{Lf} - S_{O_2}^{Bf}\Big|_{x=\delta_{Bf}}\right)$$

(Transfer from air) *(Transfer from tank)* *(Transfer to biofilm)* (6.8)

For other substrates:

$$\frac{dS_i^{Lf}}{dt} = K_{S_i}.\frac{A_{sub}}{V_{Lf}}\left(S_i^{T} - S_i^{Lf}\right) - K_{S_i}.\frac{A}{V_{Lf}}\left(S_i^{Lf} - S_i^{Bf}\Big|_{x=\delta_{Bf}}\right) \quad (6.9)$$

(Transfer from tank) *(Transfer to biofilm)*

where

V_{Lf}	Average volume of the liquid film, i.e. $\delta_{Lf}.A$ [L^3]
δ_{Lf}	Average thickness of the liquid film over the whole disc area [L]
A_{sub}	Submerged area of the disc into the bulk liquid [L^2]
A_{exp}	Exposed area of the disc in air [L^2]
$S_{O_2}^{Lf}$	Dissolved oxygen concentration in the liquid film [ML^{-3}]
$S_{O_2}^{Bf}\Big\|_{x=\delta_{Bf}}$	Dissolved oxygen concentration at the biofilm surface [ML^{-3}]
$S_{O_2}^{T}$	Dissolved oxygen concentration in tank [ML^{-3}]
S_i^{T}	Concentration of substrate i in tank [ML^{-3}]
S_i^{Lf}	Concentration of substrate i in liquid film [ML^{-3}]
$S_i^{Bf}\Big\|_{x=\delta_{Bf}}$	Concentration of substrate i at the biofilm surface [ML^{-3}]
$S_{O_2}^{*}$	Equilibrium concentration of oxygen in the bulk at a given temperature [ML^{-3}]
K_L^{air}	Oxygen transfer coefficient from the air into the liquid film [LT^{-1}]
K_L	Average oxygen transfer coefficient in the liquid film (at liquid film- bulk liquid interface or liquid film –biofilm interface), i.e. $\frac{D_{O_2}}{\delta_{Lf}}$ [LT^{-1}]
K_{S_i}	Average mass transfer coefficient of substrate S_i in the liquid film (at liquid film- bulk liquid interface or liquid film –biofilm interface), i.e. $\frac{D_{S_i}}{\delta_{Lf}}$ [LT^{-1}]

At a given temperature, the diffusivity coefficient values of oxygen (D_{O_2}) and various substrates (D_{S_i}) diffusing into biofilm is lower than that in pure water and listed in Table 16 (page 141).

The first term on the right of equation 6.8 represents the diffusive mass transfer from the gas phase (oxygen) to the liquid film through the exposed sector of the disc. This is valid for gaseous components only and is absent for the soluble components as shown in equation 6.9. The next term denotes the mass transfer with the bulk liquid and the last term signifies the transfer to the biofilm. It is same for gaseous as well as dissolved components. Like in the biofilm layers, the advection term has been avoided here because of the small magnitude and simplification of numerical calculations. The liquid film is assumed to be non-reactive as the reactions occurring in the liquid film are negligible compared to that of the biofilm. The boundary layer thickness δ_{Lf} may vary in the exposed and submerged sectors of the disc and therefore the average value may be used to calculate V_{Lf} in determination of the average concentrations in the liquid film. Equations 6.8 and 6.9 are new process definition expressions incorporated by the author for the specific case of RBC based upon the assumptions for the liquid film boundary explained previously (6.3.3.1).

Reactor model equations

The RBC reactor is assumed to be completely mixed in any stage, i.e. concentration of all substrate and particulate components are assumed to be uniform in the bulk liquid for any cascade. The mass balance terms are considered for advection, transfer to or from the liquid film (and subsequently biofilm), transfer of oxygen into the bulk liquid by air drive apparatus and reactions arising from the volatile suspended solids present inside the reactor (equation 6.10 and 6.11). The first two terms represent the major fraction of mass transfer. The fourth term reflects oxygen transfer through the air drive mode which is often used for external aeration in the bulk reactor. This may or may not be activated depending upon the system configuration. In the current lab-scale experiments, there was no external aeration and therefore this term remained deactivated in the model code by putting $K_l a$ equal to zero. Direct transfer of oxygen from air into the bulk liquid through the air-bulk liquid interface is assumed to be negligible.

For Oxygen:

$$V_T.\frac{dS_{O_2}{}^T}{dt} = Q\left(S_{O_2}{}^T{}_{ini} - S_{O_2}{}^T\right) - K_L.A_{sub}\left(S_{O_2}{}^T - S_{O_2}{}^{Lf}\right) + R_{S_{O_2}}{}^T.V_T + K_l a.\left(S_{O_2}{}^* - S_{O_2}{}^T\right)V_T \quad (6.10)$$

(Advection) (Transfer to liquid film) (Reaction) (Transfer from air drive)

For other substrates:

$$V_T.\frac{dS_i{}^T}{dt} = Q\left(S_i{}^T{}_{ini} - S_i{}^T\right) - K_{S_i}.A_{sub}\left(S_i{}^T - S_i{}^{Lf}\right) + R_{S_i}{}^T.V_T \quad (6.11)$$

(Advection) (Transfer to liquid film) (Reaction)

where

V_T Tank volume [L^3]
Q Volumetric flow rate through the tank [L^3T^{-1}]
$S_{O_2}{}^{T}{}_{ini}$ Initial concentration of oxygen in the tank [ML^{-3}]
$S_i{}^{T}{}_{ini}$ Initial concentration of soluble substrate i in the tank [ML^{-3}]
$R_{S_i}{}^{T}$ Reaction rate of soluble substrate i in tank [$ML^{-3}T^{-1}$]
K_1a Oxygen transfer coefficient of the air drive unit [T^{-1}]

The advection term may incorporate and account for a concentration change due to flow recirculation. Where the flow is recycled, equation 6.12 may be used to modify the advective transport term *A1* in the first tank for a recycle from a subsequent stage to the first stage.

$$A1 = \left(Q.S_i{}^{T1}{}_{ini} + Q_r.S_i{}^{Tr}\right) - \left(Q + Q_r\right).S_i{}^{T1} \qquad (6.12)$$

where

$A1$ Advective transport term (First term on the right of equation 6.8 or 6.9) [MT^{-1}]
Q_r Recycle flow rate to the tank [L^3T^{-1}]
$T1$ First stage tank
Tr Tank stage from where the recycle flow is initiated

6.3.3.3 Model equations for particulate components: Slow dynamics

Biofilm model equations

The solids are believed to be displaced in the biofilm matrix by a combined effect of advective and diffusive transport forces. The advective transport is dominant in nature and arises due to the expansion or contraction of the fixed biomass as a consequence of its production or consumption (degeneration) in successive biofilm layers. This movement is further influenced by the attachment and detachment processes occurring at the biofilm surface. A mass balance for particulate species across a differential element dx of the biofilm (Figure 35) will result in the following equation for the state of a particulate matter in that element:

$$\frac{\partial X_j{}^{Bf}}{\partial t} = -\frac{\partial N_{X_j}}{\partial x} + R_{X_j} \qquad (6.13)$$

with

$$N_{X_j}\Big|_x = u\Big|_x . X_j{}^{Bf}\Big|_x - D_{X_j}.\frac{\partial X_j{}^{Bf}}{\partial x} \qquad (6.14)$$

(Advection) *(Diffusion)*

where

$X_j{}^{Bf}$ Concentration of particulate species j within the biofilm in terms of COD [ML^{-3}]

x Space coordinate representing distance from biofilm from sub-stratum [L]

N_{X_j} Flux of particulate species j within the biofilm [$ML^{-2}T^{-1}$]

u Advective velocity of displacement of the particulate species j [LT^{-1}]

D_{X_j} Effective diffusive coefficient of particulate species j [L^2T^{-1}]

R_{X_j} Rate of production of particulate species j within the biofilm [$ML^{-3}T^{-1}$]

Equation 6.13 is of the same form as the substrate transport in the biofilm (equation 6.4). The particulate flux (equation 6.14) contains terms for advective transport as well as diffusive transport similar to Fick's law.

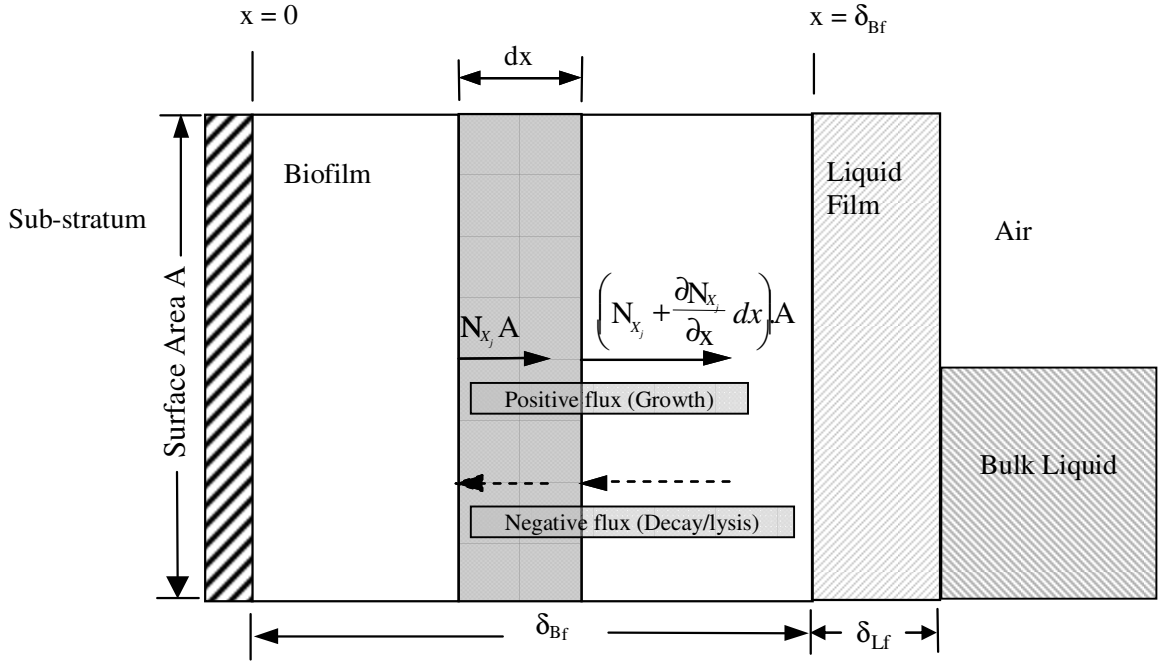

Figure 35 Particulate mass flux through a differential element of the biofilm

This is adopted from the biofilm model of Wanner and Reichert (1996). For the particulate species, advective transport is considered to be of major importance and arises as a result of the difference in the net production (or consumption) rates of various particulate species present in the biofilm. The advective velocity 'u' at a given location x in the biofilm is calculated by the summation of the effective production rates of all particulate species (ΣR_{Xj}) in each individual layer and then the integration of the average growth rate across all the layers starting from the substratum to the location x. This is expressed in equation 6.15 (Wanner and Gujer 1990). The production or the average growth rate varies with the local concentration of nutrients in the biofilm layers.

$$u\big|_x = \int_{x=0}^{x=\delta_{Bf}} \sum_j \left(\frac{R_{X_j}}{\rho}\right) dx' \qquad (6.15)$$

where

ρ Density of the biofilm in units of COD , i.e. the sum of concentrations of all particulate species within the biofilm [ML^{-3}]

The density of biofilm ρ is assumed to be a specific constant property of the system and only the solids are assumed to be displaced within the biofilm matrix. This movement of solids causes a volumetric change of the biofilm layers. As the interfacial biofilm area is assumed to be fixed, this change in volume of the biofilm layers is reflected by a corresponding change in the thickness of each layer (*dx*). Thus, the thickness of the biofilm layers is continuously changing till steady-state is attained. When the net reaction rate is positive (production), then the excess particulate species with its relative local composition is displaced away from the media support towards the surface biofilm layers. On the other hand, a negative reaction rate (net consumption) will push the solids from the upper biofilm layers adjoining the liquid film towards the media support (Figure 35). Equation 6.13 may be rewritten as shown in 6.16.

$$\frac{\partial X_j^{Bf}}{\partial t} = -u\big|_x \cdot \frac{\partial X_j^{Bf}}{\partial x} + D_{X_j} \frac{\partial^2 X_j^{Bf}}{\partial x^2} + R_{X_j} \qquad (6.16)$$

(Advection) (Diffusion) (Reaction)

The transport by diffusion is again a second order motion compared to advection and depends primarily upon the effective diffusivity coefficient D_{X_j} of the particulate components into biofilm. However, this coefficient for particulates is substantially small compared with the diffusivity coefficient of dissolved components D_{S_i} into the biofilm. In case of dissolved components, the small size of the species enables more intrinsic Brownian motion and hence a high value of $D_{Si.}$ The diffusive transport term for solids is empirical in nature, as there is no experimentally measured data available for the coefficient as a separate parameter (Wanner and Reichert, 1996). Rather, this equation accounts for the mixing of the particulate species inside the biofilm matrix, which would otherwise be stratified if there is only advective motion. In other words, without D_{X_j}, the attached solids will virtually stay at the biofilm surface and likewise the effect of detached biomass at the surface will be not be carried through inside the biofilm. In reality, the mixing may arise as a result of the surface forces such as attachment and detachment of particulate components at the biofilm surface, non-homogenous structure of the biofilm matrix, pore channels, movement of bacteria inside the matrix (motility) etc. These surface forces lead to a mechanical deformation of the matrix and hence a change in overall biofilm thickness as well as the concentration of the particulate species in the individual biofilm layers. The movement of solids inside the biofilm matrix and

the physical processes occurring at the bulk liquid-biofilm surface can be visually interpreted as shown in Figure 36.

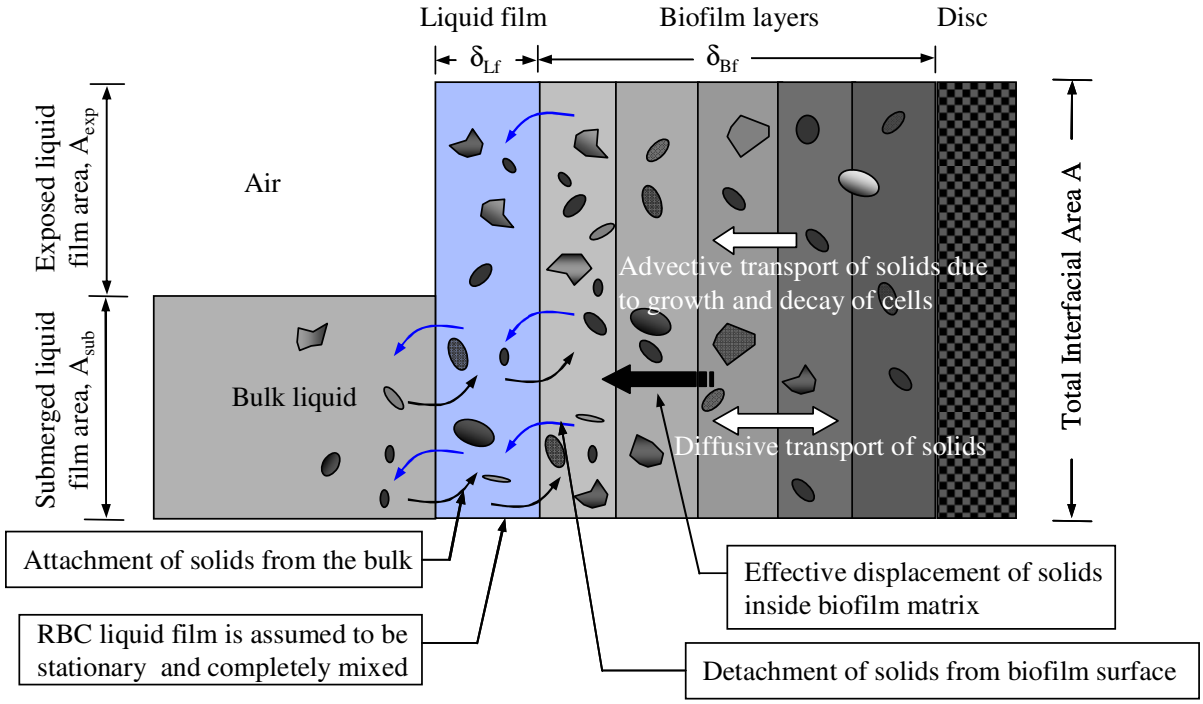

Figure 36 Transport and detachment of solids occurring in a RBC biofilm

The boundary conditions pertaining to the application for a biofilm system represented by equation 6.16 is described by equation 6.17 and 6.18 (Wanner and Reichert, 1996).

Flux of particulate components at the support media - biofilm interface ($x = 0$):

$$N_{X_j}\Big|_{x=0} = 0 \qquad (6.17)$$

i.e.

$$\left(u\big|_{x=0}\right) = 0, \text{ and}$$

$$\left(-D_{X_j} \cdot \frac{\partial X_j^{Bf}}{\partial x}\Big|_{x=0}\right) = 0 \qquad (6.18)$$

As it is assumed that no particulate component is exchanged between the substratum and the biofilm, the net effective particulate flux there is zero. Thus, equation 6.17 effectively stops all transport at the media. The boundary condition existing at the biofilm surface (i.e. $x = \delta_{Bf}$) is described in equations 6.29 and 6.30.

Attachment and detachment mechanisms at the biofilm surface

Although it is well established that the exchange reactions are dominant at the biofilm surface, the mechanism is very complicated and mathematically still empirical in nature. It is believed that loss of biomass from a biofilm occurs through regular erosion (or shear) from the surface and irregular loss by sloughing from the entire biofilm. Simultaneously, attachment is

initiated by particulate flocs suspended in the bulk liquid, which try to attach to the biofilm surface. These detachment and attachment processes depend upon a number of factors such as biofilm thickness, rotational speed, influent loading, influent quality, species growth rate, media roughness, biofilm age and density, temperature and denitrification gases formed in the inner layers The entire biofilm presents a moving boundary problem since the thickness of the film varies due to a combination of various processes governing the attachment and detachment phenomena.

$$\frac{d\delta_{Bf}}{dt} = f(u, \delta_{Bf}, \omega, Q, S_i, t, \tau, T.....) \tag{6.19}$$

where

δ_{Bf} Thickness of biofilm at time t [L]
ω Rotational speed of RBC [rpm]
τ Shear stress at the biofilm surface
Q Volumetric flow rate [L^3T^{-1}]
S_i Substrate loading rate [$ML^{-2}T^{-1}$]
T Ambient temperature [°]

Many attempts have been made to quantify these processes, but most of them are only approximate assumptions in nature. In the current model, attachment and detachment of biomass have been modelled considering mathematical expressions based upon first-order or second-order forms of biomass density and biofilm thickness. The expressions use rate constants for attachment and detachment whose approximate values are available in literature and exact values are guided by trial calibration runs.

Attachment of biomass

Particulate attachment by flocculation is modelled as a linear (first order) process depending upon the particulates concentration in the tank (Wanner and Boller, 1990). The attachment flux of particulate matter from the bulk liquid to the biofilm surface is given by the following equation:

$$N_{att,j} = k_{att,j}.X_j^T \tag{6.20}$$

where

$N_{att,j}$ Attachment flux of the particulate species j [$ML^{-2}T^{-1}$]
$k_{att,j}$ Attachment rate coefficient of the particulate species j [LT^{-1}]
X_j^T Concentration of particulate species j in the bulk liquid [ML^{-3}]

As a result of the attachment flux, the biofilm surface would move with a velocity u_{att} which may be represented as follows:

$$u_{att} = \sum_{j} \frac{N_{att,j}}{\rho} \tag{6.21}$$

where

u_{att} Attachment velocity at the biofilm surface [LT^{-1}]
ρ Density of the biofilm [ML^{-3}]

Detachment of biomass

The detachment mechanism in a RBC biofilm is assumed in the form of regular mass loss by shear from the biofilm surface. This loss is determined by a shear rate coefficient which depends upon the biofilm thickness. The shear can be modelled as linear or second-order equation with respect to the biofilm thickness. In case of linear representation of biomass erosion at the surface, the detachment flux is as shown in 6.22. This is based upon the biofilm model of Gujer and Boller (1990).

$$N_{det,j} = k_{det,j} . \delta_{Bf} . \rho \tag{6.22}$$

For second-order biomass loss, the detachment flux may be expressed as shown in 6.23. This is based upon the multi-species biofilm model of Wanner and Gujer (1986).

$$N_{det,j} = k'_{det,j} . \delta^{2}_{Bf} . \rho \tag{6.23}$$

where

$N_{\det,j}$ Detachment flux of particulate species j [$ML^{-2}T^{-1}$]
$k_{\det,j}$ Detachment rate coeff. of particulate species j in case of linear biomass loss [T^{-1}]
$k'_{\det,j}$ Detachment coeff. of the particulate species j in case of exponential biomass loss [$L^{-1}T^{-1}$]

The selection of a specific detachment mode would be guided by the growth and density of the biofilm in a real system. Both of the above forms of mass loss are empirical in nature and try to simplify the cumulative effect of various processes occurring at the biofilm surface (6.19). There are many other forms of empirical representation of biomass loss. The current model was initially coded with both the options of detachment (6.22 and 6.23) for loss of biomass. However, when the second-order detachment expression (6.23) was used, the model results for the current RBC set-up exhibited more accurate estimation of the biofilm thickness at steady-state for each cascade. Moreover, the rate coefficients are easy to obtain from literature. The second-order detachment function has been subsequently validated by many authors (Chen and Li, 1999, Xavier et al. 2005). Xavier et al. quoted Stewart (1993) as having mentioned that the second-order dependence ensured the existence of steady-state thickness even for extreme cases of unlimited growth. Biofilm in reactors for secondary and tertiary treatment are more compact and homogenous in nature while those in primary reactors are more porous and fluffy and therefore less compact. Therefore, the detachment coefficients

may be chosen accordingly with lower $k'_{det,j}$ values for the low erosion regime while a higher value for the high erosion regimes of biofilm (Xavier et al. 2005). Different literature cite different values for $k'_{det,j}$ depending upon their biofilm growth and thickness stabilisation, some of which are listed below:

$k'_{det,j}$ value	Units	Reference
750	$m^{-1}d^{-1}$	Wanner and Gujer (1986)
23 to 2300	$m^{-1}d^{-1}$	Xavier et al. (2005)
0 to 4000	$m^{-1}d^{-1}$	Merkey, Rittmann and Chopp (2006)

The current model used $k'_{det,j}$ values from 66 $m^{-1}d^{-1}$ to 750 $m^{-1}d^{-1}$ in the runs to stabilise the biofilm thickness with experimental values.

The detachment flux would result in the removal of particulate species from the biofilm surface with a detachment velocity u_{det} which may be represented as shown in equation 6.24.

$$u_{det} = \sum_j \frac{N_{det,j}}{\rho} \tag{6.24}$$

where

u_{det} Detachment velocity at the biofilm surface [LT^{-1}]

Biofilm thickness

It has been observed that results from mathematical models assuming a fixed biofilm thickness is often misleading while predicting the performance of systems with large variations in thickness in time (Morgenroth et al. 2000). Although biofilters with backwashing or trickling filters are most susceptible to large fluctuations in thickness, the effect has to be considered for every system including RBCs. The temporal variation of biofilm thickness is based upon the dynamics of attachment and detachment mechanisms and the advective transport phenomenon of the solids inside the biofilm matrix. The progression of biofilm thickness δ_{Bf} with time may be represented mathematically as shown in equation 6.25 (Gujer and Boller, 1990).

$$\frac{d\delta_{Bf}}{dt} = u\Big|_{x=\delta_{Bf}} + u_{att} - u_{det} \tag{6.25}$$

By combining equations 6.15, 6.21 and 6.24, the temporal variation of biofilm thickness in equation 6.25 may be represented mathematically as expressed below:

$$\frac{d\delta_{Bf}}{dt} = \int_0^{\delta_{Bf}} \sum_j \left(\frac{R_{X_j}}{\rho}\right) dx' + \sum_j \left(\frac{N_{att,j}}{\rho}\right) - \sum_j \left(\frac{N_{det,j}}{\rho}\right) \tag{6.26}$$

(Advective vel. due to growth/decay) (Attach. vel.) (Detach. vel.)

In the current model, it is assumed that the RBC will be treating pre-sedimented secondary effluent which contains very little suspended matter and hence the flocculation is assumed to be negligible. So the effect of $N_{att,j}$ is neglected by substituting $k_{att,j}$ as zero as it makes little difference to the particulate density in the biofilm layers and thereby the concentration fluxes. As a simplified approach many modellers including Horn et al. (1997) hypothesized detachment as a linear function of advective velocity u at the biofilm surface and gave the following formulation:

$$if\ u\Big|_{x=\delta_{Bf}} \leq 0 \text{ then } u_{det} = 0 \tag{6.27}$$

$$if\ u\Big|_{x=\delta_{Bf}} > 0 \text{ then } u_{det} = u \cdot k''_{det} \tag{6.28}$$

where

k''_{det} Detachment coefficient which can be any decimal fraction [-]

$k''_{\text{det,}}$ value had been arbitrarily chosen as 0.1 by Horn et al.(1997) and 0.8 by Wanner et al. (1996) in their mixed-culture biofilm models based upon the growth of biofilm. However, in the current RBC model, only equation 6.27 has been included while the detachment is modelled more realistically as a function of biofilm thickness (6.23). Equation 6.27 literally symbolises that when the advective transport of solids is from biofilm surface towards the substratum, there would be no detachment. The negative *u* can be due to net consumption e.g. endogenous respiration or excess decay of biomass under starvation conditions. In such cases, the biofilm starts to shrink. For a constant influent loading, the steady-state growth and detachment rates should ideally balance each other. Time taken to reach the steady-state thickness from initial conditions in the model can also be correlated with the experimental growth of biofilm when data is available.

Boundary condition at the biofilm surface

The loss of particles at the biofilm surface due to the detachment and the simultaneous attachment of particulates from the bulk fluid make it necessary to reconsider the mass balance for particulate components at the surface layer of the biofilm. So the equation 6.16 is rewritten for the biofilm surface (i.e. $x = \delta_{Bf}$) as follows.

In case of a linear form of biomass loss (corresponding to 6.22):

$$\frac{\partial X_j^{Bf}}{\partial t}\Big|_{x=\delta_{Bf}} = -u\Big|_{x=\delta_{Bf}} \cdot \frac{\partial X_j^{Bf}}{\partial x}\Big|_{x=\delta_{Bf}} + R_{X_j}\Big|_{x=\delta_{Bf}} + \left(k_{att,j}.X_j^T - k_{det,j}.\delta_{Bf} \cdot X_j^{Bf}\Big|_{x=\delta_{Bf}}\right) \cdot \left(\frac{A}{V_{Bf}\Big|_{x=\delta_{Bf}}}\right) \tag{6.29}$$

(Advection) (Reaction) (Attached biomass - detached biomass)

In case of second-order dependence for biomass loss (corresponding to 6.23):

$$\left.\frac{\partial X_j^{Bf}}{\partial t}\right|_{x=\delta_{Bf}} = -u\Big|_{x=\delta_{Bf}} \cdot \left.\frac{\partial X_j^{Bf}}{\partial x}\right|_{x=\delta_{Bf}} + R_{X_j}\Big|_{x=\delta_{Bf}} + \left(k_{att,j}.X_j^{T} - k'_{det,j}.\delta_{Bf}^{2} \cdot X_j^{Bf}\Big|_{x=Bf}\right).\left(\frac{A}{V_{Bf}\Big|_{x=\delta_{Bf}}}\right) \quad (6.30)$$

(Advection) (Reaction) (Attached biomass - detached biomass)

where

$V_{Bf}\Big|_{x=\delta_{Bf}}$ Control volume i.e. volume of the surface biofilm layer, i.e. $A.dx$ [L^3]

$X_j^{Bf}\Big|_{x=\delta_{Bf}}$ Concentration of particulate component j at the biofilm surface [ML^{-3}]

Equations 6.29 and 6.30 consider the effect of attachment as well as biomass loss by shear through the interfacial surface area of biofilm A as defined by $N_{att,j}$ and $N_{det,j}$ in 6.20, 6.22 and 6.23 respectively. In the current model, the second-order detachment expression (6.30) was used to calibrate the biofilm thickness with the experimental results. To maintain a constant density of biofilm, the time derivative, i.e. left hand side of equations 6.29 or 6.30 need to be 0. In the model, this is obtained by adjusting the shear rate constant $k'_{det,j}$ as explained previously. This balances the mass added by growth and attachment with the mass lost as a result of detachment at any given time.

The gain and loss of biomass at the biofilm surface need to be compensated by considering an equal amount of mass change in the bulk liquid reactor so as to maintain the mass balance. The control volume is the reactor volume in that case. The attachment and detachment of solids at the surface get slowly transferred into the deeper layers by the effective diffusivity coefficient D_{X_j} for the particulate components inside the biofilm.

Liquid boundary layer

The liquid film boundary at the biofilm surface acts as a mass transfer corridor as described previously (section 6.3.3.2). However, for the particulate components, the advective effects, diffusion and biochemical transformation processes are neglected due to their small magnitude. The particulates detached from the biofilm surface simply get transported through this layer into the bulk liquid. Similarly, biomass flocculating from the bulk move through this layer into the biofilm surface. As the liquid film is assumed to be non-reactive and no reaction processes have been incorporated in that layer, therefore, the gain or loss of biomass due to attachment or detachment at the biofilm surface can be substituted directly into the reactor. This reduces the numerical complexity while maintaining the mass balance across the total system.

Reactor model equations

The completely mixed bulk liquid compartment may contain volatile suspended solids (VSS) i.e. biomass, which could participate in the substrate degradation process as well. A part of the suspended biomass is generated by solids detaching from the biofilm surface. Therefore, the mass balance for the reactor needs to consider the reaction processes due to this VSS in the bulk liquid in addition to advection term. The solids also reattach to the biofilm surface and penetrate it (Drury et al. 1993). Equations 6.31 and 6.32 show the mass balance equations that have been considered in the RBC model corresponding to the attachment and selective detachment method based on linear or exponential forms as explained previously.

In case of a linear form of biomass loss (corresponding to 6.22):

$$V_T . \frac{dX_j{}^T}{dt} = Q\left(X_j{}^T{}_{ini} - X_j{}^T\right) + \left(k_{det,j} . \delta_{Bf} \cdot X_j{}^{Bf}\Big|_{x=\delta_{Bf}} - \quad k_{att,j} . X_j{}^T\right) \cdot A \quad + \quad R_{X_j}{}^T . V_T \qquad (6.31)$$

(Advection) (Biomass detached - biomass attached) (Reaction)

In case of second-order expression for biomass loss (corresponding to 6.23):

$$V_T . \frac{dX_j{}^T}{dt} = Q\left(X_j{}^T{}_{ini} - X_j{}^T\right) + \left(k'_{det,j} . \delta_{Bf}^2 \cdot X_j{}^{Bf}\Big|_{x=\delta_{Bf}} - \quad k_{att,j} . X_j{}^T\right) \cdot A \quad + \quad R_{X_j}{}^T . V_T \qquad (6.32)$$

(Advection) (Biomass detached - biomass attached) (Reaction)

where

$R_{X_j}{}^T$ Reaction rate of particulate species j in the tank [$ML^{-3}T^{-1}$]

The first term on the right represents the advection in the tank which can be substantial due to the large volume of the tank. The last term represents the reaction rate of the particulate species j in the tank based upon its concentration. The same kinetic model (modified ASM No. 3) has been used for the calculation of the reaction rates. Although all gain or loss of biomass at the biofilm surface occur through the liquid film, these mass changes are directly balanced between the tank and the surface biofilm layer in the model code.

When the flow is recycled, equation 6.33 may be used to modify the advective transport term $A1'$ in the first tank for a recycle from a subsequent stage to the first stage.

$$A1' = \left(Q . X_j{}^{T1}{}_{ini} + Q_r . X_j{}^{Tr}\right) - \left(Q + Q_r\right) . X_j{}^{T1} \qquad (6.33)$$

where

$A1'$ Advective transport term (First term on the right of equation 6.29 or 6.30) [MT^{-1}]

$T1$ First stage tank

Tr Tank stage from where recycle flow is initiated

$X_j{}^{T1}$ Concentration of particulate species j in the first stage tank [ML^{-3}]

$X_j{}^{Tr}$ Concentration of particulate species j in the recycle flow [ML^{-3}]

6.4 Numerical method as a solution strategy

The numerical method is the feasible and relatively precise approach as a solution tool to the partial and ordinary differential equations involved in the mass balance of the various components in the multi-species model. The simulations involve the calculation of the variables in the non-steady differential terms at consecutive time steps till a steady state value is achieved. Finite difference methodology is one of the approaches which help to solve the problem. For the process solution of the partial differential equations (pdes), the method of lines is used which is a technique to transform the partial differential equations into a set of ordinary differential equations (odes) by spatial discretization. The solution methodology is discussed in detail in Appendix-III.

6.4.1 Model features

The calibration and validation of the current RBC model is based upon the laboratory-scale experimental set-up with 3 cascades. In other cases, the model behaviour has been verified with available resources from the literature. The same code algorithm can be used for pilot-scale and field-scale set-up, provided it is further calibrated for such set-ups based on available data.

The large scale of temporal variation in the value of the variables (S_i, X_j, δ_{Bf}) made long-term steady-state simulations virtually impossible when fixed time-steps were used in meeting the stability and convergence criteria of the fully explicit finite-difference methodology (Appendix –III). To overcome this difficulty, a fully implicit variable time-step solver (ode 15s) was employed in Matlab which could easily and efficiently handle the stiff nature of the problem. Although the fixed step non-stiff solvers like Runga-Kutta-4 are relatively more accurate numerically, they are very slow for long runs and often not so vital when many other aspects of biofilm modelling are based upon hypothetical assumptions. Apart from the truncation error generated by neglecting the higher terms of the Taylor expansion, the other rounding off error originates from a finite accuracy in the computer, up to a significant number of digits. In every case, the resultant truncation error during the semi-discretization of the pdes into odes would exist. To minimize the effect, a high number of biofilm layers (N ≅ 15-20) have been considered in the model structure. The high spatial discretization eventually made the problem algorithm very stiff and consequently a stiff ode solver based on backward differentiation techniques was necessary. The stiff ode solver is a variable time step solver which uses linearly implicit backward differentiation techniques (Gear's method) as well as

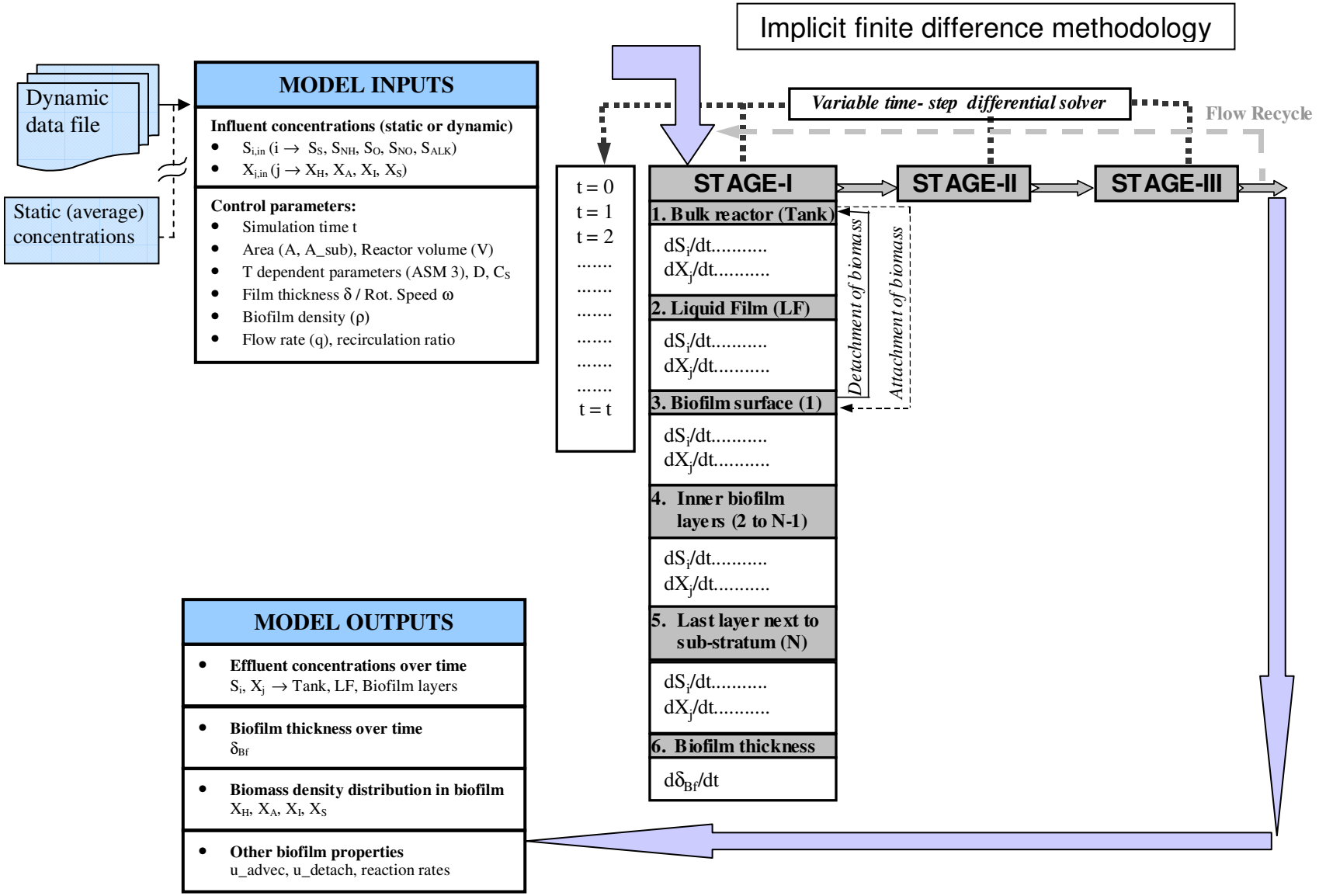

Figure 37 Schematic representation of the functional structure of the RBC model

numerical differentiation formulae to generate a stable and consistent solution. The solver generates numerical Jacobians from time to time to check the sensitivity of the parameter values.

6.4.2 Functional structure of the model

The functional structure of the model is schematically represented in the flow chart in Figure 37. The code is built in the form of an array (matrices) of N biofilm layers with each layer containing the discretized variable differentials which are solved simultaneously. The input data may be fed into the code from a pre-formatted text file representing dynamic influent loading data based on day to day measurement. For steady-state runs, the influent concentrations may be directly typed into the code. In case of dynamic data input, Matlab interpolates the data at intermediate time steps using its built-in functions. The differential equation solver in Matlab calculates the differential value 'dS' for each variable parameter by providing the time step 'dt' based upon the simultaneous behaviour of change of all state variables in all the stages of the RBC. When a variable has a high dS value, i.e. it is changing too fast (whether positive or negative), the solver reduces the time step dt to a tiny value. The stiff algorithm based on Gear's method is used for this purpose. The run gets slowed down and numerical calculations are intensive. Once the processes get more steady and dS values are very small, the solver may increase the step size for time. At steady-state, the dS values should be ideally zero. However, if the variables again change (e.g. dynamic data input), the solver may go back to small step size and the runs take longer time. In fact, with dynamic data input, a steady-state value is not relevant contrary to the case of static inputs. The runs are in fact guided by the duration of the input data, or in case of data from online measurements, it can run continuously.

The model output of all the state variables is obtained in graphical format over time for each stage and can be further processed and analysed using the output file in data processing software like MS-Excel or Origin. The program code of the RBC model with a detailed description for implementation in Matlab is added in Appendix-II.

7 Results and discussions of the RBC model

7.1 Model calibration

A detailed description of the model structure is included in Chapter 6. The input values are based upon the experimental data obtained from my colleague Mr. A. Blank for the experimental set-up-I. The unit of calculation in the differential equations for the concentrations has been kept in gm^{-3} at every time step. This can also be represented by surface fluxes ($gm^{-2}d^{-1}$) for the RBC at every stage as the interfacial area has been assumed to be constant. Many corrections and numerous pre-runs were required before the model could be adequately calibrated with an experimental data. The dry density of the biofilm was measured in the laboratory and used as an input into the numerical model. Table 14 shows the density data obtained from experiment. For model calibration, the experimental results obtained at a temperature of 25°C have been used. Conventionally, the biofilm is divided into two volumetric fractions, i.e. (1) the liquid fraction (ε_l) composed of interstitial fluid and extracellular polymeric substances (eps), in which the dissolved components are transported by diffusion and (2) the solids fraction (ε_S), which is composed of particulate components such as bacteria cells, inert material, and decayed biomass. There is also the intercellular fluid present inside the cell body i.e. cytoplasm and nucleus, but it is not conventionally modelled because of its small magnitude. Mathematically, the fractions may be represented by equation 7.1 as follows:

$$\varepsilon_l + \sum_{j=1}^{n_X} \varepsilon_{S_j} = 1 \tag{7.1}$$

where

n_x Number of particulate components considered [-]

ε_l Liquid phase volume fraction [-]

ε_{S_j} Solid phase volume fraction of particulate species j [-]

In the model, the liquid phase fraction (ε_l) is assumed to be constant as nearly 96-97% of the biofilm is liquid and ε_l variation shall have little effect on the steady-state component concentrations. The solids fraction of species j is represented as follows.

$$\varepsilon_{S_j} = \frac{X_j}{\rho_j} \tag{7.2}$$

where ρ_j is the density of the particulate component j, which is assumed to be a constant (Wanner and Reichert, 1996). This is based on the widespread assumption of biomass as a continuum. So, the mean biofilm density ρ which is measured experimentally can be represented as shown below.

$$\rho = \sum_{j=1}^{n_X} \left(\varepsilon_{S_j} \rho_j \right) = \sum_{j=1}^{n_X} X_j \tag{7.3}$$

Table 14 shows the density data obtained from laboratory measurement. The total solids fraction (ε_s), which is about 3-4% of the biofilm, is assumed to be composed of different particulate components and represented by relative fractions. As start-up input value, the solids are assumed to be distributed in the biofilm matrix as 40% heterotrophs, 20% autotrophs and the rest as particulate inert material (Wanner and Gujer, 1986). This initial condition for biofilm growth is only figurative in nature and does not attach real significance because the runs adjust the distribution depending upon substrate diffusion into the individual biofilm layers, the process kinetics in each layer and the displacement and detachment of the solids from the biofilm.

Table 14 Density data from experiment used as model input (set-up-I) at 25°C

Experiment data				**Simulation Input (start-up values)**		
Stage-I	Biofilm density (Wet)	1060	Kg/m^3	Assumed particulates distribution		gCOD/m^3
	Water content, ε_l	97	%	Solids fraction, ε_S	3 %	
	Dry biofilm density	28573	gTSS/m^3	Heterotrophic fraction, ε_{Het}	0.40* ε_S	**18200**
	Inorganic Inerts	0	%	Autotrophic fraction, ε_{Aut}	0.20* ε_S	**9200**
	Active biomass density	28573	gVSS/m^3	Inert fraction, ε_{In}	0.40* ε_S	**18200**
	COD of active biomass	**45500**	gCOD/m^3	Total biofilm density, ρ		**45600**
Stage-II	Biofilm density (Wet)	1040	Kg/m^3	Assumed particulates distribution		gCOD/m^3
	Water content, ε_l	96	%	Solids fraction, ε_S	4 %	
	Dry biofilm density	38167	gTSS/m^3	Heterotrophic fraction, ε_{Het}	0.40* ε_S	**24300**
	Inorganic Inerts	0	%	Autotrophic fraction, ε_{Aut}	0.20* ε_S	**12200**
	Active biomass density	38167	gVSS/m^3	Inert fraction, ε_{In}	0.40* ε_S	**24300**
	COD of active biomass	**60700**	gCOD/m^3	Total biofilm density, ρ	3 %	**60800**
Stage-III	Biofilm density (Wet)	1010	Kg/m^3	Assumed particulates distribution		gCOD/m^3
	Water content, ε_l	97	%	Solids fraction, ε_S	3 %	
	Dry biofilm density	30394	gTSS/m^3	Heterotrophic fraction, ε_{Het}	0.40* ε_S	**19400**
	Inorganic Inerts	0	%	Autotrophic fraction, ε_{Aut}	0.20* ε_S	**9800**
	Active biomass density	30394	gVSS/m^3	Inert fraction, ε_{In}	0.40* ε_S	**19400**
	COD of active biomass	**48400**	gCOD/m^3	Total biofilm density, ρ		**48600**

The density of the solids phase ρ_j is assumed to be a specific constant property of the biofilm and only the distribution of the solid species (ε_s %) changes with time.

For calibration, the model assumed that there would be no suspended biomass in the tank initially and all the biomass that arises subsequently in the tank resulted from the detachment of solids from the biofilm. Density data from the experimental biofilm was taken as initial values. In order to study the growth of the biofilm, the model assumed as initial value, a biofilm thickness of 90µm in stage-1, 60µm in stage-2 and 30µm in stage 3. Second order detachment mechanism (equation 6.23) was used in the model to steady the thickness of the biofilm and calibrate it with experimental value. The kinetic parameters and diffusivity coefficients of the soluble components were taken from references as shown in Table 12, Table 13 and Table 16. The diffusivity coefficient for soluble organic substrate (molasses) was assumed to be similar to acetate and taken as 60% of the value in pure water. For all other soluble components, the diffusivity value was assumed to be 80% of that in pure water (Stewart 1998). The influent concentrations for the simulations are based on the experimental set-up and detailed in chapter 4. All the kinetic and stoichiometric parameters are detailed in chapter 6. As it is difficult to maintain a constant loading rate of organic substrate and ammonia throughout the experiment, the mean value of the daily variations over a period of nearly three months has been used in the steady-state simulation runs. During the first phase of experiments from Sept. 2005 to Dec. 2005, the ambient temperature was maintained at about 25°C. In the second phase from Jan. 2006 to May 2006, temperature was increased to 30°C. An accurate measurement of the laminar liquid layer thickness was not possible in the experiment because of the rough biofilm surface. It is often difficult to ascertain whether the attached film is part of the liquid film or the eps surrounding the biofilm. It was estimated that the average thickness would be about 60µm at the considered rotational speed of 2-3 rpm. A higher rotational speed was avoided because it caused the biomass to shear-off. Moreover, a thick boundary layer as a consequence of high rotational speed would offer greater diffusive resistance to oxygen, while it would possibly prevent substrate limitation inside the biofilm during the air exposure cycle. So the biofilm has higher chances of getting oxygen limited instead. Similarly, a thin boundary layer at low rotational speed would provide deeper oxygen diffusion, while the biofilm could get substrate limited especially near the end of the air exposure phase under low loading rates. For the purpose of model calibration, the experimental set-up-I has been used since both of the laboratory-scale configurations have the same loading rates and showed nearly similar performance. The hydraulic retention time in the system was 5.0 hours and hydraulic loading rate q was 22.0 l $m^{-2}d^{-1}$ (Chapter 4). The simulation run time of 300 days for steady-state runs

is chosen randomly although most variables stabilise within 30-60 days. The particulate species and biofilm thickness however take longer time to get steady down.

7.1.1 Dissolved components

7.1.1.1 Steady state concentration of DO

Figure 38 shows the simulated and experimental DO concentration in the mixed bulk liquid in the 3-stages of the experimental set-up. The rotational speed was around 2 rpm and the

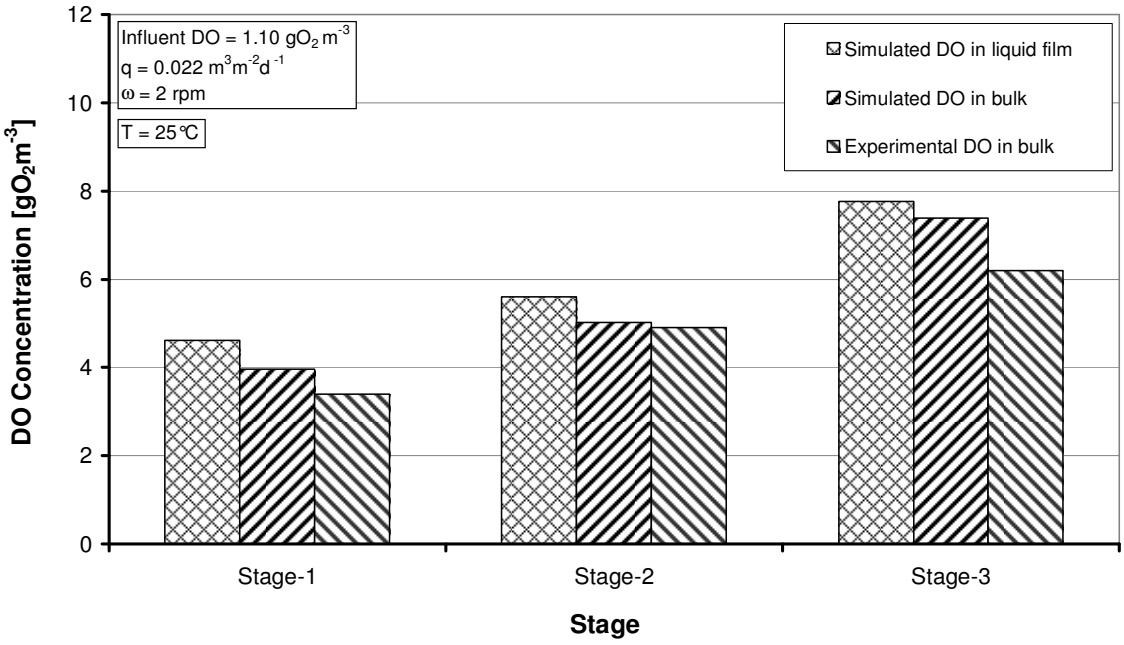

Figure 38 Simulated and experimental DO concentration in bulk liquid in RBC stages

overall hydraulic loading rate q on the system was maintained at about 0.022 $m^3m^{-2}d^{-1}$. The DO concentration is significantly high in the latter stages and approaches near the saturation value when the organic and the ammonium loads are lower and the biofilm thinner. The high uptake rate of oxygen by the biomass in the stage-1 results in lower concentrations. This is due to increased oxygen requirement by the mixed culture biofilm. The experiments show sufficient DO concentrations in the bulk and this annuls the requirement for external aeration in the tank. This is particularly relevant in the laboratory-scale set-up for the given maximum organic loading rate of 5.0 g COD $m^{-2}d^{-1}$. The laminar liquid film has typically higher concentration of DO as compared to the tank owing to direct air exposure. The DO gets limited inside the biofilm due to diffusive resistance and uptake.

The diffusive penetration of oxygen through the liquid boundary layer can be studied through simulation as a special case (snapshot view of oxygen diffusion in one RBC cycle) as shown in Figure 39. This was obtained from a special simulation scenario where an RBC disc with a fixed biofilm thickness of 900µm and constant species density under average nutrient

loading as in stage-1 is assumed to be switching between alternate air and bulk liquid exposure cycles. The disc along with the liquid boundary layer was divided into two equal parts, which exchange the concentrations through the boundary layer every half-cycle.

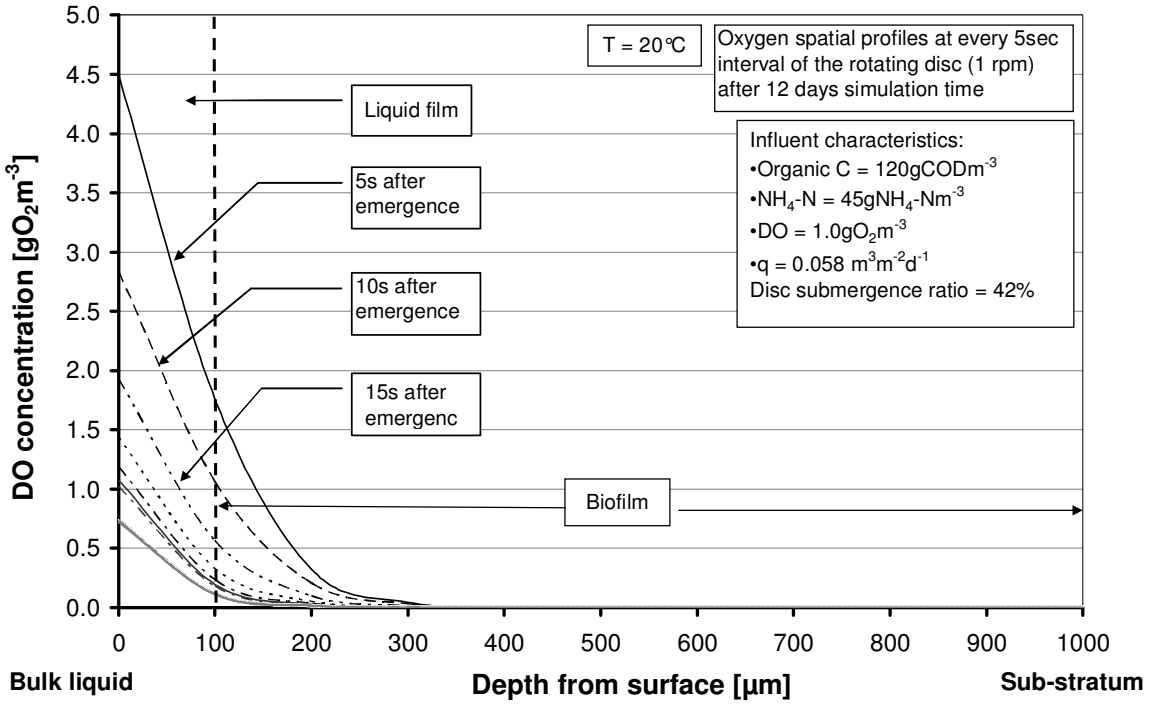

Figure 39 Diffusive penetration of oxygen during one cycle of RBC in stage-1

The DO concentration of the liquid film inside the bulk liquid was assumed to be nearly same as that of the bulk liquid. An average liquid film thickness of about 100µm was taken for both parts of the disc. The DO concentration in the liquid film represents the average value over its thickness. The plots generated after a 12 day simulation show that most of the oxygen gets uptaken beyond a biofilm depth of 250-300µm. As the disc emerges out from the bulk liquid, oxygen diffusion from air into the liquid boundary is faster than the uptake by the bacteria, and results in a higher initial concentration in the liquid film (upper curves in Figure 39). But as the disc continues to rotate, the high uptake rate by the aerobic bacteria lower the average concentration in the liquid film, so that it decreases towards the end when the disc submerges into bulk liquid. As there is continuous uptake by the bacteria even after the disc submerges back into the bulk liquid, so oxygen concentration keeps decreasing till re-emergence when the above profile gets repeated.

7.1.1.2 Steady state concentration of soluble organic substrate

The synthetic wastewater fed into the system is composed of diluted molasses, which is assumed to be soluble biodegradable organic substrate (equivalent to the filtered COD as described in ASM no.3). The carbonaceous substrate removal is relatively more stable than

ammonia removal and varies less with small fluctuations in the influent loading rates. The average influent organic loading rate on the entire system is 4.70gCOD$m^{-2}d^{-1}$ while the stage-1 loading is kept at 12gCOD$m^{-2}d^{-1}$. These are within the range of conventional design loading rates for RBC (section 4.3), which permit an overall loading of 2.5 to 8.0 g sol.BOD_5 $m^{-2}d^{-1}$ for combined nitrification, while the stage-1 loading could go up to 12 g sol.BOD_5 $m^{-2}d^{-1}$ (Table 2). Figure 40 compares the removal in the modelled RBC set-up with the experiment at different stages. All simulation runs were carried out assuming an

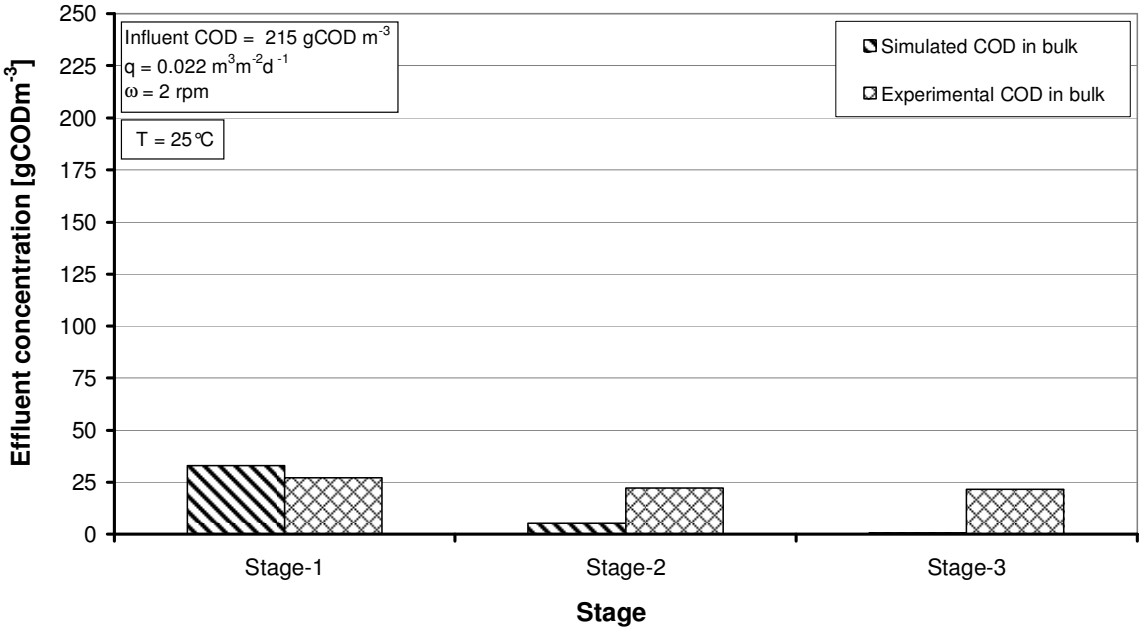

Figure 40 Simulated and experimental effluent COD concentrations in the RBC stages

ambient temperature of 25°C and no recirculation of flow between the stages. The stage-1 shows a maximum removal efficiency as observed by many authors (Rodgers et al. 2003, Famularo et al. 1978). The simulated results fit in closely with the experimental bulk liquid concentration in stage-1 but there is evidently not much removal in subsequent stages in the experiment. The simulated results show nearly 85% removal in stage-1 and an overall removal efficiency of 99% in the system. There is a steady decrease of concentration after stage-1. However, the overall removal efficiency in the real plant is only about 90% as shown by the measured data points (average COD in effluent) in Figure 40 and the COD remains nearly static after the stage-1. The decline in real plant removal could be accounted for due to the lower biofilm growth in stage-2 and stage-3 where the measured biofilm thickness is comparatively less than predicted in the runs. The simulated biofilm thickness in different stages is compared with the experiment in Figure 50. However, the most plausible reason for such experimental behaviour could be the presence of soluble inert in the remaining substrate after stage-1 which cannot get degraded in the subsequent RBC

stages. The model assumes the influent soluble substrate to be completely biodegradable and hence further degradation is possible.

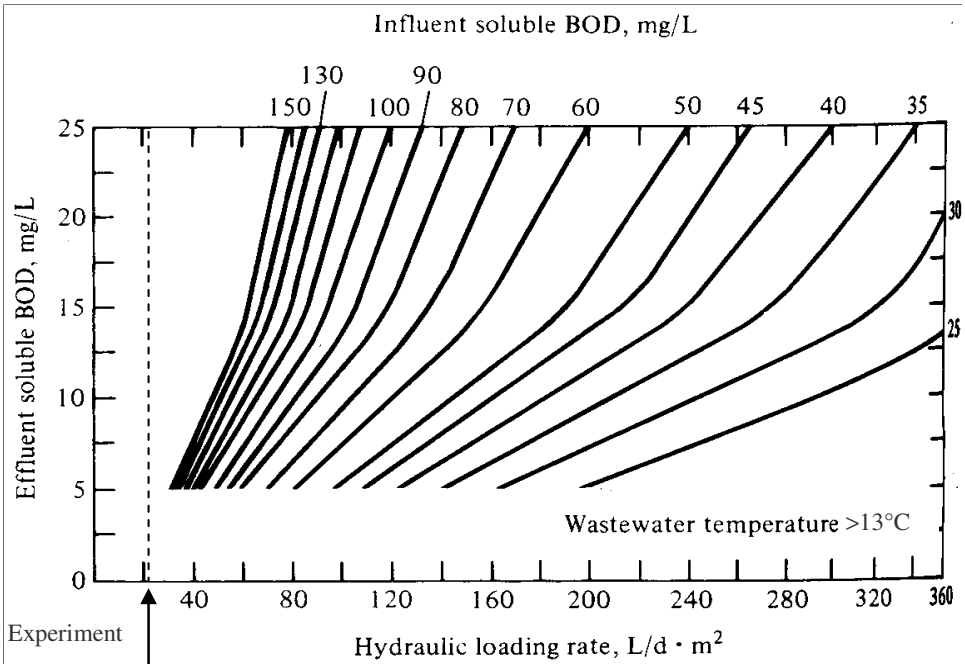

Figure 41 RBC process design curves for efficiency and loading rate for treating municipal wastewater. (Based on USEPA-600/2-84-106, June 1984 (Peavy et al. 1985))

The simulation predictions comply with the ATV-DVWK (A 281E, 2001) standards for the considered experimental set-up. The observed removal of soluble BOD in RBCs is further documented in the USEPA process design chart shown in Figure 41. At an influent organic concentration of 215mg/l, which is assumed to be soluble and readily biodegradable, and a hydraulic loading of 22.0 $lm^{-2}d^{-1}$, extrapolated curves predict nearly 95-96% removal at temperatures above 13°C as reflected by the simulations. At high organic loads, substantial removal occurs during the stage-1 which apparently points to higher heterotrophic fraction in the biofilm compared to the autotrophic species. The removal rates vary with the loading rate and temperature and these scenarios will be discussed in the subsequent sections.

7.1.1.3 Steady state concentration of nitrogen compounds

The nitrification and denitrification processes are more sensitive to external variations in loading rates compared to soluble organic substrate. Temperature and oxygen availability as well as competition between autotrophs and heterotrophs also dictate the system performance in the various stages. The calibrated scenario between simulation output and experimental results are reflected in the plots shown in Figure 42. Similar to section 7.1.1.2, stage-1 shows a closer fit when compared to the subsequent stages as displayed in Figure 42.

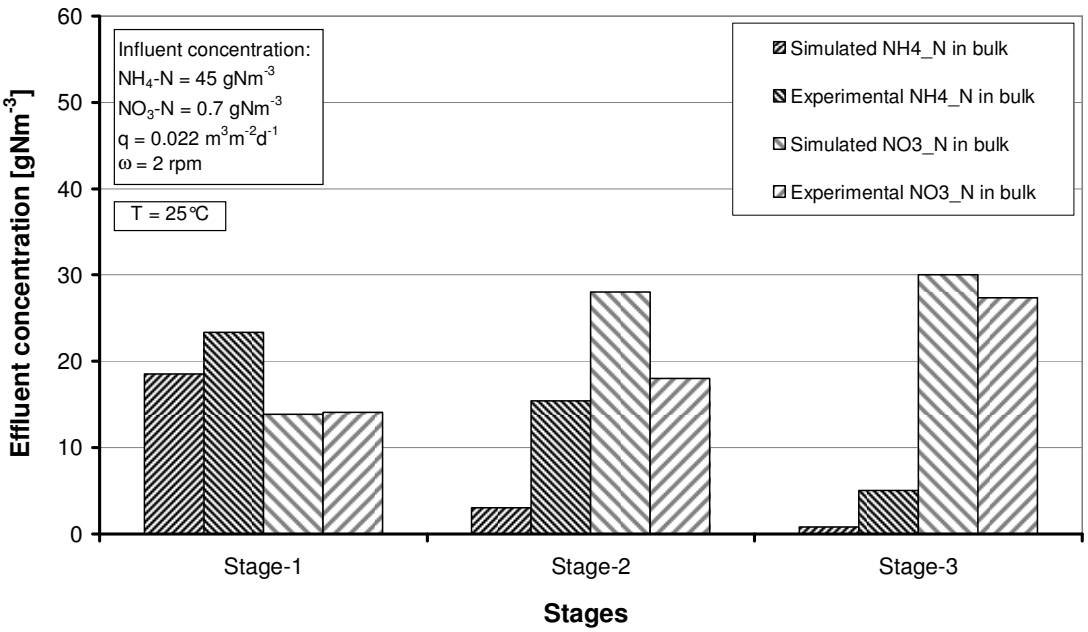

Figure 42 Simulated and experimental effluent NH_4-N concentrations in the RBC stages

The influent ammonium nitrogen loading rate over the system is about 1.0 $gNm^{-2}d^{-1}$. According to the design criteria for RBC, ammonium-nitrogen loading should be in the range of 0.75-1.6 $gNm^{-2}d^{-1}$ for optimal performance (Table 2). Stage-1 shows the NH_4-N concentration in the bulk liquid getting reduced by 55% from 45 mg/l to around 20 mg/l. The subsequent stages show further ammonia removal in both simulations and experiment. However, experimental removal is relatively less and this may be accounted for by the scarce biofilm thickness in the latter stages in the experimental RBC. But the slightly increased removal efficiency of ammonium compared to the nearly static soluble organic substrate removal in the identical stages points to the increased growth of autotrophs in the latter stages of the RBC. The simulation results however predict complete ammonia-nitrogen removal and effluent concentrations go below 1.0mg/l. This is coherent with the DIN: 4261 (II) as well as ATV-DVWK standards (2001) under the given ammonia loading.

The autotrophs appear to thrive and perform steadily once the organic substrate concentration is substantially reduced after stage-1. In the mixed-culture biofilm model, the biomass distribution inside the biofilm reveals a higher autotrophic dominance after the stage-1 as shown in sub-section 7.1.2.1. The soluble organic substrate concentration in the effluent from stage-1 is about 24 mg/l and the simulation results predict it to get reduced to below 15 mg/l in stage-2 as shown in Figure 40 earlier. This creates the optimum ambience for a good nitrification and the total ammonium removal in the system is predicted to be 95-96%. Apart from the autotrophs, heterotrophs are also partly responsible for the removal of NH_4-N removal because they use it as N-source for cell synthesis (Gujer et al.1999).

Radwan et al. (1997) had earlier observed highest ammonia removal in stage-1 under varying COD/NH_4-N ratio in their experiments at 28 ± 2°C. This was reasoned to be due to higher availability of nutrients for both heterotrophs and autotrophs in the mixed-culture biofilm in the stage-1 compared to the subsequent stages. This could explain the high NH_4-N removal apart from organic substrate minimisation in the stage-1 under similar temperature conditions in the present work. Figure 42 shows that the average measured final effluent concentration of nitrate-nitrogen is around 30 mg/l which compares well with the predicted model results. For stage-2 and stage-3, the removal of ammonia and the production of nitrate-nitrogen are corresponding to each other in both experiment and simulations and reveal little denitrification in these stages. It is observed that an influent concentration of 45 mg/l ammonium-nitrogen fed into the system is nitrified to produce 30 mg/l of effluent nitrate-nitrogen The rest is partly used in cell synthesis and partly denitrified into gaseous nitrogen. Most of the denitrification occurs in the stage-1 where heterotrophic fraction is higher than the subsequent stages. The denitrification rate in stage-1 is predicted in the model to be at 0.176gN$m^{-2}d^{-1}$. The latter stages show a low denitrification rate, while ammonia oxidation is more prominent due to less heterotrophic dominance.

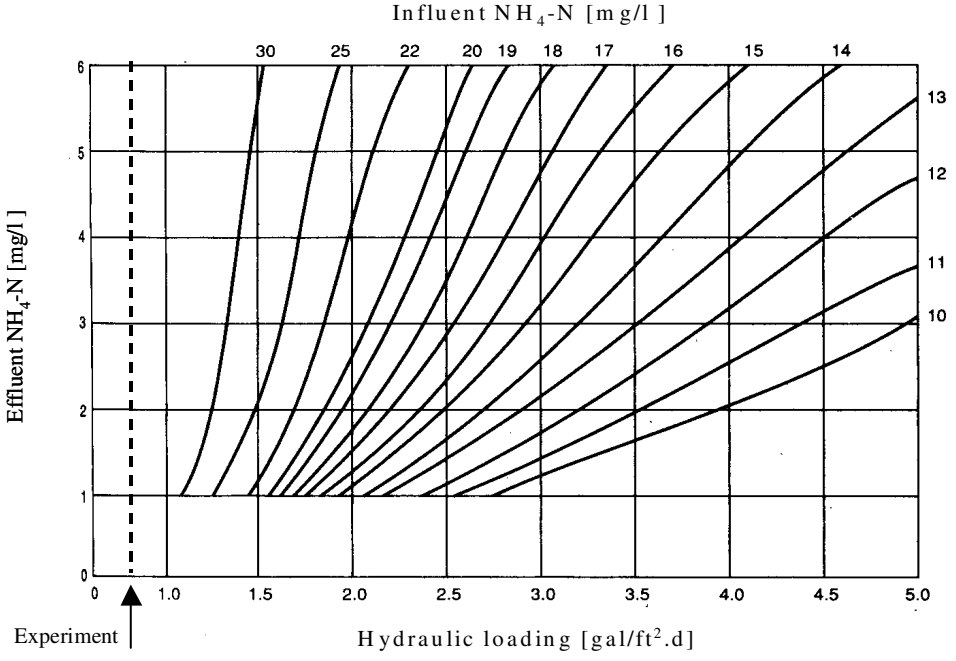

Figure 43 RBC nutrient removal and loading rate relationship in treating municipal wastewater
(Based on WPCF Manual of practice, FD-7, 1983 at T > 13°C (Tchobanoglous et al. 1995)
(1gal/ft^2.d = 40.74 l/m^2.d)

The predicted removal of NH_4-N in RBCs can be further compared with the standard charts from WPCF manual (1983) for nutrient removal which is shown in Figure 43. At influent NH_4-N concentrations above 30 mg/l and a hydraulic loading rate of 22.0 l $m^{-2}d^{-1}$, the

curves may be extrapolated to reveal removal efficiency above 95%. The model was checked for mass balance of nitrogen in each of the biofilm layers and in each stage.

7.1.1.4 Steady state concentrations of bicarbonates

Alkalinity and pH are important parameters which change during the treatment process and could become a limiting factor for the micro-organisms (section 3.5.3.1 and 3.5.3.2). The bicarbonates are the main constituent of alkalinity in domestic sewage at pH 7.

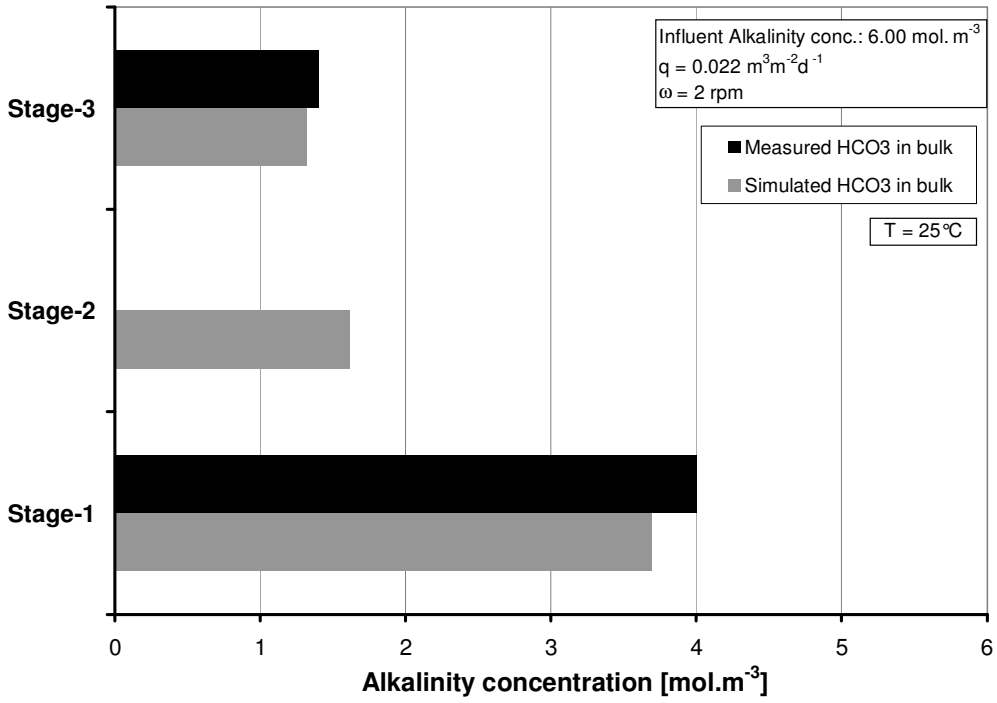

Figure 44 Simulated and experimental alkalinity concentration in the RBC stages

Both the heterotrophs and the nitrifying bacteria need HCO_3^- to sustain their cell processes. Not only that, alkalinity is also an essential requirement in ammonia oxidation. For every mole of NH_4^+-N which is oxidised, approximately two moles of HCO_3^- are consumed which corresponds to two equivalents of alkalinity, and expressed in units of mol/m^3. The nitrification process is pH dependent and an optimum range would be around 8-9. However, denitrification produces alkalinity and causes the pH to rise slightly. The simulated and measured concentrations of HCO_3^- in the bulk liquid in the 3-stages are shown in Figure 44 above. Stage-1 shows a reduction of alkalinity from 6.0 to about 4.0 mol/m^3, which gets further reduced to about 1.50 mol/m^3 in stage-2. This reduction could be correlated to the ammonium oxidation taking place in the identical stages where ammonium concentration is reduced from 45 to 20 mg/l in stage-1 and to about 3 mg/l in stage-2. There is not much nitrification after stage-2 as most of the ammonia has been oxidised and this is simultaneously reflected by a low reduction in alkalinity in stage-3.

7.1.2 Particulate components and biofilm parameters

7.1.2.1 Microbial species distribution inside biofilm matrix

The displacement of solids inside the biofilm matrix is modelled as a combined effect of advective and diffusive transport processes. The density fluxes in the matrix are affected by surface activities such as detachment and attachment of biomass, growth of the biofilm and the supply of nutrients and oxygen inside the biofilm. The solids distribute themselves based upon substrate and oxygen limitations and availability of specific nutrients for the specific species. The particulate displacement inside the biofilm is an extremely complex phenomenon and it has not been possible to measure the actual solids distribution experimentally. The net effect of biofilm growth, solids displacement and detachment is the biofilm thickness which could be measured over a period of time. Experimental data was not available to study the development of biofilm with time and compare the simulated growth. However, the steady-state biofilm thickness in simulation was based upon the measured value.

The observed yield of different species in the tank obtained from simulation could be used to give a measure of the steady-state system performance. The Y_{obs} for heterotrophs was around 0.20 and for AOM about 0.05 in the stage-1 tank. As stated in section 3.5.3.1, the observed yield is much lower in a multi-species biofilm compared to ASP process due to the presence of more than one organism type. In case of low organic loadings, as in the deeper biofilm layers, cells enter into endogenous respiration phase in which they start consuming their own cell protoplasm. The decay and endogenous respiration processes dominate there and produce high inactive particulate inerts. By way of particulate diffusion, these inerts are made to move towards the surface layers. The effective diffusive coefficient for all the particulate species D_X was adsjusted at 6×10^{-9} m^2/d, based upon a similar value (5×10^{-9} m^2/d) in the extended MCB model of Wanner and Reichert (1996). It allowed the species to get mixed inside the biofilm. The effect of attachment and detachment of the microbial cells and particles at the biofilm surface could be easily carried forward from the surface into the deeper layers. Figure 45 shows the distribution of the particulate species inside the biofilm matrix in stage-1 of the RBC. Since the heterotrophs offer strong competition for food and space, the autotrophic organisms are able to grow in the deeper layers of the biofilm and in the latter stages of the RBC when the organic load is substantially reduced. It is evident that the heterotrophs flourish near the surface layers where there is plenty of organic substrate and oxygen diffusion.

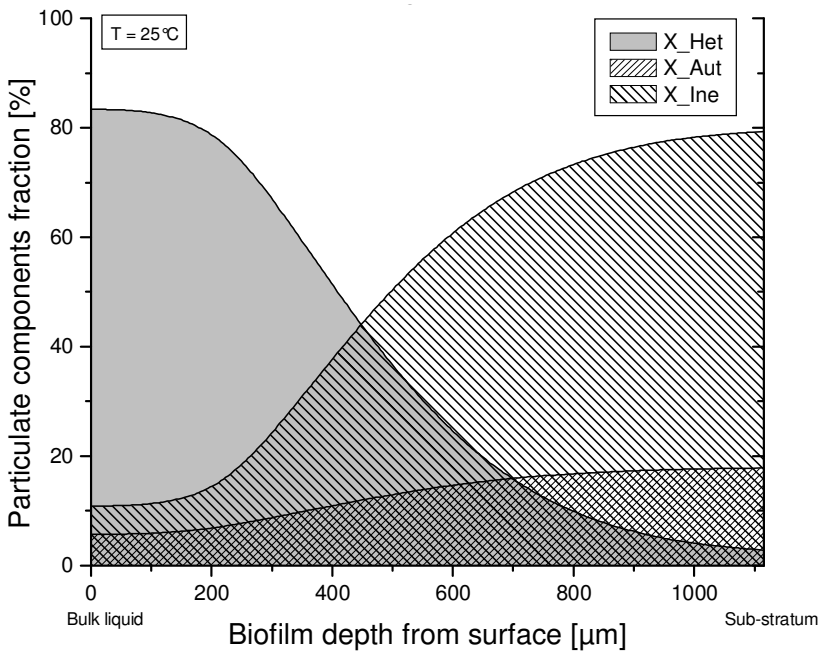

Figure 45 Relative abundance of particulate species inside biofilm matrix in stage I

In the deeper regions of the biofilm beyond 300µm, the heterotrophs drop in abundance and give way to the autotrophic species, which grow a little more abundantly. However, there is a high content of particulate inert towards the sub-stratum which rise mostly as a result of decay and lysis of the heterotrophic species. It has been observed previously (Figure 39) that most of the diffused oxygen gets uptaken within a depth of about 250-300µm from surface at temperatures around 20-25°C for a biofilm of density between 45 to 60 KgCOD/m^3. Therefore, bacterial activity is more active in this region and diminishes afterwards. Wanner and Reichert (1996) showed a similar volume fraction of microbial species in their biofilm model results with a multi-substrate feed. Okabe et al. (1990) observed that the metabolically active cell fraction decreased from 35 ± 15% in the outer layer to 15 ± 5% in the innermost biofilm, which shows a high inert content in the deeper layers. However, this fractionation of active and inactive biomass depends upon many factors such as nutrient loading, biofilm density, thickness, temperature and biofilm texture, i.e. compact and homogenous or fluffy and heterogeneous.

By means of modelling, the difference in the fractionation of the biomass in each stage of the RBC can be studied. This fractionation undergoes substantial variation in the subsequent stages as shown in Figure 46 for stage-2 and Figure 47 for stage-3. The relative fraction of heterotrophic species reduces from 85% in stage-1 to 60% in stage-2 near the biofilm surface. On the other hand, the nitrifying species show a rise from 6% in stage-1 to 25% in the surface layers in stage-2.

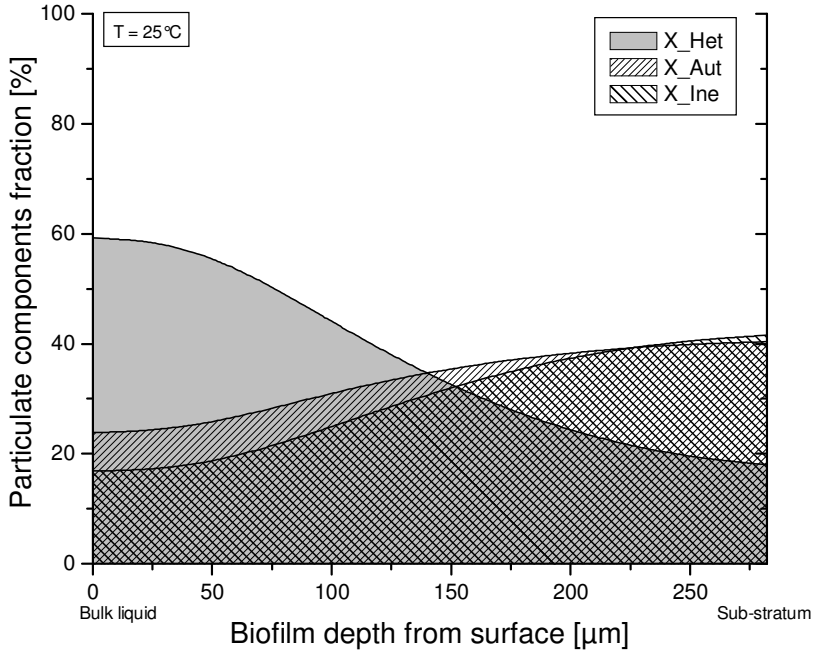

Figure 46 Relative abundance of particulate species inside biofilm matrix in stage II

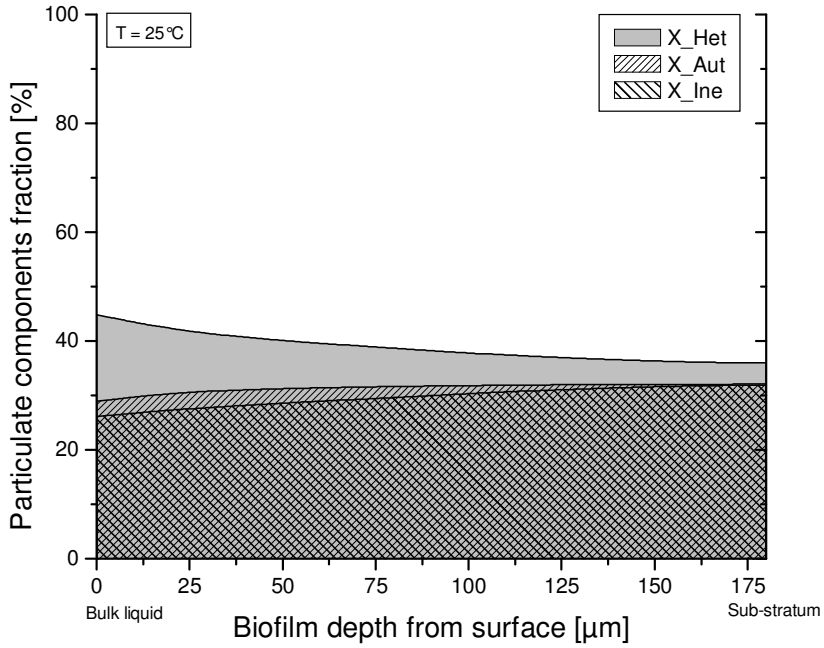

Figure 47 Relative abundance of particulate species inside biofilm matrix in stage III

Like in stage-1, autotrophic micro-organisms grow more towards the depth. It can be therefore inferred that the stage-2 biofilm comprises mainly of active biomass fraction throughout the depth. The biofilm is relatively thinner here and therefore oxygen diffusion is better. In stage-3, Figure 47 shows a nearly uniform distribution of species throughout the depth of the biofilm. The autotrophs show further rise in relative fraction, while heterotrophs get more diminished than in previous stage. It can be inferred that the biofilm is not substrate or oxygen limited. It would be more homogenous in composition. The lower

thickness of the biofilm compared to previous stages allow easy diffusion of the soluble components and oxygen inside the matrix.

7.1.2.2 Concentration of dissolved components inside the biofilm matrix

The steady-state concentration of dissolved components inside the biofilm matrix reflects a similar trend as the biomass fractions in the respective stages. Due to the high population of

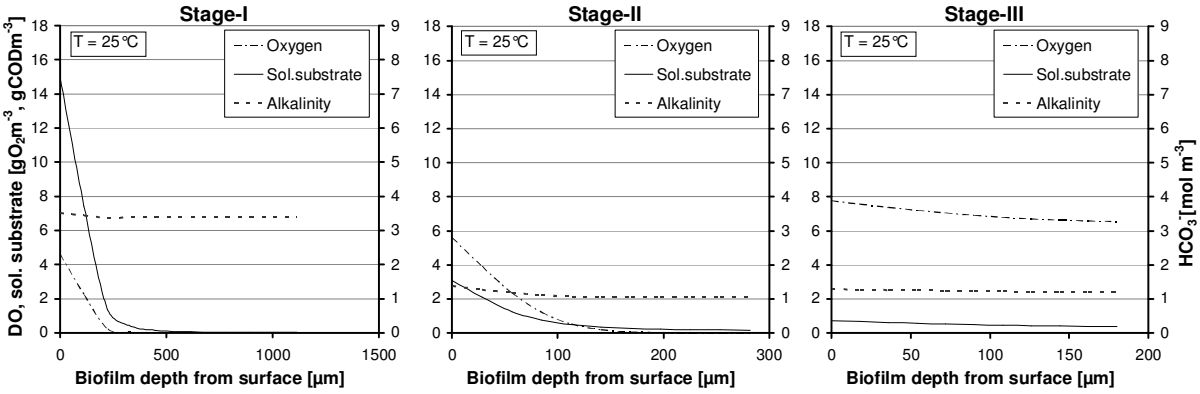

Figure 48 Concentration profiles of organic substrate, dissolved oxygen and alkalinity inside the biofilm in RBC stages

heterotrophs (Figure 45) and the availability of adequate DO in the upper layers of stage-1 biofilm, most of soluble organic substrate is degraded towards the surface and the biofilm gets substrate limited in the deeper layers as reflected in Figure 48 for stage-1. This stage compares well with the profile shown by Wanner and Reichert (1996) in their model results at steady state. The alkalinity concentration remained almost steady at 3.70 mol/m^3 inside the biofilm in stage-1 and showed a decrease from the influent value of 6 mol/m^3 due to the uptake by the bacteria. Although there might be some production in alkalinity due to the high denitrification in stage-1 vis-à-vis the subsequent stages, the net affect is decrease due to utilisation of the HCO_3^- by the cells. Stage-2 showed similar trend as in stage-1, although the concentration of soluble substrates was considerably lower due to diminished organic loading as shown in Figure 48, stage-2. Both oxygen and soluble organic substrate is limited in the deeper layers although the biofilm thickness is less than half of that in stage-1. Alkalinity showed a further decrease from stage-1 due to uptake by the microbial species and reached around 1.20mol/m^3. In stage-3, there appears to be a complete penetration of oxygen in the relatively thin biofilm. Moreover, the concentration of DO is much high inside the biofilm due to low uptake by the bacteria. Little substrate is left for the sustenance of the bacterial species as shown in stage-3 (Figure 40). There is little consumption of alkalinity after stage-2 as there is less ammonium left to be oxidised. These steady-state concentration profiles of organic substrate and oxygen inside the biofilm are only reflective of the possible nutrients supply available at the different depths of the biofilm as

a consequence of molecular diffusion, utilisation by the mixed-culture biomass and many other processes occurring inside the biofilm. The real profile of concentration of nutrients inside the biofilm is hard to verify experimentally.

Unlike the organic substrate however, the N-compounds exhibit a rather uniform concentration profile throughout the depth of the biofilm as shown in the steady-state model output in Figure 49. This reflects their relatively deeper presence compared to the organic substrate and therefore

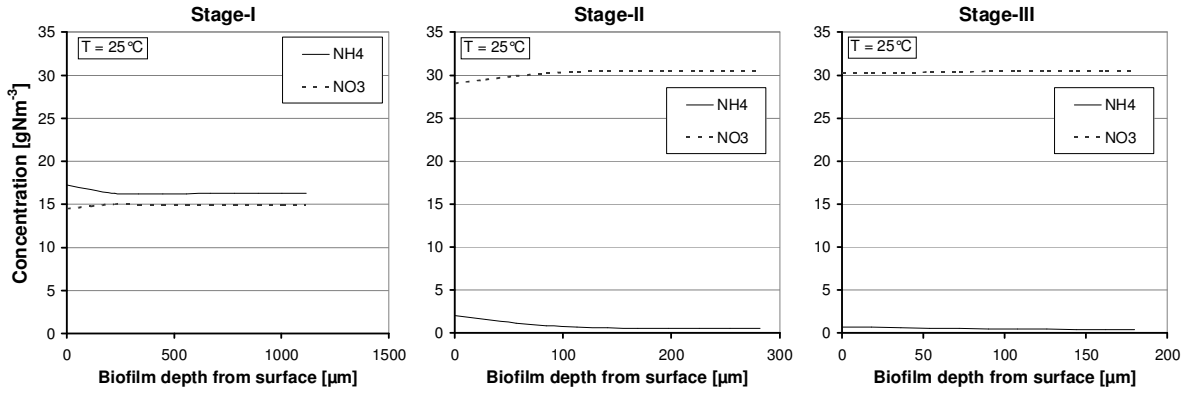

Figure 49 Concentration profiles of N compounds in 3 stages of RBC

the existence of nitrifiers at the biofilm depths. On the other hand, the heterotrophs consume all the substrate and oxygen in the surface layers especially in stages 1 and 2, and dwindle in population thereafter.

In stage-1 there is a considerable denitrification as reflected by the low nitrate concentrations in the biofilm. The reduction in the NH_4-N concentration is more than 55% while the NO_3-N concentration is only half of the total amount of ammonium oxidised. Although a small part of ammonium-nitrogen gets utilised for cell synthesis, the rest is denitrified into gaseous nitrogen. In stage-2, there is not much denitrification and the nitrate concentration soars up to almost an equivalent amount by which ammonium-nitrogen concentration sinks as shown in Figure 49. In the stage-3, there is little ammonia left for oxidation and consequently the nitrate concentration does not show much change from the previous stage. There is little denitrification in stage-3 due to the availability of oxygen even in the depths of the thin film.

7.1.2.3 Biofilm growth and surface phenomena

Due to the nutrient removal, there would be continuous accumulation of particulate matter in any biofilm system such as RBC. Since the biofilm thickness is observed to be finite, the biomass must be shed into the reactor by a detachment mechanism to conserve the mass balance. Two forms of empirical detachment mechanisms have been discussed previously (chapter 6). However, the linear form of detachment was found inadequate to check the growth of the biofilm thickness vis-à-vis experimental findings. Therefore, the second-order

detachment function with respect to biofilm thickness has been adopted in the simulation runs. In reality, the loss of biomass occurs from the biofilm either by way of regular erosion

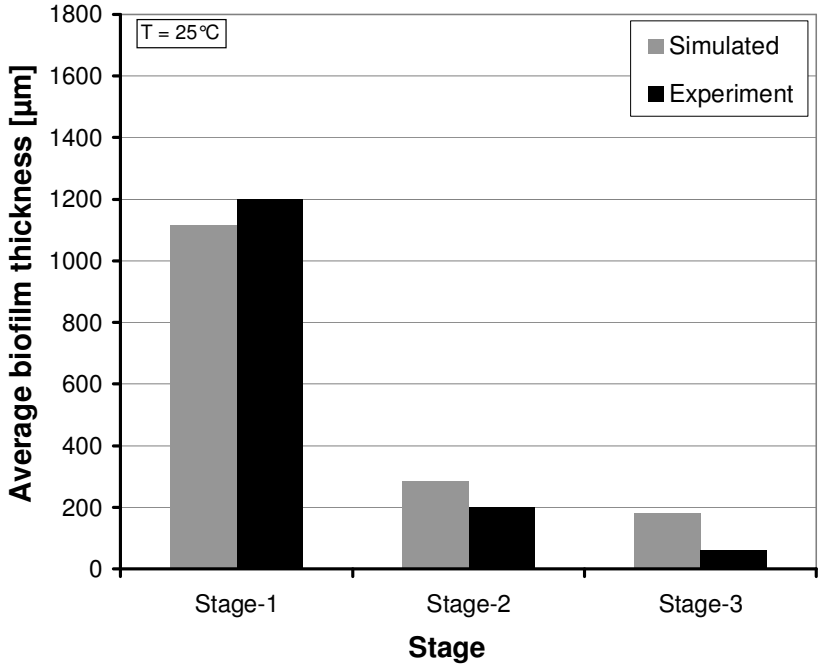

Figure 50 Simulated and experimental steady-state biofilm thickness in the RBC stages

or irregular sloughing. However, sloughing is difficult to model mathematically in a composite MCB and can be studied separately, assuming a fixed nutrient composition. Heterotrophs are the main contributors to the growth of the biofilm due to their high growth rates. Figure 50 compares the simulated steady-state biofilm thickness against the average measured thickness in the three stages of the RBC. There is comparatively less biofilm growth in stage-2 and very little growth in stage-3 in the experiment. The experimental values of thickness are averaged over the whole interfacial area of the disc, while in reality the thickness is non-uniform and irregular in nature. It is thicker at the beginning where the high nutrient content influent enters stage-1 and gradually reduces towards the end. In stage-2, the biofilm grows in sporadic patches over the disc surface while stage-3 shows little growth in most locations. So the average value over the disc surface is very less. This seems to deviate from the simulated scenario. There could be a number of reasons related to the low biofilm growth in the experiment during the latter stages. It could be due to low organic loading rates after stage-1 coupled with a smooth disc surface in the laboratory-scale set-up which might prevent the clinging of the bacteria onto the media surface. However, scaled-up set-ups might overcome such a problem. Given the substrate and oxygen, there seems to be no other apparent reason why the biofilm should not grow adequately unless the substrate is mostly inert in composition or there has been a shock loading condition. The model process kinetics are kept the same in all the three stages. The nutrient concentration in the stage-1

effluent is still high enough to initiate biofilm growth in the subsequent stages. Therefore, the predicted biofilm growth in the latter stages should be in order.

The variation of the film thickness with time is assumed to be a function of the advective velocity u and the resultant of the attachment and detachment velocity at the biofilm surface (6.3.3.3). The advective velocity sums up the net average growth rate of the biofilm layers from the bottom (media support) to the surface layer.

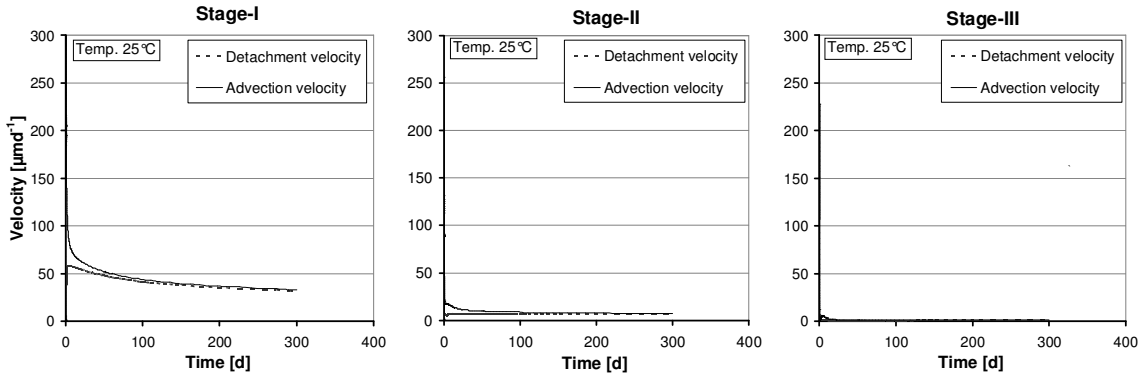

Figure 51 Solids displacement and detachment velocity at biofilm surface in RBC stages

On the other hand, the detachment velocity signifies the steady rate of erosion of biomass depending upon the biofilm thickness and the density of the surface layer. Although the above processes are simplified mathematical considerations to estimate the displacement velocity of particulate species in the biofilm matrix, it nevertheless helps to predict an average thickness value under a given loading condition. Figure 51 shows that detachment and advective velocities are highest in magnitude for stage-1 and it gets lowered in the subsequent stages. This symbolises higher displacement of solids in the biofilm of stage-1 compared to the subsequent stages. In stage-3 there is little displacement and the biofilm is more uniform and homogenous in its microbial composition. The stage-1 biofilm shows more heterogeneity and high displacement velocities due to the high content of particulate inerts in the deeper layers, which tend to move out towards the surface. Then again, the surface layers have more active biomass which tends to get displaced into deeper regions. For the film thickness to be stable the two velocities should narrow down to a single value at steady state, which is apparent from the plots.

The detached biomass from the biofilm enters the bulk reactor in each stage. It undergoes further reaction in the reactor as per equations 6.31 and 6.32 based on the same kinetics as assumed for the biofilm (Table 10, Table 11). Therefore, a part of the nitrification is taking place due to this detached biomass in the reactor.

7.2 Scenario-I: Model validation with dynamic simulation

Dynamic simulation represents running a model using input-data which varies with time. In case of biological wastewater treatment, the governing time-based variables are the influent nutrient loading rate and hydraulic loading rate (or HRT when volume of reactor is fixed). This can vary over a period of time. There may be seasonal as well as diurnal fluctuations and the current model is capable to read data from a time-based data-series file and run with such variations in input. It interpolates the intermediate variable values (in-between the measured data values in the file) based upon the time step it takes during the runs.

To test the performance of the calibrated model and verify the results based on nutrient loading variations with time, dynamic runs were performed using two different experimental data-sets (Phase-1 data at 25°C and phase-2 data at 30°C in Table 4). The simulation output from both the data-sets have been compared with the experimental results. The runs at 25°C are based on the calibrated scenario (7.1) and that at 30°C are intended to validate the model. The experimental data were obtained from my colleague Mr. A. Blank for the experimental set-up-I for a period of 9 months beginning from September 2005. The simulation runs were made with high spatial discretization of the biofilm (N ≅ 20 layers) for greater numerical accuracy of the solutions.

The simulation results from dynamic runs based upon variation of hydraulic loading rate (i.e. hydraulic retention time) has been discussed in section 7.5 (Scenario-IV).

7.2.1 Organic substrate removal

Figure 52 shows the dynamic variation of the simulated and experimental soluble organic substrate concentrations with time. As observed previously (section 7.1), most of the organic substrate gets removed in the first stage of RBC at both the temperatures. For stage-I, the simulation results show a corresponding trend with the influent loading. Under the applied loading rates (< 8gBOD$m^{-2}d^{-1}$), almost all the soluble biodegradable organic substrate should be removed according to the ATV-DVWK (2001) standards for a 3-stage cascade. The simulation results reflect the same in the final effluent. Although molasses are believed to be completely biodegradable, it may contain small amounts of soluble inert (~10%) as well as some ammonium-nitrogen. This would explain the possible reason behind only up to 90% removal of measured COD (filtered) in the final effluent. A peak loading of 450gCOD/m^3 on 6th March, 2006 was smoothened out in the final effluent which emphasizes the capability of biofilm to tackle shock loadings effectively. The black bar in the plot demarcates the results from the two date sets (Phase-1 data at 25°C and phase-2 data at 30°C).

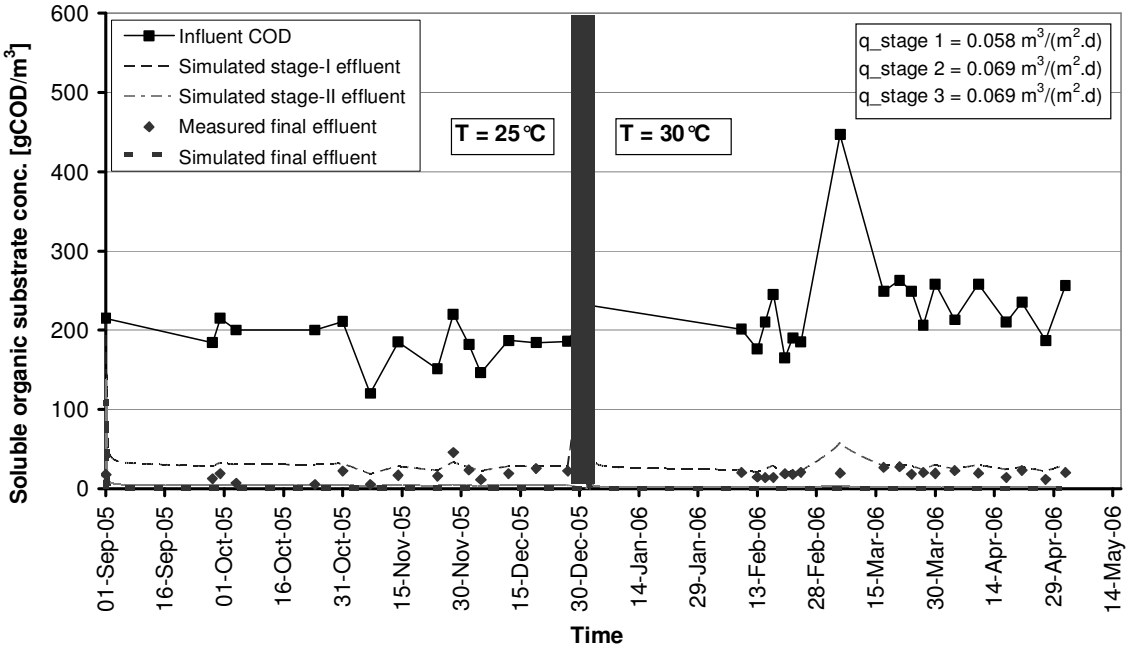

Figure 52 Simulated and experimental soluble org. substrate concentrations over time

7.2.2 Nitrification

The dynamic run results for NH_4-N removal in the 3-stage RBC is shown in Figure 53 below.

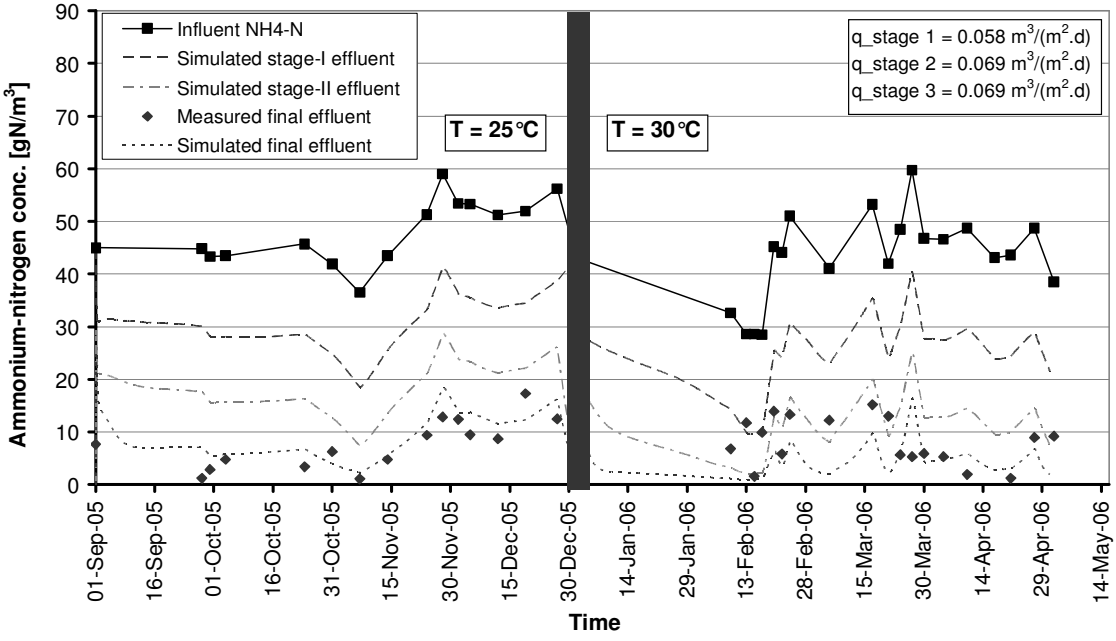

Figure 53 Simulated and experimental ammonium-nitrogen concentrations over time

Being a sensitive parameter because of the low growth rate of autotrophs, NH_4-N removal in each stage is guided by the prevalence of the autotrophic population over heterotrophs. The simulation results in each stage show a trend reflective of the influent ammonia loading and show comparable results with the measured final effluent concentrations. Average removal observed is about 95% of influent NH_4-N.

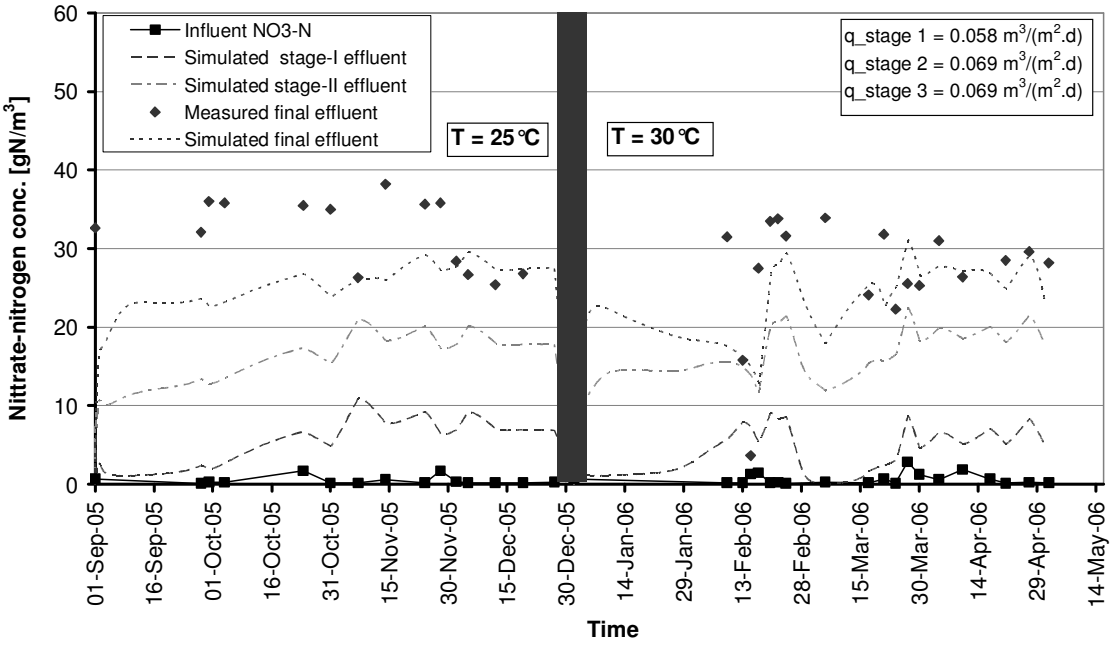

Figure 54 Simulated and experimental nitrate-nitrogen concentrations over time

In Figure 54, the measured NO_3-N concentration is compared with the simulation results. At 25°C, the measured nitrate-nitrogen concentration in the final effluent is higher than the simulated results while the data are comparable at 30°C. As the model results for ammonium show close fit with experimental results at 25°C, the high measured nitrate concentrations in the effluent can be attributed to be due to reduced denitrification in experiments. The model already uses an anoxic denitrification reduction factor (η_{den}) of 0.3 during calibration which is below the usual literature values of 0.5-1.0. However, the same η_{den} value yields better match in the plots at 30°C. The average effluent NO_3-N concentration is slightly less at 30°C as compared to 25°C. This is due to increased denitrification with temperature and also slightly reduced ammonia loading in the influent. Denitrification can be observed to be maximum in the first stage cascade which explains the difference between ammonia removal and nitrate production in that stage as compared to the second and third stage effluents.

7.2.3 Dissolved oxygen in bulk

The DO concentrations in the bulk is shown in Figure 55 below. The average DO in the influent was about 1.10gO_2/m^3 although it reached up to about 2.0gO_2/m^3 on some days. At 25°C, the measured final effluent concentration of about 6.0gO_2/m^3 matched well with the simulation results. However, at 30°C, the measured DO in the final effluent was found to be less than the simulated prediction. The most probable cause for such behaviour in the experiment is the oxygen uptake by the detached biomass in the bulk liquid. The high

endogenous respiration rates of the bacteria at 30°C would also consume oxygen and reduce DO. Both the results confirm that DO concentration decreases with temperature.

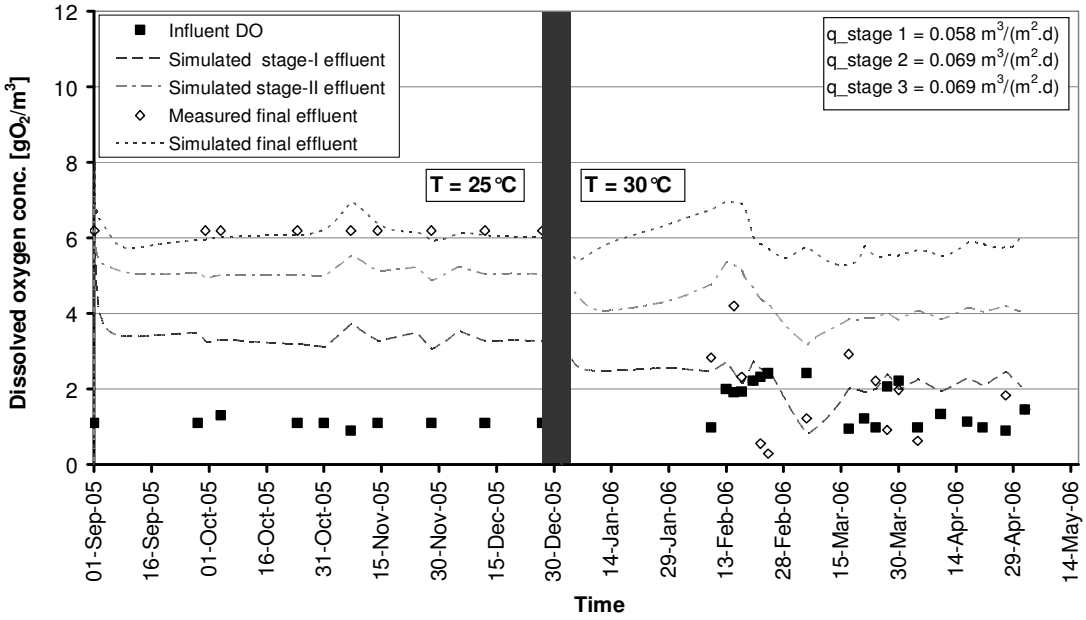

Figure 55 Simulated and measured DO concentrations in the bulk liquid over time

It can be concluded that average bulk DO concentrations remain above $1.5gO_2/m^3$ in the RBC stages which is the required minimum for achieving nitrification in aerobic systems. This makes the RBCs' an efficient aerobic treatment system.

7.2.4 Biofilm thickness

The thickness of the biofilm is non-uniform over the disc surface. It also varies with the location of the disc from the inflow point.

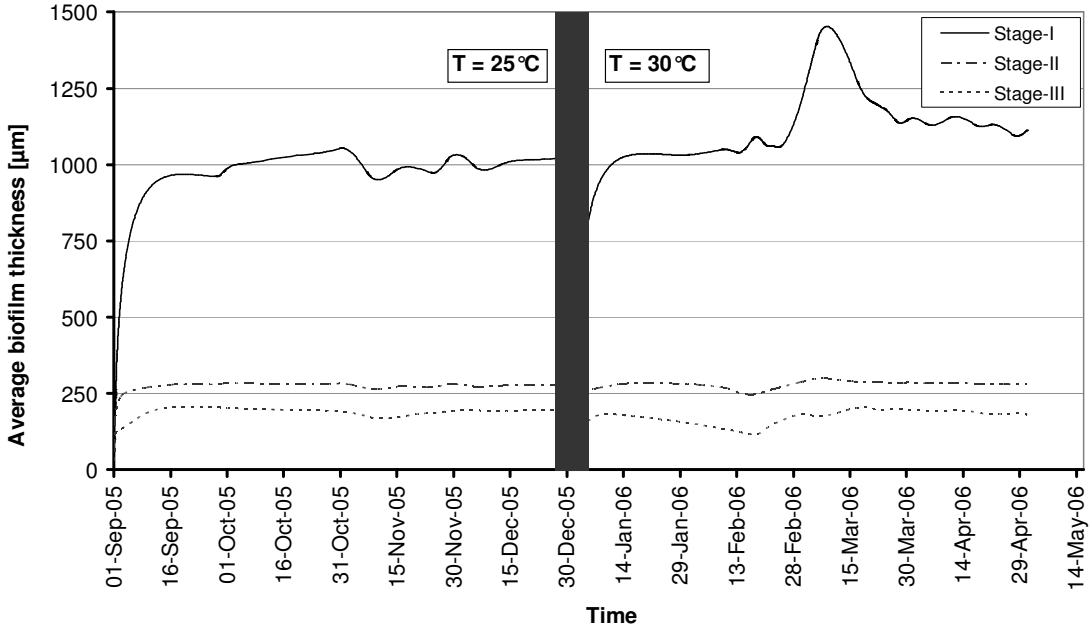

Figure 56 Simulated average biofilm thickness in the 3-stage RBC

So it is difficult to specify a single value for any stage based upon the experimental measurements. Due to the high nutrient loading, the stage-1 cascade shows a typically high biofilm thickness ranging from 600µm to1500µm. The stage-2 biofilm thickness is found to vary between 100µm to 300µm, while stage-3 cascade shows a thickness of the order of 30-90µm. The latter two stages show less variation which can be explained by the dominance of nitrifying bacteria. The simulated profile in each stage for the dynamic runs is shown in Figure 56. The thickness of the biofilm is stabilised around an average value for the measured range in each stage where possible. A peak organic loading on 6th March, 2006 resulted in increased growth of heterotrophs and corresponding rise in biofilm thickness in stage-1 around that point. It also identifies heterotrophs as the key bacterial species which are mainly responsible for a given biofilm thickness. The model used a fixed biofilm density of 45-60KgCOD/m^3 at 25°C (Table 14) and 47 KgCOD/m^3 at 30°C which were obtained from experimental measurements.

7.3 Scenario-II: Temperature sensitivity

The temperature has a substantial influence on the performance of a biofilm system. In case of the RBC biofilm, the effect is more intense because of the additional effect of changes in the saturation concentration of oxygen in the air and the diffusion coefficient of oxygen diffusing into the biofilm through the boundary layer. The growth and decay rate of the microbial species vary with temperature and this affects the nutrient removal efficiency. The diffusivity coefficients of various substrates also vary with temperature. These effects of temperature changes are normally corrected by applying temperature correction factors to the parameters involved. In ASM series, the temperature correction factor is based on the typical value of the parameters at 10°C and 20°C. However, the correction factor can be applied only within a certain range which is normally from 10°C to 32°C. Beyond that range, bacterial composition as well as kinetics may undergo transition. It is established that each microbial species has an optimum temperature range beyond which it remains dormant or ceases to exist. Other species may take control and the kinetics may change accordingly. Consequently, the present model attempts to calculate the removal of nutrients in the 3-stage RBC from 10°C to 32.5°C. Nitrification is relatively more affected by temperature changes than COD removal as the nitrifying organisms are more susceptible to temperature variations compared to heterotrophs. Table 15 shows the parameter values for the bacterial kinetics at different temperatures that have been used in the model based on the temperature correction correlation shown in equation 7.4.

$$k_T = k_{20}\, e^{\theta_T (T-20)} \tag{7.4}$$

where

$$\theta_T = \frac{\ln\left(k_{T°C}/k_{20°C}\right)}{\left(T-20\right)} \tag{7.5}$$

This equation is taken from ASM No. 3 which is based on van't Hoff exponential expression (equation 3.10). It differs from the approximate expression used in determining the physical oxygen transfer coefficient at different temperature (equation 5.29, Tchobanoglous et al. 1995). The stoichiometric coefficients have been assumed to remain unaltered with temperature as in ASM No. 3 and as shown in Table 12. The temperature correction factor for nitrification is a little higher than for COD removal because the nitrifying organisms are more temperature sensitive.

Using the Wilke-Chang equation, $D_{O_2-H_2O}$ has been determined at different temperatures (Table 9). For other nutrients, D values are taken from standard tables at 25°C only (Henze et al. 2002). The ratio $\frac{D_{T°C}}{D_{25°C}}$ for oxygen diffusivity into water at different temperatures is used for estimating the diffusivity values of other nutrients as well. However, the diffusivity coefficients of the nutrients diffusing into the biofilm are usually lower than that in pure water. This is due to the presence of microbial cells, extra-cellular polymeric substances and gaseous matter formed inside the biofilm. The effective diffusion coefficient inside biofilm D_E is a fraction of the value in pure water D_{AQ} and different values have been cited for this fraction in different literature. Siegrist (1986) determined the effective diffusion coefficient in the biofilm matrix as 50-80% of that in pure water at a biofilm density of about 15-25 kg TSS/m^3. Sophisticated methods exist to calculate this fraction (Wood et al. 2002) although there is no exact consensus over a definite value. Stewart (1998) reviewed the D_e values of some solutes in biofilm and based on his compilation, the following ranges have usually been observed: For inorganic ions such as NH_4^+, NO_3^- and light gases like O_2, CO_2, N_2O, $\frac{D_E}{D_{AQ}} = 0.60 \text{ to } 0.85.$ and for organic ions such as glucose, acetate, phenol, $\frac{D_E}{D_{AQ}} = 0.40 \text{ to } 0.60.$

Table 15 Kinetic parameters at different temperature used in the model
(Based on Table 12 values at 20°C)

Parameter	Description	Temperature(°C)						Units	θ_T (ASM 2)	Reference (at 20°C)
		10	15	20	25	30	32.5			
Kinetic parameters										
Hydrolysis										
K_{Hyd}	Hydrolysis rate constant	1.50	1.50	1.50	1.50	1.50	1.50	g X_S/(gX_H.d)		Fruhen-Hornig thesis (1997)
K_{XS}	Saturation constant for Hydrolysis	0.02	0.02	0.02	0.02	0.02	0.02	g X_S/gX_H		Fruhen thesis (1997)
Heterotrophic organisms, X_H										
μ_H	Max. growth rate of X_H	2.00	3.17	4.50	6.39	9.06	10.79	1/d	0.07	Wanner & Reichert (1996); Wanner & Gujer (1986)
K_{Ss}	Saturation constant for substrate S_S	5.00	5.00	5.00	5.00	5.00	5.00	gCOD/m^3		Wanner & Reichert (1996); Wanner & Gujer (1986)
$K_{O_2,H}$	Saturation constant for oxygen S_O	0.20	0.20	0.20	0.20	0.20	0.20	gO_2/m^3		ASM No.3 (1999); Fruhen-Hornig thesis (1997)
$K_{NH,H}$	Saturation constant for ammonium S_{NH}	0.10	0.10	0.10	0.10	0.10	0.10	gN/m^3		Fruhen-Hornig thesis (1997)
$K_{NO,H}$	Saturation constant for nitrite-nitrate S_{NO}	0.50	0.50	0.50	0.50	0.50	0.50	gNO_3^--N/m^3		Fruhen-Hornig thesis (1997)
$K_{ALK,H}$	Saturation constant for bicarbonate S_{ALK}	0.10	0.10	0.10	0.10	0.10	0.10	mol HCO_3^-/m^3		ASM No.3 (1999)
b_H	Aerobic end. respiration rate of X_H	0.10	0.14	0.20	0.28	0.40	0.48	1/d	0.07	Wanner & Reichert (1996); Wanner & Gujer (1986)
η_H	Anoxic reduction factor for end. respiration	0.47	0.49	0.50	0.51	0.52	0.53	-		ASM No.3 (1999)
η_{den}	Anoxic reduction factor for denitrification	0.30	0.30	0.30	0.30	0.30	0.30	-		Model calibration
Autotrophic organisms (X_A)										
μ_A	Max. growth rate of X_A	0.35	0.59	1.00	1.69	2.86	3.72	1/d	0.105	Koch et al. (2000); ASM No.3 (1999)

Parameter	Description	Temperature(°C)						Units	θ_T (ASM 2)	Reference (at 20°C)
		10	15	20	25	30	32.5			
$K_{O_2,A}$	Saturation constant for oxygen S_O	0.30	0.30	0.30	0.30	0.30	0.30	gO_2/m^3		Fruhen et al. (1991)
$K_{NH,A}$	Saturation constant for ammonium S_{NH}	1.00	1.00	1.00	1.00	1.00	1.00	gN/m^3		Wanner & Reichert (1996); Fruhen thesis (1997)
$K_{NO,A}$	Saturation constant for nitrite-nitrate S_{NO}	0.50	0.50	0.50	0.50	0.50	0.50			ASM No.3 (1999)
$K_{ALK,A}$	Saturation constant for bicarbonate S_{ALK}	0.50	0.50	0.50	0.50	0.50	0.50	mol HCO_3^-/m^3		ASM No.3 (1999)
b_A	Aerobic end. respiration rate of X_A	0.05	0.09	0.15	0.25	0.43	0.56	1/d	0.105	ASM No.3 (1999); Fruhen-Hornig thesis (1997)
η_A	Anoxic reduction factor for end. respiration	0.001	0.001	0.001	0.001	0.001	0.001	-		Personal correspondence with Prof. Siegrist
Stoichiometric parameters										
Y_{H,O_2}	Aerobic yield of heterotrophic biomass	0.63	0.63	0.63	0.63	0.63	0.63	g X_H/gS_S		ASM No.3 (1999); Fruhen-Hornig thesis (1997)
$Y_{H,NO}$	Anoxic yield of heterotrophic biomass	0.54	0.54	0.54	0.54	0.54	0.54	g X_H/gS_S		ASM No.3 (1999)
Y_A	Aerobic yield of X_A	0.24	0.24	0.24	0.24	0.24	0.24	g X_A/gN S_{NH}		ASM No.3 (1999); Fruhen et al. (1991)
i_{NBM}	Nitrogen content of biomass, X_H, X_A	0.07	0.07	0.07	0.07	0.07	0.07	gN/g $X_{H/A}$		ASM No.3 (1999); Fruhen-Hornig thesis (1997)
i_{NXI}	Nitrogen content of inerts, X_I	0.02	0.02	0.02	0.02	0.02	0.02	gN/g X_I		ASM No.3 (1999)
f_I	Production of X_I in end. respiration	0.20	0.20	0.20	0.20	0.20	0.20	g X_I/g $X_{H/A}$		ASM No.3 (1999)
Biofilm parameters										
ρ	Biofilm density (dry)	46-60						$KgVSS/m^3$		Experimental measurement
ε_l	Water fraction in biofilm	0.96-0.97								Experimental measurement

Table 16 Diffusivity coefficient values of soluble components at different temperature

Temperature	$D_T/D_{25°}$ *	D_Oxygen	D_Glucose	D_Acetate	D_Ammonia-N	D_Nitrite-N	D_Nitrate-N	D_Alkalinity	Reference
℃		m^2/d	m^2/d	m^2/d	m^2/d	m^2/d	m^2/d	m^2/d	
Diffusion into Pure water									
25℃	1.000	2.10E-04	.60E-04	1.00E-04	1.70E-04	.90E-04	1.60E-04	1.00E-04	Henze et al./ Perry Handbook
10℃	0.647	1.36E-04	.39E-04	.65E-04	1.10E-04	.58E-04	1.04E-04	.65E-04	Calculated
15℃	0.756	1.59E-04	.45E-04	.76E-04	1.29E-04	.68E-04	1.21E-04	.76E-04	Calculated
20℃	0.874	1.84E-04	.52E-04	.87E-04	1.49E-04	.79E-04	1.40E-04	.87E-04	Calculated
30℃	1.135	2.38E-04	.68E-04	1.14E-04	1.93E-04	1.02E-04	1.82E-04	1.14E-04	Calculated
32.5℃	1.207	2.53E-04	.72E-04	1.21E-04	2.05E-04	1.09E-04	1.93E-04	1.21E-04	Calculated
Diffusion into Biofilm									
25℃	1.000	1.68E-04	.36E-04	.60E-04	1.36E-04	.72E-04	1.28E-04	.80E-04	Calculated
10℃	0.647	1.09E-04	.23E-04	.39E-04	.88E-04	.47E-04	.83E-04	.52E-04	Calculated
15℃	0.756	1.27E-04	.27E-04	.45E-04	1.03E-04	.54E-04	.97E-04	.60E-04	Calculated
20℃	0.874	1.47E-04	.31E-04	.52E-04	1.19E-04	.63E-04	1.12E-04	.70E-04	Calculated
30℃	1.135	1.91E-04	.41E-04	.68E-04	1.54E-04	.82E-04	1.45E-04	.91E-04	Calculated
32.5℃	1.207	2.03E-04	.43E-04	.72E-04	1.64E-04	.87E-04	1.54E-04	.97E-04	Calculated
D_E/D_{AQ}.			0.80	0.60	0.60	0.80	0.80	0.80	

*(D x μ)/T is constant for each solute-solvent pair. Value estimated from the Wilke-Chang correlation

Table 16 shows the diffusivity values for different substrate in pure water and in biofilm which has been used in the model. For soluble organic substrate the diffusivity into biofilm is assumed to be 60% of that of pure water, while for all other soluble components, this value is assumed to be 80% of that in pure water (Stewart et al. 1998).

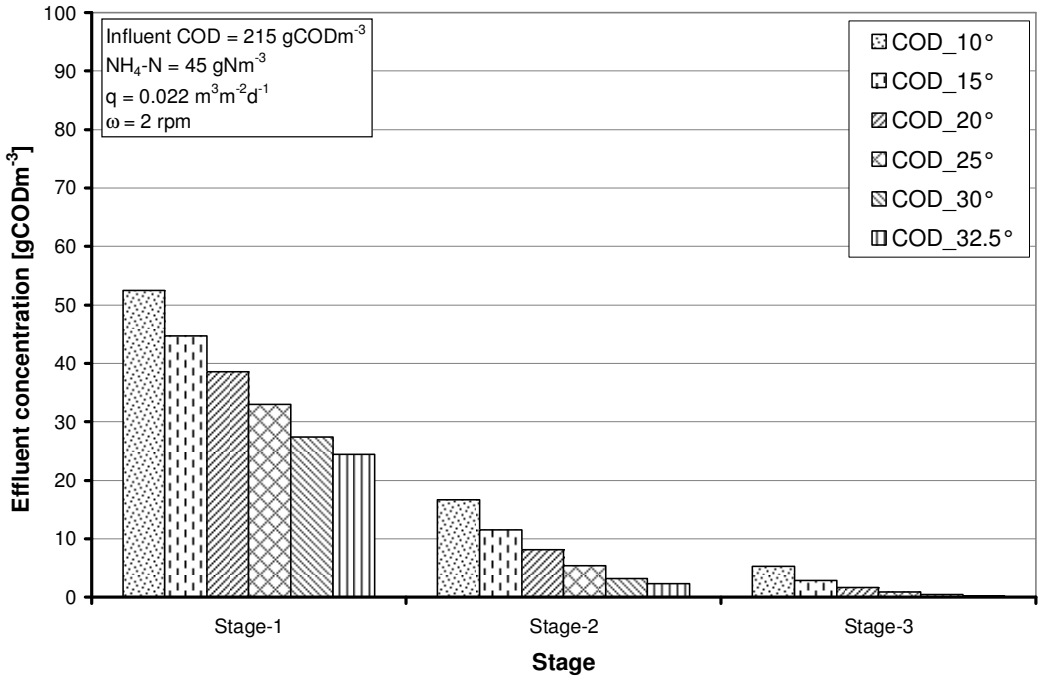

Figure 57 Simulated variation in the removal of soluble organic substrate at different temperature

The effect of temperature on the removal efficiency of the RBC system is evident from Figure 57, which shows the effluent concentration of organic substrate in each stage under different temperatures. The runs have been using the calibrated RBC model based upon the considered experimental set-up. As expected, the removal rates show an increasing trend with temperature. This is more evident in stage-1 where the COD removal rate increases from about 9.0 g/m^{2}d at 10°C to 11.0 g/m^{2}d at 32.5°C. However, the gap narrows down in the subsequent stages when substrate loading gets lowered. It is also observed that there is a sharp increase in removal efficiency in the initial temperature rise from 10 to 25°C. The subsequent range of temperature from 25 to 32.5°C shows a decelerating trend of removal. It has been observed previously that after 32-33°C, the heterotrophic growth rates remains essentially constant till about 40°C and thereafter start decreasing rapidly (Henze et al 2002). Antonio et al. (1976) is one among the earliest authors who substantiated that an increase in temperature caused an increase in BOD removal rate in biofilm systems. Banerjee (1997) reported that an increase in temperature of the RBC system led to an increase in the phenol removal rate up to a temperature of about 36°C, beyond which it remained essentially constant. As the exact kinetic constants have been unavailable at higher temperatures, further predictions could not be made using the model.

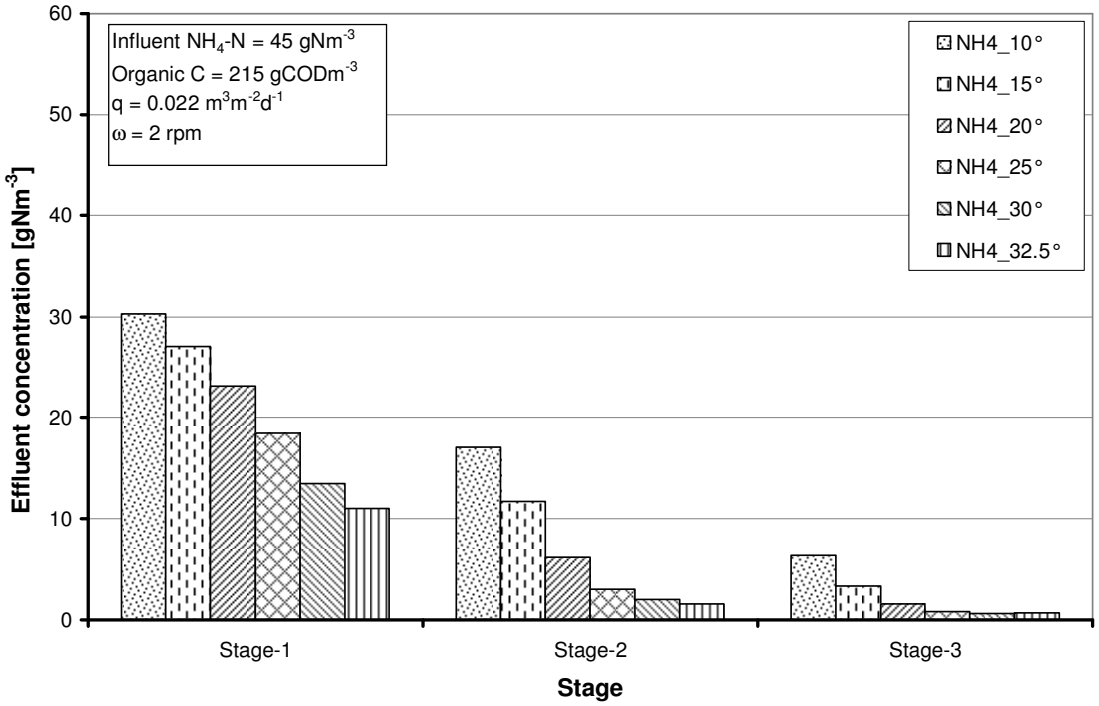

Figure 58 Simulated variation in the removal of NH_4-N at different temperature

Figure 58 shows the variation of ammonia nitrogen removal in the RBC stages with temperature. Nitrification is more sensitive to temperature than BOD removal which is evident from the above plot. In stage-1, for an influent loading rate of 2.60 gNH_4-N/m^2d, the ammonia-nitrogen removal increases more than double from 0.85 gNH4-N/m^2d at 10°C to 1.96 gNH4-N/m^2d at 32.5°C. This is much higher than the increase observed in the COD removal. The latter was only 17% for the same temperature range. At higher temperatures above 32°C, the growth rate of nitrifying bacteria remains constant till about 35°C, after which it starts to decline rapidly (Buswell et al. 1954). Nitrifiers in the thermophilic range are unknown and nitrification is often a big problem at temperatures above 32°C (Henze et al. 2002). Nitrifying bacteria are especially sensitive to sudden variations in temperature. The plots emphasize that the highest ammonia removal could be observed in the temperature range of 25-32°C when the effluent ammonium concentration is lowest. Moreover, at high temperatures, most of ammonia-nitrogen gets removed in the first two stages and there is little left to be removed in stage-3. However, at temperatures between 10-25°C, ammonia removal would occur in all stages at nearly the same rate.

Figure 59 shows nitrate-nitrogen concentrations in the bulk in the RBC stages. In stage-1, nitrate concentration increases with temperature as ammonia gets oxidized. However, there is a decline in NO_3-N concentration at high temperatures in stage-2 and 3. This may be attributed to reduced availability of NH_4-N and its assimilation for cell synthesis by the bacteria.

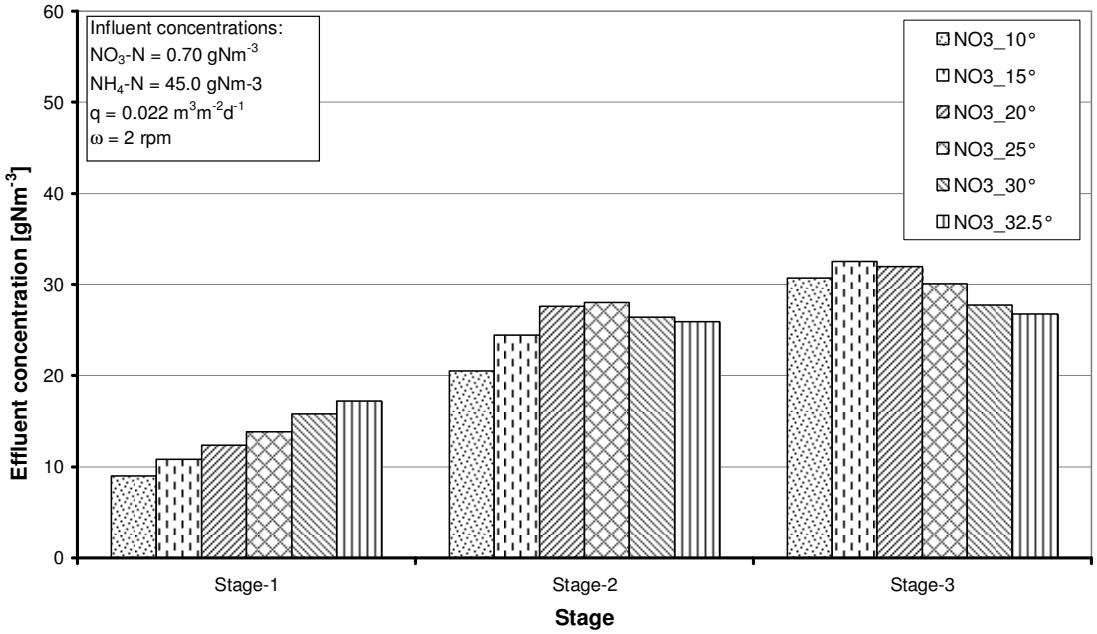

Figure 59 Simulated nitrate-nitrogen concentrations in the bulk at different temperature

Denitrification is also sensitive to temperature and exhibits a dependency similar to that of the nitrate-nitrogen. Usually, it increases with increase of temperature up to an optimum level. It gets inhibited in the presence of oxygen and so most of the denitrification takes place in the deeper biofilm layers which are essentially oxygen limited but dwelled by heterotrophs. The facultative heterotrophs which are mainly responsible for the denitrification seem to thrive with temperature when a source of organic carbon is kept available. Figure 60 highlights the correlation between denitrification rate and temperature in stage-1 and stage-2 of the RBC biofilm.

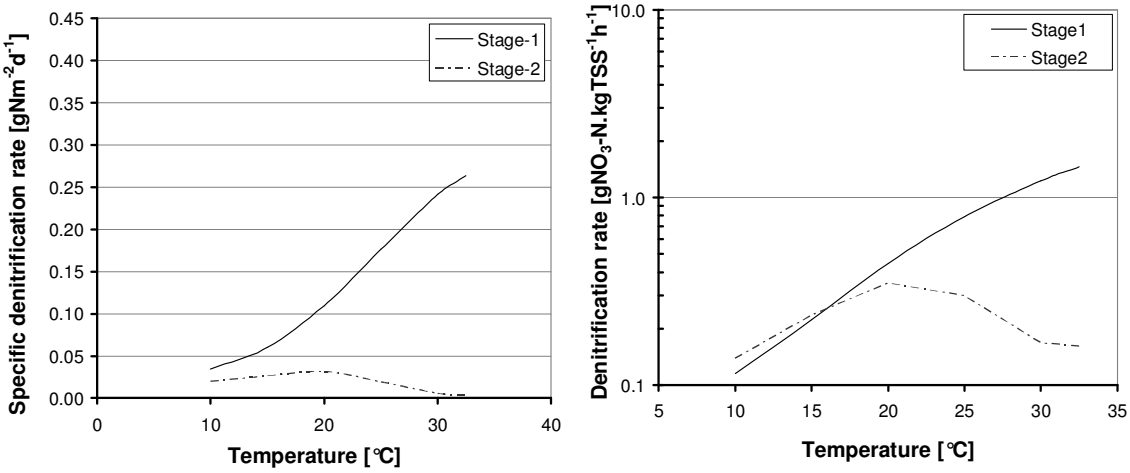

Figure 60 Effect of temperature on denitrification rate in the RBC biofilm

The rate has been calculated by summing up the volumetric production rate of gaseous nitrogen in the individual biofilm layers and then dividing it by the interfacial area of the respective stage. Up to about 20°C, denitrification rate increases with the temperature in

both stages but after that there is a reduction in the rate in stages 2. The reduction could be accounted for due to the similar drop in the nitrate concentrations as revealed in Figure 59 earlier. Moreover, contrary to stage-1, oxygen is able to penetrate deep inside the biofilm in stage-2 and 3 as shown in Figure 48. This inhibits denitrification in the latter stages. Davies (1975) also found that denitrification would slow down at temperatures above 32°C when heterotrophic activity gets static and declines afterwards. As kinetic constants above 32°C are not justified to be calculated using temperature functions and no experimental data were available, further model predictions have not been attempted. In fact, there seems to be little documentation in literature with denitrification at thermophilic temperature ranges. Similarly below 10°C, there is a substantial reduction in bacterial activity and therefore the efficiency falls down.

The DO content in the bulk liquid gets reduced with rise in temperature. This is reflected in Figure 61. Stage-3 has a higher DO content in the bulk as there is less biofilm growth and hence low uptake of oxygen. However, in stage-1, a high biofilm growth and uptake of oxygen reduces the DO concentration in the bulk.

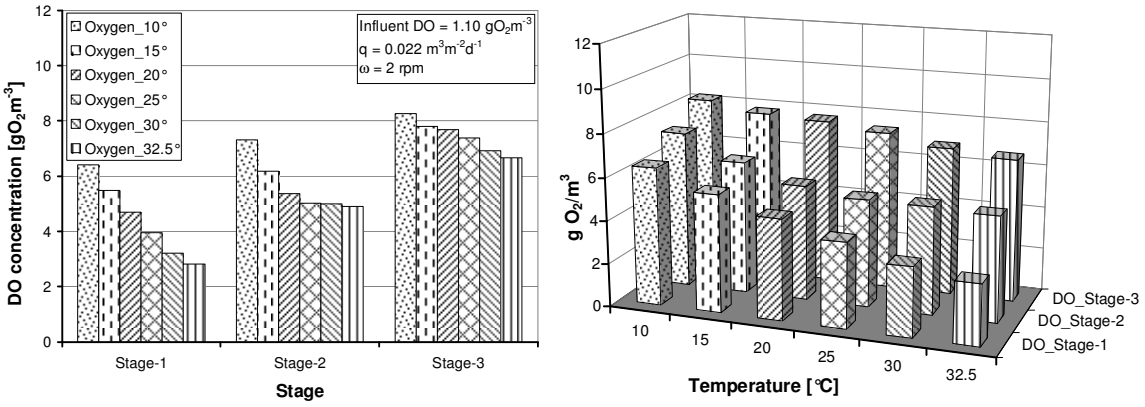

Figure 61 Simulated variation of the DO content in the bulk with temperature in the RBC stages

Simulations show that the DO content may vary from 6.40 g/m^3 at 10°C to 2.80 g/m^3 at 32.5°C, which is a reduction of more than 50% in stage-1. This reveals the temperature sensitivity of DO in biofilm systems for aerobic treatment. It may easily become a limiting factor at higher temperatures. Fortunately in RBCs, there appears to be sufficient DO left at 32°C due to the high oxygen exchange from the air through the boundary layer and so the system efficiency does not necessarily get affected. In spite of the increased bacterial growth and decay rates at higher temperature, the surface oxygen concentrations are aplenty and so the nutrient removal efficiency shows the normal trend of rise with temperature.

Temperature also affects the biofilm thickness because of the increase in the growth and decay rates of the microbial species (Table 15). This can be observed through simulation

results of the steady biofilm thickness as shown in Figure 62. Stage-2 and stage-3 clearly illustrates a decrease in thickness with temperature, while in stage-1, the high loading rate of substrate negates the effect of temperature rise and the biofilm thickness does not show substantial variation. Usually, an increase of temperature reduces the biofilm thickness under low substrate loading conditions. The increased growth rate cannot be sustained due to substrate limitations in the biofilm while the cells undergo high endogenous respiration and decay. The endogenous respiration rates get enhanced at high temperatures. This is also evidenced from the experimental observations at 30°C as well.

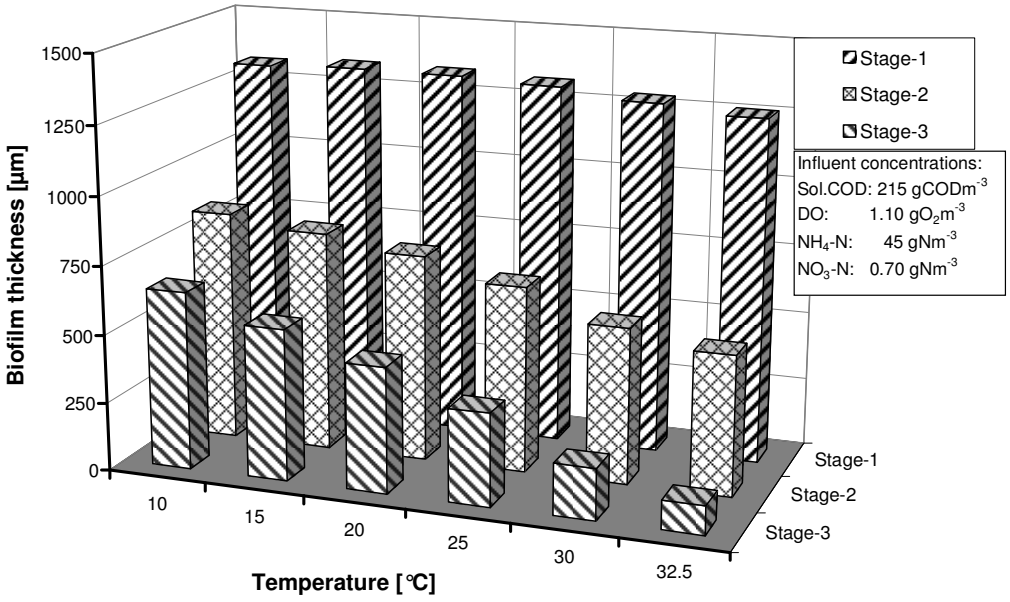

Figure 62 Effect of temperature on the biofilm thickness in the 3-stage RBC

The above results were obtained for the considered laboratory experimental set-up and the exact results may vary depending upon the hydraulic loading rate. However, the general trend of observation should remain identical with the increase in temperature.

7.4 Scenario-III: Nutrient load variation (25°C and 10°C)

A variation of influent loading rates may occur in real plants due to changes in the influent concentration of substrate or the hydraulic flow rate. The RBCs are usually designed for optimum performance under a range of influent loading rates for a given surface area. Stage-1 has a slightly higher surface area (1.18 m^2) compared to the subsequent stages (0.98 m^2). This is intended to meet the increased organic load compared to the subsequent stages.

7.4.1 Removal rates at 25°C

7.4.1.1 Organic carbon degradation

It is observed that for a given hydraulic loading rate, the removal flux in a RBC stage increases with influent substrate loading rate within a range. Beyond that range, removal rates are fairly constant for that stage and any further increase in influent loading does not increase the removal efficiency at the given temperature and loading rate. For soluble biodegradable organic substrate, the maximum removal flux stands in the range of 20-24gCODm^{-2}d^{-1} for any stage of the RBC. This is illustrated in Figure 63 for each stage of the present RBC model. The plot helps to find the optimum operating conditions for the system and defines the media surface area required for each treatment stage. For example, in stage-1, the highest carbon oxidation rate of 24gCODm^{-2}d^{-1} would occur at an influent loading of about 30gCODm^{-2}d^{-1}.

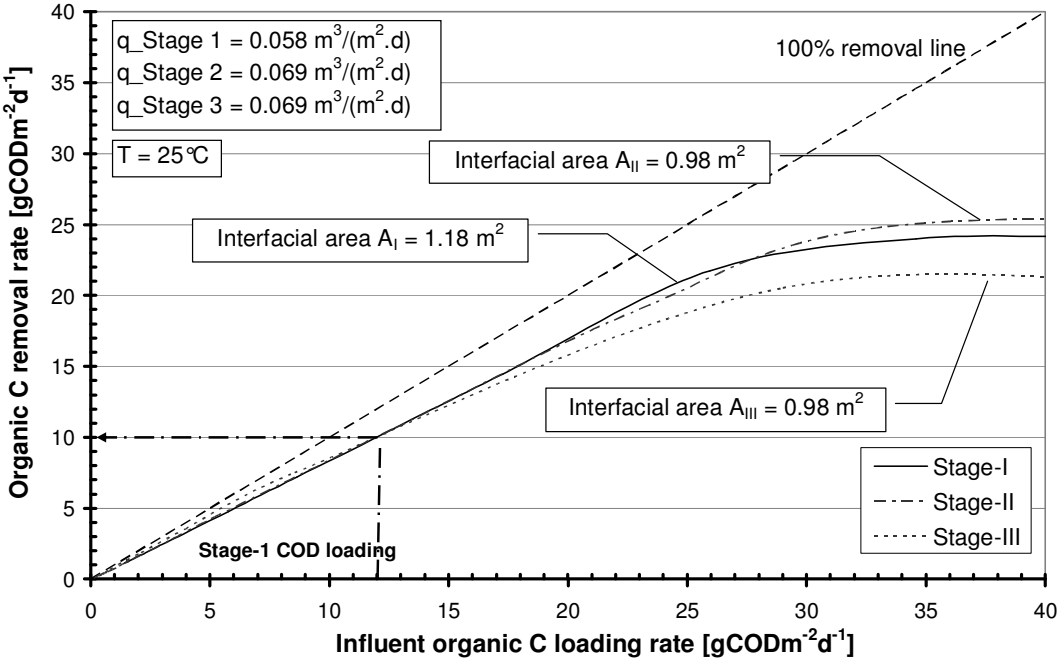

Figure 63 Simulated organic C removal rates in RBC stages under varied applied loading rates at 25°C

The highest removal rate of organic substrate is observed in the first two stages of the RBC, whereas the removal rate in stage-3 seems to be slightly lower due to less availability of nutrients and decline in the population of heterotrophic species. The hydraulic loading rate is slightly higher in stage-2 and stage-3 due to the reduced interfacial area. Figure 63 shows that the maximum removal efficiency achievable in stage-1 is about 85% at an influent organic loading rate of 12gCODm^{-2}d^{-1}. This data may be used to design and size the subsequent stages. However, in case of combined organic carbon removal and nitrification, the size of the stages of the RBC depends upon the nitrification rates as well. For the entire system, the simulated scenario of the overall removal rate of organic substrate under

different influent loading rates is compared with experimental findings as displayed in Figure 64. The removal rate keeps increasing with the increase of the influent organic loading rate and shows close fit with the available experimental results.

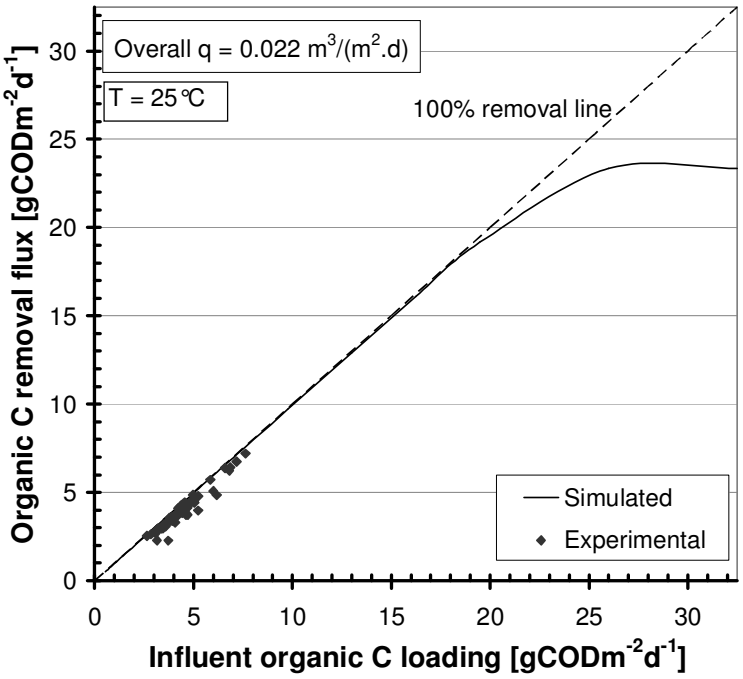

Figure 64 Experimental and simulated organic C removal rates in the overall RBC system under varied influent loading rates at 25°C

The simulation results show a high overall efficiency with nearly 99% organic substrate removal up to about 24gCOD $m^{-2}d^{-1}$ organic loading as reflected from the slope of the line. In case of the experiments, the removal efficiency is slightly lower due to the reduced removal in stage-2 and stage-3 where biofilm growth is substantially lower compared to that predicted in the simulations. The experimental results of the removal rate of the system at higher influent loading rates are due to be obtained.

7.4.1.2 Nitrification

In a combined nitrification system, nitrification rates are the driving criteria in sizing of the RBC stages. This is because the optimum nitrification rates are much lower compared to organic substrate removal rates and therefore serve as the limiting criteria in design of RBC stages. Temperature is also a big factor in the operational design of RBC units tailored for combined nitrification. The nitrification activity is highly influenced by ammonium-nitrogen loading rate. The nitrification rate increases with the increase of the loading rate up to a certain limit. Thereafter, it does not show any improvement and remains static (Gujer and Boller, 1990). Figure 65 shows the ammonia removal flux in each stage of the RBC. At 25°C, the ammonia flux in the first two stages of the considered experimental set-up reaches

a maximum at about 1.5gNH_4-N $m^{-2}d^{-1}$ after which it remains nearly steady and does not rise with further increase of the influent ammonium loading rate.

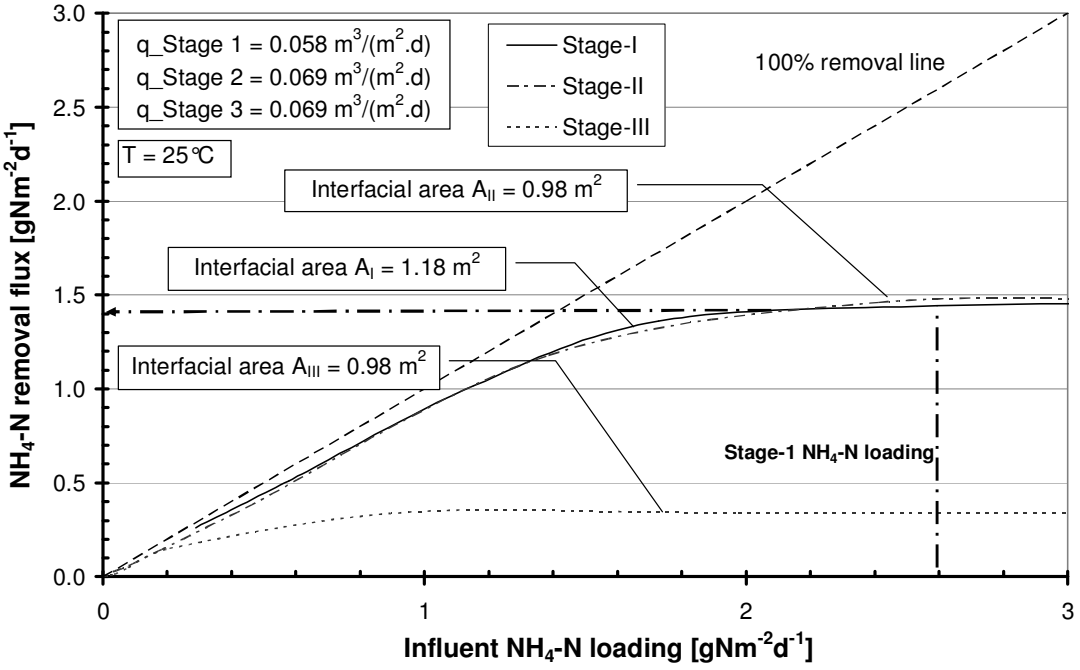

Figure 65 Simulated ammonia removal flux in RBC stages under varying influent loading rates at 25°C

The slight increase in the optimum removal rate for stage-2 compared to stage-1 is due to the increased hydraulic loading rate in the stage-2. Considering the current experiment, an influent ammonium load of 2.60gNH_4-N $m^{-2}d^{-1}$ in stage-1 is relatively higher than the optimum load necessary for complete removal and shows about 55% ammonium removal in stage-1. However, there is more than 93% overall removal of ammonium nitrogen at the end of stage-2 when the influent loading rate to that stage is 1.40gNH_4-N $m^{-2}d^{-1}$ based upon a biofilm surface area of 0.98 m^2. It is observed that maximum nitrification occurs in stage-1 compared to the latter stages due to the highest nutrient concentration in that stage. Radwan et al. (1997) made similar observations for the ammonia nitrogen removal in their 4-stage RBC (section 7.1.1.3). Stage-3 has the least nitrification potential. This is due to the low concentration of ammonia-nitrogen in the bulk after stage-2, most of which gets utilised for cell synthesis by the bacteria in stage-3. Gujer and Boller (1990) also found in their simulation predictions at 15°C that for an influent load of 6.67gNH_4-N $m^{-2}d^{-1}$ in stage-1, the last stage had least nitrification potential than the former stages. There is a limitation of substrate when nitrification is complete by the end of the earlier stage and consequently, decay and inactivation processes start taking dominance over the growth of autotrophic micro-organisms. This leads to a poor nitrifying bacteria density and hence a reduction in the removal rates compared to the former stages.

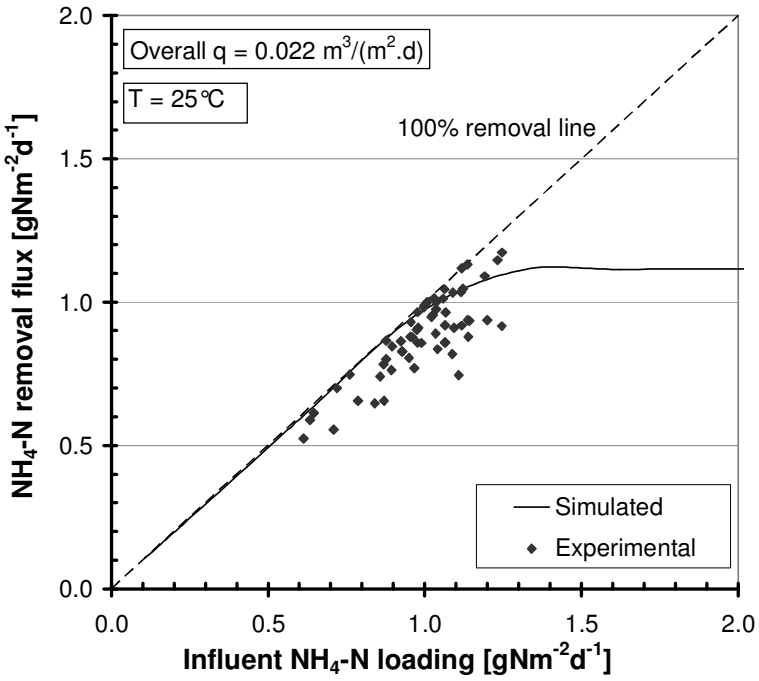

Figure 66 Experimental and simulated ammonia removal flux in the overall RBC system under varied influent loading rates at 25°C

Boller and Gujer (1989) verified that when such a stage is subjected to peak loading of ammonia nitrogen, a breakthrough will occur. The simulated and experimental scenario of nitrification for the overall system is illustrated in Figure 66. The influent load and the nitrification rate show a first order dependency till an influent loading of 1.10gNH_4-N $m^{-2}d^{-1}$. After that, it transforms into a non-linear relationship and finally steadies to a constant zero-order relationship at higher loading rates. Temperature has a big influence on the optimum range of influent loading rates for complete nitrification in the system. The results at 25°C are compared with that at 10°C in section 7.4.2.

7.4.1.3 Organic carbon oxidation vis-à-vis nitrification

For the considered experimental set-up, simulations can be done to know the probable effluent organic substrate and ammonia nitrogen concentrations in the three stages under different influent concentrations. This is displayed in Figure 67. The threshold concentration appears to be 900g$CODm^{-3}$ for biodegradable organic substrate, beyond which an increase will not initiate 100% removal in the final effluent. This corresponds to an organic loading rate of 19.8g$CODm^{-2}d^{-1}$. Up to an influent concentration of about 600g$CODm^{-3}$, maximum organic C removal occurs in stage-1. From 750g$CODm^{-3}$ upwards, both stage-1 and stage-2 show equal removal. This is evident from the line joining the effluent concentrations of the first two stages becoming straight (green dotted line in Figure 67). Further increase of the influent COD beyond this threshold level gives equal removal rates in all the 3-stages. This

can be concluded from the straight lines joining the effluent concentrations in the 3-stages (red and purple lines in the top plot in Figure 67).

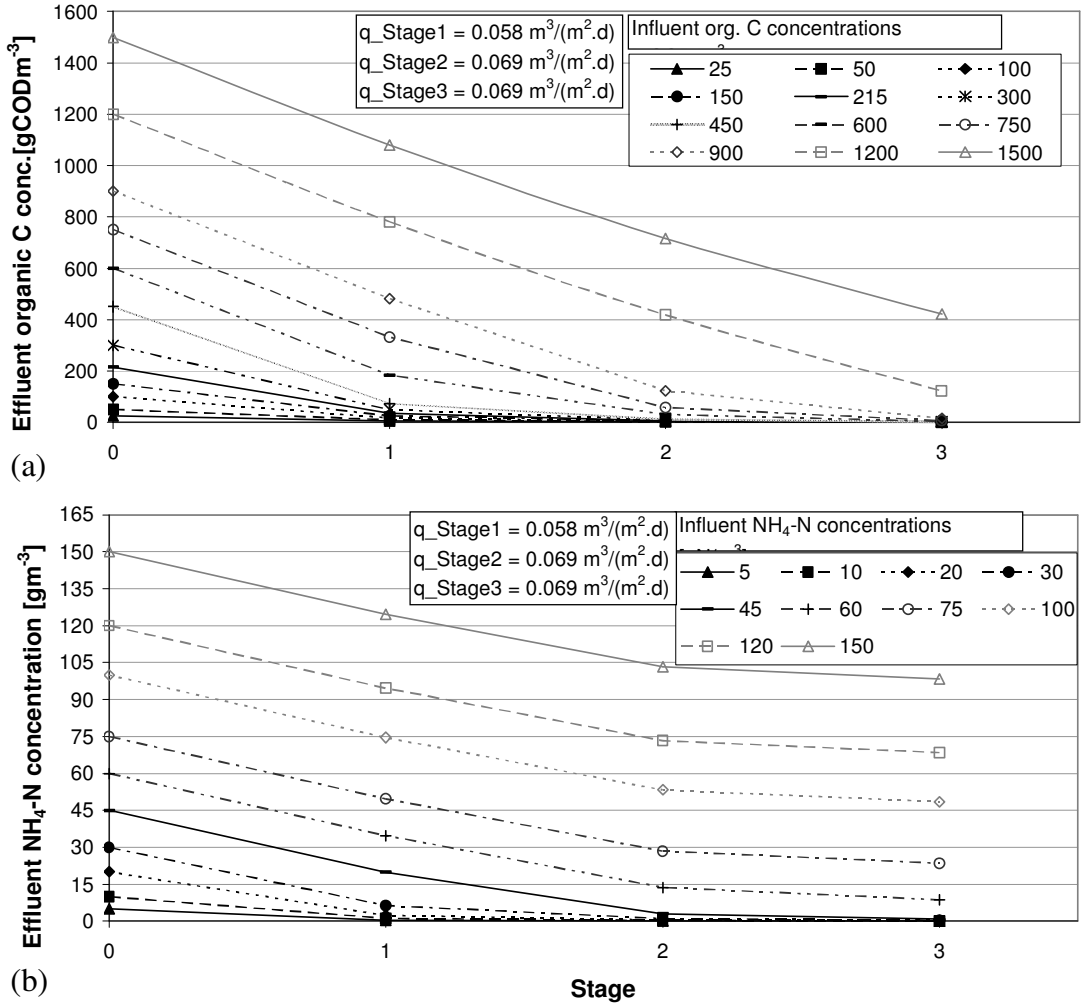

Figure 67 Effluent organic C and NH_4-N concentration at different influent loading in the RBC stages

In case of ammonium nitrogen, Figure 67 reveals a similar trend although the removal is maximum in the first two stages of the RBC. This is evident from the line joining the effluent concentrations of the first two stages becoming nearly straight after an influent concentration of 45gNH_4-Nm^{-3}. A further rise to about 60 gNH_4-Nm^{-3} results in incomplete nitrification and additional treatment of the final effluent is needed. Although it has been the design practice in RBCs to attain a maximum removal of organic substrate in the initial stages while nitrification should occur in the latter stages, the current observation differs from this practice. Both experiment and simulations show maximum nitrification in the stage-1. Radwan et al. (1997) reasoned that at higher hydraulic loading rates, mass transfer and availability of oxygen could be the limiting factors in the latter stages of the RBC. However, temperature can make a huge difference and the mixed culture biofilm at 25°C certainly would not show the same kinetics as observed at 10°C by Gujer and Boller (1990).

The autotrophs in stage-1 of the biofilm compete better with the heterotrophs at higher temperatures and once the organic substrate starts getting limited, the autotrophic species underneath the surface layers start to nitrify. The large thickness of the biofilm in the stage-1 ensures the presence of nitrifying bacteria in sufficient numbers and under aerobic conditions, nitrification is high.

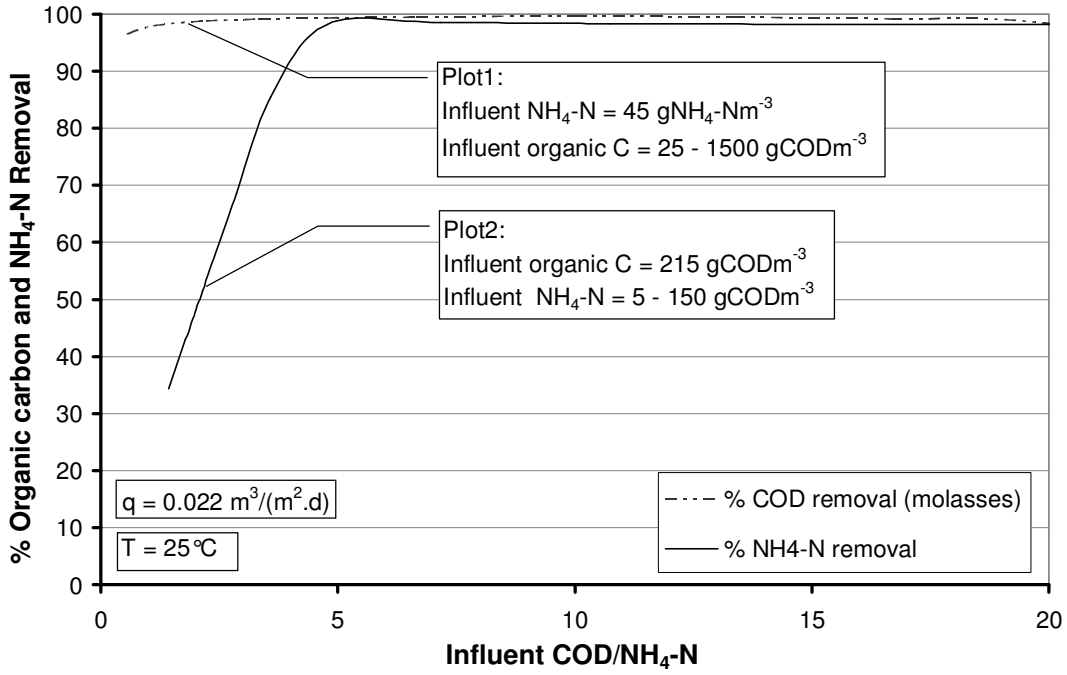

Figure 68 Effect of influent COD/NH_4-N ratio on the RBC performance

The effect of COD/NH_4-N on the RBC performance can be studied from Figure 68. The removal efficiency of organic substrate is studied by keeping the influent NH_4-N concentration constant at 45gNm^{-3} while the influent COD is varied from 25 gm^{-3} to 1500 gm^{-3} (Plot 1). Similarly, the other curve is based upon a constant influent organic carbon concentration of 215g COD m^{-3} while the influent NH_4-N concentration is varied from 5 to 150gNm^{-3} (Plot 2). At high C/N ratios, both the organic substrate and the ammonia removal seem to be high and the RBC performance is good. However, at low values of the ratio (below 5), the ammonia nitrogen removal efficiency drops down sharply while the organic substrate removal is not affected. The NH_4-N concentration in the influent rises above the optimum load for nitrification and system fails to achieve sufficient ammonia nitrogen removal at the end of stage-3. However, the benchmark ratio would vary depending upon the system configuration and hydraulic load conditions. Moreover, temperature can influence this value in a big way. Nevertheless, the C/N plots reveal that the NH_4-N concentration remains the governing criteria in the design of a RBC system. Therefore, the allowed loading range of NH_4-N needs to be carefully considered owing to its high

sensitivity in affecting the system performance during influent load fluctuations. Domestic wastewater can vary in ammonia concentration over the day but normally within a tolerable range. Based upon the considered experimental set-up, the simulation results show a tolerable NH_4-N concentration would be about 45 to 50gNm^{-3}, corresponding to an influent loading rate of 1.0 - 1.1$gNm^{-2}d^{-1}$.

7.4.2 Removal rates at 10°C

The effect of temperature on the removal rates can be studied with the help of simulation runs. As a case study, the scenario at 10°C has been selected and compared with the calibrated results obtained at 25°C in the above section. The optimization plots for the RBC stages change substantially due to the decreased bacterial activity as well as diffusivity values of the substrate. The temperature change will also affect the thickness of the liquid boundary layer which will be thicker due to the increased viscosity and can offer a higher diffusive mass transfer resistance than at 25°C. However, this variation is neglected as it was not possible to determine the boundary layer thickness accurately in the experiments.

7.4.2.1 Organic carbon degradation

Although the DO content in the bulk liquid is higher at 10°C (Figure 61), the bacterial growth rate and activity is substantially reduced as reflected from Table 15. This will invariably leave a mark on the removal rates for organic substrate degradation and nitrification. Gujer et al. (1990) had used similar kinetic parameters in their RBC model at 10°C. However, the current model is based on the ASM No. 3 process kinetics which separates the decay process (lysis) of the cells into aerobic and anoxic endogenous respiration processes. Figure 69 illustrates the organic carbon removal rates in each stage under different influent organic loading at a temperature of 10°C. The ammonia nitrogen concentration in the influent is kept steady at 45gNm^{-3}. The maximum removal rate in stage-1 and stage-2 is reduced when compared with the plots at 25°C (Figure 63). The optimum range of influent COD loading is also less when compared with 25°C. For stage 1, the maximum carbon oxidation rate of 19.4$gCODm^{-2}d^{-1}$ occurs at an influent loading of 26$gCODm^{-2}d^{-1}$ (blue dotted line in Figure 69). There appears to be a drop of about 19% in the maximum removal rate achievable in stage-1 for a temperature dip of 15°C. Stage 2 and 3 show a drop in the maximum removal rate compared to stage-1 and this would be due to the increased hydraulic loading rate in these stages. However, stage-3 shows the same removal efficiency as in stage-2. Unlike the scenario at 25°C, the last stage is not nutrient limited here, due to comparatively reduced removal in the earlier stages and so there is no

dearth of heterotrophic species and all stages take part in removal and exhibit almost equal efficiency. The cell decay rates are also less at lower temperatures and so there is less production of particulate inerts in the depths of the biofilm compared to the scenario at 25°C.

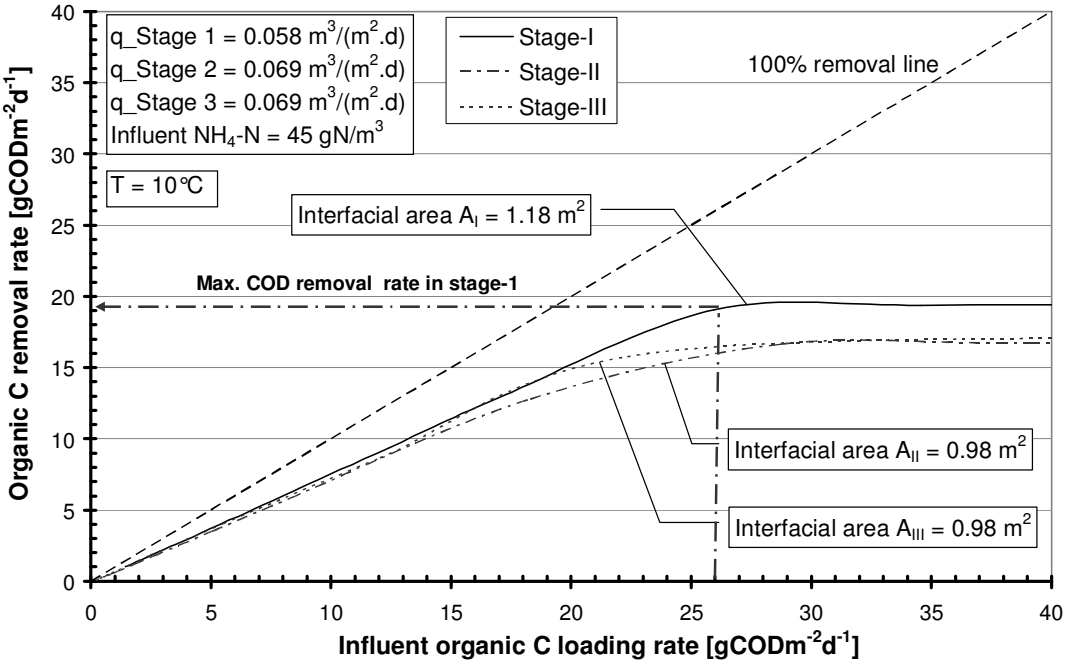

Figure 69 Simulated organic C removal rates in RBC stages under varied applied loading rates at 10°C

7.4.2.2 Nitrification

The effect of temperature on the nitrification rate is more evident as compared to 25°C scenario due to the high sensitivity of the nitrifying bacteria vis-à-vis heterotrophs in the mixed-culture biofilm. Figure 70 illustrates the simulated ammonia removal rates in the three stages of the RBC at 10°C. The predicted ammonium removal flux is reduced substantially in stage-1 and stage-2 compared to the scenario at 25°C (Figure 65). The simulated reduction is nearly 41% for stage-1 for a temperature change of 15°C and establishes the high sensitivity of autotrophic organisms compared to the heterotrophs. The maximum removal flux of 0.86gNm^{-2}d^{-1} in stage-1 would occur at an influent ammonium loading of 1.3gNm^{-2}d^{-1}. It is worthwhile to mention that there is considerable nitrification in stage-3 and it does not show a reduced removal potential as it had been observed at 25°C. Unlike the previous scenario at 25°C when stage-3 got nitrogen limited, the reduced ammonia removal in the first two stages at 10°C leaves behind sufficient nitrogen in stage-3 for the sustenance of the autotrophic species. Moreover, the slowing down of the decay rate of autotrophs at lower temperatures as well as a relatively thicker biofilm compared to 25°C (Figure 62) may additionally account for the improved nitrification potential. Gujer et al. (1990) showed a similar trend in their model runs for primary effluent although they observed a higher ammonia removal rate in the latter stages. However, their experimental

set-up was slightly different as they had considered a four stage RBC with an applied hydraulic loading rate of $0.133 m^3 m^{-2} d^{-1}$ which is much higher than that in the present scenario.

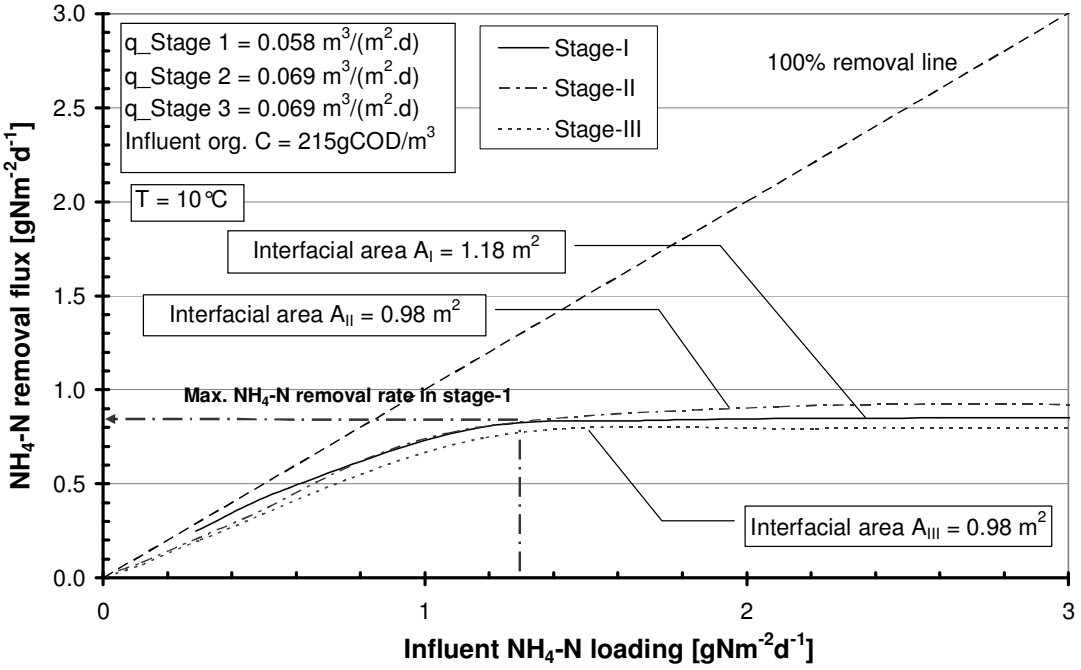

Figure 70 Simulated ammonia removal flux in RBC stages under varying influent loading rates at 10°C

7.5 Scenario-IV: Hydraulic load variation

7.5.1 Organic carbon oxidation

The removal of nutrient per unit media surface is related to the hydraulic loading rate. For soluble organic substrate, the correlation is illustrated in Figure 71 for each stage of the RBC. At higher hydraulic loading rates, the biofilm develops mass transfer as well as oxygen limitations. This will affect the removal rates but only after a threshold level. The optimum hydraulic load applicable for the organic substrate removal in each stage can be determined with the help of such a plot. The flow rate has been varied from 0.01 to $0.45 m^3 d^{-1}$ while the interfacial surface area of the biofilm has been kept fixed in the three stages in order to vary the hydraulic load. In stage-1, for an applied hydraulic loading of $0.058 m^3 m^{-2} d^{-1}$ and an influent organic loading of $12 gCOD m^{-2} d^{-1}$, the C-removal rate is $10.30 gCOD m^{-2} d^{-1}$. This can be verified with Figure 63. The removal rate rises with the hydraulic load up to an optimum value for each stage and then it stabilises to a fixed removal efficiency. The interfacial area of the three stages of the RBC has been proportioned with the same ratio of 1:0.83:0.83 so that stage-1 always has the largest surface area. The lowest hydraulic resilience is observed in stage-1 compared to the subsequent stages due to the high organic loading rate in this stage. The subsequent stages show a greater resilience because the organic load on that stage is less.

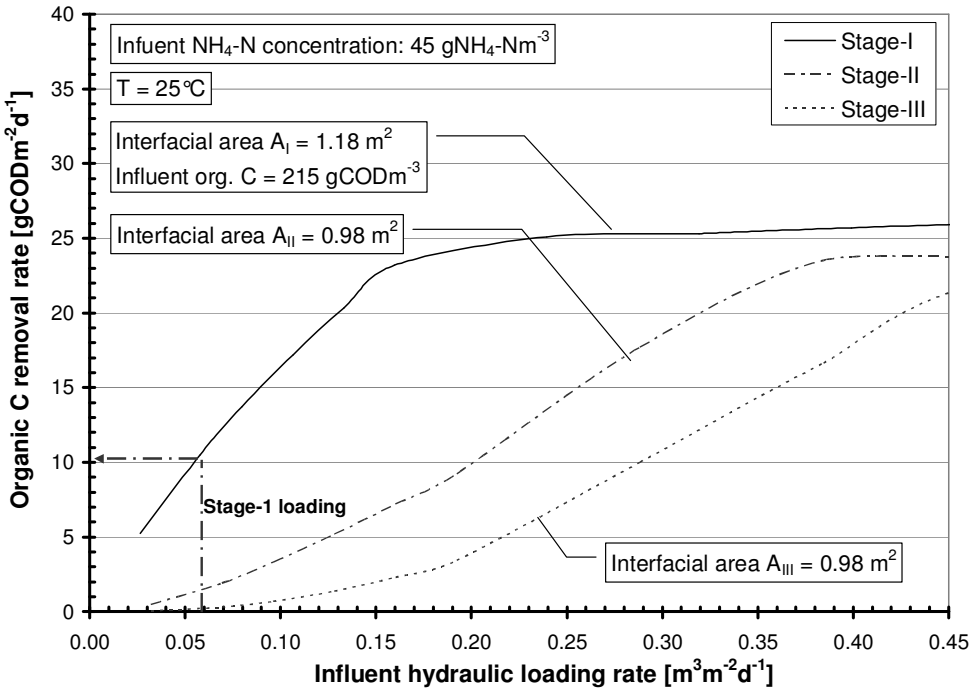

Figure 71 Org. substrate removal in RBC stages under varying hydraulic loading rates

What transpires from these plots is that RBC units can sustain fluctuations in the hydraulic loading rate within a range when designed properly and this range is dependent upon the organic load applied to that stage. As the threshold value of organic loading for a stage is constant (Figure 63), the higher the organic substrate concentration becomes, the lower the hydraulic loading sustenance gets. For a given stage of RBC, increase of the hydraulic loading rate at a fixed organic substrate concentration leads to an increase in the nutrient supply per unit area in that stage and thereby improves the removal rate within an optimum level. Beyond this threshold point, due to nutrient overloading, there is no further increase in removal rate. Famularo et al. (1978) found a similar correlation in their study on RBC mass transfer. The high DO content in the system is responsible for the high removal rates up to an optimum point. The influent DO is kept at $1.10 gO_2m^{-3}$ in all the runs. The maximum organic carbon removal rate achievable in stage-1 of the RBC seems to be about $24 gCODm^{-2}d^{-1}$ at 25°C beyond which it remains static. For stage-2 and stage-3, maximum removal rate is a little lower than in stage-1 and comes to about $20 gCODm^{-2}d^{-1}$. The latter stages have less surface area compared to the stage-1. However, the optimum range of hydraulic loading varies in each stage corresponding to the influent organic load in that stage. As a matter of fact, the hydraulic load variation plots (Figure 71) are a reflection of the influent loading charts (Figure 63) and may be read in conjunction since these plots are co-related to each other and necessary for the optimum design of any RBC system. Banerjee (1997) had also observed that an increase in the hydraulic loading at constant C concentration leads to an increase in the phenol removal rate.

7.5.2 Nitrification

Figure 72 displays the response of the ammonia removal rates in the RBC stages with a variation of the hydraulic loading rate. It is evident that nitrification is more sensitive to changes in the hydraulic loading rates than organic carbon removal. The ammonia removal flux increases with the hydraulic loading rate and then stabilises at a certain value. The stage-1 shows the lowest optimum range of applied hydraulic load compared to the subsequent stages. This is again an effect of the high ammonium concentration in this stage vis-à-vis the latter stages. In stage-1, an applied influent ammonia loading of $2.60 gNH_4\text{-}Nm^{-2}d^{-1}$ (corresponding to a concentration of $45 gNH_4\text{-}Nm^{-3}$) and a hydraulic loading rate of $0.058 m^3m^{-2}d^{-1}$ shows a maximum removal rate of $1.50 gNm^{-2}d^{-1}$. This can be verified from Figure 65. However, the removal flux reduces after reaching an optimum point and this may be due to the flow through conditions in the reactor. Thereafter, it stabilises at a lower value due to the nitrogen requirement for assimilation in cell biomass.

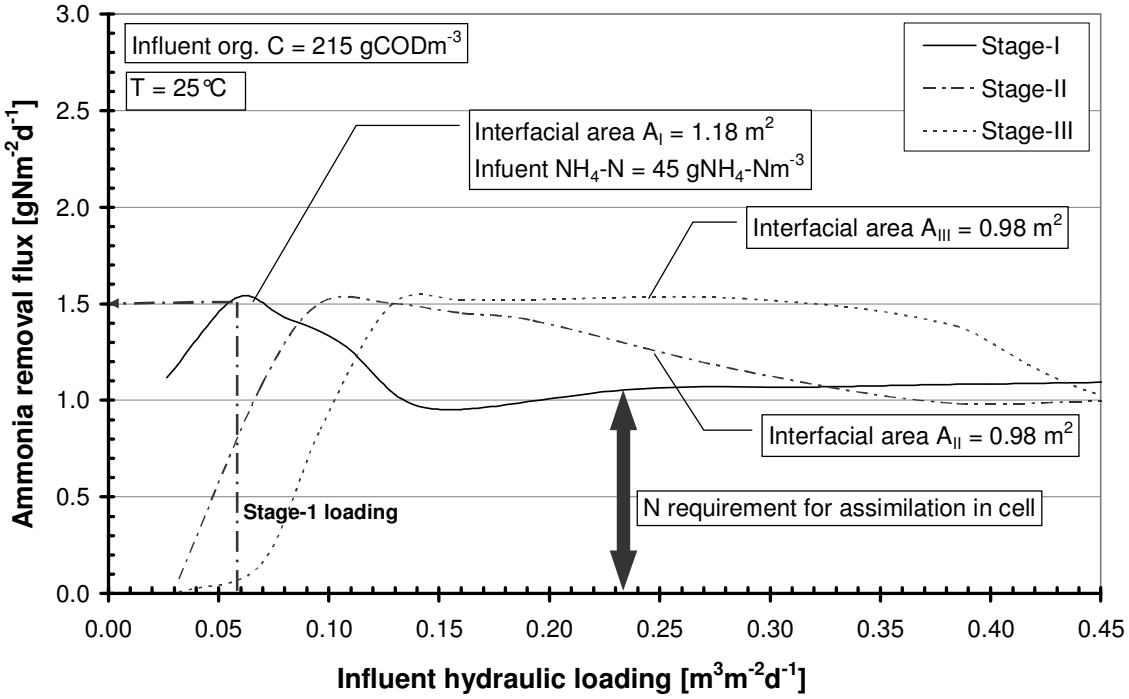

Figure 72 Nitrification in the 3-stage RBC under varying hydraulic loading rates

As only a part of the ammonium load gets removed in stage-1, there is nitrification in the subsequent stages. The optimum range of ammonia removal flux varies in the latter stages corresponding to the applied ammonium load in that stage. Nitrification plots under varying influent ammonium load (Figure 65) are usually read in conjunction with the hydraulic load variation charts (Figure 72) for an optimum process design of the RBC stages. For any RBC system design, simulations like this may be used to obtain such plots under different temperatures since the nitrification process is highly temperature sensitive.

7.5.3 Dynamic simulation results

To observe the effect of fluctuations in the hydraulic loading rate with time, dynamic runs have been conducted based upon an assumed variation of flow rate over a period of time. This is shown in Figure 73 below. The model is also capable of reading data files containing 24-hrs (diurnal) variation of flow rate when such data is available from measurements.

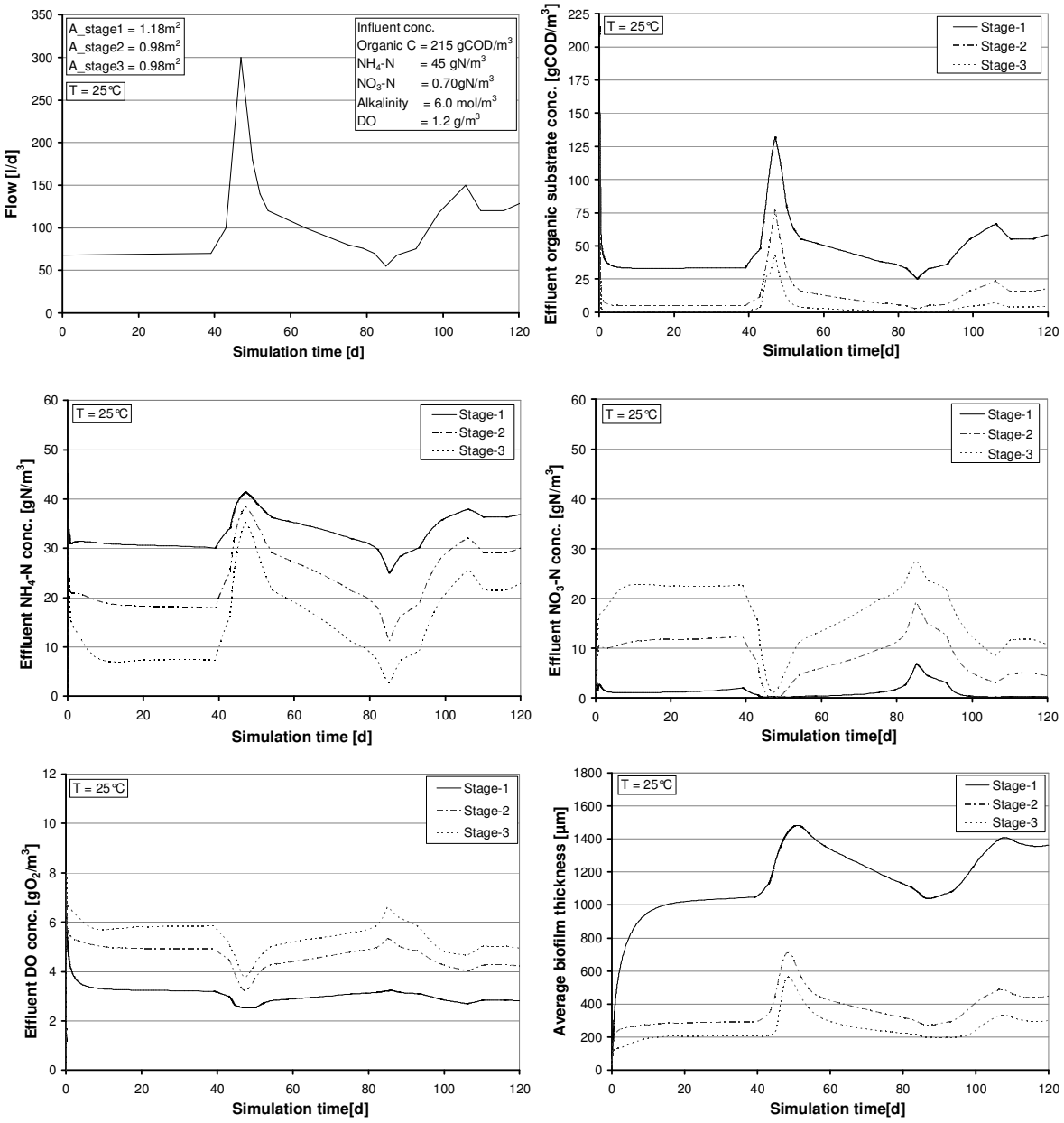

Figure 73 Simulated variation of effluent nutrient concentrations and biofilm thickness with flow

Variation of hydraulic loading rate by changing the flow rate with time in the framework of the current experimental set-up reveals corresponding effects on the overall removal rate of organic C and N-compounds. Increasing the flow rate nearly five-fold from the designed flow of 68 l/d after 45days shows a drop of 20% in the organic C removal, while NH_4-N oxidation is reduced by 77%. NO_3-N concentration follows a matching reverse trend with

ammonia and dip down where effluent NH_4-N concentrations are high due to reduced less nitrification. The results confirm that NH_4-N removal efficiency is very sensitive to fluctuations in hydraulic loading and can make big difference to the functional efficiency of a system under wide fluctuations of the flow rate. DO levels in the bulk reactor dip on the 45th day due to increased demand as a result of nutrient overloading (g/d) and thereby increased bacterial growth. The latter is evident from the biofilm thickness in the last plot where the average biofilm thickness in stage-1 increases to about 1500µm from a steady value of 1100µm. In the current simulations, the nutrient concentrations have been kept constant in the dynamic data file so as to study the individual effect of flow variation on the system performance.

7.6 Scenario-V: Recirculation ratio variation

In order to study the effect of flow recirculation by simulation, a recycle ratio varying from 0.25 to 2.0 is applied to the inflow. The recycled flow is added from the effluent of stage-3 to the influent in stage-1 of the experimental RBC set-up.

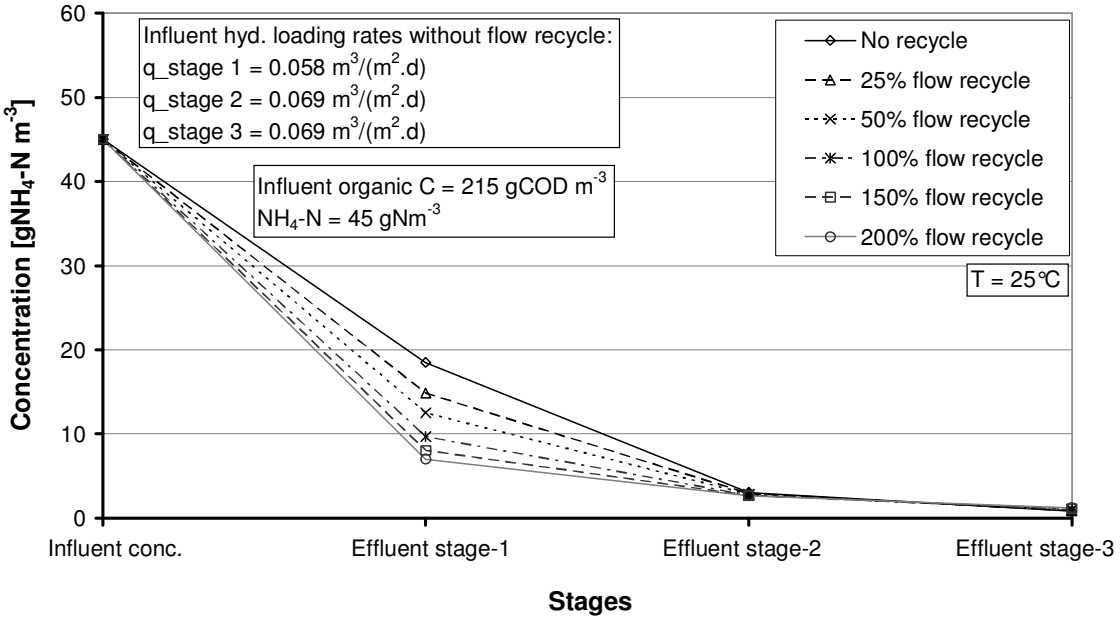

Figure 74 Effect of flow recycle on ammonia removal in the RBC stages

The concentration dilution due to this recirculation has been taken into consideration in the model as expressed in equation 6.12. The nutrient concentrations in the influent have been kept identical as in the previous runs. Due to reduction of the organic carbon concentration by way of dilution, ammonia removal improved in the first two stages as evident from the effluent NH_4-N concentrations in Figure 74. Stage-1 shows maximum removal efficiency while it is less in stage-3 due to lower availability of nutrients. The ammonia removal efficiency in

stage-1 increased from 55% for no recycled flow to 78.5% for 100% recycled flow and 84.4% for 200% recycled flow. Nevertheless, the effluent concentration after stage-3 remains nearly constant in all cases. There is little improvement in the overall removal rate for an influent ammonia nitrogen concentration of $45gNm^{-3}$. This shows that the latter stages of the RBC can capable in removing the remaining ammonium load in all cases and therefore, no additional recirculation will be required in the considered experimental set-up. This would be valid within the optimal range of the hydraulic and ammonium loading rates (Figure 72 and Figure 65). In fact, the lower the nutrient load becomes, the lower the removal efficiency of a stage gets. This is partially due to the starvation conditions generated as a consequence of low nutrient load when the cells start to undergo high degeneration and the endogenous respiration process nullifies the growth effect of the cells. Therefore, flow recycle can only be recommended for achieving a better nitrification when the ammonium loading is very high in the influent. Klees and Silverstein (1992) reported that flow recirculation improved nitrification in a RBC stage. However, when the recirculation ratio was increased beyond a certain point, it did not lead to any further improvement in the performance. It can be observed in Figure 74 that in the case of stage-1, the difference in effluent concentration narrows down with increase of the recycle ratio.

In the case of organic substrate, the simulation results showed that flow recirculation does not enhance the overall removal efficiency in any way. Wilson and Lee (1997) also observed that recirculation did not improve the overall removal efficiency of organic substrate significantly.

7.7 Scenario-VI: Submergence ratio variation

All the runs for sensitivity so far have been carried out with a constant submergence ratio (immersion ratio) of 42% of the total disc area inside the bulk liquid. However, it remains to be seen as part of the sensitivity analysis as to what happens with the variation of this submergence ratio. The current RBC model offers this feature and the exposed and submerged disc areas can be varied as explained in section 6.3.3.2 (equations 6.8, 6.9).

7.7.1 Dissolved Oxygen

The most immediate effect of changing the submergence ratio is the DO concentration. The DO tends to dip down with the increase of the submergence ratio as evident from the Figure 75. The influent DO has been kept at $1.10gO_2m^{-3}$ as in the experiment in all cases. Rodgers et al. (2003) commented that when deeper submerged RBC units are used to treat wastewater aerobically, DO in the bulk liquid will be lower and external aeration would be needed. For

the considered experimental set-up, when the submergence ratio is increased from 25% to 90% in all the RBC stages, the DO concentration gets reduced correspondingly. Submergence beyond 60% shows a sharp decrease, especially in the latter stages. In case of 90% submergence, the DO concentration is changed very little from the influent concentration and it may initiate oxygen limitation conditions which would lead to high degeneration and decay in the aerobic biofilm and thereby affect the removal rates. It may be entirely possible that the process kinetics and the bacterial strains change completely under deep submergence conditions and anaerobic conditions set in. Rodgers and Zhan (2003) quoted Lu et al. (1997) as having observed that deeper submerged RBC units, especially completely submerged RBCs can be used as anaerobic RBCs. In such cases, the present model based on aerobic species kinetics and stoichiometry will not be able to predict the effluent concentrations.

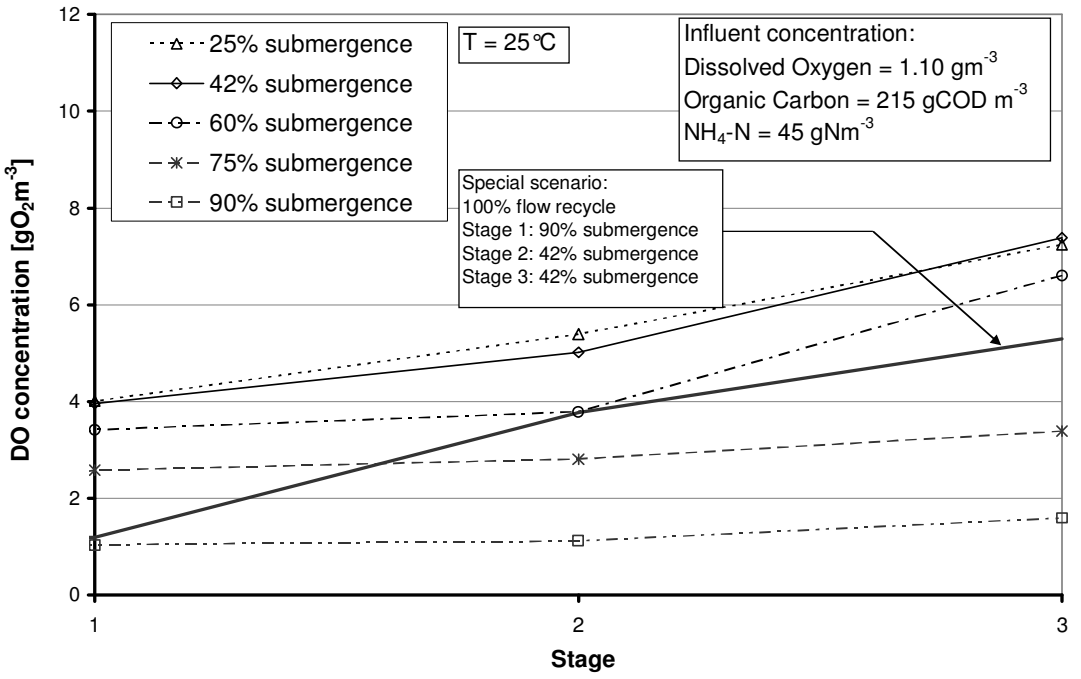

Figure 75 The DO concentration in bulk liquid under varying submergence ratio in RBC stages

As a special case study, a scenario with 100% flow recirculation and a varying submergence ratio in different stages has been attempted. The stage-1 is kept at 90% submergence, while the latter two stages have been maintained at 42% submergence as in the experiment. The DO in stage-1 remains low although there is concentration increase from flow recycle and subsequent dilution. The bulk liquid DO concentration in stage-1 is 1.19gO_2m^-3 which is slightly above the influent value. The low aeration due to high submergence would diminish aerobic activity in that stage. However, as soon as the submergence ratio increases to 42%

in the subsequent stages, the DO level rises and the removal efficiency improves as discussed in the subsequent sections.

7.7.2 Nitrification

With the change in the DO concentrations by variation of the submergence ratio, the ammonia removal and denitrification process is extremely affected. Figure 76 shows the ammonia nitrogen removal under varying submergence ratio for an influent ammonia concentration of 45gNH_4-Nm^{-3}. As the submergence ratio increases, nitrification is lowered and removal efficiency gets reduced.

Figure 76(a) indicates that submergence above 60% reduces the ammonia removal rate rapidly. The nitrifying species cannot perform optimally due to a low DO concentration in the bulk liquid and less diffusion from air. The optimum submergence seems to be around 42% for maximum ammonia nitrogen removal when the effluent concentration reaches 0.83gNH_4-Nm^{-3} with an overall removal efficiency of 98%. Submergence up to 60% would also yield good ammonia removal. The removal reflects a matching trend with the bulk oxygen concentration in the respective stages. The higher the DO content gets, the greater the ammonia removal occurs.

In the special scenario with 100% flow recycle and 90% submergence in stage-1, nitrification reveals a different trend as shown by the bold line in Figure 76(b). Due to the flow recycle and thereby the dilution effect, the DO concentration in bulk increases and hence, ammonia removal in stage-1 is comparable with the cases of 42 to 60% submergence under no recycle scenario. As there is less submergence in the latter stages, further nitrification occurs and the effluent ammonia concentration is 2.86gNH_4-Nm^{-3} depicting an overall removal efficiency of 94%. This is slightly less than the overall removal observed in the case of 42% submergence with no flow recycle. In effect, it can be inferred that varying submergence ratio below or above 42% or recycling does not lead to a significant improvement on the overall ammonia removal efficiency. The removal without recirculation is already high enough as can be seen from the previous plots. However, if the submergence is changed from 90% to about 60% in stage-1 under the above scenario with the flow recycle, the overall removal rate may improve a little more.

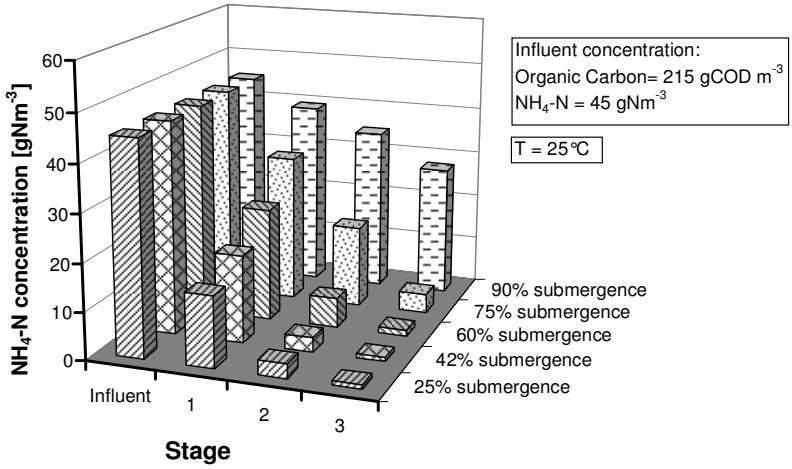

(a)

	Influent	1	2	3
25% submergence	45.00	15.03	3.06	0.91
42% submergence	45.00	18.50	3.03	0.83
60% submergence	45.00	23.91	6.31	1.27
75% submergence	45.00	31.28	17.29	4.12
90% submergence	45.00	39.35	34.67	27.75

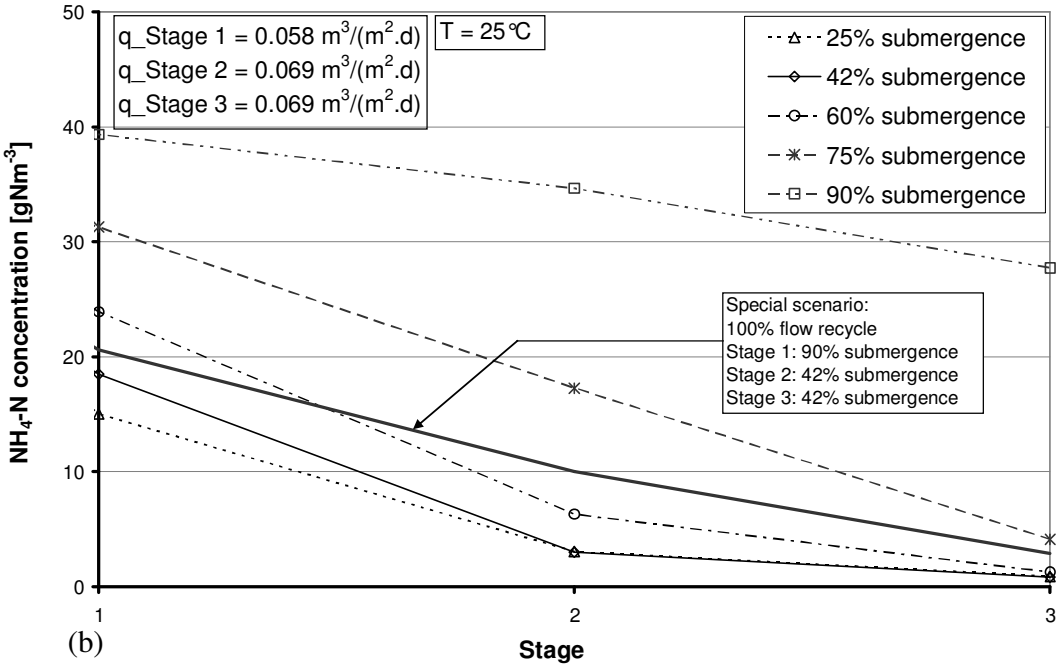

(b)

Figure 76 The effect of varying submergence ratio on ammonia removal in RBC stages

7.7.3 Denitrification

Denitrification can occur in the RBC system under two circumstances:

- In the deeper regions of the biofilm where oxygen is significantly limited while organic substrate and nitrate-nitrogen are present. This happens in the anoxic layers of the biofilm just underneath the surface of the aerobic zone especially in the stage-1 with high surface organic loading.
- Reduction of the oxygen supply in a stage by nearly completely submerging the discs and supply of adequate nitrate by flow recirculation from the latter stages. Although

flow recirculation will cause dilution of organic substrate concentration, there would be usually sufficient organic carbon in the domestic sewage.

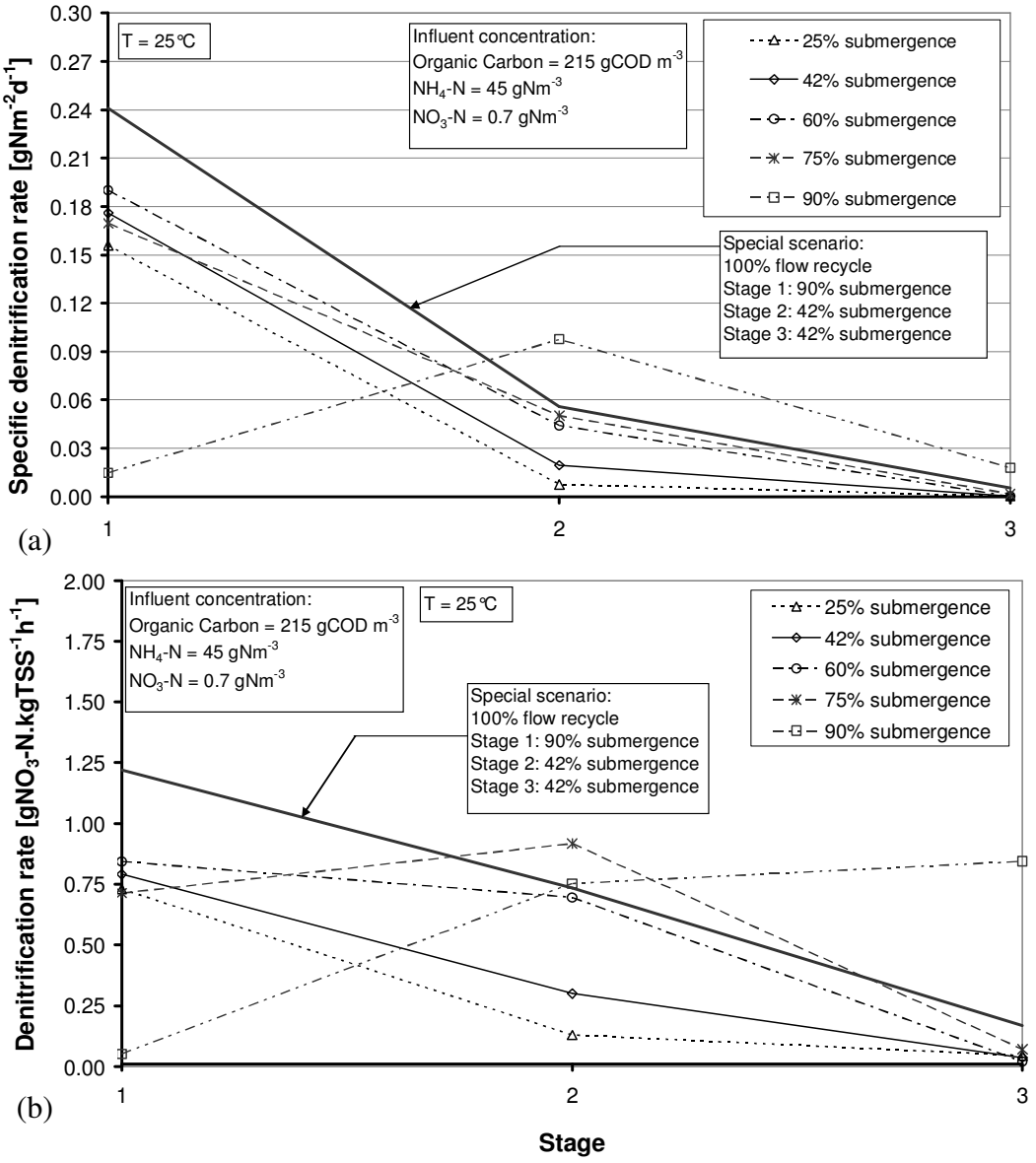

Figure 77 Effect of submergence on denitrification rate in the biofilm in each stage of the 3-stage RBC

One of the purposes of higher submergence in the simulation study here was to verify higher denitrification by increasing the submergence ratio. This advantage is clearly reflected in the denitrification plots in Figure 77. The first plot, i.e. Figure 77(a) reflects the specific denitrification rate per unit surface area of each stage, while Figure 77(b) shows the denitrification rate per unit biomass in the biofilm. The latter plot is related to the total solids present in the biofilm and helps to compare denitrification in RBC systems with conventional activated sludge processes. For instance, in stage-1, as the submergence ratio increases from 25% to 60%, denitrification also increases. However, it drops down at 75% submergence and above since little nitrification takes place as a consequence of inadequate

oxygenation and so little nitrate is left to be denitrified. Up to about 60% submergence, maximum denitrification takes place in stage-1. However, the denitrification seems to get slightly better in stage-2 at a very high submergence due to the availability of some nitrate nitrogen there. The influent nitrate is $0.70gNO_3\text{-}Nm^{-3}$ in all cases.

In the special scenario with 100% flow recycle and 90% submergence in stage-1, the denitrification is improved due to the addition of nitrate rich effluent from stage-3, while 90% submergence ensures prevalence of anoxic conditions. Moreover, there is also no dearth of organic substrate as the organic carbon concentration is high in the influent. In stage-2 and stage-3 under the current scenario, 42% submergence provides increased DO concentration (Figure 75) and anoxic conditions are no longer maintained. Consequently, the denitrification rate comes down in the latter stages as shown by the bold line in Figure 77. It is observed that the final effluent nitrate nitrogen concentration in the special scenario is about $24.48gNO_3\text{-}Nm^{-3}$. On the other hand, it is about $30gNO_3\text{-}Nm^{-3}$ in the case without recirculation with 42% submergence in all stages (Figure 42). Gujer et al. (1990) mentioned that partial denitrification can be achieved in the RBC if the effluent of the RBC is returned to a non-aerated first stage reactor. They also remarked that denitrification might be slightly improved if the recirculation ratio is reduced which will result in less dilution of organic substrate and hence more availability of it in the anoxic layers of the biofilm in the stage-1. However, as observed previously, higher submergence would simultaneously cause lower nitrate and DO levels in the first reactor and the nitrification rate of the first reactor will get lowered. Teixeira et al. (2001) also observed that RBC systems can be used for denitrification by varying the submergence ratio.

8 Discussions

The aim of the current work has been to build suitable mathematical models to study the performance of a RBC system and to predict the optimised conditions of operation for a given geometry of the system. Both the model codes, i.e. physical oxygen transfer model as well as the biofilm model were built in Matlab. Initially the programme codes were written in version 5.3 (release 11) but later updated to version 6.5 (release 13). The models run in all Matlab versions although it is a little faster in the latter versions. The author had little prior knowledge of programming in Matlab at the beginning of the work. Therefore it was a difficult task considering the dynamism of RBC operation, the adoption of process kinetics from the accepted ASM No.3 for the biofilm model and the numerical solution using finite-difference methodology employed in the models. The advantage of using Matlab especially in the biofilm model is that it offers a very strong numerical engine to solve the system of ordinary and partial differential equations by using its variable time step stiff solver and the built-in mathematical functions. It is very flexible in operation and helps to do steady-state as well as dynamic simulations with ease.

8.1 Physical oxygen transfer model

It is an established fact that the oxygen transfer phenomenon is one of the important aspects in the functioning of biofilm processes like RBC. Oxygen limitation in aerobic treatment of wastewater is not desirable and should be avoided. Understanding the physical nature of oxygen transfer into a pure water liquid film formed on the surface of a rotating disc helps to determine the boundary conditions for efficient oxygen transfer that is possible in such a system. The physical aspects of mass transfer by molecular diffusion of oxygen from air into the liquid boundary layer have been studied with the help of the physical model. This model helps to determine the oxygen transfer coefficient (K_L) and oxygen concentration in the liquid film at a specific location on the disc based upon the exposure time and the film thickness at that location of a rotating disc. It has also been used to determine the average K_L values in the liquid film based upon an average exposure time. For a 25 cm diameter disc, the following points were observed:

- At a given temperature and 42% disc submergence, the oxygen transfer coefficient is non-uniform and varies spatially over the exposed disc surface. At a fixed rotational speed, it decreases towards the end of the air exposure cycle when the liquid film gets

nearly saturated in comparison to the high values at the point of emergence from the trough. Moreover, it tends to increase with rotational speed and radial distance from the disc center. In practice however, at very low rotational speed ($\omega < 5$ rpm) of small diameter discs (lab-scale), a shearing off of the liquid film can occur due to the dominating effect of gravity over centrifugal and viscous forces. This may reduce the actual K_L value. Similarly, very high rotational speeds ($\omega > 30$ rpm) would also render shearing off of the film due to dominance of centrifugal forces and thereby reduce the measured K_L value.

- At low rotational speeds (i.e. reduced liquid film thickness), the K_L value varies directly with the film thickness. The simulation results establish the findings of Yamane and Yoshida (1972) and Bintanja et al (1975). The results are based upon the calculation of average exposure time of the disc at a given rotational speed using Bintanja's expression.
- At higher rotational speeds, the K_L value tends to get steady for a given film thickness. Its dependency on film thickness is reduced and the exposure time dominates the value. In this case, the depth of oxygen penetration into the liquid film is limited compared to the thickness of the film. The simulation results re-establish Higbie's theory (Higbie, R., 1935).
- Simulation results show that with the increase in the submergence depth, the average K_L value on the disc increases. The results are based upon the Bintanja's estimation of average exposure time at a given rotational speed. Incomplete saturation of the film due to reduced exposure time with increase of submergence results in the increase of K_L. The results establish Zeevalkink's observations (1979).
- Temperature affects the average K_L on the exposed disc surface. At rotational speeds up to about 30 rpm, the average K_L value on the disc surface decreases with increasing temperature. This is because the average film thickness decreases while the diffusivity coefficient of oxygen increases with temperature and tends to saturate the film faster at a given rotational speed. However, this trend gets reversed at higher rotational speeds (25-30 rpm). In this case, the effect of rotational speed towards increasing the average film thickness would exceed its decrease due to temperature rise and the reduced average exposure time makes the film less saturated, thereby increasing the K_L value.
- At a given rotational speed, the overall average rate of oxygen mass transfer on the disc surface, i.e. $K_L*(Cs-C_0)*A$ decreases with increasing temperature. This is due to the dominating effect of the decrease in the temperature correction factor θ' for the

concentration gradient ($Cs-C_0$) in comparison to the change in correction factor θ for the K_L value. Thus lower temperatures initiate higher oxygen diffusion in a physical disc.

The physical model helps to make the above interesting findings by its application for a plain disc rotating in water and shows the sensitivity of oxygen transfer to the physical boundary conditions defining such a system. This model could be used to determine the oxygen transfer coefficient in other liquids also if the physical properties of this liquid are known.

8.2 RBC model

To simulate the dynamic nature of the boundary conditions in a rotating biofilm disc, the laminar liquid boundary was assumed to be divided into two parts at all times, viz, exposed liquid film surface and submerged liquid film surface. The film was assumed to be completely mixed and the concentrations were averaged over the entire layer thickness. All mass transfer into the biofilm passed through this liquid layer. The layer was assumed to be non-reactive (Wanner and Reichert 1996). The basic model structure was devised on the principles of mass transfer and transport of dissolved and particulate components in one dimensional space inside the biofilm matrix which was assumed to be homogenous (Wanner and Gujer, 1986; Gujer and Boller, 1990). The reaction kinetics of the model considered the aerobic degradation of soluble organics, nitrification and denitrification (anoxic degradation) processes based upon the Activated Sludge Model No. 3. The integrity of the model was verified from the mass balance of components in the individual biofilm layers and in the bulk liquid for each stage. Calibration and validation of the model with the available experimental data from the laboratory scale RBC was essential before the application of the model to explore different scenarios. The results based upon the considered scenarios are discussed below.

Scenario-I: Model validation with dynamic simulation

- After calibration with experimental data at 25°C, simulations were performed for model verification with dynamic data sets from experimental measurements at 30°C. The organic carbon showed complete degradation under the applied overall loading rate of about $4.7 gCOD m^{-2} d^{-1}$ although the experimental results deviated by about 10% in the overall removal efficiency. This can be attributed to the possible presence of soluble inert in the synthetic wastewater (molasses).

- Ammonia nitrogen removal was more sensitive than organic carbon and effluent concentrations showed fluctuations corresponding to the influent concentrations. Overall NH_4-N removal at 30°C was observed to be about 95% at an influent loading of about 1.0 gNH_4-N $m^{-2}d^{-1}$. The removal efficiency at 30°C is a little better than at 25°C due to increased biomass activity.
- Maximum removal efficiency for organic carbon as well as ammonium was observed in the first stage. However, more than 80% organic C gets removed in first stage while only about 50-55% of NH_4-N gets oxidized in this stage. The designed organic C loading in stage-1 was $12gCODm^{-2}d^{-1}$ and ammonium nitrogen loading was $2.60gNH_4\text{-}Nm^{-2}d^{-1}$. The results show that heterotrophs are the dominant species in the biofilm matrix at high substrate loading rates, i.e. in the first stage. However, due to the limited penetration depth of oxygen, the deeper regions of the thick biofilm in the first stage showed a high fraction of particulate inerts. Autotrophs are subdued in the surface layers due to their low growth rate and competition from the heterotrophs. But they start to flourish once the heterotrophic species dwindle due to the limitation of substrate, especially in the latter stages of treatment when the soluble organic substrate concentration gets lowered in the bulk.
- The experiment results show a little higher NO_3-N concentration in the effluent at 25°C as compared to the model predictions. The difference could be possibly due to reduced denitrification in stage-1 in the experiments, provided concentration measurements were carried out accurately. The effluent NO_3-N concentrations at 30°C fitted better with the simulations results.
- DO in the bulk was high at 25°C and simulations showed close resemblance to experimental measurement. However, DO concentrations dropped to influent levels at 30°C due to possible increased consumption by the detached and accumulated biomass in the reactors. Both results reveal that periodic exposure of the discs to air in RBCs exhibit good oxygen transfer through the boundary layer. The dissolved oxygen concentration levels in the bulk liquid remained high enough to maintain nitrification. This ruled out the requirement for additional oxygenation in the bulk liquid by external means.
- The biofilm thickness in the stage-1 varied between 600 to 1500µm, while it was observed to be considerably less in the stage-2 (100-300µm) and stage-3 (30-90µm). The average thickness decreased in consecutive stages which could be attributed to the decrease in the nutrient loading rates. The model used a measured biofilm density of about $47kgCOD/m^3$ at 30°C.

Scenario-II: Temperature sensitivity

- Within the considered range of temperature between 10°C to 32.5°C, an increase of temperature increased the overall removal efficiency of the RBC system. Nitrification was found to be more sensitive compared to organic substrate removal and the rate increased by more than two-fold for an increase from 10°C to 25°C.
- The average biofilm thickness decreased with increasing temperature. This is more evident at relatively low substrate loading conditions in the latter stages. The high growth rates at higher temperature cannot be sustained due to substrate limitations in the deeper layers and the cells are presumed to undergo high endogenous respiration and decay.
- Specific denitrification rate increases with temperature in stage-1 as observed from simulations up to 32.5°C. However, stage-2 shows a drop after 20°C which may be accounted for due to corresponding reduction in effluent NO_3-N concentrations as a result of NH_4-N limitations. The high removal rate of NH_4-N in stage-1 and assimilation of the remaining amount by the biomass would result in this N-limitation in latter stages at higher temperatures.

Scenario-III: Nutrient load variation

- At a given hydraulic loading rate and temperature, nutrient removal flux in any stage of the RBC increased with increasing nutrient loading rates but within a certain optimal range. Beyond that range, the removal efficiency reached the maximum capacity. This shows that the RBC biofilm can sustain nutrient load fluctuations easily up to a limit.
- In combined nitrification systems, the optimal nitrification rate is the guiding factor in system design and sizing of discs. However, the optimum values change with temperature and it is important to take the operating temperature range into consideration during the design of an RBC system. The simulation scenario at 10°C revealed a drop of nearly 41% in the optimum nitrification rate compared to that at 25°C.
- COD/N ratio of 4-5 and above provides optimum removal efficiency in the system.

Scenario-IV: Hydraulic load variation

- At a constant organic and ammonia loading rate, the removal rate in any stage of an RBC increased with the hydraulic loading rate but again up to a certain limit. In other words, both of the above scenario point out that increasing the nutrient supply per unit time in any stage increases the removal rate up to a maximum value. The dynamic simulation results under varying flow rates confirm that RBCs can tolerate hydraulic load surges

within a certain range. The optimum range depends upon the system configuration and can be determined using the model.

Scenario-V: Recirculation ratio variation

- Flow recirculation did not improve the overall removal efficiency significantly. Although the nitrification capacity was a little better in the first stage with an increase of the recirculation ratio, the overall removal efficiency was not affected. The dilution of the organic substrate concentration in the first stage made better nitrification in that stage possible.

Scenario-VI: Submergence ratio variation

- Denitrification is found to be partial in an RBC system. At a given temperature, maximum denitrification occurs in the first stage due to the presence of anoxic zones in the deeper layers and higher heterotrophic abundance. However, substrate limitations and high DO concentration inhibits denitrification in the latter stages of the RBC. Varying submergence ratio up to 60% increases denitrification in the first stage. Beyond that submergence level, denitrification is reduced due to reduced nitrification.
- The increase of the disc submergence ratio above 42% decreased the dissolved oxygen concentrations in the bulk liquid in all stages of the RBC. Consequently, the nitrification rate lowered down and the removal efficiency was reduced in all stages.
- With 100% flow recirculation and a variation of the submergence ratio in the stages (90% in first stage and 42% in the subsequent stages), denitrification could be better controlled in the first stage and the nitrate concentration in the effluent is predicted to be lower than that attained with a submergence ratio of 42% in all stages and no recirculation. However, the overall nitrification would be slightly lower in this case compared to the latter case and this might be improved by reducing the submergence in the first stage to 60% only. Although such a process modification could be slightly beneficial for achieving better denitrification, it would involve additional costs for recirculation.

General observation

- Alkalinity is observed to decrease in the system from about 4.0mol/m^3 in stage-1 to about 1.0 mol/m^3 in stage-3 bulk liquid for an influent concentration of about 6.0mol/m^3. Maximum reduction occurs in stage-1 due to maximum removal of substrates in this stage.

8.3 Limitations of the biofilm model

Understanding the underlying concepts of the RBC processes and its implementation into computer code in Matlab had been very time-consuming and rigorous. Apart from requirement of the knowledge of programming, the making of the model involved awareness from several disciplines such as mathematics, physics and bio-chemistry to comprehend the biofilm dynamics and its process kinetics and to solve the system of mass balance equations numerically.

In reality, models represent artificial tools for estimation and prediction of the behaviour of a system based on well-known and defined physical and biological phenomena. However, it is limited by the knowledge of many processes which are still unknown or scarcely defined mathematically. The underlying assumptions can often become generalisations and in extreme cases, crude approximations of the reality which can be vastly more complex. For example, temporal variation of the biofilm thickness or the rate of displacement of solids inside the biofilm matrix are complicated dynamic processes and difficult to be predicted accurately by means of mathematical simulations. Biomass detachment by sloughing is another unpredictable phenomenon so far. The ability to predict a natural biological process like wastewater treatment using biofilm is dependent upon many factors such as accurate estimation of the biological and chemical parameter values and the boundary environment. Many parameter values are often difficult to obtain directly and are guided by indirect means such as data fitting or by reference. The biofilm morphology (rigid and dense vis-à-vis flexible and porous) varies spatially within the matrix as well as with the type of the system used. Apart from the experimental determination of the average biofilm density and the average biofilm thickness, there is very little that can be accurately measured at such a micro-scale. Fortunately, leaving apart the modelling of the processes taking place inside biofilm matrix at micro-level which are based upon many hypothesis, biofilm models today can predict removal rates rather effectively once they are calibrated properly for a given system geometry. Although the current model has been calibrated and validated for the laboratory-scale set-up, it may need further calibration during scale-up operations or temperature changes for accurate value based predictions. The model code has been defined for a 3-stage RBC configuration, but it is possible to upgrade it to multiple-stages. In the end, it must be realised that a model cannot be expected to predict all the aspects of a system with equal accuracy.

9 Conclusions and recommendations

9.1 Conclusions

Modelling in an important and integral part of research today. Although there are many biofilm models in use today, each model has its inherent advantages and limitations. The current work was undertaken with a purpose to build a mixed-culture biofilm model which is specifically tailored for a RBC system. The RBC environment differs from other biofilm systems due to the dynamic nature of its operation. It was intended to study the performance of such a system under various physical and biochemical environment and take note of the effects of the process modifications in their essence. The model was built and calibrated at 25°C based on a laboratory-scale experimental set-up. It was validated at 30°C with another data-set. Although the model structure was primarily based upon the biofilm models of Wanner and Gujer (1986) and Gujer and Boller (1990), it offers the following innovative features:

- It includes a new concept for calculating the average concentrations of oxygen and substrate in the liquid boundary layer. The boundary layer equations consider the effect of diffusion of gases (oxygen and nitrogen) from air into the exposed liquid film as well as substrate and gas transfer into the submerged liquid film. This hydraulic film diffusion is very crucial in case of RBCs as observed from the higher DO content in the film compared to that in the bulk liquid. The earlier models did not explore this aspect in RBCs.
- The process kinetics and stoichiometry is based upon the activated sludge model no.3. This is considered to be the state-of-the-art model developed by the IAWQ task group on mathematical modelling of biological processes in wastewater treatment. It is generally accepted in the modelling world after proper calibration. In the current model, apart from the biofilm layers, the bulk liquid in the reactor also considers the same reaction kinetics. This helps to take into account the reactions taking place in the reactor as a consequence of suspended biomass in the reactor.
- The detachment function for biomass loss by shear in the RBC biofilm is based upon a second order dependence on biofilm thickness and a first order dependence on surface density of biofilm. It helps to control and stabilize the biofilm thickness in each RBC stage in an efficient manner.
- As the current model divides the total interfacial area of the liquid boundary layer into two parts, i.e. submerged surface for bulk-liquid film transfer and exposed surface for gas-liquid film transfer, the effect of variation of disc submergence can be easily studied.

Apart from the innovative aspects, the model simultaneously incorporates the following features of a conventional biofilm model:

- The model is flexible and can perform steady-state as well as dynamic simulations based on available input data. The dynamic simulations are possible with diurnal and seasonal variations of influent nutrient concentrations and hydraulic flow rates for a given geometry of a RBC.
- Due to its inherent flexibility, the model can be used for any scaled-up RBC configuration. The system geometry for each cascade can be easily defined in case of such scale-up operations. The key physical parameters are biofilm surface area, liquid film thickness, reactor volumes, flow rate and recirculation ratio.
- Although the model is customized for RBCs, it is flexible enough to be used for any conventional biofilm process. In such cases, the diffusive oxygen transfer from air through the exposed liquid film area needs to be switched off by putting A_exp to 0 and switching on the K_La value for the oxygen transfer rate through external aeration devices in the reactors.

For scale-up operations, it may be again necessary to have new measured data for subsequent calibration as the known kinetics and stoichiometry may not exactly fit into the new system. Although the process kinetics would still be guided by the ASM No.3 values which are assumed to be constant at a given temperature in the simulations, it could vary with type of the substrate feed. With the increase in the size of the reactor, a small change in observed value of the kinetic parameter may affect the end results in a substantial way.

The simulated and experimental results under different scenario discussed before help to draw the following conclusions about RBC systems:

- RBCs enable high DO concentrations in the bulk liquid due to diffusive transfer of oxygen from air into the exposed liquid film surface. Therefore, requirement of external aeration in the reactor compartment can be avoided. The adoption of the new boundary layer concept reveals that average DO levels in the liquid film usually remains higher than in the bulk liquid.
- Under high nutrient loading conditions, most of the diffused oxygen gets utilized beyond a biofilm depth of 250-300µm.
- Under variations of nutrient and hydraulic loading rates in influent, RBCs can sustain such fluctuations within a tolerable range and perform efficiently. Although this is valid for most biofilm systems, RBCs may provide an economical advantage. The tolerable limit for such performance depends upon system configuration and temperature which can be determined from simulations.

- In a mixed-culture biomass environment subjected to multi-substrate feed, the ammonia removal flux serves as the governing criteria in system design for optimal performance. The removal flux is highly sensitive to temperature, hydraulic loading rates and C/N ratio. Simulations show that low C/N ratio (below 4 or 5) deteriorates the N-removal efficiency.
- The RBC stages under high nutrient loading rates show a non-uniform biomass distribution with heterotrophs dominating the surface layers where soluble organic substrate concentration remains high. The nitrifying species with a slower growth rate than heterotrophs become dominant once the heterotrophs start to dwindle. The latter stages of RBC show a more homogenous biofilm matrix than the first stage.
- Temperature increase shows an improvement in the overall removal efficiency.
- Denitrification is only partial in RBC systems and occurs predominantly in the initial stages of the RBC where high heterotrophic population and anoxic ambience is readily available.
- Flow recirculation reveals little improvement in the overall removal efficiency of the RBC system.
- Increasing submergence ratio in the first stage increases denitrification. However, changing the submergence affects the removal efficiency of other nutrients and a submergence level of 40-42% is optimum for all stages and shows best results.

Although most the above conclusions drawn regarding the performance of RBC has been observed in practice, the current work proves them through simulations based upon a calibrated and subsequently validated model. Practice proves the knowledge of the established physical phenomena and thereby the validity of the model in its essence. The RBC model can now be used as an engineering tool for design or process optimization, a scientific tool for studying biofilm kinetics or simply as a tool to predict system performance during scale-up or other such system modifications. Upon scale-up, the model can be used to predict performance trends in the absence of real data for further calibration.

9.2 Recommendations and future scope

In practice, RBCs treating wastewater are usually rotated at low angular velocities due to operational restrictions. The physical model results show that at low angular velocities, the oxygen transfer coefficient K_L is predominantly controlled by the average thickness of the laminar liquid film rather than the average exposure time. A higher film thickness by way of higher rotational speed may increase the K_L value provided the biomass does not get sheared off due to high peripheral velocity in large diameter discs. In fact, the peripheral velocity would then become the guiding criteria for determining the maximum size of the RBC disc.

The results show that a 3-stage RBC system provide efficient removal under organic C loading up to 20gBOD$m^{-2}d^{-1}$ and NH_4-N loading up to 1.10g$Nm^{-2}d^{-1}$ at a hydraulic loading of 0.022$m^3m^{-2}d^{-1}$ and temperatures between 25-30°C. The effluent is able to meet the prevailing standards of disposal for BOD and NH_4-N. Therefore, a higher number of stages may be avoided without compromising the overall efficiency under such loading conditions. However the COD/N ratio needs to be maintained above 4-5 for optimum performance. The reduced surface area in the second and third stage of the experimental set-up reveals a potential cost saving measure without compromising the overall efficiency of the system. Experiments show that flat discs may be used with good efficiency at designed nutrient loading conditions in treating wastewater. The shaft supporting the discs in the first stage need to be strongly built compared to the subsequent stages due to high biofilm growth in this stage. For better denitrification, the submergence ratio in the first stage may be increased up to 60% with 100% flow recirculation.

Modelling in the real plants today employ real-time simulators which are connected to online measuring devices. Such calibrated simulators help to provide information about the expected performance of a plant under the current operating conditions and compare with the actual measured data. If a unit malfunctions or the system performance falls below the expected level, it can be easily pin-pointed and fault diagnosed. Matlab offers such features and with suitable modifications and point to point calibration, the current scientific model for RBC biofilm could be upgraded to do such modern operations in a real RBC plant. For the present, the current RBC model can be better calibrated for application to a pilot-scale or a full-scale RBC plant.

10 References

Antonie, R.L., Kluge, D.L. and Mielke, J.H. (1974). Evaluation of rotating disk wastewater treatment plant. Journal of Water Pollution Control Fed. Vol. 46, No. 3, pp. 498 - 511.

Arvin, E. and Harremoës, P. (1990). Concepts and models for biofilm reactor performance. Water Science and Technology. Vol. 22, No. ½, pp. 171 –192.

ATV-DVWK-A 281E (2001) German Rules and Standards: Dimensioning of Trickling filters and rotating biological contactors.

Ayoub, G.M. and Saikaly, P. (2004). The combined effect of step-feed and recycling on RBC performance. Water Research. Vol. 38, pp. 3009 – 3016.

Bae, W. and Rittmann, B.E. (1996). A structured model of dual-limitation kinetics. Biotechnology and Bioengg. Vol. 49, pp. 683 – 689.

Banerjee, G. (1997). Hydraulics of bench-scale rotating biological contactor. Water Research. Vol. 31, pp. 2500 – 2510.

Bintanja, H.H.J., Van der Erve, J.J.V.M. and Boelhouwer, C. (1975). Oxygen transfer in a rotating disc treatment plant. Water Research. Vol. 9, pp. 1147 - 1153.

Bird, R.B., Stewart, W.E. and Lightfoot, E.N. (1960). "Transport Phenomena", John Wiley, New York.

Bishop, P.L., Zhang, T.C. and Fu,Y.C. (1995). Effects of biofilm structure, microbial distributions and mass transport on biodegradation processes. Water Science and Technology. Vol. 31, pp. 43 – 53.

Blank, A (2006). Quantifizierung des Sauerstoffeintrages in Scheibentauchkörperanlagen. DFG-Geschäftszeichen: HA 679/42-1.

Boller, M., Gujer, W. and Nyhuis, G. (1990). Tertiary rotating biological contactors for nitrification. Water Science and Tech. Vol. 22, No. 1/2, pp. 89 - 100.

Boller, M., Gujer, W. and Tschui, M. (1994). Parameters affecting nitrifying biofilm reactors. Water Science and Technology. Vol. 29, No. 10 – 11, pp. 1 –11.

Boumansour, B.-E. and Vasel, J.-L. (1998). A new tracer gas method to measure oxygen transfer and enhancement factor on RBC. Water Research. Vol. 32, No. 4, pp. 1049 – 1058.

Buswell, A.M. et al. (1954). Laboratory studies on the kinetics of the growth of nitrosomonas with relation to the nitrification phase of the B.O.D. Test. Applied Microbiol. Vol 2, pp. 21 – 25.

Chadwick, A. and Morfett, J. (1998). "Hydraulics in Civil and Environmental Engineering", 3rd edition, E & FN Spon, UK.

Characklis, W. G. (1973). In: Attached microbial growths-II. Frictional resistance due to microbial slimes. Water Res. Vol. 7, pp. 1249 – 58.

Characklis, W. G. and Wilderer, P. A. (1989). Structure and function of biofilms. In: Characklis, W. G. et al. (eds.): Structure and function of biofilms, Dahlem Workshop Reports (Life Sciences Research Report 46), Wiley, UK, pp. 5 – 17.

Characklis, W. G., McFeters, G. A., Marshall, K. C. (1990). Physiological ecology in biofilm systems. In: Characklis, W. G., Marshall, K. C. (eds.) Biofilms. John Wiley, New York, pp. 341 - 394.

Chen, B. and Li, Y. (1999). Numerical modeling of biofilm growth at the pore scale. In: Proceedings of the 1999 Conference on Hazardous Waste Research (Gateways to Environmental Solutions). St. Louis, Missouri, USA.

Chen, G.H., Ozaki, H and Terashima, Y. (1989). Modelling of the simultaneous removal of organic substances and nitrogen in a biofilm. Water Science and Technology. Vol. 21, pp. 791 –804.

Crank, J. (1955). "The mathematics of Diffusion", pp 45, Oxford at the Clarendon Press.

d'Antonio, G., Mendia, L., Pirozzi, F. and Polese, A. (1997). Rotating biological contactor-solid contact system for the treatment of wastewater from small communities. Water Science and Technology. Vol. 35, No. 6, pp. 109 – 118.

Davies, T.R. (1975). Denitrification with a bacterial disc unit. Water Reseach, Vol. 9, pp. 459-463.

de Beer, D., Stoodley, P. and Lewandowski, Z. (1996). Liquid flow and mass transport in heterogeneous biofilms. Water Research. Vol. 30, pp. 2761 – 2765.

DIN: 4261 (Teil 2, Juni 1984). Kleinkläranlagen: Anlagen mit abwasserbelüftung Anwendung, Bemessung, Ausführung und Prüfung.

Donlan, R. M. (2002). Biofilms: Microbial life on surfaces. In: Emerging Infectious Diseases. Vol. 8, No. 9, pp. 881 - 890.

Droste, R.L. (1997). "Theory and Practice of Water and Wastewater Treatment", John Wiley, NY.

Drury, W.J., Characklis, W.G. and Stewart, P.S. (1993). Interactions of 1µm latex particles with *Pseudomonas aeruginosa* biofilms. Water Research. Vol. 27, pp. 1119 – 1126.

Dutta, S. (2002). "Modelling and simulation of SBBR for Enhanced Biological Phosphorous Removal with post denitrification and nitrification in treatment of municipal wastewater", M.Tech. Thesis, ISWW, University of Karlsruhe and Indian Institute of Technology, New Delhi.

Dutta, S., Hoffmann, E. and Hahn, H.H. (2006). Mathematical modeling of rotating biological contactor performance. 3rd IWA International Young Researchers Conference, Singapore (May, 2006).

Dutta, S., Hoffmann, E. and Hahn, H.H. (2007). Study of rotating biological contactor performance in wastewater treatment using multi-culture biofilm model. Water Science and Tech. Vol. 55, No. 8-9, pp. 345 - 353.

Famularo, J., Mueller, J.A. and Mulligan, T. (1978). Application of mass transfer to rotating biological contactors. Journal of Water Pollution Control Fed. Vol. 50, pp. 653 - 671.

Fouad, M. and Bhargava, R. (2005). Sludge production and settleability in biofilm-activated sludge process. Journal of Environ. Engg., Vol. 131, No. 3, pp. 417 – 424.

Freitas dos Santos, L.M., Pavasant, P., Strachan, L.F., Pistikopoulos, E.N. and Livingston, A.G. (1997). Membrane attached biofilms for waste treatment-fundamentals and applications. Pure and Applied Chemistry, Vol. 69, No. 11, pp. 2459 – 2469.

Fruhen, M., Christan, E., Gujer, W. and Wanner, O. (1991). Significance of spatial distribution of microbial species in mixed culture biofilms. Water Science and Technology. Vol. 23, pp. 1365 – 1374.

Fruhen-Hornig, M. (1997). "Dynamische Simulation von Prozessen in Biofilmreaktoren zur Behandlung Kommunaler Abwässer", Ph.D. Thesis, RWTH, Aachen, Germany.

Galvan, A., Urbina, P. and de Castro, F. (2000). Characterization of filamentous micro-organisms in rotating biological contactor biofilms of wastewater treatment plants. Bioprocess Engg. Vol. 22, pp. 257 – 260.

Grady, C.P.L., Daigger, D.T., Lim, H.C. and Grady, G.L. (1980). "Biological Wastewater Treatment: Theory and Applications", Marcel Dekker, New York.

Groenveld, P. (1970). "Dipcoating by withdrawal of liquid films", Thesis, Delft.

Gujer, W. (1977). Design of a nitrifying activated sludge process with the aid of dynamic simulation. Prog. Water Technology, Vol. 9, No. 2, pp 323 – 336.

Gujer, W. and Boller, M. (1990). A mathematical model for rotating biological contactors. Water Science and Tech. Vol. 22, No. 1/2, pp. 53 - 73.

Gujer, W., Henze, M., Mino, T. and Loosdrecht, M. v. (1999). Activated Sludge Model No. 3 (IAWQ). Water Science and Tech. Vol. 39, No. 1, pp. 183 – 193.

Hahn, H. H. (1986). Water Quality Management: A review of the development and application of mathematical models. Journal of Appl. Modelling, pp. 22.

Hahn, H. H. (1994). Industrial effluent control, In: Integrated wastewater management – collection, treatment and reuse, Documentation of the EWPCA International Conference in Lisbon 1994, pp. 27 – 50.

Hahn, H. H. and Kegebein, J. (2004). Auf dem Weg zur Kläranlage von morgen. 18. Karlsruher Flockungstage. Schriftenreihe des IWG/SWW der Universität Karlsruhe (TH),. Institutsverlag-Siedlungswasserwirtschaft, Karlsruhe.

Harremoës, P. (1978). Biofilm Kinetics. In: Water Pollution Microbiology, Mitchell, R.(ed), Wiley-Interscience, New York, pp 71 – 109.

Harremoës, P. (1984). BSB-Umsetzung und Nitrifikation an Scheibentauchkörpern-Bemessung und Maßstabserfassung. GWF-Wasser/Abwasser. Vol. 125, No. 5, pp. 227 – 238.

Henze, M. and Harremoës, P. (1978). Nitrification and Denitrification in Wastewater Treatment. Chap.15. In: Mitchell, R. (ed.) Water Pollution Microbiology, Vol. 2, pp. 391 – 414. John Wiley, New York.

Henze, M., Grady, C.P.L., Jr., Gujer, W., Marais, G.v.R. and Matsuo, T. (1987). Activated Sludge Model No. 1. IAWPRC Scientific and Technical Report No. 1, IAWPRC, London.

Henze, M., Gujer, W., Mino, T., Matsuo, T., Wentzel, M.C., Marais, G.v.R.and Loosdrecht, M. v. (1999). Activated Sludge Model No. 2D (IAWQ). Water Science and Tech. Vol. 39, No. 1, pp. 165 – 182.

Henze, M., Harremoës, P., Jansen, J.-C. and Arvin, E. (2002). "Wastewater Treatment-Biological and chemical processes", 3rd edition, Springer-Verlag.

Heukelekian, H. and Heller, A. (1940). Relation between food concentration and surface for bacterial growth. In: J Bacteriol. Vol. 40, pp. 547 – 558.

Higbie, R. (1935). *Trans.* A.I.Ch.E. Journal. Vol. 31, pp. 365.

Horn, H. and Hempel, D.C. (1997). Growth and decay in an auto-/heterotrophic biofilm. Water Research. Vol. 31, No.9, pp. 2243 – 2252.

Horn, H. and Hempel, D.C. (2000). Simulationsrechnungen zur Beschreibung von Biofilmsystemen. Chemie Ingenieur Technik. Vol. 72, No.10, pp. 1234 – 1237.

Horn, H., Reiff, H. and Morgenroth, E. (2003). Simulation of growth and detachment in biofilm systems under defined hydrodynamic conditions. Biotechnology and Bioengineering. Vol. 81, No. 5, pp. 607 – 617.

Horn, H., Staudt, C., Neu, T., Leon-Ohl, A., Böbmann, M. and Hempel, D.C. (2004). Untersuchungsmethoden für Biofilmsysteme. Chemie Ingenieur Technik. Vol. 76, No.3, pp. 333 – 337.

Jansen, J.-C. and Harremoës, P. (1985). Removal of soluble substrates in fixed films. Water Science and Technology. Vol. 17, No. 2/3, pp. 1 –14.

Jeppsson, U. (1996). "Modelling Aspects of Wastewater Treatment Processes", Dissertation, Lund Institute of Technology, Stockholm.

Jones, H. C., Roth, I. L., Saunders, W. M. (1969). Electron microscopic study of a slime layer. In: J Bacteriol. Vol. 99, No. 1, pp. 316 – 325.

Kim, B-J. and Molof, A.H. (1982). The scale-up and limitation of physical oxygen transfer in rotating biological contactors. Water Science and Technology. Vol. 14, pp. 569 – 579.

Kissel, J.C:, McCarty, P.L. and Street, R.L. (1984). Numerical simulation of mixed-culture biofilm. Journal of Environ. Engg., Vol. 110, No. 2, pp. 393 – 411.

Knowles, G., Downing, A.L. and Barrett, M.J. (1965). Determination of kinetic constants for nitrifying bacteria in mixed culture, with the aid of an electronic computer. J. Gen. Microbiol. Vol. 38, pp. 263 - 278.

Koch, G, Kühni, M., Gujer, W. and Siegrist, H. (2000). Calibration and validation of Activated Sludge Model No. 3 for Swiss municipal wastewater. Water Research. Vol. 34, No. 14, pp. 3580 – 3590.

Koch., G., Egli, K., Van der Meer, J.R. and Siegrist, H. (2000). Mathematical modelling of autotrophic denitrification in a nitrifying biofilm of a rotating biological contactor. Water Science and Tech. Vol. 41, No. 4 – 5, pp. 191 – 198.

Kubsad, V., Chaudhari, S. and Gupta, S.K. (2004). Model for oxygen transfer in rotating biological contactor. Water Research. Vol. 38, pp. 4297 – 4304.

Laudie (1974). Am.Inst.Chem.Eng. Vol. 20, pp. 611.

Lazarova, V. and Manem, J. (2000). Innovative biofilm treatment technologies for water and wastewater treatment. In: Bryers, J.D.(ed.), Biofilms II: Process Analysis and Applications, Wiley-Liss, New York, pp. 159-206.

Lu, C., Li, H-C., Lee, L.Y. and Lin, M.R. (1997). Effects of disc rotational speed and submergence on the performance of an anaerobic rotating biological contactor. Environ. Int. Vol. 23, pp 253 – 263.

Maier, W., J. et al. (1967). Simulation of the trickling filter process. Journal of Amer. Soc. of Civil Engr., Sanit. Engg. Divn., Vol. 93, pp 91.

Martin-Cereceda, M., Alvarez, A.M., Serrano, S. and Guinea, A. (2001). Confocal and light microscope examination of protozoa and other micro-organisms in the biofilms from a rotating biological contactor wastewater treatment plant. Acta Protozool. Vol. 40, pp. 263 – 272.

Masuda, S., Watanabe, Y. and Ishiguro, M. (1991). Biofilm properties and simultaneous nitrification and denitrification in aerobic rotating biological contactors. Water Science and Technology. Vol. 23, pp. 1355 – 1363.

Matlab Reference Guide (1992), The Mathworks, Inc., USA

Mba, D., Bannister, R.H. and Findlay, G.E. (1999). Mechanical redesign of the rotating biological contactor. Water Research. Vol. 33, pp. 3679 – 3688.

Merkey, B. V., Rittmann, B. E. and Chopp, D. L. (2006). A Multi-species, Multi-component Biofilm Model (under review).

Morgenroth, E. and Wilderer, P.A. (2000). Influence of detachment mechanisms on competition in biofilms. Water Research. Vol. 34, No. 2, pp. 417 – 426.

Müller, J.A., Paquin, P. and Famularo, J. (1980). Nitrification in rotating biological

contactors. Journal of Water Pollution Control Fed. Vol. 52, No.4, pp. 688 – 710.

Nishidome, K., Kusuda, T., Watanabe, Y., Yamauchi, M. and Mihara, M. (1994). Determination of oxygen transfer rate to a rotating biological contactor by microelectrode measurement. Water Science and Technology. Vol. 29, No. 10 – 11, pp. 471 – 477.

Noguera, D.R. and Morgenroth, E. (2004). Introduction to the IWA Task Group on biofilm modeling. Water Science and Technology. Vol. 49, No. 11 – 12, pp. 131 –136.

Okabe, S., Hiratia, K., Ozawa, Y. and Watanabe, Y. (1996). Spatial microbial distributions of nitrifiers and heterotrophs in mixed-population biofilms. Biotechnology and Bioengineering. Vol. 50, pp. 24 – 35.

Paolini, A.E. (1986). Effect of biomass on oxygen transfer in RBC systems. Journal of Water Pollution Control Fed. Vol. 58, No. 4, pp. 306 – 311.

Paolini, A.E., Sebastiani, E. and Variali, G. (1979). Development of mathematical models for the treatment of an industrial wastewater by means of biological rotating disc reactors. Water Research. Vol. 13, pp. 751 – 761.

Patwardhan, A.W. (2003). Rotating biological contactors: A Review. Ind. Engg. Chem. Research. Vol. 42, pp. 2035 – 2051.

Peavy, H.S., Rowe, D.R. and Tchobanoglous, G. (1985). "Environmental Engineering", International edition, McGraw-Hill, Singapore.

Perry, R H., Green, D.W. and Maloney, J.O. (1984). "Chemical Engineers' Handbook", 6th edition, McGraw-Hill, New York. Pp. 3 – 273 and 3 – 286.

Picioreanu, C. (1999). "Multidimensional modeling of biofilm structure", Ph.D. Thesis, Delft University of Technology, Netherlands.

Radwan, K.H. and Ramanujam, T.K. (1997). Influence of COD/NH_3-N ratio on organic removal and nitrification using modified RBC. Bioprocess Engineering. Vol. 16, pp. 77 – 81.

Rauch, W., Vanhooren, H. and Vanrolleghem, P.A. (1999). A simplified mixed-culture biofilm model. Water Research. Vol. 33, No. 9, pp. 2148 – 2162.

Reichert, P. (1994). A tool for simulation and data analysis of aquatic systems. Water Science and Technology. Vol. 30, No. 2, pp. 21 – 30.

Reichert, P. and Wanner, O. (1997). Movement of solids in biofilms: Significance of liquid phase transport. Water Science and Technology. Vol. 36, No. 1, pp. 321 –328.

Rittmann, B.E. and Manem, J.A. (1992). Development and experimental evaluation of a steady-state multispecies biofilm model. Biotech. And Bioeng. Vol. 39, pp. 914 – 922.

Rittmann, B.E. and McCarty, P.L. (1978). Variable-order model for bacterial-film kinetics. Journal of Environ. Engg., Vol. 104, pp. 889 – 900.

Rittmann, B.E., Schwarz, A.O., Eberl, H.J., Morgenroth, E., Perez, J., Van Loosdrecht, M.C.M. and Wanner, O. (2004). Results from the multi-species Benchmark Problem using one-dimensional models. Water Science and Technology. Vol. 49, No. 11 – 12, pp. 163 –168.

Rittmann, B.E., Suozzo, R. and Romero, B.R. (1983). Temperature effects on oxygen transfer to rotating biological contactors. Journal of Water Poll. Con. Fed. Vol. 55, No. 3, pp. 270 – 277.

Rodgers, M. and Zhan, X.-M. (2003). Moving-medium biofilm reactors. Reviews in Environmental Science and Biotechnology. Vol. 2, pp. 213 – 224.

Schlichting, H. (1960). "Boundary Layer Theoy", Mcgraw-Hill, New York.

Shampine, L.F. and Reichelt, M.W.(1997). The Matlab ODE Suite. SIAM Journal on Scientific Computing, Society for Industrial and Applied Mathematics, Vol. 18, No. 1, pp. 1 – 22.

Smith, G.D. (1985). "Numerical solution of partial differential equations: finite difference methods", 3rd edition. Oxford at the Clarendon Press.

Stewart, P.S. (1998). A review of experimental measurements of effective diffusive permeabilities and effective diffusion coefficient in biofilms. Biotechnology and Bioengineering. Vol. 59, pp. 261 – 272.

Suga, K. and Boongorsrang, A. (1984). A new model of mass transfer in a rotating disc contactor. Chemical Engineering Science, Vol. 39, No. 4, pp. 767-773.

Surampalli, R.Y. and Baumann, E.R. (1997). Role of supplemental aeration in improving overloaded first-stage RBC performance. Water Air Soil Poll. Vol. 98, pp. 1 – 15.

Tchobanoglous, G. and Burton, F. (1995). "Wastewater Engineering-Treatment, disposal and reuse", Metcalf and Eddy, Inc. 3rd edition, McGraw-Hill, New York.

Tchobanoglous, G. and Burton, F., Stensel, M.D. (2003). "Wastewater Engineering-Treatment and reuse", Metcalf and Eddy, Inc., McGraw-Hill, New York.

Teixeira, P. and Oliveira, R. (2001). Denitrification in a closed rotating biological contactor: effect of disk submergence. Process Biochem. Vol. 37, pp. 345 – 349.

Tijhuis, L., van Loosdrecht, M. C. M., Heijnen, J. J. (1994). Formation and growth of heterotrophic aerobic biofilms on small suspended particles in airlift reactors. Biotechnol. Bioeng. Vol. 44, No. 5, pp. 595 – 608.

Trulear, M.G. and Characklis, W.G. (1982). Dynamics of biofilm processes. Journal of Water Pollution Control Fed. Vol. 54, No. 9, pp. 1288 – 1301.

Van Loosdrecht, M. C. M., Pot, M. A., Heijnen, J. J. (1997). Importance of bacterial storage polymers in bioprocesses. Water Science and Technology. Vol. 35, No. 1, pp. 41 – 47.

Vanhooren, H. (2002). "Modelling for optimization of biofilm wastewater treatment

processes: A complexity compromise", Ph.D. Thesis, University Gent, Belgium.

Vijayraghvan, K. and Gupta, J.P. (1982). Thickness of the film on a vertically rotating disk partially immersed in a Newtonian liquid. Ind. Engg. Chem. Fundam. Vol. 21, pp. 333 – 336.

Wanner, O. and Gujer, W. (1985). Competition in biofilms. Water Science and Technology. Vol. 17, pp. 27 –44.

Wanner, O. and Gujer, W. (1986). A multi-species biofilm model. Biotechnology and Bioengineering. Vol. 28, pp. 314 – 328.

Wanner, O. and Reichert, P. (1996). Mathematical modeling of mixed-culture biofilms. Biotechnology and Bioengineering. Vol. 49, pp. 172 – 184.

Watanabe, Y. and Ishiguro, M. (1978). Denitrification kinetics in a submerged rotating biological disc unit. Prog. Water Tech. Vol. 10, pp. 187 – 195.

Watanabe, Y., Masuda, S., Nishidome, K. and Wantawin, C. (1984). Mathematical model of simultaneous organic oxidation, nitrification and denitrification in rotating biological contactors. Water Science and Technology. Vol. 17, pp. 385 – 397.

Weast, R.C. (ed) "Handbook of Chemistry and Physics" (1964), 45th edition, Chemical Rubber Co., Cleveland, Ohio.

WEF and ASCE (1998). "Design of Municipal Wastewater Treatment Plants", Water Environment Federation and American Society of Civil Engineers, Alexandria and Reston, USA.

Wik, T. (1999). "On Modeling the Dynamics of Fixed Biofilm Reactors", Ph.D. Thesis, Chalmers University of Technology, Göteborg, Sweden.

Wilke, C. R. and Chang, P. (1955). Correlation of diffusion coefficients in dilute solutions. A.I.Ch.E. Journal. Vol. 1, pp. 264 – 270.

Williamson, K. and McCarty, P.L. (1976). A model of substrate utilization by bacterial films. Journal of Water Pollution Control Fed. Vol. 48, pp. 9 – 24.

Wilson, F and Lee, W.M. (1997). Rotating biological contactors for wastewater treatment in an equatorial climate. Water Science and Technology. Vol. 35, No. 8, pp. 177 – 184.

Winkler, M.A. (1981). "Biological Treatment of Wastewater", John Wiley, New York.

Xavier, J.-B., Picioreanu, C. and Van Loosdrecht, M.C.M. (2005). A general description of detachment for multidimensional modeling of biofilms. Biotechnology and Bioengineering. Vol. 91, No. 6, pp. 651 – 669.

Yamane, T. and Yoshida, F. (1972). Absorption in a rotating disc gas-liquid contactor. Journal of Chemical Engg. Of Japan. Vol. 5, No. 4, pp. 381 – 385.

Zeevalkink, J.A., Kelderman, P. and Boelhouwer, C. (1978). Liquid film thickness in a

rotating disc gas-liquid contactor. Water Research. Vol. 12, pp. 577 – 581.

Zeevalkink, J.A., Kelderman, P., Visser, D.C. and Boelhouwer, C. (1979). Physical mass transfer in a rotating disc gas-liquid contactor. Water Research. Vol. 13, pp. 913 – 919.

Zhang, T.C. and Bishop, P.L. (1994). Density, porosity and pore structure of biofilms. Water Research. Vol. 28, No. 11, pp. 2267 – 2277.

Zobell, C. E. (1946). The effect of solid surfaces on bacterial activity. J Bacteriol. Vol. 46, pp. 39 – 56.

Appendix I Program code for determination of K_L in pure water

The code is written in the programming language of Matlab for interactive determination of K_L and the concentration profile of oxygen in a liquid film. The code is stored in the working directory of Matlab with a filename and this file is called in Matlab window to execute the program every time. The syntax is given below.

```
% Input parameters are nt, nx, cini, cs, D, dx, dt and time.
% time  = contact time or time of exposure of the film in air
% dx    = elemental thickness of the liquid film = delta/nx
% delta = measured or calculated film thickness in air
% nx    = number of discretization points (say 20 for a 100µm film)
% dt    = 0.5 * (dx)^2   (Required to satisfy stability criteria in
explicit method of solution)
% nt    = number of time steps = time/dt
% cini  = Initial concentration of oxygen in the liquid film
% cs    = Concentration of oxygen in air at temperature T°C
% D     = Diffusivity coefficient of oxygen at temperature T°C
clear;
% Example Input values
cini    = 0.01;             % g/m3
cs      = 9.08;             % g/m3
D       = 0.0019723;        % mm2/s
delta   = 87.292*1.00e-03; % mm
nx      = 28;
time    = 0.738;            % s

%Calculations
dx      = delta/(nx-1);     % mm
dt      = 0.5*(dx)^2;       % s
nt      = round(time/dt)+1;

c=zeros(nt,nx);
c(1,2:nx)=cini;  c(1:nt,1)=cs;
   for i=2:nt
     for j=2:nx
      if j<nx
      c(i,j)=c(i-1,j)+D*(dt/dx^2)*(c(i-1,j+1)-2*c(i-1,j)+c(i-1,j-1));
      else
      c(i,nx)=c(i,nx-1);
      end
     end
   end

n=zeros(nt,1);
for k=1:nt
   n(k,1)=(D/dx)*(c(k,1)-c(k,2));
end
n1=n.*(1.00e-06);

t=zeros(nt,1);
for i=2:nt
   t(i,1)=dt;
end
m=n1.*t;
```

```
s=sum(m);
K=s/time;
KL=K*1.0e+6/((cs-cini)*0.001)  % Units in 1.0e-06 m/s

%save K_L_20°_86.73µm_40rpm.txt KL -ascii -tabs
%save time_O2_20°_86.73µm_40rpm.txt t c -ascii -tabs

%save <set path and filename.txt> KL -ascii -tabs
%save <set path and filename.txt> t c -ascii -tabs
%Output parameters, i.e. K_L, concentration grid c with time matrix t may
%be stored in a file by defining a path and giving file name in .txt or
%.dat format.
```

Implementation of the code

- The necessary software required is Matlab. The code is saved as a Matlab file with '.m' extension. All input values need to be given in this file. Storage location of output need to be specified in this code file.
- For a given temperature, input values for diffusivity coefficient of oxygen into water/liquid, initial concentration of oxygen in liquid film and the saturation concentration of oxygen in water may be determined from the tables in Chapter 5.
- The film thickness is obtained from measurement at a given point or the average value calculated using equation 5.13 in Chapter 5.
- The time of exposure of a point on the disc surface may be calculated using equation (5.19). For an average value over the entire disc, equation 5.23 may be used in case of considered disc geometry with 42% disc submergence. For other sizes and submergence ratio, it needs to be calculated using equation 5.20.
- The code is run by calling the file with the filename in the Matlab command window.
- The output data is stored in the user specified location with the given file name as tab separated ASCII text. This may be further processed in other data processing tools like MS-excel or Ultra-edit if required.

Appendix II Program code for the mixed culture biofilm model of RBC

The code is written in the programming language of Matlab. The code is divided into six function files (a to f), one file for saving the output data (g) and two input data files (h and i). The first function file 'substrate.m' is the main file which contains the ode solver. It is to be called in Matlab command window by typing the filename for running the simulations. This file calls the ode function file 'biofilm.m' and executes the program. The file 'biofilm.m' contains the code for the solution of the set of differential equations based on the solution methodology. This file is linked to sub-function files 'bioflux.m' and 'biokinetics.m' to calculate the advective flux of particulate components and the reaction kinetics at every time step. The variables are protected against negative values by the sub-routine 'maxcode.m'. The file 'Initial_cond.m' is contains the initial values in matrix form which is required for the simulations. It takes the values from the input files 'Input_data.m' and time-series data file (user inputs). The file 'filesave.m' saves the output in '.dat' form in the desired location as defined by the user. The relevant code files for the 3-stage RBC model are listed chronologically as shown below and annexed herewith in the subsequent pages:

a) substrate.m
b) biofilm.m
c) biokinetics.m
d) bioflux.m
e) maxcode.m
f) Initial_cond.m
g) filesave.m
h) Input_data.m
i) Time series data file (e.g. daten_Sept_Dez.dat)

The relevant codes of the biofilm model are annexed below.

a) substrate.m

```
% *********ode solver call for 3-stage RBC system*********************

clear;

[ft So_in Ss_in Snh_in Sno_in Sn2_in Salk_in Q] =
textread('daten_Sept_Dez.dat','%f %f %f %f %f %f %f %f','headerlines',2);

Input_data;

tic,[T,Y] =
ode15s('biofilm',[],[],[],time,N,rho1,rho2,rho3,dx1,dx2,dx3,ft,So_in,Ss_in
,Snh_in,Sno_in,Sn2_in,Salk_in,Xs_in,Xh_in,Xa_in,Xi_in,...

Do,Ds,Dnh,Dno,Dn,Dalk,S_o_sat,S_n2_sat,K_la,P1,P2,P3,k_floc1,k_floc2,k_flo
c3,k_shear1,k_shear2,k_shear3,dlf1,A_tot1,A_sub1,V_lf1,...

Q,Qr,V1,dlf2,A_tot2,A_sub2,V_lf2,V2,dlf3,A_tot3,A_sub3,V_lf3,V3);toc;

Length=length(Y)

%*****************************SAVE OUTPUT**************************

% Define save path in filesave.m
%filesave;
```

b) biofilm.m

```
% *************** Biofilm model code for 3-stage RBC system***********
% Comments
% For each stage, N = Number of biofilm layers + 2; the extra 2 layer
component represents the reactor tank and the liquid film layer for that
stage.
% Code is vectorised to represent a set of equations with each layer
having 10 ode equations.
% Solution for the set of vectorised odes is done simultaneously in this
ode function file calling other sub-function files not shown here.
% Last ode equation for each stage represents the biofilm thickness. It
helps to calculate layer thickness dx.

function varargout =
biofilm(t,y,flag,time,N,rho1,rho2,rho3,dx1,dx2,dx3,ft,So_in,Ss_in,Snh_in,S
no_in,Sn2_in,Salk_in,Xs_in,Xh_in,Xa_in,Xi_in,Do,Ds,Dnh,Dno,Dn,Dalk,
S_o_sat,S_n2_sat,K_la,P1,P2,P3,k_floc1,k_floc2,k_floc3,k_shear1,k_shear2,k
_shear3,dlf1,A_tot1,A_sub1,V_lf1,Q,Qr,V1,dlf2,A_tot2,A_sub2,V_lf2,V2,dlf3,
A_tot3,A_sub3,V_lf3,V3)

if nargin < 4 | isempty(N)
  N = 17;
end

switch flag
case ''                              % Return dy/dt = f(t,y).
varargout{1} =
f(t,y,N,rho1,rho2,rho3,dx1,dx2,dx3,ft,So_in,Ss_in,Snh_in,Sno_in,Sn2_in,Sal
k_in,Xs_in,Xh_in,Xa_in,Xi_in,Do,Ds,Dnh,Dno,Dn,Dalk,S_o_sat,S_n2_sat,K_la,P
1,P2,P3,k_floc1,k_floc2,k_floc3,k_shear1,k_shear2,k_shear3,dlf1,A_tot1,A_s
ub1,V_lf1,Q,Qr,V1,dlf2,A_tot2,A_sub2,V_lf2,V2,dlf3,A_tot3,A_sub3,V_lf3,V3)
;

case 'init'                          % Return default [tspan,y0,options].
```

```
[varargout{1:3}] =
Initial_cond(time,N,dx1,dx2,dx3,rho1,rho2,rho3,So_in,Ss_in,Snh_in,Sno_in,S
n2_in,Salk_in,Xs_in,Xh_in,Xa_in,Xi_in);
otherwise
error(['Unknown flag ''' flag '''.']);
end

%******************** 2nd order PDE solution ******************

function dS =
f(t,y,N,rho1,rho2,rho3,dx1,dx2,dx3,ft,So_in,Ss_in,Snh_in,Sno_in,Sn2_in,Sal
k_in,Xs_in,Xh_in,Xa_in,Xi_in,Do,Ds,Dnh,Dno,Dn,Dalk,S_o_sat,S_n2_sat,K_la,P
1,P2,P3,k_floc1,k_floc2,k_floc3,k_shear1,k_shear2,k_shear3,dlf1,A_tot1,A_s
ub1,V_lf1,Q,Qr,V1,dlf2,A_tot2,A_sub2,V_lf2,V2,dlf3,A_tot3,A_sub3,V_lf3,V3)

So_in = interp1(ft,So_in,t); Ss_in = interp1(ft,Ss_in,t); Snh_in =
interp1(ft,Snh_in,t); Sno_in = interp1(ft,Sno_in,t); Sn2_in =
interp1(ft,Sn2_in,t); Salk_in= interp1(ft,Salk_in,t); Q = interp1(ft,Q,t);

% Stage-I
dx1 = (y(10*N+1,1)*1000)/(N-2);
co1 = Do/dx1.^2; cs1 = Ds/dx1.^2; cnh1 = Dnh/dx1.^2; cno1 = Dno/dx1.^2;
cn1 = Dn/dx1.^2; calk1= Dalk/dx1.^2; ps1 = P1/dx1.^2;

% Stage-II

dx2 = (y(20*N+2,1)*1000)/(N-2);
co2 = Do/dx2.^2; cs2  = Ds/dx2.^2; cnh2 = Dnh/dx2.^2; cno2 = Dno/dx2.^2;
cn2 = Dn/dx2.^2; calk2= Dalk/dx2.^2; ps2  = P2/dx2.^2;

% Stage-III
dx3 = (y(30*N+3,1)*1000)/(N-2);
co3 = Do/dx3.^2; cs3  = Ds/dx3.^2; cnh3 = Dnh/dx3.^2; cno3 = Dno/dx3.^2;
cn3 = Dn/dx3.^2; calk3= Dalk/dx3.^2; ps3  = P3/dx3.^2;

dS = zeros(30*N+3,size(y,2));
R  = zeros(30*N+3,size(y,2));
J  = zeros(30*N+3,size(y,2));

%.....................FIRST STAGE REACTION RATES, FLUXES.............%
i=1:10:10*N-9;
S_O = y(i,:); S_S = y(i+1,:); S_NH = y(i+2,:); S_NO = y(i+3,:); S_ALK=
y(i+5,:); X_S = y(i+6,:); X_H = y(i+7,:); X_A = y(i+8,:); X_I = y(i+9,:);

[R_So,R_Ss,R_Snh,R_Sno,R_Sn2,R_Salk,R_XS,R_XH,R_XA,R_XI] =
biokinetics(S_O,S_S,S_NH,S_NO,S_ALK,X_S,X_H,X_A);

R(i,:) = R_So; R(i+1,:) = R_Ss; R(i+2,:) = R_Snh; R(i+3,:) = R_Sno;
R(i+4,:)= R_Sn2; R(i+5,:) = R_Salk; R(i+6,:) = R_XS; R(i+7,:) = R_XH;
R(i+8,:)= R_XA; R(i+9,:) = R_XI;

dx    = dx1;
rho   = rho1;

[N_XS,N_XH,N_XA,N_XI,u,T,X_T]=
bioflux(R_XS,R_XH,R_XA,R_XI,X_S,X_H,X_A,X_I,dx,N,y,rho);

J(i+6,:) = N_XS; J(i+7,:) = N_XH; J(i+8,:) = N_XA; J(i+9,:) = N_XI;
u1 = u;
%X_T1 = X_T;

if u1(3,:)<0;
k_shear1 = 0;
```

```
end

%%..................... SECOND STAGE REACTION RATES, FLUXES.........%%

i=10*N+2:10:20*N-8;
S_O  = y(i,:); S_S  = y(i+1,:); S_NH = y(i+2,:); S_NO = y(i+3,:); S_ALK=
y(i+5,:); X_S  = y(i+6,:); X_H  = y(i+7,:); X_A  = y(i+8,:);
X_I  = y(i+9,:);

[R_So,R_Ss,R_Snh,R_Sno,R_Sn2,R_Salk,R_XS,R_XH,R_XA,R_XI] =
biokinetics(S_O,S_S,S_NH,S_NO,S_ALK,X_S,X_H,X_A);

R(i,:) = R_So;R(i+1,:) = R_Ss; R(i+2,:) = R_Snh; R(i+3,:) = R_Sno;
R(i+4,:) = R_Sn2; R(i+5,:) = R_Salk; R(i+6,:) = R_XS; R(i+7,:) = R_XH;
R(i+8,:) = R_XA; R(i+9,:) = R_XI;

dx    = dx2;
rho   = rho2;

[N_XS,N_XH,N_XA,N_XI,u,T,X_T]=
bioflux(R_XS,R_XH,R_XA,R_XI,X_S,X_H,X_A,X_I,dx,N,y,rho);

J(i+6,:) = N_XS; J(i+7,:) = N_XH; J(i+8,:) = N_XA; J(i+9,:) = N_XI;
u2 = u;
%X_T2 = X_T;

if u2(3,:)<0;
k_shear2 = 0;
end

%%%.............. THIRD STAGE REACTION RATES, FLUXES..............%%%

i=20*N+3:10:30*N-7;
S_O = y(i,:); S_S  = y(i+1,:); S_NH = y(i+2,:); S_NO = y(i+3,:); S_ALK=
y(i+5,:); X_S  = y(i+6,:); X_H  = y(i+7,:); X_A  = y(i+8,:); X_I  =
y(i+9,:);

[R_So,R_Ss,R_Snh,R_Sno,R_Sn2,R_Salk,R_XS,R_XH,R_XA,R_XI] =
biokinetics(S_O,S_S,S_NH,S_NO,S_ALK,X_S,X_H,X_A);

R(i,:) = R_So; R(i+1,:) = R_Ss; R(i+2,:) = R_Snh; R(i+3,:) = R_Sno;
R(i+4,:) = R_Sn2; R(i+5,:) = R_Salk; R(i+6,:) = R_XS; R(i+7,:) = R_XH;
R(i+8,:) = R_XA; R(i+9,:) = R_XI;

dx    = dx3;
rho   = rho3;

[N_XS,N_XH,N_XA,N_XI,u,T,X_T]=
bioflux(R_XS,R_XH,R_XA,R_XI,X_S,X_H,X_A,X_I,dx,N,y,rho);

J(i+6,:) = N_XS; J(i+7,:) = N_XH; J(i+8,:) = N_XA; J(i+9,:) = N_XI;
u3 = u;
%X_T3 = X_T;

if u3(3,:)<0;
k_shear3 = 0;
end

%********************** FIRST STAGE MASS TRANSPORT*********************
i=1;  % Tank
dS(i,:)  = (1/V1)*(Q*So_in  + Qr*y(20*N+3,:)  - (Q+Qr)*y(i,:))    -
((Do/dlf1)/1000) * (A_sub1/V1)*(y(i,:) - y(i+10,:)) +
R(i,:)/(3600*24)+.K_la *(S_o_sat-y(i,:));           % S_Oxygen
```

```
dS(i+1,:)= (1/V1)*(Q*Ss_in  + Qr*y(20*N+4,:) - (Q+Qr)*y(i+1,:)) -
((Ds/dlf1)/1000)  * (A_sub1/V1)*(y(i+1,:)-y(i+11,:)) + R(i+1,:)/(3600*24);
% S_BOD
dS(i+2,:)= (1/V1)*(Q*Snh_in + Qr*y(20*N+5,:)  - (Q+Qr)*y(i+2,:)) -
((Dnh/dlf1)/1000) * (A_sub1/V1)*(y(i+2,:)-y(i+12,:)) + R(i+2,:)/(3600*24);
% S_NH4
dS(i+3,:)= (1/V1)*(Q*Sno_in + Qr*y(20*N+6,:)  - (Q+Qr)*y(i+3,:)) -
((Dno/dlf1)/1000) * (A_sub1/V1)*(y(i+3,:)-y(i+13,:)) + R(i+3,:)/(3600*24);
% S_NO3
dS(i+4,:)= (1/V1)*(Q*Sn2_in + Qr*y(20*N+7,:)  - (Q+Qr)*y(i+4,:)) -
((Dn/dlf1)/1000)  * (A_sub1/V1)*(y(i+4,:)-y(i+14,:)) + R(i+4,:)/(3600*24);
% S_N2
dS(i+5,:)= (1/V1)*(Q*Salk_in+ Qr*y(20*N+8,:)  - (Q+Qr)*y(i+5,:)) -
((Dalk/dlf1)/1000)* (A_sub1/V1)*(y(i+5,:)-y(i+15,:)) + R(i+5,:)/(3600*24);
% S_Alk
dS(i+6,:)= (1/V1)*(Q*Xs_in  + Qr*y(20*N+9,:) - (Q+Qr)*y(i+6,:)) +
(1/(3600*24))*(k_shear1 * (y(10*N+1,:).^2).*y(27,:)*(A_tot1/V1)) +
R(i+6,:)/(3600*24);  % XS
dS(i+7,:)= (1/V1)*(Q*Xh_in  + Qr*y(20*N+10,:)- (Q+Qr)*y(i+7,:)) +
(1/(3600*24))*(k_shear1 * (y(10*N+1,:).^2).*y(28,:)*(A_tot1/V1)) +
R(i+7,:)/(3600*24);  % XH
dS(i+8,:)= (1/V1)*(Q*Xa_in  + Qr*y(20*N+11,:)- (Q+Qr)*y(i+8,:)) +
(1/(3600*24))*(k_shear1 * (y(10*N+1,:).^2).*y(29,:)*(A_tot1/V1)) +
R(i+8,:)/(3600*24);  % XA
dS(i+9,:)= (1/V1)*(Q*Xi_in  + Qr*y(20*N+12,:)- (Q+Qr)*y(i+9,:)) +
(1/(3600*24))*(k_shear1 * (y(10*N+1,:).^2).*y(30,:)*(A_tot1/V1)) +
R(i+9,:)/(3600*24);  % XI

i=11; % Liquid film
dS(i,:)  = ((Do/dlf1)/1000)*  ((A_sub1/V_lf1)*(y(i-10,:)-y(i,:)) -
(A_tot1/V_lf1)*(y(i,:)  - y(i+10,:)) + ((A_tot1- A_sub1)/V_lf1) *
(S_o_sat-y(i,:)));
dS(i+1,:)= ((Ds/dlf1)/1000)*  ((A_sub1/V_lf1)*(y(i-9,:)- y(i+1,:)) -
(A_tot1/V_lf1)*(y(i+1,:)- y(i+11,:)));
dS(i+2,:)= ((Dnh/dlf1)/1000)* ((A_sub1/V_lf1)*(y(i-8,:)- y(i+2,:)) -
(A_tot1/V_lf1)*(y(i+2,:)- y(i+12,:)));
dS(i+3,:)= ((Dno/dlf1)/1000)* ((A_sub1/V_lf1)*(y(i-7,:)- y(i+3,:)) -
(A_tot1/V_lf1)*(y(i+3,:)- y(i+13,:)));
dS(i+4,:)= ((Dn/dlf1)/1000) * ((A_sub1/V_lf1)*(y(i-6,:)- y(i+4,:)) -
(A_tot1/V_lf1)*(y(i+4,:)- y(i+14,:)) + ((A_tot1-A_sub1)/V_lf1)*(S_n2_sat-
y(i+4,:)));
dS(i+5,:)= ((Dalk/dlf1)/1000)*((A_sub1/V_lf1)*(y(i-5,:)- y(i+5,:)) -
(A_tot1/V_lf1)*(y(i+5,:)- y(i+15,:)));

i=21; % First biofilm layer
dS(i,:)  = co1 .* (y(i-10,:)-  2*y(i,:)   + y(i+10,:)) + R(i,:)/(3600*24);
dS(i+1,:)= cs1 .* (y(i-9,:) -  2*y(i+1,:) + y(i+11,:)) +
R(i+1,:)/(3600*24);
dS(i+2,:)= cnh1.* (y(i-8,:) -  2*y(i+2,:) + y(i+12,:)) +
R(i+2,:)/(3600*24);
dS(i+3,:)= cno1.* (y(i-7,:) -  2*y(i+3,:) + y(i+13,:)) +
R(i+3,:)/(3600*24);
dS(i+4,:)= cn1 .* (y(i-6,:) -  2*y(i+4,:) + y(i+14,:)) +
R(i+4,:)/(3600*24);
dS(i+5,:)= calk1.*(y(i-5,:) -  2*y(i+5,:) + y(i+15,:)) +
R(i+5,:)/(3600*24);
dS(i+6,:)= - (1/(3600*24))*(k_shear1 *
(y(10*N+1,:).^2).*y(i+6,:).*(1/(dx1/1000))) + R(i+6,:)/(3600*24) +
(1/(dx1/1000)).*(1/(3600*24)).*(J(i+16,:)-J(i+6,:));
dS(i+7,:)= - (1/(3600*24))*(k_shear1 *
(y(10*N+1,:).^2).*y(i+7,:).*(1/(dx1/1000))) +  R(i+7,:)/(3600*24) +
(1/(dx1/1000)).*(1/(3600*24)).*(J(i+17,:)-J(i+7,:));
```

```
dS(i+8,:)= - (1/(3600*24))*(k_shear1 *
(y(10*N+1,:).^2).*y(i+8,:).*(1/(dx1/1000))) +  R(i+8,:)/(3600*24) +
(1/(dx1/1000)).*(1/(3600*24)).*(J(i+18,:)-J(i+8,:));
dS(i+9,:)= - (1/(3600*24))*(k_shear1 *
(y(10*N+1,:).^2).*y(i+9,:).*(1/(dx1/1000))) +  R(i+9,:)/(3600*24) +
(1/(dx1/1000)).*(1/(3600*24)).*(J(i+19,:)-J(i+9,:));

i=31:10:10*N-19;  % 2nd to (N-1) biofilm layer
dS(i,:)  = co1 .* (y(i-10,:)- 2*y(i,:)  + y(i+10,:)) + R(i,:)/(3600*24);
dS(i+1,:)= cs1 .* (y(i-9,:) - 2*y(i+1,:)+ y(i+11,:)) + R(i+1,:)/(3600*24);
dS(i+2,:)= cnh1.* (y(i-8,:)-  2*y(i+2,:)+ y(i+12,:)) + R(i+2,:)/(3600*24);
dS(i+3,:)= cno1.* (y(i-7,:)-  2*y(i+3,:)+ y(i+13,:)) + R(i+3,:)/(3600*24);
dS(i+4,:)= cn1 .* (y(i-6,:)-  2*y(i+4,:)+ y(i+14,:)) + R(i+4,:)/(3600*24);
dS(i+5,:)= calk1.*(y(i-5,:)-  2*y(i+5,:)+ y(i+15,:)) + R(i+5,:)/(3600*24);
dS(i+6,:)= ps1 .* (y(i-4,:)-  2*y(i+6,:)+ y(i+16,:)) + R(i+6,:)/(3600*24)
+ (1/(dx1/1000)).*(1/(3600*24)).*(J(i+16,:)-J(i+6,:));
dS(i+7,:)= ps1 .* (y(i-3,:)-  2*y(i+7,:)+ y(i+17,:)) + R(i+7,:)/(3600*24)
+ (1/(dx1/1000)).*(1/(3600*24)).*(J(i+17,:)-J(i+7,:));
dS(i+8,:)= ps1 .* (y(i-2,:)-  2*y(i+8,:)+ y(i+18,:)) + R(i+8,:)/(3600*24)
+ (1/(dx1/1000)).*(1/(3600*24)).*(J(i+18,:)-J(i+8,:));
dS(i+9,:)= ps1 .* (y(i-1,:)-  2*y(i+9,:)+ y(i+19,:)) + R(i+9,:)/(3600*24)
+ (1/(dx1/1000)).*(1/(3600*24)).*(J(i+19,:)-J(i+9,:));

i=10*N-9;   % Last biofilm layer next to substratum
dS(i,:) = co1 .* (y(i-10,:)- y(i,:))   +  R(i,:)/(3600*24);   dS(i+1,:)=
cs1 .* (y(i-9,:) - y(i+1,:)) +  R(i+1,:)/(3600*24);
dS(i+2,:)= cnh1.* (y(i-8,:)-  y(i+2,:)) +  R(i+2,:)/(3600*24);
dS(i+3,:)= cno1.* (y(i-7,:)-  y(i+3,:)) +  R(i+3,:)/(3600*24);
dS(i+4,:)= cn1 .* (y(i-6,:)-  y(i+4,:)) +  R(i+4,:)/(3600*24);
dS(i+5,:)= calk1.*(y(i-5,:)-  y(i+5,:)) +  R(i+5,:)/(3600*24);
dS(i+6,:)= ps1 .* (y(i-4,:)-  y(i+6,:)) +  R(i+6,:)/(3600*24) +
(1/(dx1/1000)).*(1/(3600*24)).*(0-J(i+6,:));
dS(i+7,:)= ps1 .* (y(i-3,:)-  y(i+7,:)) +  R(i+7,:)/(3600*24) +
(1/(dx1/1000)).*(1/(3600*24)).*(0-J(i+7,:));
dS(i+8,:)= ps1 .* (y(i-2,:)-  y(i+8,:)) +  R(i+8,:)/(3600*24) +
(1/(dx1/1000)).*(1/(3600*24)).*(0-J(i+8,:));
dS(i+9,:)= ps1 .* (y(i-1,:)-  y(i+9,:)) +  R(i+9,:)/(3600*24) +
(1/(dx1/1000)).*(1/(3600*24)).*(0-J(i+9,:));

i=1:10:10*N-9;
X_SS1  =  y(i+6,:);
X_Het1 =  y(i+7,:);
X_Aut1 =  y(i+8,:);
X_Ine1 =  y(i+9,:);

X_Tot1 = X_SS1 + X_Het1 + X_Aut1 + X_Ine1;
% New X_tot at current time step. Units in g/m3

U_attach1   = (k_floc1  *   X_Tot1(1,:))/(rho1); % units m/d
U_shear1    = (k_shear1 *  (y(10*N+1,:).^2));    % units m/d

i=10*N+1;   % Biofilm thickness
dS(i,:) = (1/(3600*24))*(u1(3,:) + (U_attach1 - U_shear1)); % Units m

%%**********************SECOND STAGE MASS TRANSPORT***************%%
i=10*N+2;   % Tank
dS(i,:)  = ((Q+Qr)/V2)*(y(1,:) - y(i,:))-((Do/dlf2)/1000)*
(A_sub2/V2)*(y(i,:) - y(i+10,:))+  R(i,:)/(3600*24)+ K_la * (S_o_sat-
y(i,:));
dS(i+1,:)= ((Q+Qr)/V2)*(y(2,:) - y(i+1,:)) -((Ds/dlf2)/1000)  *
(A_sub2/V2)*(y(i+1,:)-y(i+11,:))               +  R(i+1,:)/(3600*24);
dS(i+2,:)= ((Q+Qr)/V2)*(y(3,:) - y(i+2,:)) -((Dnh/dlf2)/1000) *
(A_sub2/V2)*(y(i+2,:)-y(i+12,:))               +  R(i+2,:)/(3600*24);
```

```
dS(i+3,:)= ((Q+Qr)/V2)*(y(4,:) - y(i+3,:)) -((Dno/dlf2)/1000) *
(A_sub2/V2)*(y(i+3,:)-y(i+13,:))                +  R(i+3,:)/(3600*24);
dS(i+4,:)= ((Q+Qr)/V2)*(y(5,:) - y(i+4,:)) -((Dn/dlf2)/1000)  *
(A_sub2/V2)*(y(i+4,:)-y(i+14,:))                +  R(i+4,:)/(3600*24);
dS(i+5,:)= ((Q+Qr)/V2)*(y(6,:) - y(i+5,:)) -((Dalk/dlf2)/1000)*
(A_sub2/V2)*(y(i+5,:)-y(i+15,:))                +  R(i+5,:)/(3600*24);
dS(i+6,:)= ((Q+Qr)/V2)*(y(7,:) - y(i+6,:)) + (1/(3600*24))*(k_shear2 *
(y(20*N+2,:).^2).*y(10*N+28,:)*(A_tot2/V2))     +  R(i+6,:)/(3600*24);
dS(i+7,:)= ((Q+Qr)/V2)*(y(8,:) - y(i+7,:)) + (1/(3600*24))*(k_shear2 *
(y(20*N+2,:).^2).*y(10*N+29,:)*(A_tot2/V2))  +  R(i+7,:)/(3600*24);
dS(i+8,:)= ((Q+Qr)/V2)*(y(9,:) - y(i+8,:)) + (1/(3600*24))*(k_shear2 *
(y(20*N+2,:).^2).*y(10*N+30,:)*(A_tot2/V2))     +  R(i+8,:)/(3600*24);
dS(i+9,:)= ((Q+Qr)/V2)*(y(10,:)- y(i+9,:)) + (1/(3600*24))*(k_shear2 *
(y(20*N+2,:).^2).*y(10*N+31,:)*(A_tot2/V2))     +  R(i+9,:)/(3600*24);

i=10*N+12;  % Liquid film
dS(i,:)  = ((Do/dlf2)/1000)*  ((A_sub2/V_lf2)*(y(i-10,:)-y(i,:))  -
(A_tot2/V_lf2)*(y(i,:)-  y(i+10,:)) + ((A_tot2-A_sub2)/V_lf2)*(S_o_sat-
y(i,:)));
dS(i+1,:)= ((Ds/dlf2)/1000)*  ((A_sub2/V_lf2)*(y(i-9,:)- y(i+1,:))-
(A_tot2/V_lf2)*(y(i+1,:)-y(i+11,:)));
dS(i+2,:)= ((Dnh/dlf2)/1000)* ((A_sub2/V_lf2)*(y(i-8,:)- y(i+2,:))-
(A_tot2/V_lf2)*(y(i+2,:)-y(i+12,:)));
dS(i+3,:)= ((Dno/dlf2)/1000)* ((A_sub2/V_lf2)*(y(i-7,:)- y(i+3,:))-
(A_tot2/V_lf2)*(y(i+3,:)-y(i+13,:)));
dS(i+4,:)= ((Dn/dlf2)/1000) * ((A_sub2/V_lf2)*(y(i-6,:)- y(i+4,:))-
(A_tot2/V_lf2)*(y(i+4,:)-y(i+14,:)) + ((A_tot2-A_sub2)/V_lf2)*(S_n2_sat-
y(i+4,:)));
dS(i+5,:)= ((Dalk/dlf2)/1000)*((A_sub2/V_lf2)*(y(i-5,:)- y(i+5,:))-
(A_tot2/V_lf2)*(y(i+5,:)-y(i+15,:)));

i=10*N+22;  % First biofilm layer
dS(i,:)  = co2 * (y(i-10,:)- 2*y(i,:)  + y(i+10,:))+ R(i,:)/(3600*24);
dS(i+1,:)= cs2 * (y(i-9,:) - 2*y(i+1,:)+ y(i+11,:))+R(i+1,:)/(3600*24);
dS(i+2,:)= cnh2* (y(i-8,:) - 2*y(i+2,:)+ y(i+12,:))+R(i+2,:)/(3600*24);
dS(i+3,:)= cno2* (y(i-7,:) - 2*y(i+3,:)+ y(i+13,:))+R(i+3,:)/(3600*24);
dS(i+4,:)= cn2 * (y(i-6,:) - 2*y(i+4,:)+ y(i+14,:))+R(i+4,:)/(3600*24);
dS(i+5,:)= calk2*(y(i-5,:) - 2*y(i+5,:)+ y(i+15,:))+R(i+5,:)/(3600*24);
dS(i+6,:)= - (1/(3600*24))*(k_shear2 *
(y(20*N+2,:).^2).*y(i+6,:)*(1/(dx2/1000))) +  R(i+6,:)/(3600*24) +
(1/(dx2/1000))*(1/(3600*24))*(J(i+16,:)-J(i+6,:));
dS(i+7,:)= - (1/(3600*24))*(k_shear2 *
(y(20*N+2,:).^2).*y(i+7,:)*(1/(dx2/1000))) +  R(i+7,:)/(3600*24) +
(1/(dx2/1000))*(1/(3600*24))*(J(i+17,:)-J(i+7,:));
dS(i+8,:)= - (1/(3600*24))*(k_shear2 *
(y(20*N+2,:).^2).*y(i+8,:)*(1/(dx2/1000))) +  R(i+8,:)/(3600*24) +
(1/(dx2/1000))*(1/(3600*24))*(J(i+18,:)-J(i+8,:));
dS(i+9,:)= - (1/(3600*24))*(k_shear2 *
(y(20*N+2,:).^2).*y(i+9,:)*(1/(dx2/1000))) +  R(i+9,:)/(3600*24) +
(1/(dx2/1000))*(1/(3600*24))*(J(i+19,:)-J(i+9,:));

i=10*N+32:10:20*N-18;   % 2nd layer to the (N-1) biofilm layer
dS(i,:)  = co2 * (y(i-10,:)- 2*y(i,:)  + y(i+10,:))  + R(i,:)/(3600*24);
dS(i+1,:)= cs2 * (y(i-9,:) - 2*y(i+1,:)+ y(i+11,:))  + R(i+1,:)/(3600*24);
dS(i+2,:)= cnh2* (y(i-8,:) - 2*y(i+2,:)+ y(i+12,:))  + R(i+2,:)/(3600*24);
dS(i+3,:)= cno2* (y(i-7,:) - 2*y(i+3,:)+ y(i+13,:))  + R(i+3,:)/(3600*24);
dS(i+4,:)= cn2 * (y(i-6,:) - 2*y(i+4,:)+ y(i+14,:))  + R(i+4,:)/(3600*24);
dS(i+5,:)= calk2*(y(i-5,:) - 2*y(i+5,:)+ y(i+15,:))  + R(i+5,:)/(3600*24);
dS(i+6,:)= ps2 * (y(i-4,:) - 2*y(i+6,:)+ y(i+16,:))  + R(i+6,:)/(3600*24)
+ (1/(dx2/1000))*(1/(3600*24))*(J(i+16,:)-J(i+6,:)); dS(i+7,:)= ps2 *
(y(i-3,:) - 2*y(i+7,:)+ y(i+17,:))  + R(i+7,:)/(3600*24) +
(1/(dx2/1000))*(1/(3600*24))*(J(i+17,:)-J(i+7,:));
```

```
dS(i+8,:)= ps2 * (y(i-2,:) - 2*y(i+8,:)+ y(i+18,:))  + R(i+8,:)/(3600*24)
+ (1/(dx2/1000))*(1/(3600*24))*(J(i+18,:)-J(i+8,:));
dS(i+9,:)= ps2 * (y(i-1,:) - 2*y(i+9,:)+ y(i+19,:))  + R(i+9,:)/(3600*24)
+ (1/(dx2/1000))*(1/(3600*24))*(J(i+19,:)-J(i+9,:));

i=20*N-8;   % Last biofilm layer next to substratum
dS(i,:)  = co2 * (y(i-10,:)- y(i,:))   +  R(i,:)/(3600*24);
dS(i+1,:)= cs2 * (y(i-9,:) - y(i+1,:)) +  R(i+1,:)/(3600*24);
dS(i+2,:)= cnh2* (y(i-8,:) - y(i+2,:)) +  R(i+2,:)/(3600*24);
dS(i+3,:)= cno2* (y(i-7,:) - y(i+3,:)) +  R(i+3,:)/(3600*24);
dS(i+4,:)= cn2 * (y(i-6,:) - y(i+4,:)) +  R(i+4,:)/(3600*24);
dS(i+5,:)= calk2*(y(i-5,:) - y(i+5,:)) +  R(i+5,:)/(3600*24);
dS(i+6,:)= ps2 * (y(i-4,:) - y(i+6,:)) +  R(i+6,:)/(3600*24) +
(1/(dx2/1000))*(1/(3600*24))*(0-J(i+6,:));
dS(i+7,:)= ps2 * (y(i-3,:) - y(i+7,:)) +  R(i+7,:)/(3600*24) +
(1/(dx2/1000))*(1/(3600*24))*(0-J(i+7,:));
dS(i+8,:)= ps2 * (y(i-2,:) - y(i+8,:)) +  R(i+8,:)/(3600*24) +
(1/(dx2/1000))*(1/(3600*24))*(0-J(i+8,:));
dS(i+9,:)= ps2 * (y(i-1,:) - y(i+9,:)) +  R(i+9,:)/(3600*24) +
(1/(dx2/1000))*(1/(3600*24))*(0-J(i+9,:));

i=10*N+2:10:20*N-8;
X_SS2  =  y(i+6,:);
X_Het2 =  y(i+7,:);
X_Aut2 =  y(i+8,:);
X_Ine2 =  y(i+9,:);

X_Tot2 = X_SS2 + X_Het2 + X_Aut2 + X_Ine2;
% New X_tot at current time step. Units in g/m3

U_attach2   = (k_floc2  *   X_Tot2(1,:))/(rho2); % units m/d
% units m/d (k_floc2 is in m/d)
U_shear2    = (k_shear2 *  (y(20*N+2,:).^2)); units m/d

i=20*N+2;   % Biofilm thickness
dS(i,:) = (1/(3600*24))* (u2(3,:) + (U_attach2 - U_shear2));% Units m

%%%******************** THIRD STAGE MASS TRANSPORT********************%%%
i=20*N+3;   % Tank
dS(i,:)  = ((Q+Qr)/V3)*(y(10*N+2,:) - y(i,:))  -((Do/dlf3)/1000)  *
(A_sub3/V3)*(y(i,:) - y(i+10,:))          +  R(i,:)/(3600*24) + K_la *
(S_o_sat-y(i,:));
dS(i+1,:)= ((Q+Qr)/V3)*(y(10*N+3,:) - y(i+1,:))-((Ds/dlf3)/1000)  *
(A_sub3/V3)*(y(i+1,:)-y(i+11,:))          +  R(i+1,:)/(3600*24);
dS(i+2,:)= ((Q+Qr)/V3)*(y(10*N+4,:) - y(i+2,:))-((Dnh/dlf3)/1000) *
(A_sub3/V3)*(y(i+2,:)-y(i+12,:))          +  R(i+2,:)/(3600*24);
dS(i+3,:)= ((Q+Qr)/V3)*(y(10*N+5,:) - y(i+3,:))-((Dno/dlf3)/1000) *
(A_sub3/V3)*(y(i+3,:)-y(i+13,:))          +  R(i+3,:)/(3600*24);
dS(i+4,:)= ((Q+Qr)/V3)*(y(10*N+6,:) - y(i+4,:))-((Dn/dlf3)/1000)  *
(A_sub3/V3)*(y(i+4,:)-y(i+14,:))          +  R(i+4,:)/(3600*24);
dS(i+5,:)= ((Q+Qr)/V3)*(y(10*N+7,:) - y(i+5,:))-((Dalk/dlf3)/1000)*
(A_sub3/V3)*(y(i+5,:)-y(i+15,:))          +  R(i+5,:)/(3600*24);
dS(i+6,:)= ((Q+Qr)/V3)*(y(10*N+8,:) - y(i+6,:))+ (1/(3600*24))*(k_shear3 *
(y(30*N+3,:).^2).*y(20*N+29,:)*(A_tot3/V3))  +  R(i+6,:)/(3600*24);
dS(i+7,:)= ((Q+Qr)/V3)*(y(10*N+9,:) - y(i+7,:))+ (1/(3600*24))*(k_shear3 *
(y(30*N+3,:).^2).*y(10*N+30,:)*(A_tot3/V3))  +  R(i+7,:)/(3600*24);
dS(i+8,:)= ((Q+Qr)/V3)*(y(10*N+10,:)- y(i+8,:))+ (1/(3600*24))*(k_shear3 *
(y(30*N+3,:).^2).*y(10*N+31,:)*(A_tot3/V3))  +  R(i+8,:)/(3600*24);
dS(i+9,:)= ((Q+Qr)/V3)*(y(10*N+11,:)- y(i+9,:))+ (1/(3600*24))*(k_shear3 *
(y(30*N+3,:).^2).*y(10*N+32,:)*(A_tot3/V3))  +  R(i+9,:)/(3600*24);

i=20*N+13;  % Liquid film
```

```
dS(i,:)  = ((Do/dlf3)/1000)*  ((A_sub3/V_lf3)*(y(i-10,:)-y(i,:))  -
(A_tot3/V_lf3)*(y(i,:)-  y(i+10,:)) + ((A_tot3-A_sub3)/V_lf3)*(S_o_sat-
y(i,:)));
dS(i+1,:)= ((Ds/dlf3)/1000)*  ((A_sub3/V_lf3)*(y(i-9,:)- y(i+1,:))-
(A_tot3/V_lf3)*(y(i+1,:)-y(i+11,:)));
dS(i+2,:)= ((Dnh/dlf3)/1000)* ((A_sub3/V_lf3)*(y(i-8,:)- y(i+2,:))-
(A_tot3/V_lf3)*(y(i+2,:)-y(i+12,:)));
dS(i+3,:)= ((Dno/dlf3)/1000)* ((A_sub3/V_lf3)*(y(i-7,:)- y(i+3,:))-
(A_tot3/V_lf3)*(y(i+3,:)-y(i+13,:)));
dS(i+4,:)= ((Dn/dlf3)/1000) * ((A_sub3/V_lf3)*(y(i-6,:)- y(i+4,:))-
(A_tot3/V_lf3)*(y(i+4,:)-y(i+14,:)) + ((A_tot3-A_sub3)/V_lf3)*(S_n2_sat-
y(i+4,:)));
dS(i+5,:)= ((Dalk/dlf3)/1000)*((A_sub3/V_lf3)*(y(i-5,:)- y(i+5,:))-
(A_tot3/V_lf3)*(y(i+5,:)-y(i+15,:)));

i=20*N+23;  % First biofilm layer
dS(i,:)  = co3 * (y(i-10,:)- 2*y(i,:)  + y(i+10,:))+R(i,:)/(3600*24);
dS(i+1,:)= cs3 * (y(i-9,:) - 2*y(i+1,:)+ y(i+11,:))+R(i+1,:)/(3600*24);
dS(i+2,:)= cnh3* (y(i-8,:) - 2*y(i+2,:)+ y(i+12,:))+R(i+2,:)/(3600*24);
dS(i+3,:)= cno3* (y(i-7,:) - 2*y(i+3,:)+ y(i+13,:))+R(i+3,:)/(3600*24);
dS(i+4,:)= cn3 * (y(i-6,:) - 2*y(i+4,:)+ y(i+14,:))+R(i+4,:)/(3600*24);
dS(i+5,:)= calk3*(y(i-5,:) - 2*y(i+5,:)+ y(i+15,:))+R(i+5,:)/(3600*24);
dS(i+6,:)= - (1/(3600*24))*(k_shear3 *
(y(30*N+3,:).^2).*y(i+6,:)*(1/(dx3/1000))) +  R(i+6,:)/(3600*24) +
(1/(dx3/1000))*(1/(3600*24))*(J(i+16,:)-J(i+6,:));
dS(i+7,:)= - (1/(3600*24))*(k_shear3 *
(y(30*N+3,:).^2).*y(i+7,:)*(1/(dx3/1000))) +  R(i+7,:)/(3600*24) +
(1/(dx3/1000))*(1/(3600*24))*(J(i+17,:)-J(i+7,:));
dS(i+8,:)= - (1/(3600*24))*(k_shear3 *
(y(30*N+3,:).^2).*y(i+8,:)*(1/(dx3/1000))) +  R(i+8,:)/(3600*24) +
(1/(dx3/1000))*(1/(3600*24))*(J(i+18,:)-J(i+8,:));
dS(i+9,:)= - (1/(3600*24))*(k_shear3 *
(y(30*N+3,:).^2).*y(i+9,:)*(1/(dx3/1000))) +  R(i+9,:)/(3600*24) +
(1/(dx3/1000))*(1/(3600*24))*(J(i+19,:)-J(i+9,:));

i=20*N+33:10:30*N-17;    % 2nd layer to the (N-1) biofilm layer
dS(i,:)  = co3 * (y(i-10,:)- 2*y(i,:) + y(i+10,:))+ R(i,:)/(3600*24);
dS(i+1,:)= cs3 * (y(i-9,:) - 2*y(i+1,:)+ y(i+11,:))+R(i+1,:)/(3600*24);
dS(i+2,:)= cnh3* (y(i-8,:) - 2*y(i+2,:)+ y(i+12,:))+R(i+2,:)/(3600*24);
dS(i+3,:)= cno3* (y(i-7,:) - 2*y(i+3,:)+ y(i+13,:))+R(i+3,:)/(3600*24);
dS(i+4,:)= cn3 * (y(i-6,:) - 2*y(i+4,:)+ y(i+14,:))+R(i+4,:)/(3600*24);
dS(i+5,:)= calk3*(y(i-5,:) - 2*y(i+5,:)+ y(i+15,:))+R(i+5,:)/(3600*24);
dS(i+6,:)= ps3 * (y(i-4,:) - 2*y(i+6,:)+ y(i+16,:))+ R(i+6,:)/(3600*24) +
(1/(dx3/1000))*(1/(3600*24))*(J(i+16,:)-J(i+6,:));
dS(i+7,:)= ps3 * (y(i-3,:) - 2*y(i+7,:)+ y(i+17,:))+ R(i+7,:)/(3600*24) +
(1/(dx3/1000))*(1/(3600*24))*(J(i+17,:)-J(i+7,:));
dS(i+8,:)= ps3 * (y(i-2,:) - 2*y(i+8,:)+ y(i+18,:))+ R(i+8,:)/(3600*24) +
(1/(dx3/1000))*(1/(3600*24))*(J(i+18,:)-J(i+8,:));
dS(i+9,:)= ps3 * (y(i-1,:) - 2*y(i+9,:)+ y(i+19,:))+ R(i+9,:)/(3600*24) +
(1/(dx3/1000))*(1/(3600*24))*(J(i+19,:)-J(i+9,:));

i=30*N-7;   % Last biofilm layer next to substratum
dS(i,:)  = co3 * (y(i-10,:)- y(i,:)) +  R(i,:)/(3600*24);
dS(i+1,:)= cs3 * (y(i-9,:) - y(i+1,:)) +  R(i+1,:)/(3600*24);
dS(i+2,:)= cnh3* (y(i-8,:) - y(i+2,:)) +  R(i+2,:)/(3600*24);
dS(i+3,:)= cno3* (y(i-7,:) - y(i+3,:)) +  R(i+3,:)/(3600*24);
dS(i+4,:)= cn3 * (y(i-6,:) - y(i+4,:)) +  R(i+4,:)/(3600*24);
dS(i+5,:)= calk3*(y(i-5,:) - y(i+5,:)) +  R(i+5,:)/(3600*24);
dS(i+6,:)= ps3 * (y(i-4,:) - y(i+6,:)) +  R(i+6,:)/(3600*24) +
(1/(dx3/1000))*(1/(3600*24))*(0-J(i+6,:));
dS(i+7,:)= ps3 * (y(i-3,:) - y(i+7,:)) +  R(i+7,:)/(3600*24) +
(1/(dx3/1000))*(1/(3600*24))*(0-J(i+7,:));
```

```
dS(i+8,:)= ps3 * (y(i-2,:) - y(i+8,:)) +  R(i+8,:)/(3600*24) +
(1/(dx3/1000))*(1/(3600*24))*(0-J(i+8,:));
dS(i+9,:)= ps3 * (y(i-1,:) - y(i+9,:)) +  R(i+9,:)/(3600*24) +
(1/(dx3/1000))*(1/(3600*24))*(0-J(i+9,:));

i=20*N+3:10:30*N-7;
X_SS3  =  y(i+6,:);
X_Het3 =  y(i+7,:);
X_Aut3 =  y(i+8,:);
X_Ine3 =  y(i+9,:);

X_Tot3 = X_SS3 + X_Het3 + X_Aut3 + X_Ine3;
% New X_tot at current time step. Units in g/m3

U_attach3   = (k_floc3 * X_Tot3(1,:))/(rho3); % units m/d
U_shear3    = (k_shear3 * (y(30*N+3,:).^2));    % units m/d

i=30*N+3;   % Biofilm thickness
dS(i,:) = (1/(3600*24))*(u3(3,:) + (U_attach3 - U_shear3)); %Units m

format long
```

c) biokinetics.m

```
function [R_So,R_Ss,R_Snh,R_Sno,R_Sn2,R_Salk,R_XS,R_XH,R_XA,R_XI] =
biokinetics(S_O,S_S,S_NH,S_NO,S_ALK,X_S,X_H,X_A)

% Kinetic and stoichiometric coefficients at 25°C
% For Heterotrophs
mhu_H=6.39;
b_H=0.28;

% Kinetic and stoichiometric coefficients at 30°C
% For Heterotrophs
%mhu_H=9.06;
%b_H=0.40;

K_H_O2=0.20;
K_SS=5.0;
K_H_NH=0.10;
K_H_NO=0.5;
K_H_ALK=0.10;
eta_H=0.5;
theta_DEN=0.3;
Y_H_O2=0.63;
Y_H_NO=0.54;

% For Autotrophs at 25°C
mhu_A=1.69;
b_A=0.25;

% For Autotrophs at 30°C
%mhu_A=2.86;
%b_A=0.43;

K_A_O2=0.30;
K_A_NH=1.0;
K_A_NO=0.5;
K_A_ALK=0.5;
eta_A=0.001;
Y_A=0.24;
```

```
% Stoichiometric Fractions
i_nbm=0.07; % gN/gCOD X_H (or X_A);
i_nxi=0.02; % gN/gCOD X_I;
f_i=0.2;    % gCOD X_I/gCOD X_H (or X_A);
K_HYD   = 1.5;
K_XS    = 0.02;

% Heterotrophic process kinetics
P1H= (mhu_H).*(S_S./(S_S+K_SS)).*
(S_O./(S_O+K_H_O2)).*(S_NH./(S_NH+K_H_NH)).*(S_ALK./(S_ALK+K_H_ALK));
P2H= theta_DEN.* (mhu_H).*(S_S./(S_S+K_SS)).*
(K_H_O2./(S_O+K_H_O2)).*(S_NH./(S_NH+K_H_NH)).*.
(S_ALK./(S_ALK+K_H_ALK)).*(S_NO./(S_NO+K_H_NO));
P3H= b_H.*(S_O./(S_O+K_H_O2));
P4H= eta_H*b_H.*(K_H_O2./(S_O+K_H_O2)).*(S_NO./(S_NO+K_H_NO));
R_XH=(P1H+P2H-P3H-P4H).* X_H;  % Units in g/m3.d

% Autotrophic process kinetics
P1A=(mhu_A).*(S_O./(S_O+K_A_O2)).*(S_NH./(S_NH+K_A_NH)).*(S_ALK./(S_ALK+K_
A_ALK));
P2A= b_A.*(S_O./(S_O+K_A_O2));
P3A= eta_A*b_A.*(K_A_O2./(S_O+K_A_O2)).*(S_NO./(S_NO+K_A_NO));
R_XA=P1A-P2A-P3A).* X_A;  % Units in g/m3.d;
%R_HYD=K_HYD*((X_S./(X_H))./(K_XS + (X_S./(X_H )))).*X_H; % Hydrolysis

% Substrate and product stoichiometry in biofilm
R_So=(((Y_H_O2-1)/Y_H_O2).* P1H -(1-f_i).*P3H).* X_H +(((Y_A-4.57)/Y_A)
.* P1A -(1-f_i).*P2A).* X_A; % Units in g/m3.d
R_Ss  = ((-1/Y_H_O2).* P1H -(1/Y_H_NO).*P2H).*X_H ; %+ R_HYD;
R_Snh = (-i_nbm.*P1H - i_nbm.*P2H + (i_nbm-f_i*i_nxi).*P3H + (i_nbm-
f_i*i_nxi).*P4H).* X_H +(-(i_nbm + 1/Y_A).*P1A + (i_nbm-f_i*i_nxi).*P2A +
(i_nbm-f_i*i_nxi).*P3A).* X_A;
R_Sno = (((Y_H_NO-1)/(2.86 * Y_H_NO)).*P2H - ((1-f_i)/2.86).*P4H).*X_H +
((1/Y_A).*P1A).* X_A + ((-(1-f_i)/2.86).*P3A).* X_A;
R_Sn2 = (-((Y_H_NO-1)/(2.86 * Y_H_NO)).*P2H +((1-f_i)/2.86).*P4H).*X_H +
((1-f_i)/2.86).*P3A.* X_A;
 R_Salk= (-(i_nbm/14).*P1H + ((1-Y_H_NO)/(40*Y_H_NO)-(i_nbm/14)).*P2H
+.(i_nbm-f_i*i_nxi)/14).*P3H + ((i_nbm-f_i*i_nxi)/14 + (1-f_i)/40).*P4H).*
X_H +(-((i_nbm/14)+1/(7*Y_A)).*P1A +((i_nbm-f_i*i_nxi)/14).*P2A +
(1/14).*(i_nbm-f_i*i_nxi+((1-f_i)/2.86)).*P3A).* X_A;
R_XI= f_i.*((P3H+P4H).* X_H + (P2A+P3A).* X_A);
%R_XS = - R_HYD;
R_XS = 0;
```

d) bioflux.m

```
function [N_XS,N_XH,N_XA,N_XI,u,T,X_T]=
bioflux(R_XS,R_XH,R_XA,R_XI,X_S,X_H,X_A,X_I,dx,N,y,rho);

N_XS = zeros(N,size(y,2));
N_XH = zeros(N,size(y,2));
N_XA = zeros(N,size(y,2));
N_XI = zeros(N,size(y,2));

u    = zeros(N,size(y,2));

X_T  = X_S + X_H + X_A + X_I;             % units in g/m3
T    =(R_XS + R_XH + R_XA + R_XI)./(rho); % units in 1/d

U    = T.*(dx/1000);                      % units in m/d

u(N,:)= U(N,:);
```

```
for int=1:N-1;   % integration of N_Xnh in each of the strips at any time
                 % step given by k
k = N-int;
u(k,:)      = u(k+1,:) + U(k,:);          % units in m/d
end

u(1:2,:)    = 0;
T(1:2,:)    = 0;
N_XS        = X_S.*u;                     % units in g/m2.d
N_XH        = X_H.*u;
N_XA        = X_A.*u;
N_XI        = X_I.*u;

format long
```

e) maxcode.m

```
% User inputs are N, rho and k_shear from main files

function [t,y] = maxcode(t,y,flag)  % Input_data;
C = 0;

if nargin < 3 | isempty(flag)| strcmp (flag,'init')
y = max(C,y);
```

f) Initial_cond.m

```
% Input parameters file
function [tspan,y0,options] =
Initial_cond(time,N,dx1,dx2,dx3,rho1,rho2,rho3,So_in,Ss_in,Snh_in,Sno_in,S
n2_in,Salk_in,Xs_in,Xh_in,Xa_in,Xi_in)

tspan = [0 3600*24*time]; % Time in sec

% STAGE I
a = zeros(10,N);
% Influent tank concentrations in g/m3

a(1,1)      = So_in(1);             % Oxygen in Tank
a(2,1)      = Ss_in(1);             % sol.substrate in Tank
a(3,1)      = Snh_in(1);            % Ammonium in Tank
a(4,1)      = Sno_in(1);            % Nitrate in Tank
a(5,1)      = Sn2_in(1);            % Nitrogen in Tank
a(6,1)      = Salk_in(1);           % Alkalinity in Tank
a(7,1)      = Xs_in(1);             % SS in tank
a(7,2)      = 0;                    % SS in LF
a(8,1)      = Xh_in(1);             % Het. in tank
a(8,2)      = 0;                    % Het. in LF
a(9,1)      = Xa_in(1);             % Autotrophs in tank
a(9,2)      = 0;                    % Autotrophs in LF
a(10,1)     = Xi_in(1);             % Particulate Inerts in tank
a(10,2)     = 0;                    % Particulate Inerts in LF

% Liquid film and Biofilm concentrations
a(1,2:N)    = 0;                    % Oxygen in biofilm
a(2,2:N)    = 0;                    % sol.COD in biofilm
a(3,2:N)    = 0;                    % Ammonium in biofilm
a(4,2:N)    = 0;                    % Nitrate in biofilm
a(5,2:N)    = 0;                    % Nitrogen in biofilm
a(6,2:N)    = 0;                    % Alkalinity in biofilm

a(7,3:N)    = 0;                    % Suspended solids in biofilm
```

```
a(8,3:N)    = 0.50*rho1;            % Heterotrophs in biofilm
a(9,3:N)    = 0.20*rho1;            % Autotrophs in biofilm
a(10,3:N)   = 0.30*rho1;            % Inerts in biofilm

a=a(:);

% STAGE II
b = zeros(10,N);

b(1,1)      = 0;                    % Oxygen
b(2,1)      = 0;                    % sol.COD
b(3,1)      = 0;                    % Ammonium
b(4,1)      = 0;                    % Nitrate
b(5,1)      = 0;                    % Nitrogen
b(6,1)      = 0;                    % Alkalinity
b(7,1:2)    = 0;                    % SS in tank and LF
b(8,1:2)    = 0;                    % Heterotrophs in tank and LF
b(9,1:2)    = 0;                    % Autotrophs in tank and LF
b(10,1:2)   = 0;                    % Particulate Inerts in tank & LF

b(1,2:N)    = 0;
b(2,2:N)    = 0;
b(3,2:N)    = 0;
b(4,2:N)    = 0;
b(5,2:N)    = 0;
b(6,2:N)    = 0;

b(7,3:N)    = 0;                    % Suspended solids in biofilm
b(8,3:N)    = 0.50*rho2;            % Heterotrophs in biofilm
b(9,3:N)    = 0.20*rho2;            % Autotrophs in biofilm
b(10,3:N)   = 0.30*rho2;            % Inerts in biofilm

b=b(:);

% STAGE III
c = zeros(10,N);

c(1,1)      = 0;                    % Oxygen
c(2,1)      = 0;                    % sol.COD
c(3,1)      = 0;                    % Ammonium
c(4,1)      = 0;                    % Nitrate
c(5,1)      = 0;                    % Nitrogen
c(6,1)      = 0;                    % Alkalinity
c(7,1:2)    = 0;                    % SS in tank and LF
c(8,1:2)    = 0;                    % Heterotrophs  in tank and LF
c(9,1:2)    = 0;                    % Autotrophs in tank and LF
c(10,1:2)   = 0;                    % Particulate Inerts in tank & LF

c(1,2:N)    = 0;
c(2,2:N)    = 0;
c(3,2:N)    = 0;
c(4,2:N)    = 0;
c(5,2:N)    = 0;
c(6,2:N)    = 0;

c(7,3:N)    = 0;                    % Suspended solids in biofilm
c(8,3:N)    = 0.50*rho3;            % Heterotrophs in biofilm
c(9,3:N)    = 0.20*rho3;            % Autotrophs in biofilm
c(10,3:N)   = 0.30*rho3;            % Inerts in biofilm

c=c(:);

y0 = zeros(30*N+3,1);
```

```
y0(1:10*N,:)         = a;
y0(10*N+1,:)        = (N-2)*(dx1)/1000; % Init. Biofilm thickness in m
y0(10*N+2:20*N+1,:)  = b;
y0(20*N+2,:)         = (N-2)*(dx2)/1000; % Init. Biofilm thickness in m
y0(20*N+3:30*N+2,:)  = c;
y0(30*N+3,:)         = (N-2)*(dx3)/1000; % Init. Biofilm thickness in m

options=odeset('Vectorized','on','BDF','on','MaxOrder',3,'OutputFcn','maxc
ode');
```

g) filesave.m

```
Tank1 = Y(:,1:10*N+1); Tank2 = Y(:,10*N+2:20*N+2); Tank3 =
Y(:,20*N+3:30*N+3);

save C:\MATLAB_data\output_tank1.dat T Tank1 -ascii -tabs;
save C:\MATLAB_data\output_tank2.dat T Tank2 -ascii -tabs;
save C:\MATLAB_data\output_tank3.dat T Tank3 -ascii -tabs;
save C:\MATLAB_data\run_time.dat T -ascii -tabs;

% CASCADE 1
S_O1  = Y(:,1:10:10*N-9);
S_S1  = Y(:,2:10:10*N-8);
S_NH1 = Y(:,3:10:10*N-7);
S_NO1 = Y(:,4:10:10*N-6);
S_N1  = Y(:,5:10:10*N-5);
S_ALK1= Y(:,6:10:10*N-4);
X_S1  = Y(:,7:10:10*N-3);
X_H1  = Y(:,8:10:10*N-2);
X_A1  = Y(:,9:10:10*N-1);
X_I1  = Y(:,10:10:10*N);
L1    = Y(:,10*N+1);

save C:\MATLAB_data\S_O1.dat S_O1 -ascii -tabs;
save C:\MATLAB_data\S_S1.dat S_S1 -ascii -tabs;
save C:\MATLAB_data\S_NH1.dat S_NH1 -ascii -tabs;
save C:\MATLAB_data\S_NO1.dat S_NO1 -ascii -tabs;
save C:\MATLAB_data\S_N1.dat S_N1 -ascii -tabs;
save C:\MATLAB_data\S_ALK1.dat S_ALK1 -ascii -tabs;
save C:\MATLAB_data\X_S1.dat X_S1 -ascii -tabs;
save C:\MATLAB_data\X_H1.dat X_H1 -ascii -tabs;
save C:\MATLAB_data\X_A1.dat X_A1 -ascii -tabs;
save C:\MATLAB_data\X_I1.dat X_I1 -ascii -tabs;
save C:\MATLAB_data\L1.dat L1 -ascii -tabs;

% CASCADE 2
S_O2  = Y(:,10*N+2:10:20*N-8);
S_S2  = Y(:,10*N+3:10:20*N-7);
S_NH2 = Y(:,10*N+4:10:20*N-6);
S_NO2 = Y(:,10*N+5:10:20*N-5);
S_N2  = Y(:,10*N+6:10:20*N-4);
S_ALK2= Y(:,10*N+7:10:20*N-3);
X_S2  = Y(:,10*N+8:10:20*N-2);
X_H2  = Y(:,10*N+9:10:20*N-1);
X_A2  = Y(:,10*N+10:10:20*N);
X_I2  = Y(:,10*N+11:10:20*N+1);
L2    = Y(:,20*N+2);

save C:\MATLAB_data\S_O2.dat S_O2 -ascii -tabs;
save C:\MATLAB_data\S_S2.dat S_S2 -ascii -tabs;
save C:\MATLAB_data\S_NH2.dat S_NH2 -ascii -tabs;
```

```
save C:\MATLAB_data\S_NO2.dat S_NO2 -ascii -tabs;
save C:\MATLAB_data\S_N2.dat S_N2 -ascii -tabs;
save C:\MATLAB_data\S_ALK2.dat S_ALK2 -ascii -tabs;
save C:\MATLAB_data\X_S2.dat X_S2 -ascii -tabs;
save C:\MATLAB_data\X_H2.dat X_H2 -ascii -tabs;
save C:\MATLAB_data\X_A2.dat X_A2 -ascii -tabs;
save C:\MATLAB_data\X_I2.dat X_I2 -ascii -tabs;
save C:\MATLAB_data\L2.dat L2 -ascii -tabs;

% CASCADE 3
S_O3  = Y(:,20*N+3:10:30*N-7);
S_S3  = Y(:,20*N+4:10:30*N-6);
S_NH3 = Y(:,20*N+5:10:30*N-5);
S_NO3 = Y(:,20*N+6:10:30*N-4);
S_N3  = Y(:,20*N+7:10:30*N-3);
S_ALK3= Y(:,20*N+8:10:30*N-2);
X_S3  = Y(:,20*N+9:10:30*N-1);
X_H3  = Y(:,20*N+10:10:30*N);
X_A3  = Y(:,20*N+11:10:30*N+1);
X_I3  = Y(:,20*N+12:10:30*N+2);
L3    = Y(:,30*N+3);

save C:\MATLAB_data\S_O3.dat S_O3 -ascii -tabs;
save C:\MATLAB_data\S_S3.dat S_S3 -ascii -tabs;
save C:\MATLAB_data\S_NH3.dat S_NH3 -ascii -tabs;
save C:\MATLAB_data\S_NO3.dat S_NO3 -ascii -tabs;
save C:\MATLAB_data\S_N3.dat S_N3 -ascii -tabs;
save C:\MATLAB_data\S_ALK3.dat S_ALK3 -ascii -tabs;
save C:\MATLAB_data\X_S3.dat X_S3 -ascii -tabs;
save C:\MATLAB_data\X_H3.dat X_H3 -ascii -tabs;
save C:\MATLAB_data\X_A3.dat X_A3 -ascii -tabs;
save C:\MATLAB_data\X_I3.dat X_I3 -ascii -tabs;
save C:\MATLAB_data\L3.dat L3 -ascii -tabs;
```

h) Input_data.m

```
time    = 120;          % Simulation time in days
N=17;
rho1   = 45600;         % User input: Biofilm density in stage-I
rho2   = 60800;         % User input: Biofilm density in stage-II
rho3   = 48600;         % User input: Biofilm density in stage-III


L_Bf1  = 90;            % Initial biofilm thickness in µm
L_Bf2  = 60;            % Initial biofilm thickness in µm
L_Bf3  = 30;            % Initial biofilm thickness in µm

dx1    = L_Bf1/1000*(N-2)); % Stage-I Biofilm layer thickness in mm
dx2    = L_Bf2/1000*(N-2)); % Stage-II Biofilm layer thickness in mm
dx3    = L_Bf3/1000*(N-2)); % Stage-III Biofilm layer thickness in mm

Xs_in  = 10.00; Xh_in = 0; Xa_in = 0; Xi_in = 0; % Units in g/m3

% Initial conc. in influent for static inputs w.r.t. steady state runs
%ft = 0; So_in = 1.10; Ss_in = 215; Snh_in = 45; Sno_in = 0.70;
%Sn2_in  = 0; Salk_in = 6.00; Salk in mmol/m3

%Q = 68.0e-03/(3600*24); % Flow rate through the tank converted from m3/d
to m3/s

% Diffusivity values at 25°C in mm2/s
```

```
Do = 1.944e-003; Ds = 0.694e-003;Dnh = 1.574e-003;Dno = 1.481e-003; Dn =
1.900e-003; Dalk = 0.926e-003;
S_o_sat= 8.24;

% Diffusivity values at 30°C in mm2/s
%Do = 2.207e-003; %Ds = 0.788e-003;%Dnh = 1.787e-003;%Dno = 1.681e-003;
%Dn = 1.900e-003;%Dalk = 1.051e-003;

%S_o_sat= 7.54;
S_n2_sat=16; % g/m3 at 25°C
K_la = 0; % Oxygen transfer coefficient to tank from air transfer drive,
Units 1/s

P1 = (6.0e-9)*((1000)^2/(3600*24));% For particulates, diffusive flux
coefficient in mm2/s
P2 = (6.0e-9)*((1000)^2/(3600*24));
P3 = (6.0e-9)*((1000)^2/(3600*24));

k_floc1 =0.0;    % Units: m/d
k_floc2 =0.0;    % Units: m/d
k_floc3 =0.0;    % Units: m/d

k_shear1=66;                    % Exponential detachment; Units 1/(m.d)
k_shear2=300;                   % Exponential detachment; Units 1/(m.d)
k_shear3=300;                    % Exponential detachment; Units 1/(m.d)

% STAGE I
dlf1   = 60.0e-03;               % Liquid film thickness in mm
A_tot1 = 1.18;                    % Total area of biofilm in m2
A_sub1 = 0.42*A_tot1;            % Submerged area of biofilm in m2
V_lf1  = A_tot1*(dlf1/1000);      % Liquidiflm volume in m3
%V_bf1 = A_tot1 * L1;            % Initial Biofilm volume in m3
Qr     = 0/(3600*24);             % Recycle flow rate in m3/d
V1     = 5.80e-03;               % Tank Volume in m3

% STAGE II
dlf2   = 60.0e-03;                % Liquid film thickness in mm
A_tot2 = 0.98;                     % Total area of biofilm in m2
A_sub2 = 0.42*A_tot2;              % Submerged area of biofilm in m2
V_lf2  = A_tot2*(dlf2/1000);       % Liquidiflm volume in m3
%V_bf2 = A_tot2 * L2;             % Initial Biofilm volume in m3
V2     = 4.20e-03;                % Tank Volume in m3

% STAGE III
dlf3   = 60.0e-03;               % Liquid film thickness in mm
A_tot3 = 0.98;                    % Total area of biofilm in m2
A_sub3 = 0.42*A_tot3;             % Submerged area of biofilm in m2
V_lf3  = A_tot3*(dlf3/1000);      % Liquidiflm volume in m3
%V_bf3 = A_tot3 * L3;
V3     = 4.20e-03;               % Tank Volume in m3
```

i) Time series data file (e.g. daten_Sept_Dez.dat)

ft	So_in	Ss_in	Snh_in	Sno_in	Sn2_in	Salk_in	Q
s	g/m3	g/m3	g/m3	g/m3	g/m3	mol/m3	m3/s
0	1.2	215	45	0.7	0	6	7.87037E-07
3369600	1.2	215	45	0.7	0	6	7.87037E-07
3715200	1.2	215	45	0.7	0	6	7.87037E-07
3888000	1.2	215	45	0.7	0	6	7.87037E-07
4060800	1.2	215	45	0.7	0	6	7.87037E-07
4320000	1.2	215	45	0.7	0	6	7.87037E-07
4492800	1.2	215	45	0.7	0	6	7.87037E-07

```
4665600          1.2   215   45    0.7   0     6     7.87037E-07
5529600          1.2   215   45    0.7   0     6     7.87037E-07
6480000          1.2   215   45    0.7   0     6     7.87037E-07
6825600          1.2   215   45    0.7   0     6     7.87037E-07
7084800          1.2   215   45    0.7   0     6     7.87037E-07
7344000          1.2   215   45    0.7   0     6     7.87037E-07
7603200          1.2   215   45    0.7   0     6     7.87037E-07
8035200          1.2   215   45    0.7   0     6     7.87037E-07
8553600          1.2   215   45    0.7   0     6     7.87037E-07
9158400          1.2   215   45    0.7   0     6     7.87037E-07
9504000          1.2   215   45    0.7   0     6     7.87037E-07
10022400         1.2   215   45    0.7   0     6     7.87037E-07
10454400         1.2   215   45    0.7   0     6     7.87037E-07
```

Implementation of the RBC biofilm code

- The software required for implementation of the code is Matlab. The code files need to be saved with '.m' extension in a Matlab folder.
- User defined input data need to be given in the following files: Input_data.m, biokinetics.m and time series data-file, e.g. daten_Sept_Dez.dat. The list of variables for substitution by user defined values in each file is given below:

Notation	**Description**	**Unit**
N	Number of discrete biofilm layers plus 2 (1 for tank and 1 for LF), [default is 17]	-
time	Run time of simulation (need to be same as in the time-series data file)	d
L_Bf1	Initial average biofilm layer thickness in stage-1	µm
L_Bf2	Initial average biofilm layer thickness in stage-2	µm
L_Bf3	Initial average biofilm layer thickness in stage-3	µm
rho1	Total density of biofilm in stage-1 (1 for stage-1)	$gCOD/m^3$
rho2	Total density of biofilm in stage-2 (2 for stage-2)	$gCOD/m^3$
rho3	Total density of biofilm in stage-3 (3 for stage-3)	$gCOD/m^3$
Do	Diffusivity coefficient of oxygen in biofilm at given temperature T°C	mm^2/s
Ds	Diffusivity coefficient of sol. biodegradable org. substrate in biofilm at T°C	mm^2/s
Dnh	Diffusivity coefficient of ammonium-nitrogen in biofilm at T°C	mm^2/s
Dn	Diffusivity coefficient of gaseous nitrogen in biofilm at T°C	mm^2/s
Dno	Diffusivity coefficient of nitrate-nitrogen in biofilm at T°C	mm^2/s
Dalk	Diffusivity coefficient of bicarbonates (alkalinity) in biofilm at T°C	mm^2/s
P1, P2, P3	Diffusivity coefficient of particulate components in biofilm in resp. stages	mm^2/s
S_o_sat	Saturation concentration of oxygen in water at T°C	gO_2/m^3
S_n2_sat	Saturation concentration of nitrogen gas in water at T°C	gN/m^3
K_la	Oxygen transfer coefficient in bulk from air drive mode	1/s
k_floc	Rate of attachment of solids from bulk to the biofilm surface in any stage	m/d
k_shear	Rate of detachment of solids from biofilm surface into tank in any stage	1/(m.d)
dlf	Liquid film thickness in any stage	mm

A_tot	Total interfacial area of biofilm in any stage	m^2
A_sub	Submerged area of biofilm in any stage (% of A_tot)	m^2
Q	Flow rate through any tank	m^3/s
Qr	Recirculation flow rate in the system	m^3/s
V	Bulk liquid volume in any stage	m^3
So_in	Influent oxygen concentration in stage-1	gO_2/m^3
Ss_in	Influent soluble biodegradable organic substrate concentration in stage-1	$gCOD/m^3$
Snh_in	Influent ammonium-nitrogen concentration in stage-1	$gNH_4\text{-}N/m^3$
Sn2_in	Influent gaseous nitrogen concentration in stage-1	$gNO_2\text{-}N/m^3$
Sno_in	Influent nitrate-nitrogen concentration in stage-1	$gNO_3\text{-}N/m^3$
Salk_in	Influent alkalinity concentration (as bicarbonate) in stage-1	mol HCO_3/m^3
Xs_in	Initial concentration of suspended solids in stage-1	$gCOD/m^3$
Xh_in	Initial concentration of heterotrophs bacteria in stage-1	$gCOD/m^3$
Xa_in	Initial concentration of autotrophs in biofilm layers in stage-1	$gCOD/m^3$
Xi_in	Initial concentration of inert particulate matter in stage-1	$gCOD/m^3$
Kinetic parameters for heterotrophic organisms, X_H		
mhu_H	Maximum growth rate of heterotrophic micro-organisms	1/d
K_H_O2	Saturation constant for oxygen S_O	gO_2/m^3
K_SS	Saturation constant for soluble organic substrate S_S	$gCOD/m^3$
K_H_NH	Saturation constant for ammonium nitrogen S_{NH}	$gNH_4\text{-}N/m^3$
K_H_NO	Saturation constant for nitrate nitrogen S_{NO}	$gNO_3\text{-}N/m^3$
K_H_ALK	Saturation constant for bicarbonate S_{ALK}	mol HCO_3/m^3
b_H	Aerobic endogenous respiration rate of heterotrophic micro-organisms	1/d
eta_H	Anoxic reduction factor for endogenous respiration	-
theta_DEN	Anoxic reduction factor for denitrification	-
Kinetic Parameters for autotrophs, X_A		
mhu_A	Maximum growth rate of ammonium oxidizing micro-organisms	1/d
K_A_O2	Saturation constant for oxygen S_O	gO_2/m^3
K_A_NH	Saturation constant for ammonium nitrogen S_{NH}	gN/m^3
K_A_NO	Saturation constant for nitrate nitrogen S_{NO}	gN/m^3
K_A_ALK	Saturation constant for bicarbonate S_{ALK}	mol HCO_3/m^3
b_A	Aerobic endogenous respiration rate ofautotrophs	-
eta_A	Anoxic reduction factor for endogenous respiration	-
Stoichiometric Parameters		
Y_H_O2	Aerobic yield of heterotrophic biomass	gCOD X_H/gCODS_S
Y_H_NO	Anoxic yield of heterotrophic biomass	gCOD X_H/gCODS_S
Y_A	Aerobic yield of autotrophs	gCOD X_A/gN S_{NH}
i_nbm	Nitrogen content of biomass	gN/gCOD $X_{H/A}$
i_nxi	Nitrogen content of inert particulate matter, X_I	gN/gCOD X_I
f_i	Production of X_I in endogenous respiration	gCOD X_I/gCOD $X_{H/A}$

- The output file can be saved at a desired location by defining the path for storage. The data may be stored as .dat or .txt format by suffixing the relevant extension. It is stored in tab separated ASCII format for further processing in data processing software like MS-excel or ultra-edit.
- After a simulation runs, Matlab provides graphical display of the variables solved with time in each RBC stage automatically. The plots may be saved in jpeg or other picture formats. If necessary, more plots can also be made in Matlab from the output data matrix.
- After the run, Matlab command window also displays the time taken in the simulation in seconds. In some cases, when an input data changes too suddenly with time, the solver may display integration time-step error and stop the simulations at that point. To overcome such cases, it is advisable to make the variation in the input variable smoother with time.

Appendix III Numerical methodology for solution of differential equations

Parabolic equations

The mathematical representation of most problems in science involving rates of change with respect to two or more independent variables such as time and space lead to partial differential equation. An important family of equation that is often encountered in engineering is based on the following equation:

$$a\frac{\partial^2 f}{\partial x^2} + b\frac{\partial^2 f}{\partial x.\partial y} + c\frac{\partial^2 f}{\partial y^2} = 0 \qquad (1)$$

where

f some variable such as concentration or velocity of a substance

If b^2-4ac = 0, equation (1) takes the form as shown below:

$$\frac{\partial f}{\partial x} = c\frac{\partial^2 f}{\partial y^2} \qquad (2)$$

Such equations are called parabolic equations which is encountered in problems involving diffusion of a property say concentration. Here x may represent the independent variable time, while y could represent the other independent variable space.

Discretization of differential equations in finite-difference approximation

When analytical solutions are not available, numerical method seem to be the best possible solution strategy. A numerical solution provides numbers that represent the behaviour of a variable, although it has its limitations. It can provide such numbers only at certain discrete locations in a space-time domain. The algebraic equations used to form the numerical model are based on finite differences. These finite difference expressions are approximations to the equivalent differential equations. Most finite difference expressions are based on Taylor series expansion. The Taylor expansion of a function for a differential increase in the value of the dependent variable x may be expressed as follows:

$$f(x+\Delta x) = f(x) + \frac{\partial f(x)}{\partial x}\Delta x + \frac{\partial^2 f(x)}{\partial x^2}\frac{\Delta x^2}{2!} + \ldots\ldots\ldots + \frac{\partial^n f(x)}{\partial x^n}\frac{\Delta x^n}{n!} \qquad (3)$$

Similarly, a small decrement in the variable value x would expand as follows:

$$f(x-\Delta x) = f(x) - \frac{\partial f(x)}{\partial x}\Delta x + \frac{\partial^2 f(x)}{\partial x^2}\frac{\Delta x^2}{2!} - \ldots\ldots\ldots \pm \frac{\partial^n f(x)}{\partial x^n}\frac{\Delta x^n}{n!} \qquad (4)$$

When the higher terms after the second order are neglected, the resultant error is known as truncation error. Rearranging the equation (3) would yield the following:

$$\underbrace{\frac{\partial f(x)}{\partial x}}_{\text{partial derivative}} = \underbrace{\frac{f(x+\Delta x)-f(x)}{\Delta x}}_{\text{forward difference}} - \underbrace{\frac{\partial^2 f(x)}{\partial x^2}\frac{\Delta x^2}{2!}}_{\text{truncation error}} + \text{higher} - \text{order terms} \tag{5}$$

This indicates that the partial differential equation is being approximated. As the finite difference is obtained by subtracting f(x) from f(x+Δx), this is known as forward difference method. Similarly for equation (4), the rearrangement would result in the following expression:

$$\underbrace{\frac{\partial f(x)}{\partial x}}_{\text{partial derivative}} = \underbrace{\frac{f(x)-f(x-\Delta x)}{\Delta x}}_{\text{backward difference}} + \underbrace{\frac{\partial^2 f(x)}{\partial x^2}\frac{\Delta x^2}{2!}}_{\text{truncation error}} + \text{higher} - \text{order terms} \tag{6}$$

Equation (6) represents the backward difference method of finite-difference approximation. When this equation is subtracted form equation (5), the solution for the second-order derivative could be obtained as shown below:

$$\frac{\partial^2 f(x)}{\partial x^2} = \frac{f(x+\Delta x)-2f(x)+f(x-\Delta x)}{\Delta x^2} + \text{truncation error} \tag{7}$$

This also represents the central difference method. Apart from the **truncation error** generated by neglecting the higher terms of the Taylor expansion, the other error called **rounding error** originates from a finite accuracy in computers up to a significant number of digits.

Explicit and implicit solutions

For the parabolic equation (2), if function f represents the concentration of a substance C, while time and space are the independent variables, x may be replaced with t and y with x. The constant c may be substituted by diffusivity coefficient D. This will result in the following equation:

$$\frac{\partial C}{\partial t} = D\frac{\partial^2 C}{\partial x^2} \tag{8}$$

This is the general form of the diffusion equation. If there is an additional process involved such as chemical transformation reaction R, the equation (8) may be represented as follows:

$$\frac{\partial C}{\partial t} = D\frac{\partial^2 C}{\partial x^2} + R \tag{9}$$

A simple finite difference application on both the sides of the equation would result in the full discretization as shown below.

$$\frac{C^{x}_{t+\Delta t} - C^{x}_{t}}{\Delta t} = D\left[\frac{C^{x+\Delta x}_{t} - 2C^{x}_{t} + C^{x-\Delta x}_{t}}{\Delta x^{2}}\right] + R^{x}_{t} \quad (10)$$

where R^{x}_{t} indicates the reaction at time t and space co-ordinate x. Therefore, the solution for the next time-step $C^{x}_{t+\Delta t}$ would be as follows:

$$C^{x}_{t+\Delta t} = C^{x}_{t} + D\left(\frac{\Delta t}{\Delta x^{2}}\right)\left[C^{x+\Delta x}_{t} - 2C^{x}_{t} + C^{x-\Delta x}_{t}\right] + R^{x}_{t}.\Delta t \quad (11)$$

Equation (11) can be easily solved in a grid-structure when the boundary values of x and initial value of t is given. The above solution represents the **explicit mode** of finite difference approximation. The boundary conditions and the initial condition define the domain of the solution.

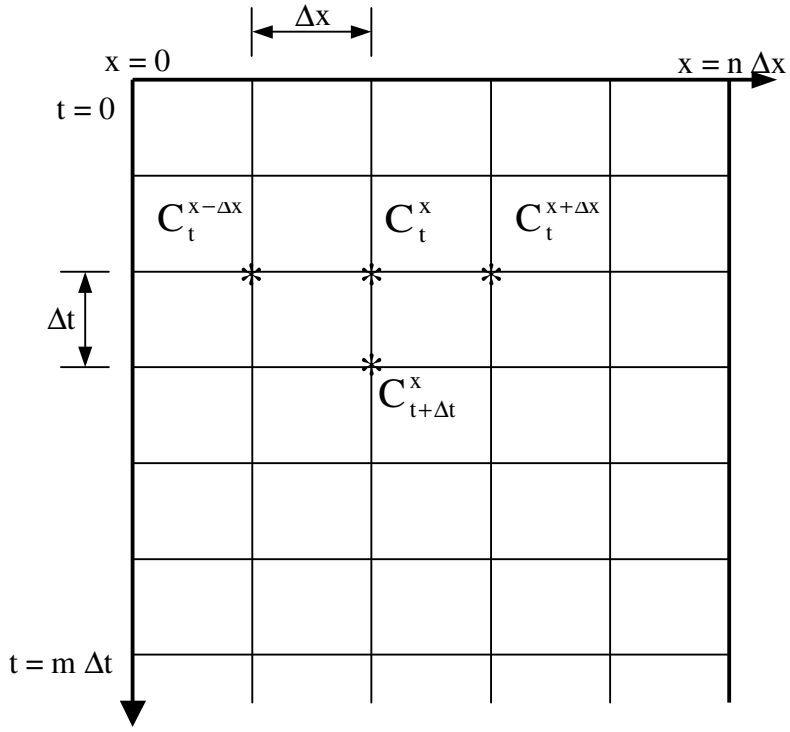

Figure 78 Grid-structure showing spatial and temporal discretization in finite-difference solution methodology

Figure 78 shows the grid-structure used in calculation of the solution to partial differential equations by finite difference method. 'm' represents the number of time steps, while 'n' represents the number of spatial discretization points. For small finite time intervals, explicit method presents the ideal solution with fixed time steps and can give high convergence. **This methodology was implemented as the solution methodology in the physical oxygen diffusion model.** Here, convergence implies that the numerical solution approaches the analytical solution as $\Delta x, \Delta t \to 0$. However, to attain stability, this method needs to satisfy a rigid criteria for r as shown below:

$$0 < r \le \frac{1}{2} \text{ where } r = \frac{\Delta t}{\Delta x^2} \tag{12}$$

$$\text{i.e } \Delta t \le \frac{1}{2}\Delta x^2 \tag{13}$$

Therefore, if Δx is very small for better accuracy, Δt would be infinitesimal and sometimes and this would require very large number of time steps and hence computational time. This is the main weakness of this method in solving equations for large time intervals.

In case of **implicit method**, the spatial properties of function C are based on the average of the values at time levels t and (t+Δt). In other words, in the right-hand side of expression (10), $C_t^{x+\Delta x}$ now becomes:

$$C^{x+\Delta x}_{t+\frac{\Delta t}{2}} = \frac{C_t^{x+\Delta x} + C_{t+\Delta t}^{x+\Delta x}}{2} \tag{14}$$

Similarly, C_t^x and $C_t^{x-\Delta x}$ now becomes:

$$C^{x}_{t+\frac{\Delta t}{2}} = \frac{C_t^{x} + C_{t+\Delta t}^{x}}{2} \tag{15}$$

$$C^{x-\Delta x}_{t+\frac{\Delta t}{2}} = \frac{C_t^{x-\Delta x} + C_{t+\Delta t}^{x-\Delta x}}{2} \tag{16}$$

Therefore, equation (9) may now be solved based on equation (10) as follows:

$$\frac{\partial C}{\partial t} = D\frac{\left[\left(C_t^{x+\Delta x} + C_{t+\Delta t}^{x+\Delta x}\right)/2\right] - \left[C_t^{x} + C_{t+\Delta t}^{x}\right] + \left[\left(C_t^{x-\Delta x} + C_{t+\Delta t}^{x-\Delta x}\right)/2\right]}{\Delta x^2} + R_t^x \tag{17}$$

To solve this form of finite-difference equation, function values at two time levels are needed. The values at time level t are known, but those at (t+Δt) are not known and need to be determined. The solution method employed for this approach requires the simultaneous solution of the finite difference equations for all x grid points. This method is superior to the explicit method for large time intervals although computationally intensive in nature. It minimizes the inflexible stability criteria of explicit solution which reduces the total volume of calculation while being valid (i.e. convergent and stable) for all values of r. This method is often referred to as Crank-Nicolson implicit method.

Due to the flexibility of implicit method, it was the ideal choice for solving the system of partial differential equations through the ode solver in the biofilm model. The first step was the discretization of the spatial derivates based on equation (5) and (7) for the first order and the second order partial differential equations respectively. This led to a system of ordinary differential equation in the time variable. In the next step, an ordinary differential equation (ode) solver was employed to solve the semi-discrete system. Although the non-stiff solvers like Runga-Kutta-4 are relatively more stable and accurate numerically, they are very

slow for long runs and often not so vital when many other aspects of biofilm modelling are hypothetical in nature. Owing to the stiff nature of problem, a variable time step solver based on implicit formulae was required. In Matlab software, ode15s is a variable order solver based on the numerical differentiation formulas (NDF). Options allowed integration of the NDF with the backward differentiation formulas (also known as Gear's method). Backward differences are very suitable for implementing the NDF's in Matlab for solving stiff problems because the basic algorithms can be coded compactly and efficiently. It generated high stability with quasi-constant step-size. So this was activated to attain steady results.

Schriftenreihe SWW - Karlsruhe

Bisher aus der Arbeit am Institut erschienen

[1] KARPE, H.-J.: Zur Wirtschaftlichkeit bei der Planung von Fernwasserversorgungen. Karlsruhe 1969 (Eigenverlag des Verfassers).

[2] PÖPEL, J.: Schwankungen von Kläranlagenabläufen und ihre Folgen für Grenzwerte und Gewässerschutz. GWF, Schriftenreihe Wasser - Abwasser, 16. Oldenbourg Verlag, München 1971.

[3] MEIER, P.M.: Möglichkeiten zur technischen und wirtschaftlichen Optimierung von Zweckverbänden. Wasser und Abwasser in Forschung und Praxis, Bd. 4. Erich Schmidt Verlag, Bielefeld 1972.

[4] ABENDT, R.; AHRENS; W.; CEMBROWICZ, R.G.; HAHN, H.H.; KNOBLAUCH, A.; ORTH, H.: Operations Research und seine Anwendung in der Siedlungswasserwirtschaft I. Wasser und Abwasser in Forschung und Praxis, Bd. 5. Erich Schmidt Verlag, Bielefeld 1972.

[5] NOLL, K.: Untersuchungen zur Grundwasserentnahme aus den pleistozänen Sedimenten des Rheintalgrabens im Rhein-Neckar-Raum. Karlsruhe 1972 (Eigenverlag des Verfassers).

[6] NEIS, U.: Experimentelle Bestimmung der Stabilität anorganischer Schwebstoffe in natürlichen Gewässern. Karlsruhe 1974 (Eigenverlag des Verfassers).

[7] AHRENS, W.: Optimierungsverfahren zur Lösung nichtlinearer Investitionsprobleme - angewandt auf das Problem der Planung regionaler Abwasserentsorgungssysteme. Quantitative Methoden der Unternehmensplanung, Bd. 4. Verlag Meisenheim/Glahn 1975.

[8] ORTH, H.: Verfahren zur Planung kostenminimaler regionaler Abwasserentsorgungssysteme. Wasser und Abwasser in Forschung und Praxis, Bd. 9. Erich Schmidt Verlag, Bielefeld 1975.

[9] MOSEBACH, K.G.: Phosphatrücklösung bei der Ausfaulung von Simultanschlämmen. Wasser und Abwasser in Forschung und Praxis, Bd. 11. Erich Schmidt Verlag, Bielefeld 1975.

[10] AHRENS, W.; CEMBROWICZ, R.G.; DEHNERT, G.; HEISS, H.-J.; HAHN, H.H.; HENSELEIT, H.J.; ORTH, H.; SENG, H.J.: Operations Research und seine Anwendung in der Siedlungswasserwirtschaft II. Wasser und Abwasser in Forschung und Praxis, Bd. 12. Erich Schmidt Verlag, Bielefeld 1976.

[11] DEHNERT, G.: Regionale Planung der Standorte für Abwasserbehandlungsanlagen mit Hilfe graphentheoretischer Algorithmen. Abfallwirtschaft in Forschung und Praxis, Bd. 1. Erich Schmidt Verlag, Bielefeld 1976.

[12] HAHN, H.H. (Hrsg.): Umweltschutz im Bereich des Wasserbaus. Wasser und Abwasser in Forschung und Praxis, Bd. 14. Erich Schmidt Verlag, Bielefeld 1976.

[13] JØRGENSEN, S.E.: Reinigung häuslicher Abwässer durch Kombination eines chemischen Fällungs- und Ionenaustauschverfahrens. Karlsruhe 1976 (Eigenverlags des Verfassers).

[14] RUF, J.: Gewässergütesimulation unter Berücksichtigung meteorologischer Einflüsse. Prognostisches Modell Neckar, Bericht 16. Dornier System. Friedrichshafen 1977.

[15] AHRENS, W.; DEHNERT, G.; DURST, F.; GERBER, J.; HAHN, H.H.; PAESSENS, H.; WEUTHEN, H.K.: Tourenplanung bei der Abfallbeseitigung. Abfallwirtschaft in Forschung und Praxis, Bd. 3. Erich Schmidt Verlag, Bielefeld 1977.

[16] KLUTE, R.: Adsorption von Polymeren an Silikaoberflächen bei unterschiedlichen Strömungsbedingungen. Karlsruhe 1977 (Eigenverlag des Verfassers).

[17] KNOBLAUCH, A.: Mathematische Simulation des Phopsphorkreisaufs in einem gestauten Gewässer. GWF, Schriftenreihe Wasser- Abwasser, Bd. 17. Oldenbourg Verlag, München 1978.

[18] ABENDT, R.: Aussagefähigkeit von Sauerstoffhaushaltsrechnungen. Hochschulsammlung Ingenieurwissenschaft, Wasserwirtschaft, Bd. 1. Hochschulverlag, Stuttgart 1978.

[19] SENG, H.J.: Systematische Beurteilung der Umweltverträglichkeit bei Abfalldeponiestandorten. Hochschulsammlung Ingenieurwissenschaft, Abfallwirtschaft, Bd. 2. Hochschulverlag, Stuttgart 1979.

[20] INSTITUT FÜR SIEDLUNGSWASSERWIRTSCHAFT: Fortschritte bei der Anwendung von Flockungsverfahren in der Abwassertechnologie. 2. Verfahrensstechnisches Seminar. Karlsruhe 1979 (Eigenverlag des Instituts, vergriffen).

[21] HAHN, H.H. (Hrsg.): Von der Abfallbeseitigung zur Abfallwirtschaft, Fachkolloquium zu Ehren von Prof. Dr.-Ing. Hans Straub, Karlsruhe 1980 (Eigenverlag des Instituts, vergriffen).

[22] INSTITUT FÜR SIEDLUNGSWASSERWIRTSCHAFT: Planung und Organisation von Einzelkläranlagen und Gruppenkläranlagen, 6. Planungstechnisches Seminar. Karlsruhe 1980 (Eigenverlag des Instituts).

[23] KÄSER, F.: Transport suspendierter Feststoffe in Fließgewässern. Karlsruhe 1981 (Eigenverlag des Instituts, vergriffen).

[24] EPPLER, B.: Aggregation von Mikroorganismen. Karlsruhe 1981 (Eigenverlag des Instituts, vergriffen).

[25] INSTITUT FÜR SIEDLUNGSWASSERWIRTSCHAFT: Fortschritte bei der Anwendung des Flotationsverfahrens in der kommunalen Abwasserreinigung, 3. Verfahrenstechnisches Seminar. Karlsruhe 1981 (Eigenverlag des Instituts).

[26] PAESSENS, H.: Tourenplanung bei der regionalen Hausmüllentsorgung. Karlsruhe 1981 (Eigenverlag des Instituts).

[27] KIEFHABER, K.P.: Versuchsanlagen zur Entspannungsflotation von Abwasser - Vergleich von Versuchsergebnissen. Karlsruhe 1982 (Eigenverlag des Instituts, vergriffen).

[28] HAHN, H.H.; SENG, H.J. (Hrsg.): Wirtschaftlichkeit in der Abfallwirtschaft. Karlsruhe 1982 (Eigenverlag des Instituts).

[29] HAHN, H.H.; PAESSENS, H. (Hrsg.): Tourenplanung in der Abfallwirtschaft II. Karlsruhe 1982 (Eigenverlag des Instituts).

[30] DICKGIESSER, G.: Betriebssichere und wirtschaftliche Klärschlammentsorgung. Karlsruhe 1982 (Eigenverlag des Instituts, vergriffen).

[31] HAHN, H.H. (Hrsg.): Wasserversorgung und Abwasserbehandlung in Entwicklungsländern. Karlsruhe 1982 (Eigenverlag des Instituts).

[32] HAHN, H.H. (Hrsg.): Schlämme aus der Abwasserfällung/-flockung. Karlsruhe 1983 (Eigenverlag des Instituts).

[33] v. FALKENHAUSEN, K.: Planung eines Entsorgungssystems für die Klärschlammbehandlung. Karlsruhe 1983 (Eigenverlag des Instituts).

[34] HEISS, H.-J.: Stabilität kostenminimaler Lösungen bei der Planung von Abwasserentsorgungssystemen. Karlsruhe 1983 (Eigenverlag des Instituts).

[35] HAHN, H.H. (Hrsg.): Planung im Gewässerschutz unter besonderer Berücksichtigung von Flussgebietsmodellen. Karlsruhe 1984 (Eigenverlag des Instituts, vergriffen).

[36] BANTZ, I.: Ein Rechenverfahren zur Darstellung der Auswirkungen von Stoßbelastungen auf die Qualität von Fließgewässern. Karlsruhe 1985 (Eigenverlag des Instituts, vergriffen).

[37] LÖHR, J.: Einfluss der Tiefendurchmischung auf die Entwicklung von Phytoplankton - dargestellt am Beispiel des Maines. Karlsruhe 1984 (Eigenverlag des Instituts).

[38] TROUBOUNIS, G.: Strukturorientierte Simulation des Kohlenstoff, Stickstoff-, Phosphor- und Sauerstoffhaushaltes flacher Gewässer. Karlsruhe 1985 (Eigenverlag des Instituts, vergriffen).

[39] DITTRICH, A.: Transport und Sedimentation organischer Stoffe in Abwasserteichen. Karlsruhe 1985 (Eigenverlag des Instituts, vergriffen).

[40] GROHMANN, A.; HAHN, H.H.; KLUTE, R. (Hrsg.): Chemical Water and Wastewater Treatment. Practical Experience and New Concepts. Proceedings from the 1st Gothenburg Symposium, 1984. Gustav Fischer Verlag, Stuttgart, New York, 1985 (vergriffen).

[41] HAHN, H.H.; NEIS, U. (Hrsg.): Belastungsschwankungen auf Kläranlagen: Auswirkungen und Möglichkeiten zur Reduktion, insbesondere durch Chemikalieneinsatz. Karlsruhe 1985 (Eigenverlag des Instituts).

[42] SCHMITT, T.G.: Der instationäre Kanalabfluss in der Schmutzfrachtmodellierung. Karlsruhe 1985 (Eigenverlag des Instituts, 2. Auflage).

[43] IOSSIFIDIS, V.: Die Rolle der Ablagerungen bei der Schmutzfrachtberechnung in Kanalisationsnetzen. Karlsruhe 1985 (Eigenverlag des Instituts, 2. Auflage).

[44] SCHMITT, T.G.; HAHN, H.H. (Hrsg.): Schmutzfrachtberechnung für Kanalisationsnetze. Karlsruhe 1986 (Eigenverlag des Instituts, 2. Auflage).

[45] DÖLL, B.: Die Kompensation der Oberflächenladung kolloidaler Silika-Suspensionen durch die Adsorption kationischer Polymere in turbulent durchströmten Rohrreaktoren. Karlsruhe 1986 (Eigenverlag des Instituts).

[46] MERTSCH, V.: Sedimentation, Eindickung und Entwässerung von Fällungs-/Flokkungsschlämmen. Karlsruhe 1987 (Eigenverlag des Instituts, vergriffen).

[47] KORDES, B.: Berechnung der Energiebilanz von Kläranlagen unter Berücksichtigung zeitlicher Schwankungen. Karlsruhe 1987 (Eigenverlag des Instituts, vergriffen).

[48] GEPPERT, B.: Tourenplanung bei der innenstädtischen Hausmüllentsorgung. Karlsruhe 1987 (Eigenverlag des Instituts).

[49] GUTEKUNST, B.: Sielhautuntersuchungen zur Einkreisung schwermetallhaltiger Einleitungen. Karlsruhe 1988 (Eigenverlag des Instituts).

[50] HAHN, H.H.; KLUTE, R.; BALMER, P. (Hrsg.): Recycling in Chemical Water and Wastewater Treatment. Proceedings from the 2nd international Gothenburg Symposium. Karlsruhe 1986 (Eigenverlag des Instituts).

[51] HAHN, H.H.; PFEIFER, R.; (Hrsg.): Abwasserreinigung in Entwicklungsländern mit besonderer Berücksichtigung der Industrie. Karlsruhe 1987 (Eigenverlags des Instituts).

[52] HOFFMANN, E.: Strömungsstrukturen in Flockungsreaktoren. (in Vorbereitung).

[53] HAHN, H.H.; PFEIFER, R. (Hrsg.): Fällung/Flockung - Erfahrungen aus Labor und Praxis. Karlsruhe 1990 (Eigenverlag des Instituts).

[54] KRÜGER, E.M.: Stabilität mineralischer Basisabdichtungen von Hausmülldeponien bezüglich des Ausbreitungsverhaltens anorganischer Schadstoffe. Karlsruhe 1989 (Eigenverlag des Instituts).

[55] Siskos, D.: Kläranlagenauslegung für stehende Vorfluter. Karlsruhe 1989 (Eigenverlag des Instituts).

[56] HOU, R.: Kontrollstrategien für Fällung und Flockung auf Kläranlagen mit einem Vorhersagemodell der Zu- und Ablauffracht. Karlsruhe 1990 (Eigenverlag des Instituts).

[57] Xanthopoulos, C.: Methode für die Entwicklung von Modellregenspektren für die Schmutzfrachtberechnung. Karlsruhe 1990 (Eigenverlag des Instituts).

[58] HAHN, H.H.; XANTHOPOULOS, C. (Hrsg.): Schadstoffe im Regenabfluss aus städtischen Gebieten - Präsentation eines BMFT - Verbundprojektes. Karlsruhe 1990 (Eigenverlag des Instituts, vergriffen).

[59] LEE, C.-M.: Tone zur physikalisch-chemischen Abwasserreinigung. Karlsruhe 1990 (Eigenverlag des Instituts).

[60] HARTMANN, K.-H.: Anaerobe Behandlung von Sickerwässern aus Hausmülldeponien. Karlsruhe 1991 (Eigenverlag des Instituts).

[61] HAHN, H.H.; PFEIFER, R. (Hrsg.): Vor-, Simultan- oder Nachfällung? – Entscheidungskriterien für Planung, Entwurf und Betrieb. Karlsruhe 1991 (Eigenverlag des Instituts).

[62] LEONHARD, D.: Eindickung und Entwässerung als Konsolidierungsvorgang. Karlsruhe 1992 (Eigenverlag des Instituts).

[63] WEISSER, M.: Untersuchungen zur Belastung kommunaler Klärschlämme durch organische Schadstoffe - Abschlußbericht zum BMFT-Forschungsvorhaben 02 WS 464/8. Karlsruhe 1992 (Eigenverlag des Instituts, 2. Auflage).

[64] HAHN, H.H.; XANTHOPOULOS, C. (Hrsg.): Schadstoffe im Regenabfluss II. Präsentation des BMFT-Verbundprojektes. Karlsruhe 1992 (Eigenverlag des Instituts, 2. Auflage).

[65] HAHN, H.H.; PFEIFER, R. (Hrsg.): Sanierung von Kläranlagen. Karlsruhe 1992 (Eigenverlag des Instituts).

[66] DÜRETH-JONECK, S.: Entwicklung eines naturnahen, praxisorientierten. Mobilitätstests für Schwermetalle und Arsen in kontaminierten Böden. Karlsruhe 1993 (Eigenverlag des Instituts).

[67] HAHN, H.H.; TRAUTH, R. (Hrsg.): Fällungs-/Flockungschemikalien. Anforderungen, Angebot, Auswahl und Qualität. Karlsruhe 1993 (Eigenverlag des Instituts, vergriffen).

[68] HAHN, H.H.; TRAUTH, R. (Hrsg.): Wechselwirkungen der biologischen und chemischen Phosphorelimination. Karlsruhe 1993 (Eigenverlag des Instituts).

[69] LANGER, S.J.: Struktur und Entwässerungsverhalten polymergeflockter Klärschlämme. Karlsruhe 1994 (Eigenverlag des Instituts).

[70] MÜLLER, N.: Gewässergütemodellierung von Fließgewässern unter Berücksichtigung qualitativer, quantitativer, flächenhafter und sozioökonomischer Informationen. Karlsruhe 1994 (Eigenverlag des Instituts).

[71] HAHN; H.H.; TRAUTH, R. (Hrsg.): Klärschlamm - Ressource oder kostenintensiver Abfall? Karlsruhe 1994 (Eigenverlag des Instituts).

[72] MIHOPULOS, J.: Wechselwirkung Flockenbildung - Flockenabtrennung unter Berücksichtigung der Durchströmungsmuster in Sedimentations- und Flotationsbecken. München 1995 (Oldenbourg Verlag).

[73] XANTHOPOULOS, C.; HAHN, H.H. (Hrsg.): Schadstoffe im Regenabfluss III. München 1995 (Oldenbourg Verlag).

[74] HAHN, H.H.; TRAUTH, R. (Hrsg.): Wirtschaftlichkeitsfragen in der Abwasserreinigung. München 1995 (Oldenbourg Verlag).

[75] SCHMID, K.: Tensidunterstützte und biologische Sanierung der Feinkornfraktion aus der Bodenwäsche bei kohlenwasserstoffhaltigen Altlasten. München 1996 (Oldenbourg Verlag).

[76] HÖLZER, D.: EDV-gestützte Planung von Belebtschlammanlagen unter Berücksichtigung betrieblicher Aspekte. München 1996 (Oldenbourg Verlag).

[77] HARITOPOULOU, T.: Polycyclische Aromatische Kohlenwasserstoffe und Schwermetalle in urbanen Entwässerungssystemen - Aufkommen, Transport und Verbleib. München 1996 (Oldenbourg Verlag).

[78] HAHN, H.H.; TRAUTH, R.: Wechselwirkung zwischen Einzugsgebiet und Kläranlage. München 1996 (Oldenbourg Verlag).

[79] FUCHS, S.: Wasserwirtschaftliche Konzepte und ihre Bedeutung für die Ökologie kleiner Fließgewässer - Aufgezeigt am Beispiel der Mischwasserbehandlung. München 1997 (Oldenbourg Verlag).

[80] BEUDERT, G.: Gewässerbelastung und Stoffaustrag von befestigten Flächen in einem kleinen ländlichen Einzugsgebiet. München 1997 (Oldenbourg Verlag) .

[81] WITT, P.CH.: Untersuchungen und Modellierungen der biologischen Phosphatelimination in Kläranlagen. München 1997 (Oldenbourg Verlag).

[82] PSCHERA, S.: Abwasserbehandlung mit Ozon: Klassifizierung von Abwasser zur optimierten Verfahrensgestaltung in der Kreislaufwirtschaft. München 1997 (Oldenbourg Verlag).

[83] TRAUTH, R.: Lokalisierung von Grundwasserschadstoffquellen in urbanen Räumen. München 1998 (Oldenbourg Verlag).

[84] JAKOBS, J.: Quantifizierung der Wirkung von Kanalnetzbewirtschaftungsmaßnahmen mit Hilfe des detailliert hydrodynamischen Schmutzfrachtmodells HAuSS. München 1998 (Oldenbourg Verlag).

[85] XANTHOPOULOS, C.: Stoffströme in der Urbanhydrologie Teil 1 – Oberfläche. München 1998 (Oldenbourg-Verlag).

[86] SCHMITT, T.G.: Stoffströme in der Urbanhydrologie Teil 2 - Kanalisaton. München 1997 (Oldenbourg Verlag).

[87] SEYFRIED, C.F.: Stoffströme in der Urbanhydrologie Teil 3 – Kläranlage. München 1998 (Oldenbourg Verlag).

[88] HAHN, H.H.; SCHÄFER, M. (Hrsg.): Stoffströme in der Urbanhydrologie Teil 4 - Emission/Immission. München 1998 (Oldenbourg Verlag).

[89] HAHN, H.H.; WILHELMI, M.: Abwasserreinigung - Reststoffproblem oder Sekundärrohstoffquelle. München 1997 (Oldenbourg Verlag).

[90] SCHULZ, ST.: Der Kanal als Reaktor: Neubildung von AOX durch Wirkstoffe in Reinigungsmitteln. München 1998 (Oldenbourg Verlag).

[91] WOLTER, CH.: Steuer- und Regelkonzepte der Vorklärung unter Einbeziehung der Vorfällung/Flockung und Schlammhydrolyse. München 1998 (Oldenbourg Verlag).

[92] PFEIFER, R.: Schmutzstoffrückhalt durch chemisch/physikalische Regenwasserbehandlung im Trennsystem. München 1998 (Oldenbourg Verlag).

[93] LIN, L.Q.: Entstabilisierung und Aggregation von Silika und Huminsäure mit Aluminiumsalzen in turbulenten Rohrströmungen. München 1998 (Oldenbourg Verlag).

[94] HAHN, H.H.; WILHELMI, M. (Hrsg.): Abwasserfällung- und Flockung. München 1998 (Oldenbourg Verlag).

[95] HUPPERT, N.: Elimination von Ibuprofen und NBBS in kommunalen Kläranlagen analysiert mittels Festphasenmikroextraktion. München 1999 (Oldenbourg Verlag).

[96] FUCHS, S.; HAHN, H.H. (Hrsg.): Schadstoffstoffe im Regenabfluss IV. Abschlusspräsentation des BMBF-Verbundprojektes NIEDERSCHLAG. München 1999 (Oldenbourg Verlag).

[97] SCHÄFER, M.: Regionalisierte Stoffstrombilanzen in städtischen Einzugsgebieten - Möglichkeiten, Probleme und Schlussfolgerungen.

[98] HAHN, H.H.; KRAUS, J. (Hrsg.): Technologische Aspekte der Wasser-, Abwasser- und Schlammbehandlung. Karlsruhe 1999 (Universität Karlsruhe - Institutsverlag Siedlungswasserwirtschaft).

[99] KISHI, R.T.: Einzugsgebietseigenschaften und Fließgewässergüte (Modellierung stofflicher Parameter mit Hilfe raumbezogener Daten). Karlsruhe 2000 (Universität Karlsruhe - Institutsverlag Siedlungswasserwirtschaft).

[100] NAUDASCHER, I.: Kompostierung menschlicher Ausscheidungen durch Verwendung biologischer Trockentoiletten - mit besonderer Berücksichtigung des Kleingartenbereichs. Karlsruhe 2001 (Universität Karlsruhe - Institutsverlag Siedlungswasserwirtschaft).

[101] ANDERS, G.: Der Einsatz von Scheibentauchkörpern zur Güllebehandlung mit dem Ziel der weitergehenden Nährstoffreduktion. Karlsruhe 2002 (Universität Karlsruhe - Institutsverlag Siedlungswasserwirtschaft).

[102] WITTLAND, C.: Angepasste Verfahren zur Industrieabwassererreinigung - Modell zur Verfahrensauswahl. Karlsruhe 2000 (Universität Karlsruhe - Institutsverlag Siedlungswasserwirtschaft).

[103] HAHN, H.H.; KRAUS, J. (Hrsg.): Projektmanagement, Maschinentechnik und gesetzliche Vorgaben. Karlsruhe 2000 (Universität Karlsruhe - Institutsverlag Siedlungswasserwirtschaft).

[104] SCHMID-SCHMIEDER, V.: Vergleich der Leistungsfähigkeit von Biofilmverfahren bei Sanierungen bzw. Erweiterungen von kommunalen Kläranlagen. Karlsruhe 2001 (Universität Karlsruhe - Institutsverlag Siedlungswasserwirtschaft).

[105] HAHN, H.H.; KRAUS, J.: Geruchsemissionen. Karlsruhe 2001 (Universität Karlsruhe - Institutsverlag Siedlungswasserwirtschaft).

[106] ANTUSCH, E.: Lokalisierung organischer Schadstoffemissionen durch Sielhaut-untersuchungen. Karlsruhe 2002 (Universität Karlsruhe - Institutsverlag Siedlungswasserwirtschaft).

[107] OBERACKER, F.E.: Verwendung und Entsorgung arsenhaltiger Wasserwerksschlämme. Karlsruhe 2002 (Universität Karlsruhe - Institutsverlag Siedlungswasserwirtschaft).

[108] HAHN, H.H.; KRAUS, J.: Bläh- und Schwimmschlamm. Karlsruhe 2002 (Universität Karlsruhe - Institutsverlag Siedlungswasserwirtschaft).

[109] HITZLER, A.: Beurteilung und Optimierung von Sandwaschanlagen auf Kläranlagen. Karlsruhe 2002 (Universität Karlsruhe - Institutsverlag Siedlungswasserwirtschaft).

[110] KLINGEL, M.: Prozess-Simulation in der Abwasser- und Abfallbehandlung. Karlsruhe 2003 (Universität Karlsruhe - Institutsverlag Siedlungswasserwirtschaft).

[111] SONG, Y.: Precipitation Chemistry of Calcium Phosphate for Phosphorous Recovery. Karlsruhe 2003 (Universität Karlsruhe - Institutsverlag Siedlungswasserwirtschaft).

[112] KRAUS, J.: Herstellung von Leichtzuschlagstoffen aus Klärschlamm. Karlsruhe 2003 (Universität Karlsruhe - Institutsverlag Siedlungswasserwirtschaft).

[113] ZHANG, P.: Herstellung und Charakterisierung und Wirksamkeit polymerer anorganischer Flockungsmittel. Karlsruhe 2003 (Universität Karlsruhe - Institutsverlag Siedlungswasserwirtschaft).

[114] HAHN, H:H.; KRAUS, J.: Wertschöpfung durch Betriebsoptimierung. Karlsruhe 2003 (Universität Karlsruhe - Institutsverlag Siedlungswasserwirtschaft).

[115] LUCAS, S.: Auftreten, Ursachen und Auswirkungen hoher Fremdwasserabflüsse – eine zeitliche und räumliche Analyse. Karlsruhe 2003 (Universität Karlsruhe - Institutsverlag Siedlungswasserwirtschaft).

[116] SCHWARZ, M.: Mikrobielle Kolmation von abwasserdurchsickerten Bodenkörpern: Nucleinsäuren zum Nachweis von Biomasse und Bioaktivität. Karlsruhe 2004 (Universität Karlsruhe - Institutsverlag Siedlungswasserwirtschaft).

[117] HOLZ, A.: Immissionsorientierte Bilanzierung punktueller und diffuser Schwermetallfrachten. Karlsruhe 2004 (Universität Karlsruhe - Institutsverlag Siedlungswasserwirtschaft).

[118] HAHN, H.H.; KEGEBEIN, J.: Auf dem Weg zur Kläranlage von morgen. Karlsruhe 2004 (Universität Karlsruhe - Institutsverlag Siedlungswasserwirtschaft).

[119] BUTZ, J.: Stoffstrombilanzen für Phosphor und sechs Schwermetalle am Beispiel des oberen Kraichbachs. Karlsruhe 2005 (Verlag Siedlungswasserwirtschaft Karlsruhe).

[120] MAHMUTSPAHIC, Z.: Projektfinanzierung – ein PPP Modell für internationale siedlungswasserwirtschaftliche Projekte. Karlsruhe 2005 (Verlag Siedlungswasserwirtschaft Karlsruhe).

[121] HAHN, H.H.; FRIEDRICH, K.: Chemikalien in der Abwasserbehandlung – was haben wir dazugelernt? Karlsruhe 2005 (Verlag Siedlungswasserwirtschaft Karlsruhe).

[122] KEGEBEIN, J.: Die Verwendung von Küchenabfallzerkleinerern (KAZ) aus abwasser- und abfallwirtschaftlicher Sicht (in Vorbereitung)

[123] HAHN, H.H.; HOFFMANN, E.; BLANK, A.: Abwasserproblemstoffe – Erfahrungen mit neuen Produkten und Technologien. Karlsruhe 2006 (Verlag Siedlungswasserwirtschaft Karlsruhe).

[124] KPONGBEGNA, K.: Wasserver- und Entsorgung in der Stadt Lomé/Togo: Analysen,Beiträge und Konzepte. Karlsruhe 2006 (Verlag Siedlungswasserwirtschaft Karlsruhe).

[125] BEKKER, M.: Charakterisierung der anaeroben Abbaubarkeit von spezifischen organischen Stoffen(in Vorbereitung).

[126] DUTTA, S.: Mathematical Modeling of the Performance of a Rotating Biological Contactor for Process Optimisation in Wastewater Treatment. Karlsruhe 2007 (Verlag Siedlungswasserwirtschaft Karlsruhe).

Bestellanschrift:

Universität Karlsruhe (TH)
Institut für Wasser und Gewässerentwicklung
Bereich Siedlungswasserwirtschaft
Forschungszentrum Umwelt
BIBLIOTHEK, Abteilung: Schriftenreihe
D – 76128 Karlsruhe